

**CANOPY CHLOROPHYLL ESTIMATION WITH HYPERSPECTRAL  
REMOTE SENSING**

By

JINCHENG GAO

B. S., Shangdong Normal University, 1986

M.S., China Southwest Normal University, 1989

M.A., Kansas State University, 2001

AN ABSTRACT OF A DISSERTATION

submitted in partial fulfillment of the requirements for the degree

DOCTOR OF PHILOSOPHY

Department of Geography

College of Arts and Sciences

KANSAS STATE UNIVERSITY

Manhattan, Kansas

2006

## **Abstract**

In this research, proximal measurements of hyperspectral reflectance were used to develop models for estimating chlorophyll content in tallgrass prairie at leaf and canopy scales. Models were generated at the leaf scale and then extended to the canopy scale. Three chlorophyll estimation models were developed, one based on reflectance spectra and two derived from derivative transformations of the reflectance spectra. The triangle chlorophyll index (TCI) model was derived from the reflectance spectrum, whereas the first and second derivative indices (FDI and SDI) models were developed from the derivative transformed spectra. The three models were found to be well-correlated with the chlorophyll content measured with solvent extraction. The result indicated that the three models were effective for the leaf scale estimates of chlorophyll content.

The three chlorophyll models developed at the leaf scale were further extended to the canopy scale and fine-scale images. The three models were found to be conditionally effective for estimating canopy chlorophyll content. The TCI model was more effective in dense vegetation, and the FDI and SDI models were better in sparser vegetation. This research suggests that the extension of chlorophyll models from the leaf scale to canopy scale is complex and affected not only by soil background, but also by canopy structure and components

CANOPY CHLOROPHYLL ESTIMATION WITH HYPERSPECTRAL  
REMOTE SENSING

By

JINCHENG GAO

B. S., Shangdong Normal University, 1986

M.S., China Southwest Normal University, 1989

M.A., Kansas State University, 2001

A DISSERTATION

submitted in partial fulfillment of the requirements for the degree

DOCTOR OF PHILOSOPHY

Department of Geography  
College of Arts and Sciences

KANSAS STATE UNIVERSITY

Manhattan, Kansas

2006

Approved by:

Major Professor

Douglas G. Goodin

## **Abstract**

In this research, proximal measurements of hyperspectral reflectance were used to develop models for estimating chlorophyll content in tallgrass prairie at leaf and canopy scales. Models were generated at the leaf scale and then extended to the canopy scale. Three chlorophyll estimation models were developed, one based on reflectance spectra and two derived from derivative transformations of the reflectance spectra. The triangle chlorophyll index (TCI) model was derived from the reflectance spectrum, whereas the first and second derivative indices (FDI and SDI) models were developed from the derivative transformed spectra. The three models were found to be well-correlated with the chlorophyll content measured with solvent extraction. The result indicated that the three models were effective for the leaf scale estimates of chlorophyll content.

The three chlorophyll models developed at the leaf scale were further extended to the canopy scale and fine-scale images. The three models were found to be conditionally effective for estimating canopy chlorophyll content. The TCI model was more effective in dense vegetation, and the FDI and SDI models were better in sparser vegetation. This research suggests that the extension of chlorophyll models from the leaf scale to canopy scale is complex and affected not only by soil background, but also by canopy structure and components.

## Table of Contents

List of Figures.....	x
List of Tables .....	xiii
Acknowledgements.....	xiv
CHAPTER 1 - INTRODUCTION.....	1
1.1 Overview of the Research.....	1
1.2 Statement of the Problems .....	4
1.3 Purposes of the Study .....	5
1.4 Significance of the Research.....	5
CHAPTER 2 - LITERATURE REVIEW.....	8
2.1 Leaf Reflectance .....	8
2.2 Canopy Reflectance .....	12
2.2.1 Radiative Transfer Models.....	14
2.2.2 Geometrical Models.....	14
2.2.3 Turbid Medium Models .....	15
2.2.4 Hybrid Models .....	15
2.2.5 Computer Simulation Models .....	16
2.3 Inversion of Canopy Reflectance Models.....	16
2.4 Empirical Retrieval with Vegetation Indices.....	17
2.5 Derivative of Reflectance Spectrum .....	20
2.6 Measurement of Chlorophyll Content .....	21
2.6.1 Destructive Measurement of Chlorophylls .....	22
2.6.2 Non-destructive Measurement of Chlorophylls.....	23
2.7 Application of Hyperspectral Remote Sensing.....	24
2.7.1 Canopy Water Content.....	24
2.7.2 Canopy Chlorophyll Content .....	25
2.8 Scaling from Canopy to Fine-scale Image.....	27
CHAPTER 3 - RESEARCH METHODS.....	29

3.1 Study Location.....	29
3.1.1 Climate.....	29
3.1.2 Geomorphology and Soils.....	32
3.1.3 Vegetation.....	33
3.1.4 Experimental Treatments at Konza Prairie Biological Station.....	34
3.2 Research Design.....	37
3.2.1 Research Sites.....	37
3.2.2 Field Data Collection.....	41
3.2.2.1 Leaf Hyperspectral Reflectance.....	41
3.2.2.2 Leaf Chlorophyll Measurement.....	41
3.2.2.3 Canopy Hyperspectral Reflectance.....	43
3.2.2.4 Canopy Multiple-spectral Reflectance.....	43
3.2.2.5 Canopy Greenness Cover.....	44
3.2.2.6 Canopy Leaf Area Index.....	44
3.2.2.7 Canopy Chlorophyll Content.....	48
3.2.3 Aircraft Image Acquisition.....	48
3.3 Derivative of Reflectance Spectrum.....	51
3.3.1 Functions of Derivative Spectra.....	51
3.3.2 Development of Derivative Spectra from Hyperspectral Reflectance.....	52
3.3.3 Development of Derivative Image from Hyperspectral Images.....	54
3.4 Data Analyses.....	54
CHAPTER 4 - LEAF REFLECTANCE MODEL TO ESTIMATE CHLOROPHYLL	
CONTENT USING HYPER-RESOLUTION SPECTROSCOPY.....	58
4.1 Introduction.....	58
4.2 Spectral Indices.....	59
4.3 Development of New Chlorophyll Index from Reflectance Spectrum.....	62
4.3.1 Spectral Reflectance and Chlorophyll Content.....	62
4.3.2 Triangle Chlorophyll Index (TCI).....	64
4.4 Development of Derivative Spectral Indices.....	65
4.5 Results and Analysis.....	70
4.5.1 Chlorophyll Contents of Solvent Extraction and Optical Measurement.....	70

4.5.2 Chlorophyll Content with the TCI Model.....	70
4.5.3 Chlorophyll Content with the FDI and SDI Models.....	76
4.5.4 Spectral Shift with Seasonal Change.....	79
4.6 Conclusions.....	79
CHAPTER 5 - APPLICATION OF LEAF-SCALE SPECTRAL MODELS FOR CANOPY CHLOROPHYLL ESTIMATION.....	83
5.1 Introduction.....	83
5.2 Correlation of Spectral Reflectance with Canopy Chlorophyll Content .....	84
5.3 Canopy Derivative Spectral Indices .....	86
5.4 Spectral Indices and Canopy Chlorophyll Content.....	91
5.4.1 Correlation between Spectral Indices and Canopy Chlorophyll Content .....	91
5.4.2 Correlation between Derivative Indices and Canopy Chlorophyll Content ....	93
5.5 Application of the Chlorophyll Models in Canopy .....	95
5.5.1 The TCI Model .....	96
5.5.2 The FDI Model .....	97
5.5.3. The SDI Model .....	98
5.5.4 Analysis of the Chlorophyll Models.....	103
5.6 Conclusions.....	105
CHAPTER 6 - APPLICATION OF LEAF-SCALE SPECTRAL MODELS FOR HYPERSPETRAL IMAGES .....	108
6.1 Introduction.....	108
6.2 Relationship between Spectral Index Images and Field Canopy Chlorophyll Measurement .....	111
6.2.1 Correlation between TCI image and Canopy Chlorophyll Content.....	111
6.2.2 Correlation between FDI Image and Canopy Chlorophyll Content .....	112
6.2.3 Correlation between SDI Image and Canopy Chlorophyll Content .....	113
6.3 Validation of Image Chlorophyll Content with Field Measurement .....	113
6.3.1 The TCI Model .....	113
6.3.2 The FDI Model .....	116
6.3.3 The SDI Model .....	118
6.4 Factors Affecting the Three Models for Chlorophyll Estimation.....	119

6.5 Conclusions.....	120
CHAPTER 7 - CONCLUSIONS .....	128
Limitation and Future Studies.....	133
References.....	135
Appendix A - Absorption Spectrum of Chlorophyll Content with Solvent Extraction in June 30, 2004.....	159
Appendix B - Absorption Spectrum of Chlorophyll Content with Solvent Extraction in July, 2004.....	161
Appendix C - Absorption Spectrum of Chlorophyll Content with Solvent Extraction in September 1, 2004 .....	163
Appendix D - Leaf Reflectance in Visible and Near Infrared, June 30, 2004 .....	165
Appendix E - Leaf Reflectance in Visible and Near Infrared, July 26, 2004 .....	167
Appendix F - Leaf Reflectance in Visible and Near Infrared, September 1, 2004.....	169
Appendix G - Canopy Reflectance and Biophysical Attributes on HQC, June 30, 2004 .....	171
Appendix H - Canopy Reflectance and Biophysical Attributes on HQC, July 26, 2004 .....	173
Appendix I - Canopy Reflectance and Biophysical Attributes on HQC, September 01, 2004 .....	175
Appendix J - Canopy Reflectance and Biophysical Attributes on 020BE, May 29, 2002 .....	177
Appendix K - Canopy Reflectance and Biophysical Attributes on 020BW, May 29, 2002 .....	179
Appendix L - Canopy Reflectance and Biophysical Attributes on 002CE, May 29, 2002 .....	181
Appendix M - Canopy Reflectance and Biophysical Attributes on 002CW, May 29, 2002 .....	183
Appendix N - Canopy Reflectance and Biophysical Attributes on 020BE, August 22, 2002 .....	185
Appendix O - Canopy Reflectance and Biophysical Attributes on 020BW, August 22, 2002 .....	187

Appendix P - Canopy Reflectance and Biophysical Attributes on 002CE, August 22, 2002  
..... 189

Appendix Q - Canopy Reflectance and Biophysical Attributes on 002CW, August 22, 2002  
..... 191

## List of Figures

Figure 2-1 Simplified model of radiance received from a single leaf (Modified from Liang 2004) .....	9
Figure 2-2 The internal structure of a healthy, green citrus leaf (Modified from Campbell, 1996) .....	10
Figure 2-3 Spectral properties of a health green leaf controlled by leaf pigment, leaf structure, and leaf water content (Modified from Liang, 2004) .....	10
Figure 2-4 Multiply-path radiation received by remote sensor for canopy structure (Modified from Liang 2004) .....	13
Figure 3-1 Location of field sampling collection: HQC, 002C, and 020B at Konza Prairie Biological Station, Kansas .....	30
Figure 3-2 The monthly precipitation in 2004 on Konza Prairie Biological Station (pink) and the monthly mean precipitation (blue) at Manhattan during 1889 - 2005 .....	31
Figure 3-3 Experimental design of KPBS with different fire and grazing treatments.....	36
Figure 3-4 The four transects and two irrigated lines in HQC treatment (Modified from Lewis 1996) .....	38
Figure 3-5 Location of field nested plots in 002C and 020B treatments .....	40
Figure 3-6 Measurement of leaf hyperspectral reflectance with ASD fiber optic probe.....	46
Figure 3-7 Leaf chlorophyll measurement with SPAD-502 chlorophyll meter .....	46
Figure 3-8 Measurement of canopy hyper-spectral reflectance with the ASD spectroradiometer by using a fiber-optic head above ground at about 1.2 meter .....	47
Figure 3-9 True RGB color reflection image taken with a reflection camera on September 1 2004 .....	49
Figure 3-10 Black-white reflection image with 79% greenness cover taken on September 1, 2004 .....	49
Figure 3-11 Vegetation reflectance spectra in zero-order ( <i>a</i> ), first-order ( <i>b</i> ), and second-order ( <i>c</i> ) derivative in the visible and near-infrared ranges.....	56

Figure 3-12 Data analysis flowchart and research framework .....	57
Figure 4-1 Absorption spectra of chlorophyll <i>a</i> and <i>b</i> (Ahmad <i>et al.</i> 1999) .....	59
Figure 4-2 Correlation spectra between spectral reflectance and chlorophyll content on June 30, July 26, and September 1, 2004 .....	64
Figure 4-3 The triangle (red color) at the peak of green, trough of red, and shoulder of NIR regions from the reflectance spectrum of a fresh green leaf.....	65
Figure 4-4 The peak occurrence (a and b) and the maximum trough (c) of the first derivative with 80 samples at visible and near infrared regions in different growing seasons.....	68
Figure 4-5 The maximum peak (a) and maximum trough (b) of second derivative with 80 samples at visible and near infrared regions in different growing seasons.....	69
Figure 4-6 Correlation between optical measurement with a SPAD meter and solvent chlorophyll content (N=80), July 26, 2004 .....	71
Figure 4-7 Correlation between optical measurement with a SPAD meter and solvent chlorophyll content (N=80), September 1, 2004.....	72
Figure 4-8 Correlation between optical measurement with a SPAD meter and solvent chlorophyll content with 240 leaf samples collected in June, July, and September 2004 .....	72
Figure 4-9 Regression of leaf chlorophyll content with TCI within 160 leaf samples collected in July and September 2004 .....	74
Figure 4-10 Regression of leaf chlorophyll content with first derivative index (FDI) within 240 leaf samples collected in June, July, and September 2004 .....	77
Figure 4-11 Regression of leaf chlorophyll content with second derivative index (SDI) within 240 leaf samples collected in June, July, and September 2004 .....	78
Figure 5-1 Correlation of spectral reflectance with chlorophyll content in June, July, and September 2004 .....	86
Figure 5-2 Wavelength occurrence frequency of peaks and trough in the first derivative spectra (N=80): (a) peak in the green edge around 523 nm, (b) peak in the red edge around 717 nm, and (c) trough around 570 nm.....	89
Figure 5-3 Wavelength occurrence frequency of peak (a) and trough (b) in the second derivative spectra (N=80) .....	90
Figure 5-4 Regression (red line) of canopy Chl from TCI Model in June, July, and September 2004 (black solid line is 1:1 line).....	100

Figure 5-5 Regression (red line) of canopy Chl from FDI Model in June, July, and September 2004 (black solid line is the 1:1 line).....	101
Figure 5-6 Regression (red line) of canopy chlorophyll from SDI Model in June, July, and September 2004 (black solid line is the 1:1 line).....	102
Figure 6-1 Ground sample location in 020B plotted on a 1-m false color image with bands of 508, 636, and 783 nm (black points represent the location of field sampling plots).....	110
Figure 6-2 The TCI image was derived from the spectral reflectance with green, red edge, and NIR bands of the hyperspectral image acquired in May 2002.....	110
Figure 6-3 Regression of canopy chlorophyll content from the TCI model (Red line) in May image at 002C and 020B treatments in East and West slopes. The solid blank line represents the 1:1 line.....	122
Figure 6-4 Regression of canopy chlorophyll content from the TCI model (Red line) in August image at 002C and 020B treatments in the East and West slopes. The solid blank line represents the 1:1 line .....	123
Figure 6-5 Regression of canopy chlorophyll content from the FDI model (Red line) in May image at 002C and 020B treatments in East and West slopes. The solid blank line represents the 1:1 line.....	124
Figure 6-6 Regression of canopy chlorophyll content from the FDI model (Red line) in August image at 002C and 020B treatments in East and West slopes. The solid blank line represents the 1:1 line.....	125
Figure 6-7 Regression of canopy chlorophyll content from the SDI model (Red line) in May image at 002C and 020B treatments in East and West slopes. The solid blank line represents the 1:1 line.....	126
Figure 6-8 Regression of canopy chlorophyll content from the SDI model (Red line) in August image at 002C and 020B treatments in East and West slopes. The solid blank line represents the 1:1 line.....	127

## List of Tables

Table 3-1 Summary of field data collection with date, location, and instruments .....	45
Table 3-2 The band wavelengths (nm) of AISA imagery acquired on May 30 and August 29, 2002, with 1-m, 2-m, and 3-m resolution .....	50
Table 4-1 Correlation between spectral indices and chlorophyll content measured with dissolvent extraction and a SPAD chlorophyll meter .....	75
Table 4-2 Regression equations and parameters of leaf chlorophyll content with SPAD units and spectral indices derived from original and derivative spectra .....	75
Table 4-3 Correlations between derivative spectral indices and chlorophyll contents measured with dissolvent extraction and optical chlorophyll meter .....	78
Table 5-1 Correlations of spectral indices with canopy chlorophyll content measured with a SPAD chlorophyll meter and canopy LAI and greenness cover (n=80 for each sampling date).....	92
Table 5-2 The correlations between derivative indices and canopy chlorophyll content, LAI, and greenness cover in 2004 (n=80 for each sampling date).....	94
Table 5-3 Validation statistics of TCI, FDI, SDI chlorophyll models.....	99
Table 6-1 The correlations (r) of canopy chlorophyll content and canopy LAI with the TCI, FDI, and SDI indices from hyperspectral images in May and August 2002 at 002C and 020B treatments on Konza Prairie.....	115
Table 6-2 Validation of the TCI, FDI, and SDI models with field estimation of canopy chlorophyll in May and August hyperspectral images at 002C and 020B treatment on the Konza Prairie .....	117

## **Acknowledgements**

I would like to express sincere gratitude to my major professor and mentor, Dr. Douglas G. Goodin, for his constant support, patience, and encouragement during the entire process for my doctoral research and dissertation. Without his good guidance and financial support, I would not complete this long journey. I want to thank Dr. John A. Harrington, Jr. and Dr. Max Lu for their warm-hearted help, support, and suggestions throughout my doctoral program either through formal meetings or informal chat over a cup of tea. I also sincerely thank all the other professors who serve on my graduate committee, Dr. David A. Gustafson, Dr. Michael A. Herman, and Dr. Alan K. Knapp, for their feedback, encouragement, and support given to my doctoral research.

I would also take this opportunity to thank those who have helped me during my research process. Dr. John Blair, my supervisor of the current position, has given me lots of support while I'm working full time and writing my dissertation. Dr. Anthony Joern and Mr. Duncan M<sup>c</sup>Kinley reviewed my dissertation and shared their constructive suggestions. I would also give my thanks to all the faculty members in the Departments of Geography and the Division of Biology for sharing their knowledge with me.

Last but not least, I would like to give my special thanks to my beloved wife and best friend, Dr. Hong Wang, for her love, support, and encouragement in all the seasons of my life. I would also thank my dear parents, Zhenqi Gao and Yuying Diao, and my brothers and sisters for their support during my oversea study.

# CHAPTER 1 - INTRODUCTION

Remote sensing has provided powerful techniques for addressing questions concerning biogeophysical patterns across multiple spatial scales. The purpose of this dissertation is to evaluate the application of hyperspectral remote sensing in estimating canopy chlorophyll content and to study the influence of rescaling on remotely sensed data. This introductory chapter is organized in the following sections: (a) overview of the research, (b) statement of the problem, (c) purpose of the study, and (d) significance of the research.

## 1.1 Overview of the Research

Biogeophysical attributes are important parameters for many ecological and climatic models. Remote sensing provides the possibility to supply these parameters at various spatial and temporal resolutions based on model requirements. For example, vegetation indices derived from Landsat images are important parameters in models of global climate change (Quattrochi and Goodchild 1997). Global net primary production estimated with remote sensing is an important component of biogeochemical cycling models (Turner *et al.* 2001).

With the development of advanced optical-electronic technology, remote sensing spectroradiometers can provide fine-scale remotely sensed data with small spatial and spectral resolutions. For example, airborne hyperspectral images are available with bands ranging from 400 nm to 2450 nm, spectral resolution approaching 1 nm, and spatial resolution less than 1 meter. Compared to multi-spectral images, hyperspectral images

have more detailed spectral information with finer spectral resolution. Hyperspectral remote sensing has been increasingly used to acquire more accurate ground biophysical attributes such as leaf area index (LAI) (Knyazikhin *et al.* 1998, Fang and Liang 2003) and canopy water content (Gao 1996, Sanderson 1998, Bowyer and Danson 2004).

Hyperspectral images have also been increasingly used to extract canopy biochemical variables such as foliar nitrogen (Huang *et al.* 2004) and chlorophyll content (Hu *et al.* 2004). Canopy biochemistry can relate to modeling of productivity and nitrogen dynamics (Patel *et al.* 1983, Van Cleve *et al.* 1983). Concentrations of N and C can be estimated with remote sensing by our increasing ability to understand and measure foliar spectra (Card *et al.* 1988, Curran 1989). By making such estimates remotely, remote sensing can provide information for studying vegetation quality and nutrient cycles from local to regional and global scales. Remote sensing is playing an increasingly critical role in the study of global biogeochemical cycling and global climate change. The role of remote sensing was noted in the 1990 U.S. agenda for the study of global change:

“New, high spectral resolution remote sensing techniques show promise of estimating canopy chemical composition parameters that can be used to elucidate ecosystem properties. Basic understanding and wider validation of this approach are needed” (Committee on Earth Sciences 1989).

Remote sensing provides a potential application in estimating vegetation chlorophyll content (Jensen 1983). Plant chlorophylls absorb light in the visible region of the electromagnetic spectrum (400-700 nm). There is high absorption in the blue and red regions of the visible spectrum, and a relative high reflectance in the green wavelength region (around 540 nm). When plants are under stress or plant chlorophyll content

decreases, the lack of chlorophyll pigments causes the plants to absorb less in the red and blue wavelength regions, and to reflect more in the red portion of the spectrum. The plants become yellowish (Hoffer 1978).

Several spectral indices have been developed to estimate plant chlorophyll content based on the chlorophyll spectral reflectance. For example, the ratios of R675/R760, R675/R700, and R760/R500 were highly correlated to chlorophyll *a*, chlorophyll *b*, and the total carotenoid concentration in soybean leaves (Chappelle *et al.* 1992). The ratios of R750/R550 and R750/R700 were also well correlated with the total chlorophyll content of maple, chestnut, and cotoneaster leaves (Gitelson and Merzlyak 1996). The ratio of R672/(R555\*R708) was found related to total chlorophyll content, and the ratio of R672/R550 was a good indicator for chlorophyll *b* (Datt 1998). Daughtry *et al.* (2000) found the reflectance of wavelengths at 550 nm and 715 nm were inversely related to chlorophyll concentration in corn leaves. Gitelson *et al.* (2003a) further studied the application of remote sensing to estimate chlorophyll content on irrigated and rainfed cropland and designed a concept model of chlorophyll estimation with NIR, green, and red edge wavelengths based on the absorption of pigment of interest from the reflectance spectra. The concept model was effectively used for the quantification of different pigments in fruit peels (Merzlyak *et al.* 2003) and for remote estimation of chlorophyll-*a* in turbid productive waters (Dall'Olmo *et al.* 2003). However, all of the indices to estimate chlorophyll content were derived from experimental spectral reflectance at leaf scale with foliage of crop plants or leaves of trees.

## 1.2 Statement of the Problems

Most applications of remote sensing to estimate canopy biophysical attributes were applied in relatively homogeneous canopies such as in cropland or forest. Spectral indices of chlorophyll measurement were mostly derived from individual leaves of trees or crops. Because leaf reflectance could be affected by species structure, the indices to measure chlorophyll content may vary with plant species, space, and time (Datt 1998). Canopy reflectance is affected not only by leaf chlorophyll, but also by canopy scattering and soil reflectance. Daughtry *et al.* (2000) showed that the transformation from leaf to canopy spectral response in cropland is complex, and cannot be done by simple extrapolation from leaf to canopy scale. This is especially true for complex heterogeneous canopies, because canopy reflectance varies with leaf physical condition, leaf spatial distribution, and solar angle. The transformation of reflectance from leaf to canopy scale is not a simple aggregating process.

To extract biophysical variables, remotely sensed data must be validated with field measurements. As remotely sensed data normally has a spatial extent that may range from less than one meter to over one kilometer, it is impossible to validate an image with field data at the same spatial scale. Rescaling from fine-scale field data to image scale is therefore necessary.

A landscape is normally composed of nested, hierarchically organized structures, such as sub-watersheds are nested in a watershed. Remote sensing with different spatial resolutions is needed to observe landscape patterns and diversity with multiple spatial scales. It is common for researchers to use multiple-scale images to address spatial change and seasonal difference from regional to global scales. One question arising from

these studies is how to reconcile remote sensor data obtained at varying resolutions. Addressing this question suggests a need to rescale multiple-resolution images into a common spatial resolution. Upscaling from fine-scale to coarse-scale images becomes an important issue in applications of remote sensing in order to make data comparable.

### **1.3 Purposes of the Study**

The purpose of my research is to address the above problems and find a convenient solution for the problems. The goal of this research is to develop a nondestructive and fast model from leaf hyper-spectrum in order to assess leaf chlorophyll content, and further extend this model to canopy scale and finer-resolution images to estimate canopy chlorophyll content. Three major questions will be addressed in my research:

1. Is hyperspectral remote sensing effective for estimating leaf chlorophyll content?
2. Can we transform the chlorophyll model derived from the leaf scale to canopy scale?
3. Is the chlorophyll model effective in finer-resolution image for chlorophyll estimation?

### **1.4 Significance of the Research**

Remote sensing is intensively studied and widely used at coarse scales. Applications of remote sensing with fine-scale spatial and hyper-spectral resolution are relatively new and challenging. Hyperspectral remote sensing is increasingly used to extract biogeophysical variables, such as canopy chlorophyll content, vegetation biomass, and canopy water content (Jensen 1983). Canopy chlorophylls are the component of

leaves which is related to plant photosynthesis and further affects vegetation net primary productivity (NPP). Gitelson *et al.* (2006) used the concept chlorophyll model derived from foliage of crops to effectively assess gross primary production in crops. The concept model was also found effective to remotely estimate canopy chlorophyll content in crops (Gitelson *et al.* 2003b). However, all of the effective estimation at canopy scale was conducted in crops with homogenous canopy and single species.

There is no effective approach to estimate chlorophyll content of heterogeneous canopy at a large scale. One direct reason is the influence of leaf scatter because of the irregular distribution of leaves. Another reason is the soil background reflectance and complexity of canopy components. In this research, I tried to use derivative technique to remove or minimize the influence of soil background from reflectance spectrum in order to use hyperspectral reflectance to estimate chlorophyll content.

Scale is an important issue in ecological and geographical studies. Fine-scale researches are traditional domains of ecological studies. Field samples are important data sources of the fine-scale researches. The canopy dynamics incorporating net primary productivity (NPP) has been studied from a long-term data collection from plots of 0.1 square meters on the Konza Prairie (Briggs and Knapp 1995, Knapp *et al.* 1993). Right now, the ecological studies are facing a transition from fine-scale to coarser-scale and from local to continental scale in order to extend the models and theories derived from fine-scale to coarse-scale studies. The on-going National Ecological Observatory Network (NEON) is an example of extension from fine-scale to coarse-scale study. The NEON project is a continental scale project based on a national network of field observation stations. Remotely sensed data are another important data source for NEON

project to collect land use and vegetation maps in a large extent area. However, it is difficult to use field data to validate the coarse scale images. To make a transition from fine-scale dataset to coarse-scale images, fine-scale images make it possible. We can use the fine-scale field data to validate fine-scale images, and then using fine-scale image to upscale to coarse scale images.

The First ISLSCP (International Satellite Land Surface Climatology Project) Field Experiment (FIFE) conducted on the Konza Prairie from 1987 through 1989 was designed to study the biophysical processes of energy flux, and carbon and water cycles from pixel-level information to regional scale (Sellers *et al.* 1992). The energy and mass fluxes used for rescaling were based on the relationship between canopy conductance and incident PAR flux in grasslands with similar physiology and physiognomy on the Konza Prairie (Hall *et al.*, 1992). The FIFE experiment verified that the mathematical structure relating radiation and surface energy flux to remote sensing parameters are scale invariant on a homogeneous vegetation (Sellers *et al.* 1992). This means that ground biophysical attributes in homogenous canopy could be estimated with remotely sensed data at coarse scale because of the scale invariance. However, in long term unburned areas, the homogeneous grassland has been fragmented by invasion of woody species, thus the results of FIFE need to be retested heterogeneous canopies. In this research, scale invariance was further evaluated with canopy chlorophyll on heterogeneous canopy. Canopy chlorophyll content was estimated from chlorophyll models derived from leaf scale, and the models were further extended to fine-resolution images of heterogeneous vegetation.

## CHAPTER 2 - LITERATURE REVIEW

### 2.1 Leaf Reflectance

Plant leaves are the sites at which leaf photosynthesis and respiration occur. When electromagnetic solar radiation (EMR) reaches the surface of a leaf, it is either absorbed, transmitted, or reflected (Figure 2.1). The intensity of absorption, transmission, and reflection is dependent on the wavelength of electromagnetic energy, leaf structure, and leaf pigment content.

The structure of a typical dicot leaf has four layers: cuticle, epidermis, palisade, and spongy mesophyll (Figure 2.2). The palisade parenchyma is the layer in which most chlorophyll pigments occur. This layer is the main site where photosynthetically active radiation is absorbed and converted into biochemical energy. Up to 90 percent of incident blue and red wavelength energy is absorbed, depending on the content of chlorophyll pigment (Maas and Dunlap 1989). The spongy mesophyll layer contains most of the water in the leaf and is the site where near infrared (NIR) and middle infrared (MIR) are absorbed. The spongy mesophyll reflects up to 40 or 50 percent of incident NIR energy and transmits most of the rest. In this layer, absorption of MIR varies with water content. Thus, the structure, chlorophyll pigment, and water content in a leaf would affect the absorption, transmission, and reflection of incident energy. A typical spectral reflectance property of green vegetation is shown as Figure 2.3.

At the leaf scale, the dominant factors contributing to leaf reflectance in the spectral region from 400 to 2600 nm are leaf pigments, cell structure, and water content (Hoffer 1978, Jensen 1983, Walter-Shea *et al.* 1992). Leaf pigments have an important impact on visible reflectance. Chlorophyll pigments absorb wavelengths of blue (400-500 nm) and red (600-680 nm), and reflect green wavelength (500-600 nm). Leaf cell structure also results in high reflectance of near infrared light. Water content has a strong influence in middle and far infrared region. Water molecules are strong absorbers of solar energy at 1400 nm and 1900 nm.

**Figure 2-1 Simplified model of radiance received from a single leaf (Modified from Liang 2004)**

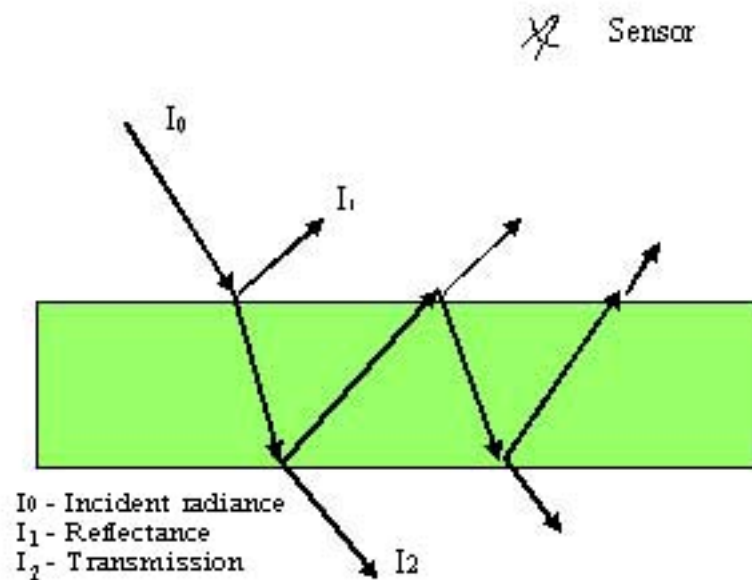


**Figure 2-2 The internal structure of a healthy, green citrus leaf (Modified from Campbell, 1996)**

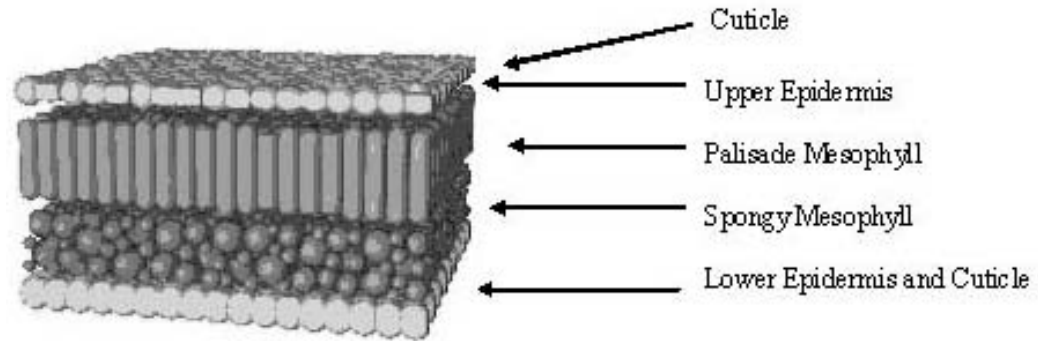
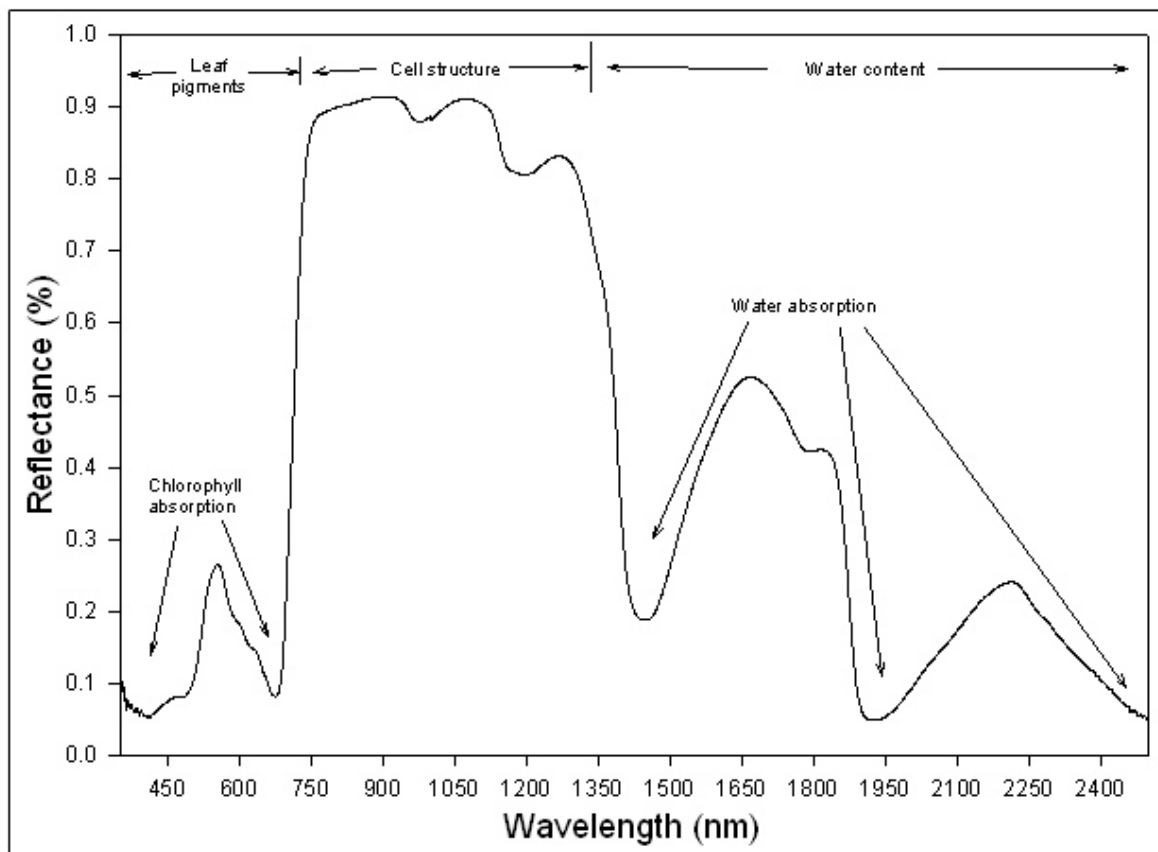


**Figure 2-3 Spectral properties of a health green leaf controlled by leaf pigment, leaf structure, and leaf water content (Modified from Liang, 2004)**



There are several leaf optical models to simulate the reflectance and transmittance of broad-leaves and needle-leaves. A common leaf reflectance model is the PROSPECT model for broadleaf canopies, first introduced by Jacquemoud and Baret (1990). PROSPECT is a radiative transfer model that calculates leaf hemispherical reflectance and transmittance from 400 to 2500 nm as a function of leaf structure and leaf biochemical parameters. Scattering is described by the refractive index of leaf materials and by a parameter characterizing the leaf mesophyll structure. Absorption is calculated from the biochemical concentrations and specific absorption coefficients. The original PROSPECT model requires only three parameters: structure, chlorophyll content, and water content to calculate reflectance and transmittance of any fresh leaf over the whole solar domain. The modified PROSPECT model added two more parameters: the protein and cellulose + lignin contents to simulate dry leaf reflectance and transmittance (Jacquemoud *et al.* 1995). This model was successful in simulating the reflectance spectra of a compact corn leaf with few air-cell wall interfaces.

The LIBERTY (Leaf Incorporating Biochemistry Exhibiting Reflectance and Transmittance Yields) model was developed to characterize spectral properties of conifer needles (Dawson *et al.* 1998). With an assumption that leaf cellular structure could be represented by spherical cells, LIBERTY performs a linear summation of the individual absorption coefficients of the major constituent leaf chemicals (chlorophyll, water, cellulose, lignin, protein) according to their content per unit area of leaf. The model needs three structure parameters: mean cell diameter, leaf thickness, and an intercellular air-gap

determinant. The model could provide accurate reflectance and transmittance spectra of both stacked and individual needles.

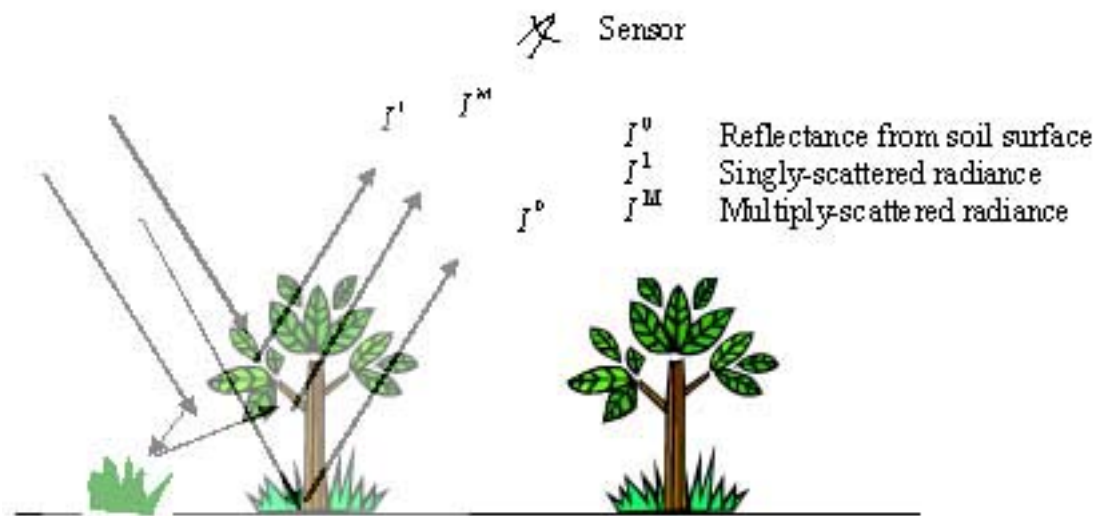
## **2.2 Canopy Reflectance**

Compared with leaf reflection, canopy reflection is more complex. Canopy reflection is the aggregation of reflection from leaves and their background (Figure 2.4). Canopy reflectance is affected by leaf reflection, canopy structure, sunlight incident angle, soil, and bi-directional reflectance. Canopy structure includes leaf size, shape, density, and orientation. Previous studies showed that the optical properties of individual leaves are not directly related to the reflectance of the canopy (Curran and Milton 1983, Campbell 1996). The signal received by remote sensor includes direct reflectance, singly scattered radiance from individual leaf, and multiple-scattered radiance from multiple leaves. Many different canopy structures could generate very similar reflectance spectra and have the same signal in remotely sensed data (Walter-Shea *et al.* 1992).

For a dense green canopy, visible reflection is primarily related to chlorophyll content in the canopy upper layer and soil reflectance can be ignored. Soil reflectance has an important influence on canopy reflectance in a sparse and open canopy (Rundquist 2000). Several factors affect soil reflectance, such as soil moisture, soil physical and chemical components, and soil surface roughness. Shadows have an important influence on canopy reflectance. Under the

**Figure 2-4 Multiply-path radiation received by remote sensor for canopy structure**

(Modified from Liang 2004)



influence of shadow, reflectance per unit of area in the visible and NIR spectral region for a canopy is less than that for an individual leaf (Knippling 1970). Shadow influence on canopy reflectance cannot be ignored in field radiation collection and fine scale aircraft imagery. To minimize the shadow effect, it is better to take radiation measurement at minimum solar zenith angle (i.e. around solar noon).

Several approaches have been developed to model radiation reflectance regimes in vegetation canopies. Goel (1988) made a detailed review of canopy reflectance models, identifying four categories: geometric models, turbid medium models, hybrid models, and computer simulation models. All these models are based on the geometrical optical, the radiative transfer theory/model, and average canopy transmittance theory.

### **2.2.1 Radiative Transfer Models**

A radiative transfer model is used to simulate radiation transfer processes in certain media, such as vegetation and atmosphere. For vegetation, it simulates the interaction between solar radiation and plants. Kubelka and Munk (1931) developed a theory of light scattering and extinction in diffusing media. There are two fluxes (downward and upward) included in the KM theory. The relations between these fluxes are expressed by two simultaneous linear differential equations with two coefficients. Allen *et al.* (1970) extended the KM two-flux model by adding a direct solar flux which made it a three-flux theory with three differential equations and five coefficients. Suits (1972) further extended Allen's three-flux model by adding the radiation in the direction of observation into a four-flux theory. The Suits model is a four-flux model with four differential equations and nine coefficients. The Suits model assumes that the canopy consists only of horizontal and vertical leaves, and is parameterized with canopy structure and solar viewing geometry (Suits 1972).

Verhoef (1984) developed the light Scattering by Arbitrarily Inclined Leaves (SAIL) model by extending the Suits model to allow for variations of leaf angles. The extinction and scattering coefficients of a layer in the SAIL model are calculated based on a given leaf area index and a leaf inclination distribution, in addition to the usual parameters describing the optical properties of single leaves and those associated with measurement conditions.

### **2.2.2 Geometrical Models**

Canopy geometric optical models assume that the canopy is made of a surface with geometrical shapes such as cylinders, spheres, cones, and ellipsoids. For sparse

canopies, reflectance is calculated with the interception of light and shadow. Li and Strahler (1985 and 1986) first introduced geometric models to study remotely sensed data with simple geometric shapes to represent tree crowns in sparse conifer forest. Li and Strahler (1985) used a Monte Carlo procedure to simulate pixels composed of cone shaped crowns. This model should adequately represent sparse canopies (shrubs, sparse forests, orchards, planted crops in the early stages of growth, etc.) at low zenith angle.

### **2.2.3 Turbid Medium Models**

Turbid medium models consider objects as small particles that scatter and absorb radiation and are distributed randomly in horizontal layer and oriented in given directions with given optical properties. Those models ignore the size of objects compared with the distance between objects. Turbid medium models for leaf reflectance were derived from Kubelka-Munk theory and consider a leaf as a slab to diffuse and to absorb radiation (Liang 2004). Several linear differential equations were used to simplify the radiative transfer theory, and with the solution of those equations to yield simple analytic formulas for the scatter and transmittance. Those models are more successful for denser and more horizontally uniform canopies in which the leaf size is much smaller compared to the height of canopy.

### **2.2.4 Hybrid Models**

Hybrid models combine elements of geometric and turbid medium models. The canopy in this approach is still approximated by a distribution of geometrically shaped leaves, while the leaf is treated as absorbing and scattering particles, except that the

multiple scattering cannot be neglected. Hybrid models are most effective at simulating medium density canopies.

### **2.2.5 Computer Simulation Models**

Computer simulation models are developed for computation of radiation distribution over a complex canopy configuration. The arrangement and orientations of vegetation elements are simulated with a computer. Monte Carlo ray tracing and radiosity are two common methods to determine light impact and random scattering to produce the statistical distribution of radiation field. Both of those methods are based on a light transport equation. Radiative transfer models and turbid media models are more suitable for dense vegetation canopies. Geometric models are better for sparse vegetation canopies with regularly shaped crowns. Computer simulation models have been used to simulate or validate simplified models.

### **2.3 Inversion of Canopy Reflectance Models**

Several canopy reflectance models have been developed based on canopy structure and measured parameters. After canopy reflectance models have been validated on experimental datasets, the inversion procedure is used to estimate canopy biophysical variables from reflectance measurements (Jacquemond 1993). The accuracy for retrieving canopy biophysical attributes is dependent on the selection of an accurate model and choice of an appropriate inversion procedure (Goel and Thompson 1984). Jacquemond (1993) analyzed the PROSPECT + SAIL reflectance model with simulated spectra of AVIRIS, and found that this model is numerically invertible. His results indicated that the leaf physiological status including chlorophyll *a* and *b*, and leaf water content can be

generally retrieved with a reasonable accuracy, but it is difficult to estimate the canopy geometrical parameters (LAI and leaf distribution angle) separately. Jacquemond *et al.* (1995) further studied the inversion of PROSPECT + SAIL models to extract vegetation biophysical parameters from a sugar beet canopy, and found the extraction of chlorophyll content and water content was reasonably accurate, but retrieval of canopy structure parameters (LAI, leaf mesophyll structure, and mean leaf inclination angle) was inaccurate. The four canopy structure parameters may have an individual effect on canopy spectral reflectance, but combinations of these parameters may produce similar spectra. For this reason, they cannot be inferred simultaneously using only spectral information, although, in theory, this should be possible with directional radiation data. To address the inaccuracy problem, vegetation indices have been increasingly used to retrieve canopy attributes.

## **2.4 Empirical Retrieval with Vegetation Indices**

Field spectroscopy has been used to estimate biophysical attributes for more than 30 years. In the early 1970s, Pearson and Miller (1972) began to use two-channel hand-held radiometer with red and near infrared (about 680 nm and 780 nm) to estimate biomass in shortgrass prairie at the Pawnee National Grasslands, CO. They found the ratio between near infrared and red is highly correlated to live green biomass ( $r=0.95$ ). Several researchers further studied the relationship between spectral reflectance and green vegetation and found that green vegetation is positively related to near infrared region and negatively related to blue and red regions (Tucker *et al.* 1975, Tucker and Maxwell 1976).

Many vegetation indices (VI) have been derived from the reflectance spectrum of vegetation. Most VIs are based on red and NIR wavelengths, because vegetation exhibits unique reflectance properties in those regions. Bunnik (1978) suggested that the ratio of NIR and red was simply related to LAI and hence LAI could be derived with the measurement of NIR and red. Several researchers further confirmed this experiment in different crop canopies, such as soybean (Holben *et al.* 1980, Kollenkark *et al.* 1982), corn (Kimes *et al.* 1981, Walburg *et al.* 1982, Gardner and Blad 1986), wheat (Aase and Tanaka 1984, Hatfield *et al.* 1985), and rice (Patel *et al.* 1983).

Richardson and Wiegand (1977) first introduced the Perpendicular-Vegetation Index (PVI). While the ratio indices are calculated independently of soil reflectance properties, PVI refers to a base line for soil background. The base line is normally defined by two coefficients of the slope and intercept as determined by linear regression of soil reflectance with Red-NIR spectral space. PVI performs relatively well at low LAI values or sparse vegetation cover, but becomes more sensitive to soil background reflectance as LAI increases (Broge and Leblanc 2000). Wardley and Curran (1984) investigated vegetation indices in detail for estimating LAI in grasslands and found the accuracy ranged from 50 to 86 percent at a 95% confidence level.

The most widely used vegetation index is Normalized Difference Vegetation Index (NDVI) proposed by Rouse (1973). NDVI is calculated with red and near infrared (NIR) bands in the formula  $NDVI = (NIR - RED) / (NIR + RED)$ . NDVI values range between -1 and 1. NDVI becomes large with the increase of green vegetation because of enhancement of NIR reflectance. NDVI tends to enhance the contrast between soil and vegetation while minimizing the effects of illumination conditions (Baret and Guyot

1991). However, NDVI has shown sensitivity to soil brightness, especially with low vegetation cover (Huete 1989, Roujean and Breon 1995). NDVI is also widely used to extract other canopy biophysical attributes such as leaf area index and biomass.

NDVI has been used to classify land cover and monitor vegetation dynamics (Tucker *et al.* 1985). NDVI is also used for predicting vegetation net primary production (NPP) (Sellers 1985, Runyon *et al.* 1994, Wylie *et al.* 1995, Rasmussen 1998), and biomass of grassland and cropland (Tucker 1979, Curran 1980, Badwhar *et al.* 1986, Running *et al.* 1986, Bartlett *et al.* 1990, Todd *et al.* 1998). Zhang *et al.* (1997) studied Pacific coast salt marshes with remote sensing and found that biomass production can be accurately estimated with vegetation indices. The accuracies ranged from 58 to 80 percent, varying with vegetation indices and plant species. Weiser *et al.* (1985, 1986) collected field spectral reflectance with two multi-band radiometers above tallgrass prairie at the Konza Prairie Biological Station, and found that vegetation biomass is linearly correlated to NDVI ( $r \approx 0.70$ ). They also found that leaf area index is highly correlated to NDVI.

Vegetation indices have also been used to estimate canopy variables such as leaf area index (LAI) and fraction of absorbed photosynthetically active radiation (fPAR). NDVI was used to estimate the LAI of wheat (Pinter *et al.* 1983, Asrar *et al.* 1984), grassland (Weiser *et al.* 1986), and corn (Kimes *et al.* 1981). Gardner and Blad (1986) developed empirical models of LAI from red and NIR reflectance in corn canopy based on field measurement and data collected by airborne sensors. NDVI is highly linear correlated to LAI ( $r = 0.76$  to  $0.85$ ), with standard error ranging from 0.6 to 0.79. Wiegand

(1992) also studied the relationships between LAI and vegetation indices in wheat canopy, and found the same conclusion as Gardner and Blad's study (1986).

Plant growth is directly related to the absorbed photosynthetically active radiation (PAR). The fraction of PAR is called fPAR and can be estimated with vegetation indices. The relationship between fPAR and VI varied with vegetation and canopy structure. The relationship demonstrated both linear (Wiegand *et al.* 1991, Daughtry *et al.* 1992) and non-linear (Wiegand *et al.* 1992, Ridao *et al.* 1998) correlation with field measurements.

Modified NDVI has been developed to improve the efficiency of vegetation index by minimizing the contribution of soil variation and atmospheric scatter (Baret and Guyot 1991, Huete *et al.* 1994). Soil adjusted vegetation index (SAVI) was designed to remove the influence of soil variation, and is useful in low canopy cover and varied soil backgrounds (Huete 1988). The atmospherically resistant vegetation index (ARVI) (Kaufman and Tanre 1992) was developed to minimize atmospheric-induced variations making the vegetation index less sensitive to spatial and temporal variations.

## **2.5 Derivative of Reflectance Spectrum**

Derivative techniques have long been applied in analytical chemistry for reduction of low frequency background noise and for resolution of overlapping spectra (Bulter and Hopkins, 1970). This technique has increasingly been used in remote sensing for the elimination of background signals. Garrison *et al.* (1979) used ratios and differences of the transmitted solar radiation in the 305-340 nm wavelength regions to remove the effects of Rayleigh and aerosol scattering in the measurement of atmosphere ozone. Demetriades-Shah *et al.* (1990) discussed the functions of derivative spectra to remove the noises of backgrounds and found the derivative spectra was superior to

conventional broad-band spectral indices for monitoring chlorosis in vegetation. Goodin *et al.* (1993) used the second-order derivative spectra for studying turbidity and suspended sediments and found the second derivative at 660 nm and 695 nm highly correlated to chlorophyll content in water. Louchard *et al.* (2002) used derivative spectroscopy to assess qualitative and quantitative information regarding seafloor types and found the major sediment pigments, chlorophyll *a* and fucoxanthin, to be identified from remotely sensed data. The derivative techniques were also used to remove signal overlaps to identify plant nutrients (Gong *et al.* 2002).

## **2.6 Measurement of Chlorophyll Content**

Chlorophyll is a photoreceptor used for the conversion of sunlight into chemical energy and plays a vital role in plant photosynthesis (Veron and Seely 1966). Chlorophyll concentration in leaves and canopies can be an indicator of photosynthetic capacity, developmental stage, plant productivity, environmental stress, and nutrient management (Whittaker and Marks 1975, Darks *et al.* 1983, Ahmad *et al.* 1999).

Chlorophyll level is related to nitrogen content of plants and regarded it as a predictor of nitrogen levels (Piekielek *et al.* 1995, Sudduth *et al.* 1997, Johnson *et al.* 2003). Because the majority of leaf nitrogen is contained in chlorophyll molecules, there is a strong relationship between leaf chlorophyll content and leaf nitrogen content (Yoder and Pettigrew-Crosby 1995). Leaf chlorophyll content is regarded as an indicator of leaf nitrogen concentration (Blackmer and Schepers 1995, Daughtry *et al.* 2000).

Measurement of leaf chlorophyll content is also an indirect approach to estimate soil nitrogen (Peterson *et al.* 1993, Wood *et al.* 1993, Blackmer *et al.* 1994).

There are many approaches to measure chlorophyll content. We can summarize the approaches into two categories based on their process: destructive and non-destructive. The destructive approach uses harvested leaf tissues, while nondestructive approach using an optical instrument does not destroy plant tissues.

### **2.6.1 Destructive Measurement of Chlorophylls**

Destructive measurement of chlorophylls is the traditional approach to extracting chlorophyll with a chemical solution (Shoadf and Lium 1976, Jiang 2001). The procedure of destructive method includes collecting leaf samples, grinding and extracting pigments with chemical liquids, and measuring those pigments with a spectrophotometer. The extraction of chlorophylls (*a* and *b*) usually uses a variety of water-miscible solvents such as methanol, ethanol, acetone, pyridine, and acetone plus ethyl acetate. The extraction method normally contains a grinding and centrifugation processes that are noticeably time consuming for a large number of samples. Chlorophyll content is then calculated using empirical equations (Arnon 1949).

Acetone is the normal solvent used to extract chlorophyll. A disadvantage of this approach is that the chlorophyll extracted from acetone solvent is not stable and it is a time-consuming process. Shoaf and Lium (1976) found that dimethyl sulphoxide (DMSO) is superior to acetone for extracting chlorophyll from a wide range of algal species. Chlorophylls could be directly extracted with DMSO solvent without grinding and centrifugation. Chlorophylls extracted with DMSO are more stable than that extracted with acetone (Hiscox and Israelstam 1979). DMSO extraction does not require grinding and centrifugation, but it is still a time-consuming process for large numbers of samples. Also, the destructive approach increases the cost of labor and chemical solvents.

A more important disadvantage of this method is the destruction of plant tissue, which would affect plant growth. In recent years, non-destructive methods have been developed based on the absorption and reflection property of chlorophyll.

### 2.6.2 Non-destructive Measurement of Chlorophylls

There are several optical chlorophyll meters available on the market to quickly and nondestructively measure chlorophyll content, such as the CCM- 200 (Opti-Sciences, Inc) and the SPAD-502 (Minolta Corporation, Japan). Both these meters use red and near infrared bands to measure chlorophyll contents. The SPAD-502 commonly used to measure chlorophyll content in field is a fast, compact, and easy-to-use meter.

The SPAD meter has a measuring area of 2 x 3 mm with a measurement accuracy of  $\pm 1.0$  SPAD unit. The measurement principle for the chlorophyll meter is transmittance, based on 650 nm (red) and 940 nm (near infrared) wavelengths using the following equation:

$$SPAD = K \log_{10} \left[ \frac{IR_1 / IR_0}{R_1 / R_0} \right]$$

SPAD: chlorophyll level (SPAD) value

K constant

$IR_1$  and  $R_1$  transmittance of NIR (940 nm) and Red (650 nm)

$IR_0$  and  $R_0$  incident power of NIR and Red

SPAD values are linearly related to leaf chlorophyll content. Unfortunately, the coefficients in the linear equation are varied with plant species and individual SPAD meter (Ahmad *et al.* 1999). Therefore, to determine the actual chlorophyll content with

the SPAD-502 meter requires a calibration against chlorophyll content determined with solvent extraction. However, the reading of the SPAD meter itself provides a reliable relative measure of chlorophyll. Thus, most applications of chlorophyll measures with SPAD-502 meter are used in cropland and forest with SPAD units.

## **2.7 Application of Hyperspectral Remote Sensing**

In contrast to the application of broadband multispectral remote sensing, narrowband hyperspectral remote sensing has been increasingly used in the Earth environment. Multispectral data usually consists of less than 10 bands of relatively broad bandwidths (70-400 nm), whereas hyperspectral data are composed of more than 10 bands with relatively narrow bandwidths (less than 10 nm). Examples of operational hyperspectral instruments include the Moderate Resolution Imaging Spectrometer (MODIS) onboard NASA's *Terra* and *Aqua* satellites with 36 bands and NASA's Airborne Visible/Infrared Imaging Spectrometer (AVIRIS) with 224 bands. Hyperspectral remote sensing has been used for collecting many biophysical and geophysical variables such as leaf water content, chlorophyll and pigment, mineral and soil types.

### **2.7.1 Canopy Water Content**

Canopy water content is normally measured by weighing water content from field samples. Hyperspectral remote sensing is increasingly used to estimate canopy water content. Several researchers have found that middle infrared wavelengths are highly absorbed by plant water (Knipling 1970, Tucker 1980, Hunt 1989) and reflectance between 1530 and 1720 nm is as an indicator of leaf water content (Fourty and Baret

1997). Tucker (1979) indicated that the ratio of red and NIR is highly correlated to total leaf water content. Penuelas *et al.* (1993) used a ratio of two near infrared wavelengths 970 and 900 nm as a water index to measure plant water content. Carter (1994) used a narrow-band hand-held spectrometer to detect plant stress and found that the ratios of 695 / 760 nm and 605 / 760 nm are strong indicators of plant stress. Zhang *et al.* (1997) also used hyperspectral spectrometer to estimate canopy water content of salt marshes and found the narrow band reflectance about 970nm is efficient to measure canopy water content with R-square of 0.63. Ceccato *et al.* (2001) found that the reflectance ratio of 1600 and 820 nm could be an indicator to predict leaf water content.

### **2.7.2 Canopy Chlorophyll Content**

Hyperspectral remote sensing is increasingly used to measure chlorophyll content based on canopy reflection spectrum. Most empirical indices of chlorophyll estimation were directly derived from the reflection spectrum.

Kim *et al.* (1994) found the ratio of 550 nm and 700 nm from leaf spectral reflectance is constant regardless of differences in chlorophyll concentration and developed the CARI index to calculate chlorophyll concentration with reflectance at 550 nm, 670 nm, and 700 nm. Lichtenthaler *et al.* (1996) studied the relationship of chlorophyll content with spectral reflectance and found that there is a strong correlation between chlorophyll concentration and reflectance ratios of R750/R700 and R750/R550. Broge *et al.* (2000) developed the triangle vegetation index called TVI by calculating the area of green peak, red valley, and near infrared shoulder. TVI is based on the fact that chlorophyll absorption causes a decrease of red reflectance and leaf tissue abundance causes an increase of NIR reflectance, which leads to the increase of the triangle area.

Several researchers have noticed that the red-edge inflection is highly correlated to leaf chlorophyll content (Horler *et al.* 1983, Curran *et al.* 1991). Red edge shifts towards shorter wavelength which indicates a decrease in density of green vegetation, while it shifts to longer wavelength means an increase of vegetation density (Liang 2004). The red-edge curve can be approximated by one half of an inverted Gaussian function (Bonham-Carter 1988). Miller *et al.* (1990) used an inverted Gaussian reflectance model to simulate the red-edge reflectance to extract chlorophyll content.

Gitelson *et al.* (2002) studied the relationships of reflectance spectroscopy with chlorophyll and carotenoid content from leaf samples of maize and soybean and found it is efficient enough to estimate carotenoid content with green and near infrared bands. Gitelson *et al.* (2003a) further introduced chlorophyll empirical indices with NIR and green wavelength to estimate leaf chlorophyll content. Gitelson *et al.* (2003b) extend the leaf chlorophyll model to canopy chlorophyll estimation of crops with high accuracy (R-square over 0.92). However, the chlorophyll model was derived and validated from homogeneous crops and the model is also highly correlated with canopy LAI.

Haboudane *et al.* (2002) introduced a new combined index (TCARI/OSAVI) by minimizing LAI influence and underlying soil background effects. The index is sensitive to chlorophyll content variations and resistant to variations of LAI and solar zenith angle and is effective at canopy scale. With a study of corn canopy, Daughtry *et al.* (2000) found that canopy spectral reflectance is affected not only by leaf chlorophyll content, but also strongly affected by soil backgrounds and canopy structure.

To remove the influence of soil reflectance and canopy scatter, derivative transformations have been applied to spectral reflectance spectra. The first derivative of

leaf reflectance spectra was used to locate the “red edge” that is related to chlorophyll content (Horler *et al.* 1983). Wessman *et al.* (1988) applied the first derivative of forest canopy reflectance spectrum for canopy chemistry study and found the first derivative at 1256 nm, 1311 nm, and 1555 nm were high correlated with canopy lignin. Demetriades-Shah *et al.* (1990) found the second-order derivative at 636 nm and 692 nm were high correlated to leaf “red edge” and suggested that the derivative spectral indices are superior to conventional broad-band spectral indices.

## **2.8 Scaling from Canopy to Fine-scale Image**

Rescaling from canopy to coarse-resolution image has received increasing attention in recent years. The First ISLSCP Field Experiment (FIFE) conducted on the Konza Prairie Biological Station in 1987 through 1989 was designed to test the scaling invariance of energy and mass process models in homogeneous vegetation. Canopy conductance derived from canopy parameters and FPAR were estimated from a series of field sampling collection. Image spectral radiation was derived from aircraft images and satellite TM data. Biophysical properties collected with field experiments were found to be linearly correlated to satellite data with scale invariance (Hall *et al.* 1992, Sellers and Hall 1992). The scale invariance was also verified with canopy spectral reflectance on the Konza Prairie. Field radiation collected with hand-held radiometers was highly linearly correlated with fine-scale helicopter-based photo and TM data (Demetriades-Shah *et al.* 1992). However, all the experiments were conducted on grassland with similar physiology. Marsh and Lyon (1980) also found that there were statistically important correlations between field data and satellite data with concurrently collected data.

Some research argued that the reflect radiation received at a sensor is not a linear aggregation of scene elements (Bian 1997). The radiation of coarse scale image is strongly related to object size and density in a landscape (Collins and Woodcock 1999). Fine-scale data are more affected by environmental factors than coarse scale data.

Rescaling has increasingly been received attention with the application of fine-scale photogrammetry. Most researchers have focused on up-rescaling from fine-scale to coarse-scale images, but a few researchers have studied the systematic rescaling from leaf to canopy and from canopy to image. Rescaling is an important part of this research that focuses on the rescaling process from individual leaf reflectance to canopy reflectance, from canopy reflectance to fine-scale image, and from fine-scale to coarse-scale images. Meanwhile, the efficiency of hyperspectral remote sensing to estimate leaf chlorophyll content was further studied in this research. Several spectral indices related to leaf chlorophyll content were compared with the absolute leaf chlorophyll content. First-order and second-order derivative spectral indices were derived from leaf spectral reflectance. The measurement of canopy chlorophyll content was also explored with the model extension from a leaf scale.

## **CHAPTER 3 - RESEARCH METHODS**

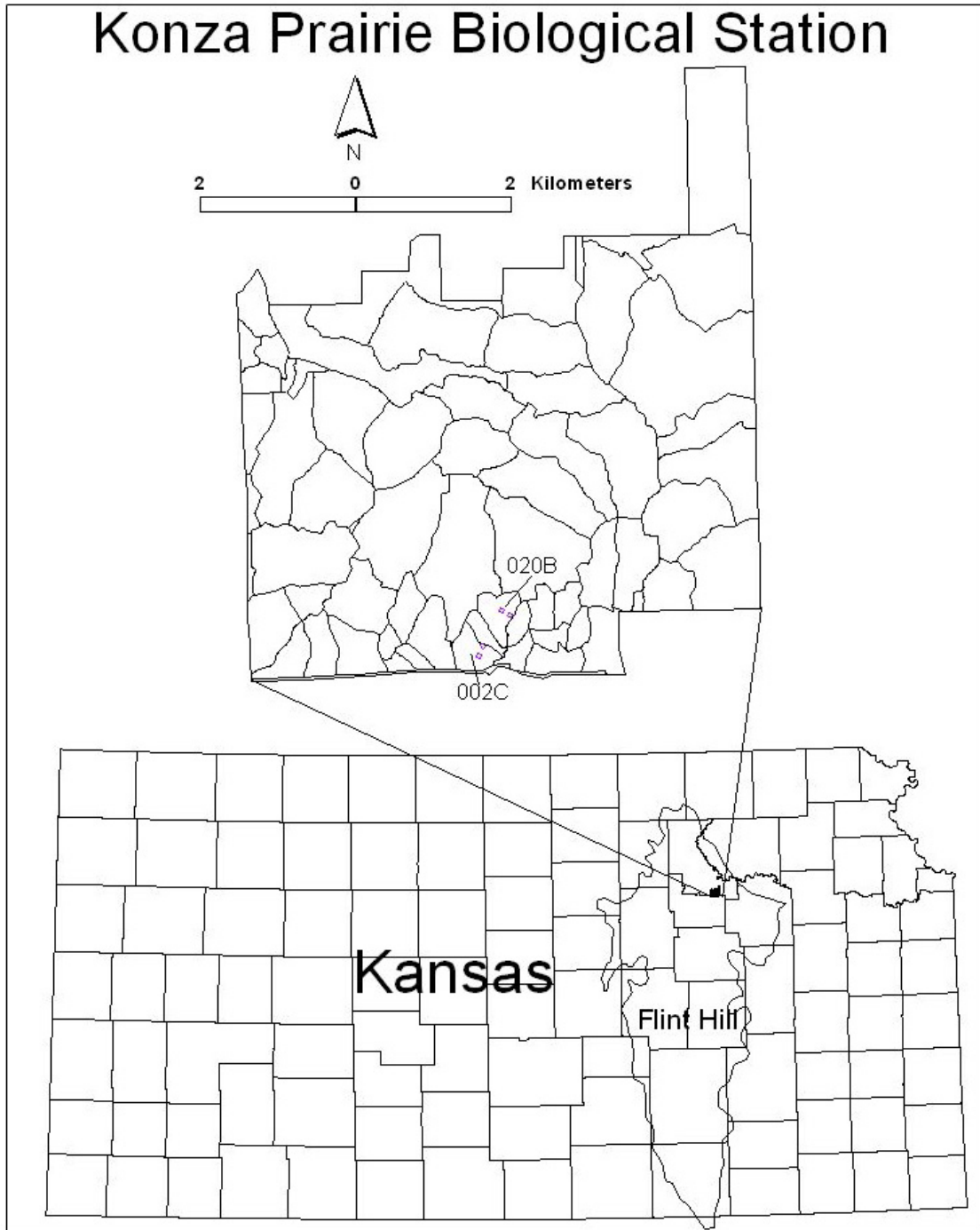
### **3.1 Study Location**

All research was conducted at the Konza Prairie Biological Station (KPBS), one of the 26 Long-Term Ecological Research sites. The KPBS is located in the northern of the Flint Hills of central Kansas (39° N, 96° W), 12 kilometers south of Manhattan, Kansas (Figure 3.1). The KPBS was established in 1972 through the efforts of Dr. Lloyd C. Hulbert as a research facility to represent a native tallgrass prairie. The land was originally purchased by the Nature Conservancy with funds provided by Katharine Ordway, and is leased to the Division of Biology, Kansas State University for research purposes. The KPBS is designed to provide experimental management of climate, fire frequency, and grazing intensity in order to understand patterns and processes in the tall-grass prairie ecosystem.

#### **3.1.1 Climate**

The climate of KPBS is continental, hot in summer and cold in winter. The weather is controlled by three air masses, a cold and dry mass from north, a warm and wet mass from the Gulf of Mexico, and a dry westerly flowing from the mountain region. The interaction of the three air masses results in large climatic variability. The mean annual temperature on the Konza Prairie is approximately 12.9 °C, with a monthly mean minimum of -1.8 °C in January and a monthly mean maximum of 26.5 °C in July. The annual precipitation is about 836.7 mm. Most of the precipitation is distributed in the

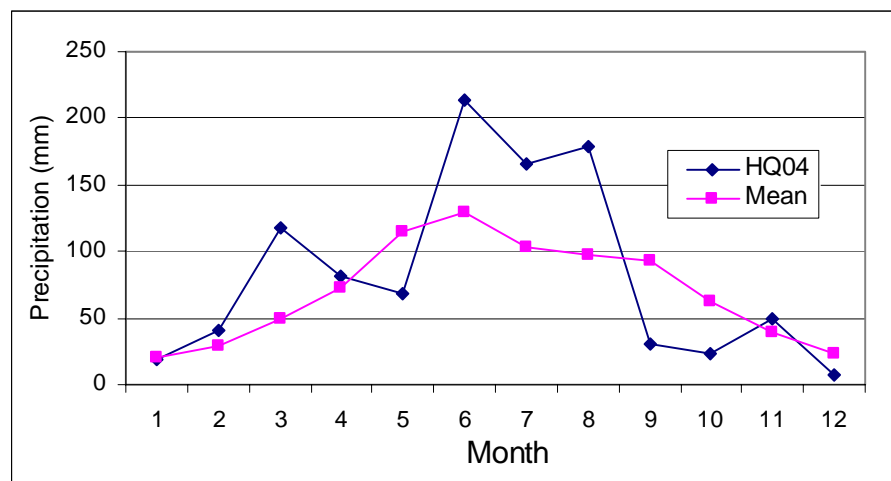
**Figure 3-1 Location of field sampling collection: HQC, 002C, and 020B at Konza Prairie Biological Station, Kansas**



early and late summer. The precipitation from May to September is more than 65 percent of the annual rainfall. There is an obvious drought season in July and early August with high temperature and low rainfall. The total precipitation in July and August is approximately with 24 percent of the total annual rainfall. High variability of precipitation is the climatic characteristics at KPBS. For example, precipitation in 1988, a dry year, was only 515.1 mm compared with 1434.6 mm in 1993, a wet year. Precipitation varies on a cycle of about 11-12 years (Weakly 1962).

It was an especially wet year in 2004 (the year of this study) with annual precipitation of 997.3 mm on the Konza Prairie. Although the total precipitation was not too high, the high distribution of rainfall in the summer was a special feature in this year (Figure 3.1). There was no obvious drought season in the growing season. The rainfall in the summer which is normally dry was obviously higher than the monthly mean precipitation in June, July, and August 2004 (Figure 3.2). The total precipitation in June, July, and August were 558 mm which was about 56 percent of the annual precipitation.

**Figure 3-2 The monthly precipitation in 2004 on Konza Prairie Biological Station (pink) and the monthly mean precipitation (blue) at Manhattan during 1889 - 2005**



### 3.1.2 Geomorphology and Soils

The Konza Prairie lies in the northeast of the Flint Hills, a region of chert-bearing limestones and shales of Permian age. Elevation at the Konza Prairie ranges from 320 to 444 m with slopes ranging from 0 to 20 degree (Knapp and Seastedt 1998). The geomorphology of the KPBS is strongly controlled by bedrock geology. Prominent in the uplands is a bench and slope topography created by erosion of contrasting bedrock units, consisting of resistant limestone layers alternating with less-resistant mudstone layers. As the landscape undergoes erosion, surface deposits are generally thin and relatively young, and are accumulated in temporary storage sites, such as ridgebone and valley bottoms.

Soil formation is the integral result of climate, organisms, topography, and parent material (Jenny 1941). Soils developed on the Konza Prairie are strongly influenced by the surface deposits and the location of landscape. With study in N04D treatment at KPBS, Wehmueller (1996) divided the Konza soils into four groups based on landscape position of summit and benches, side slopes, footslopes, and floodplains.

Dwight and Florence are typical soil series developed on interfluves and benches (Ransom *et al.* 1998). The Dwight series consists of gently sloping soils developed on a thick loess mantle. Those soils are moderately deep, moderately well drained, and slowly permeable. The soils are generally distributed on nearly level summits of benches with shale bedrock. The Florence series occurs on a shoulder slope below the summit. The Florence soils are moderately deep, sloping, and well drained. The Florence soils are mostly developed on limestone bedrock.

Soils developed on side slopes have a wide range in depth, amount of carbonate, and content of rock fragments. Tuttle soils are located on steep slopes and have a calcic

horizon of CaCO<sub>3</sub> with contents over 15% in soil pedon. Benfield and Clime soils are the most extensive soils occurring in gentle slope on the side slope. Clime soils formed in hillslope sediment over residuum weathered from shale. Benfield soils typically have a surface layer with dark silty clay loam.

Tully series are typical soils developed on the foot slopes. The soils are generally thicker than the soils on the side slopes and are deeper to bedrock. The soils in the upper reaches of the watershed are usually more than 125 cm, but less than 200 cm thick over shale or limestone bedrock. In the lower part of the watershed, the soils on the foot slopes are developed from hill-slope sediment over alluvium, and the thickness of the valley soils ranges from 200 cm to more than 400 cm. Typically, the surface layer is black or very dark brown silty clay loam with 35 to 40% clay.

Ivan series are dominant soils on terraces and floodplains. The Ivan series consists of deep, gentle sloping, and moderately to well-drained soils. The organic carbon content of the soils decreases irregularly with depth. These soils are well suited to all crops.

### **3.1.3 Vegetation**

The natural potential vegetation at KPBS is bluestem tallgrass prairie (Küchler 1974). The prairie is dominated by a few warm-season graminoid species that have wide ranges and broad ecological amplitudes (Freeman 1998). The dominant species include big bluestem (*Andropogon gerardii*), little bluestem (*Schizachyrium scoparium*), Indian grass (*Sorghastrum nutans*), and switch grass (*Panicum virgatum*) (Groffman *et al.* 1995). Forbs, also called nongraminoid herbs, are subdominant species and mosaiced into the tallgrass grassland. The forbs species include heath aster (*Aster ericoides*), daisy fleabane (*Erigeron strigosus*), slimflower scurfpea (*Psoralea tenuiflora*), pitcher sage

(*Salvia azurea*), and Missouri and Canadian goldenrod (*Solidago missouriensis* and *S. rigida*, respectively). In the upland are western ragweed (*Ambrosia psilostachya*), Louisiana sagewort (*Artemisia ludoviciana*), aromatic aster (*Aster oblongifolius*), blacksamson echinacea (*Echinacea angustifolia*), inland ironweed (*Vernonia baldwinii*), and several species of gayfeather (*Liatris*) (Freeman 1998). More shrubs are commonly found on infrequently burned treatments. Common species include leadplant (*Amorpha canescens*), roughleaf dogwood (*Cornus drummondii*), aromatic sumac (*Rhus aromatica*), smooth sumac (*R. glabara*), and Arkansas rose (*Rosa arkansana*) (Freeman 1998). Individual trees or forested areas are generally distributed in permanent drainage basins (Knight *et al.* 1994). The dominant species are bur oak (*Quercus macrocarpa*), hackberry (*Celtis occidentalis*), and chinquapin oak (*Q. muehlenbergii*) (Bark 1987).

### **3.1.4 Experimental Treatments at Konza Prairie Biological Station**

The management treatments at KPBS were designed at the watershed level, based on the tallgrass prairie ecosystem (Knapp and Seastedt 1998). There are 60 total treatments at KPBS, which combine different grazing and fire frequencies (Figure 3.3).

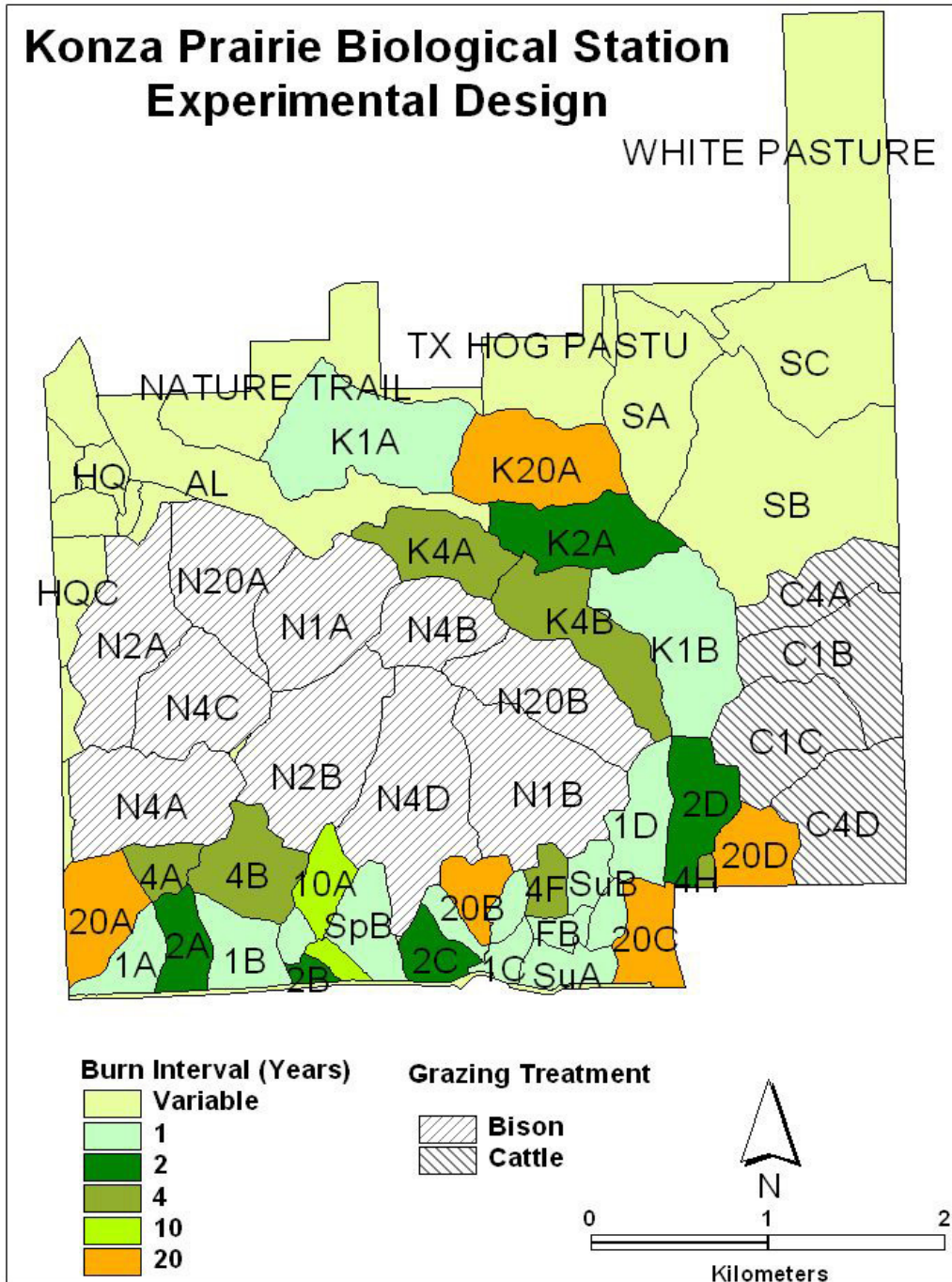
Fire is the most important landscape factor on the tallgrass prairie. It influences energy, water, and nutrient relationships primarily through the removal of detritus and subsequent alteration of the microclimate (Knapp and Seastedt 1986). The Konza Prairie has been managed by burning at 1-, 2-, 4-, 10-, and 20-year intervals. The burning time was originally set in the spring (April 10 ± 20 days depending on weather condition) for two reasons: 1) most lightning ignitions occur in autumn and spring, and 2) most grasslands in the Flint Hills were burned in late spring to increase the production of

domestic livestock (Bragg and Knapp 1995; Owensby and Anderson 1967). A small number of watersheds are burned in summer, fall, or winter.

Herbivory is the second major ecological factor influencing grasslands (McNaughton 1985; Sala *et al.* 1988). Herbivory may reduce some effects of fire (Knapp and Seastedt 1986) and change the relationships among energy, water, and nutrients (Knapp *et al.* 1993). Native ungulates (*Bos bison*) were reintroduced to the Konza Prairie in 1987 to examine effects of grazing by native herbivores. Another reason was to provide comparative studies with domesticated ungulates (cattle) on the tallgrass prairie.

The variable climate is the third major factor influencing grassland ecosystems. The weather fluctuation cycle in the Midwest is about 11-12 years (Weakly 1962). This means there will likely be a strong drought or wet year about every 12 years in this region. The climatic influence at the tallgrass prairie should be reflected at the long-term unburned treatments.

Figure 3-3 Experimental design of KPBS with different fire and grazing treatments



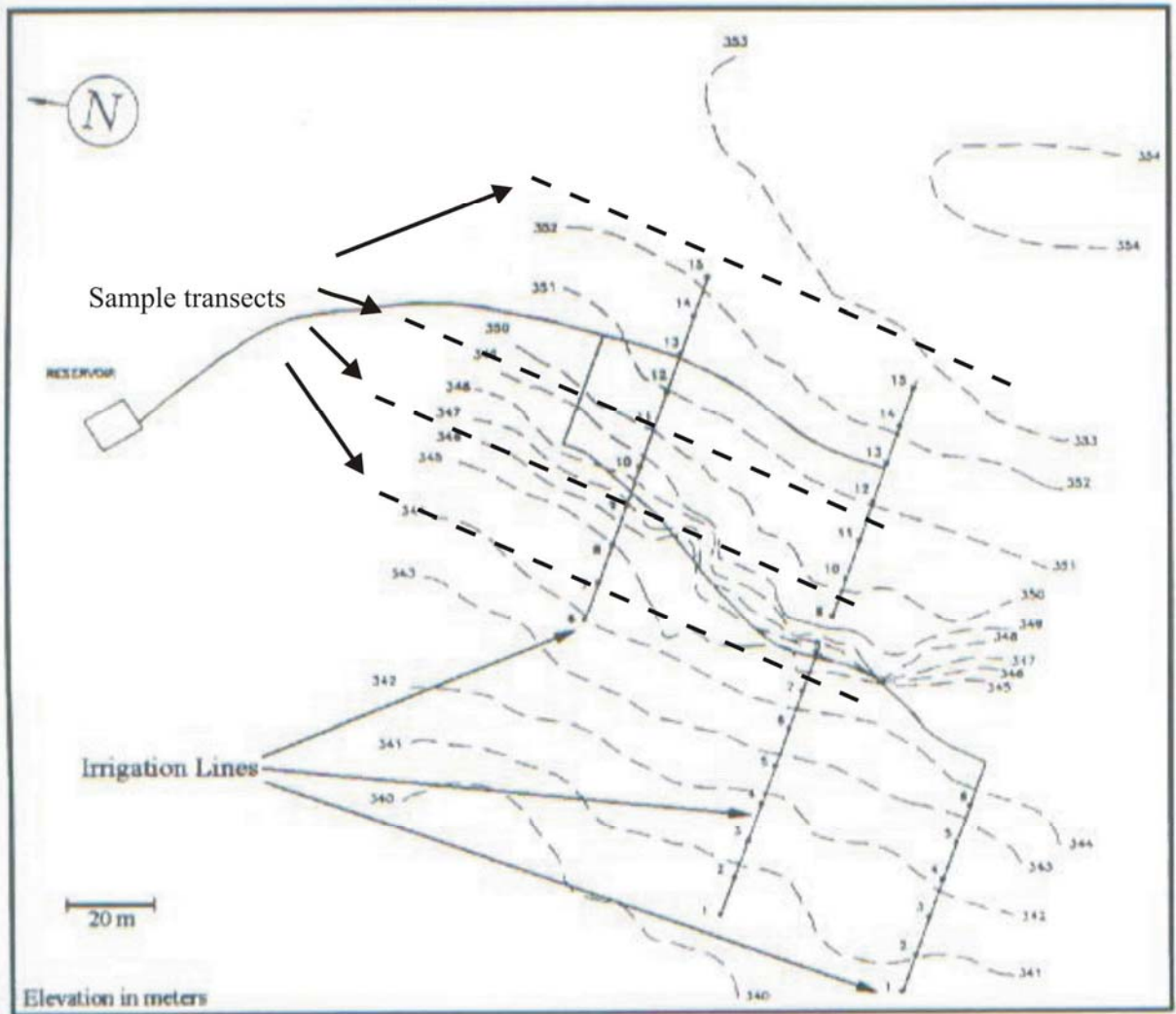
## 3.2 Research Design

### 3.2.1 Research Sites

Three watersheds at KPBS with different burn management regimes were selected for field data collection. They are an annually burned irrigated watershed (HQC), a 2-year burn treatment (002C), and a 20-year burn treatment (020B). As species diversity is strongly affected by fire frequencies (Collins 1992; Hartnett *et al.* 1996, Hartnett and Fay 1998), canopy structure in frequently burned treatments is relatively homogeneous because of dominance of grasses and lack of woody and forb species (Briggs and Knapp 2001, Knapp *et al.* 1998). Because of its relative homogeneity of canopy, HQC was used to collect leaf and canopy data in the growing season of 2004 for developing a chlorophyll model at leaf scale and for rescaling from leaf to canopy scale. The other two watersheds, 002C and 020B, were used to collect *in situ* field data with aircraft images acquired in May and August 2002. The canopy data collected in 002C and 020B was used for validating the rescale from canopy to fine-scale images and from fine-scale to coarse-scale images.

HQC is an irrigated and annually burned watershed close to Konza Headquarters. It was used to collect grass samples for measurement of chlorophyll content in both leaf and canopy scales. Vegetation in HQC is dominated by C4 perennial grasses including big bluestem (*Andropogon gerardii*), little bluestem (*Schizachyrium scoparium*), Indian grass (*Sorghastrum nutans*), and switch grass (*Panicum virgatum*). Only small amounts of woody species such as leadplant (*Amorpha canescens*) are distributed in the uplands.

Figure 3-4 The four transects and two irrigated lines in HQC treatment (Modified from Lewis 1996)



Three irrigation lines are arranged in the treatment in order to enhance the spatial variability of canopy in terms of density, percent cover, and species composition. Four transects were perpendicular to the three irrigation lines (Figure 3.4). Two transects were in the upperland, one was in the slope-land, and one was in lower-land. Twenty plots were selected in each transect with 5 meter intervals. Field data was collected in a month interval, on June 30, July 26, and September 1, 2004, including canopy hyper-spectral reflection, LAI, canopy chlorophyll content, and canopy green coverage. More detail processes of the data collection will discuss in the following section.

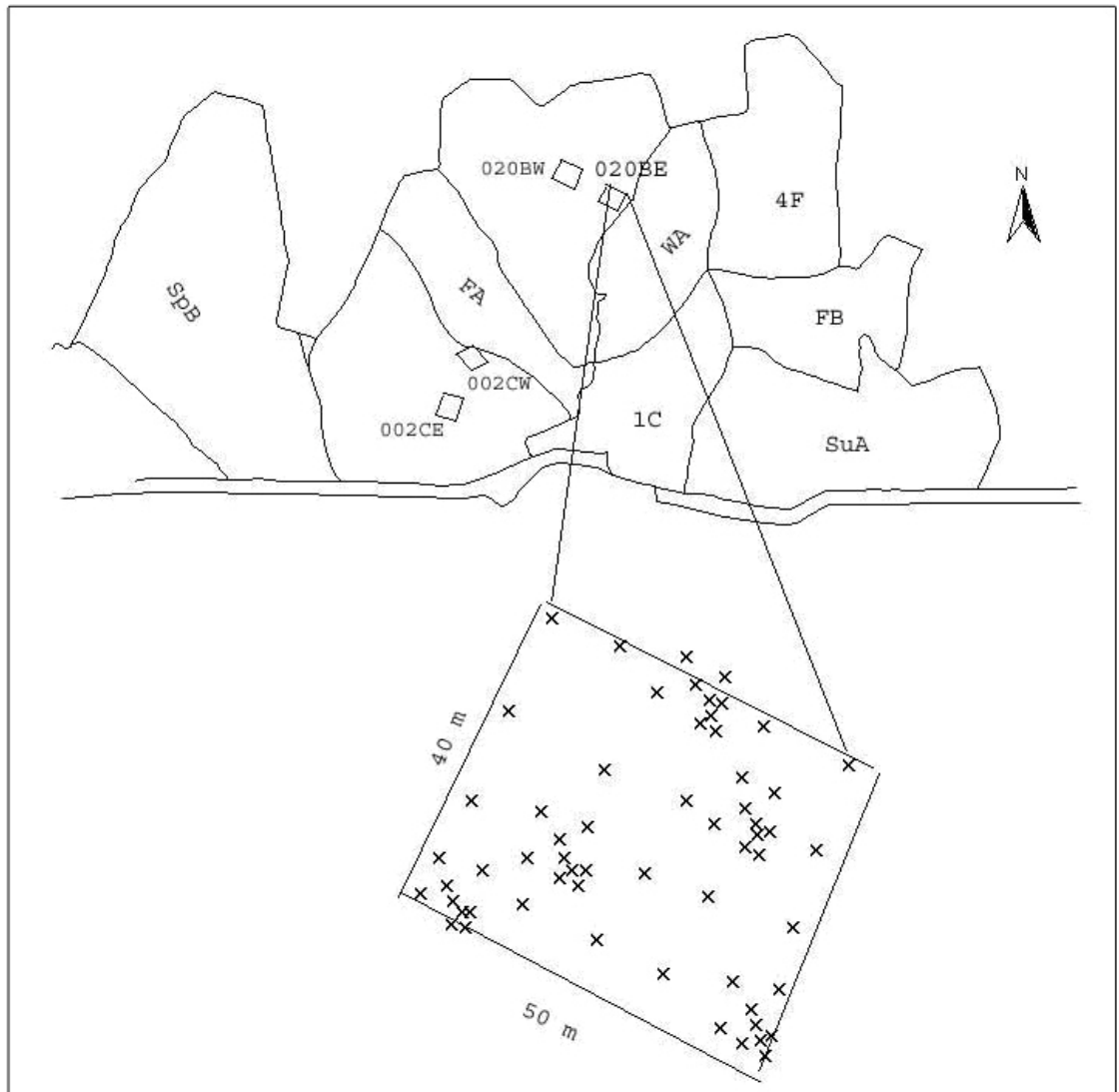
Watershed 002C is burned in two-year intervals, and was most recently burned in the spring of 2001 and 2003. It was in its second unburned year in 2002. Vegetation species was similar to that in HQC, which was dominated by C4 perennial grasses (Collins and Steinauer 1998).

Watershed 020B is an unburned treatment with 20-year burning intervals. The last burn in 020B was in the spring of 1991. It was the 12th year in 2002 after its last burn. Woody islands are the dominant vegetation that spread out through the watershed. The dominant woody species include roughleaf dogwood (*Cornus drummondii*), aromatic sumac (*Rhus aromatica*), smooth sumac (*R. glabara*), and Arkansas rose (*Rosa arkansana*).

Two grids were established in each watershed of 002C and 020B on an east-facing slope and a west-facing slope. Each grid was about 40 meters x 50 meters and 60 samples were selected in each grid within a nested structure (Figure 3.5). Field data was *in situ* collected on May 29 and August 22, 2002 that corresponded with aircraft images acquired on May 30 and August 29, 2002. Field data collected in 2002 included canopy

multi-spectral reflectance, LAI, canopy chlorophyll content, canopy water content, and soil water content. The processing of data collection will be described in detail in the following section.

**Figure 3-5 Location of field nested plots in 002C and 002B treatments**



### **3.2.2 Field Data Collection**

Field data collected in 2004 were on experimental plots located in annually burned watershed HQC, including leaf spectral reflectance, leaf chlorophyll content, and canopy biophysical variables. Canopy biophysical variables collected in 2002 were located on experimental plots in 002C, and 020B. The datasets collected in the field were summarized in Table 3.1.

#### **3.2.2.1 Leaf Hyperspectral Reflectance**

Leaf hyperspectral reflectance was measured with a leaf probe mounted on a field-portable spectroradiometer (Analytical Spectral Devices, Boulder, CO). The spot size of plant probe is about 1.00 cm in diameter. To measure leaf spectral reflectance, a leaf was cut into several sections and spread out on a calibration panel in order to completely cover the plant probe (Figure 3.6). The ASD was warming up over 20 minutes and calibrated with the calibration panel before measurement in order to minimize the influence of background. All samples collected in July and September were conducted in this process. The leaf spectral reflectance was directly measured for samples collected in June by using a leaf without cutting into pieces. The leaf measuring area was dependent on the leaf width for the directly measurement.

#### **3.2.2.2 Leaf Chlorophyll Measurement**

The same leaf used for the ASD measurement was also used to measure the leaf chlorophyll content. Leaf chlorophyll content was measured with two conventional approaches. One is an optical measurement with a SPAD-502 meter, a nondestructive and fast method. The other is a destructive measurement with dimethyl sulfoxide (DMSO)

extraction that is to measure the absolute chlorophyll content of a leaf. As chlorophyll content varies in different part of a leaf, the middle part of a leaf was used for chlorophyll measurement.

Chlorophyll content can be directly read from the SPAD-meter with a clip of leaf (Figure 3.7). The SPAD chlorophyll meter with a measuring area of 2 x 3 mm has a measurement accuracy of  $\pm 1.0$  SPAD unit. Principle of measurement for the chlorophyll meter is based on the transmission of red and near infrared wavelengths (see Chapter 2).

A small piece in the middle leaf was used for chemical extraction. A fresh leaf segment with about 0.005 to 0.01 gram was placed in a tube containing 10 ml DMSO solvent. Chlorophyll would be completely extracted with the solvent after 72 hours dark storage. After chlorophyll was completely extracted, 3-ml chlorophyll solvent with a complete stirred was transferred to a transparent cuvette and the absorption values at 645 nm and 663 nm were read in a spectrophotometer (Spectronic GeneSys 2 manufactured by Thermo Electron Corporation) with 1 nm resolution. Chlorophyll *a* and *b* were calculated with the empirical equation used by Arnon (1949). The absolute chlorophyll content per gram fresh leaf was calculated with the following formula. The total chlorophyll content is the sum of chlorophyll *a* and *b*.

$$\text{Ch}_a = (12.21 * L_{663} - 2.81 * L_{645}) / W_{\text{fresh}} \quad (3.1)$$

$$\text{Ch}_b = (20.13 * L_{645} - 5.03 * L_{663}) / W_{\text{fresh}} \quad (3.2)$$

As the empirical chlorophyll equations were derived from chlorophyll extraction with acetone solvent, Wellburn (1994) modified the two equations and used 665 nm and

649 nm wavelengths for DMSO solvent extraction. After comparing with Arnon's equations, I found the total chlorophyll content was almost the same from Arnon's and Wellburn's equations ( $R^2 = 0.999$ ), but Arnon's equations slightly underestimates chlorophyll *a* and overestimates chlorophyll *b* than Wellburn's equations. However, they are highly correlated ( $R^2 > 0.95$ ) for both chlorophyll *a* and *b* measurement.

### **3.2.2.3 Canopy Hyperspectral Reflectance**

Hyperspectral reflectance was collected in HQC with an ASD in 2004. Data collection was conducted at nadir on sunny days between 10:00 am and 2:00 pm local daylight time in order to minimize the effect of reflectance from ground surface. The ASD spectrometer has 2150 wavelengths ranged from 350 to 2500 nm with 1 nm spectral bandwidth. The fiber-optic head was suspended 1.2-meter above ground and oriented nadir (Figure 3.8). A field view of 18 degrees was a circle of approximately 60 cm diameter with about 0.283 m<sup>2</sup> ground area. The ASD was calibrated with a Spectralon white reflectance panel that was approximately 100% reflective for radiation before conducting measurement.

### **3.2.2.4 Canopy Multiple-spectral Reflectance**

Multiple-spectral reflectance was collected at 002C and 020B treatments using a Cropscan MSR-5 field-portable spectroradiometer, manufactured by Cropscan Inc, Rochester, MN. The conical field view of sensor is 28 degree. The distance from the sensor head to the ground surface was 1.4 m and yielded a circular field of about 0.4 square meters at nadir (Goodin and Gao 2004). Spectral sensitivity of the MSR-5 simulates the five corresponding bands of Thematic Mapper (TM) at 485, 560, 660, 830, and 1650 nm. The MSR-5 was calibrated using a two-point method before conducting the

field data collection (MSR 1995). Reflectance data at the two watersheds have been consistently collected every two weeks in the growing season for more than five years. All field radiation was collected on sunny days. Only two datasets collected on May 29 and August 22, 2002 were used in this research, which were used along with imagery collected on May 30 and August 29, 2002, for rescaling from canopy to image (see Chapter 5).

### **3.2.2.5 Canopy Greenness Cover**

Canopy green coverage was calculated from reflectance photos acquired with a First Growth reflection camera (Decagon Devices, Inc), which measures the percentage of green plant material covering the ground surface (Figure 3.9 and Figure 3.10). Reflectance photos were taken following ASD in the same measurement conditions, about 1.2 m above ground. The reflectance camera was calibrated with a white paper before measurement.

### **3.2.2.6 Canopy Leaf Area Index**

A Sunscan Optical Ceptometer (Delta-T Devices Ltd) was used to measure the fraction of photosynthetically active radiation (fPAR) and leaf area index (LAI). fPAR is calculated with the ratio of transmitted electromagnetic radiation (below canopy) and incident electromagnetic radiation (above canopy). LAI is defined as one-sided leaf area per unit of ground area, which can be an integration of the leaf area density function over the vertical extent of canopy (Liang 2004). The LAI value from Sunscan ceptometer is derived from fPAR with a logarithm transformation using the following formula:

$$LAI = -\ln(Q_{\text{under}}/Q_{\text{above}})/K \quad (3.3)$$

where K is a coefficient that is related to solar zenith angle (Campbell 1986).

**Table 3-1 Summary of field data collection with date, location, and instruments**

Field Datasets	Date	Location	Instruments
Leaf hyperspectral reflectance	06/30/2004	HQC	ASD Probe
	07/26/2004		
	09/01/2004		
Canopy hyperspectral reflectance	06/30/2004	HQC	ASD
	07/26/2004		
	09/01/2004		
Canopy multispectral reflectance	05/29/2002	002C	MSR5
	08/29/2002	020B	
Leaf and canopy chlorophyll content	06/30/2004	HQC	SPAD-502 Meter
	07/26/2004		
	09/01/2004		
Canopy chlorophyll content	05/29/2002	002C	SPAD-502 meter
	08/29/2002	020B	
Canopy green cover	06/30/2004	HQC	Firstgrowth Reflectance Camera
	07/26/2004		
	09/01/2004		
Canopy LAI and fPAR	06/30/2004	HQC	Sunscan Optic Ceptometer
	07/26/2004		
	09/01/2004		
Hyperspectral aircraft Imagery	05/29/2002	002C	AISA imaging spectroradiometer
	08/30/2002	020B	

**Figure 3-6 Measurement of leaf hyperspectral reflectance with ASD fiber optic probe**



**Figure 3-7 Leaf chlorophyll measurement with SPAD-502 chlorophyll meter**



**Figure 3-8 Measurement of canopy hyper-spectral reflectance with the ASD spectroradiometer by using a fiber-optic head above ground at about 1.2 meter**



### **3.2.2.7 Canopy Chlorophyll Content**

Canopy chlorophyll content was estimated with the SPAD-502 chlorophyll meter. Five leaves from the dominant species in each plot were selected as the samples to measure the leaf chlorophyll content. The average of the five sample measurements represents the canopy chlorophyll content of the plot.

### **3.2.3 Aircraft Image Acquisition**

Fine-scale hyperspectral aircraft images were acquired from low-height flight at KPBS on sunny days in 2002. To monitor the seasonal canopy change, two flights were arranged in early and later summer, respectively. One was on May 30, 2002, and the other was on August 29, 2002. Flight routes were designed from northeast to southwest direction to cover 002C and 020B burned treatments (Figure 3.5). Digital images were collected from the AISA imaging spectroradiometer boarded on a Piper Warrior aircraft operated by the Institute of Aviation and the Center for Advanced Land Management Information Technologies (CALMIT) at the University of Nebraska. Aircraft flights were conducted at three altitudes, yielding hyperspectral data with 1-m, 2-m, and 3-m spatial resolution. The spectrum of hyperspectral image ranged from visible bands to near infrared bands and varied with spatial resolution. The image of 1-m resolution acquired in May has 25 bands ranging from 497 nm to 885 nm with average bandwidths of 16 nm (Table 3.2). The image of 1-m resolution collected in August has 17 bands ranging from 480 to 884 nm with an average bandwidth of 25 nm. The images of 2-m and 3-m resolutions have 35 bands ranged from 479 to 887 nm with average bandwidth about 11.6 nm. All aircraft images were rectified with atmospheric correction and georeferenced into UTM projection with WGS-84 in zone 14.

**Figure 3-9 True RGB color reflection image taken with a reflection camera on September 1 2004**



**Figure 3-10 Black-white reflection image with 79% greenness cover taken on September 1, 2004**



**Table 3-2 The band wavelengths (nm) of AISA imagery acquired on May 30 and August 29, 2002, with 1-m, 2-m, and 3-m resolution**

Bands	May 30, 2002			August 29, 2002		
	1-m	2-m	3-m	1-m	2-m	3-m
1	497.33	479.47	479.47	480.24	479.47	479.47
2	508.2	496.55	496.55	497.33	496.55	496.55
3	515.96	507.42	507.42	525.28	507.42	507.42
4	525.28	516.74	516.74	554.79	516.74	516.74
5	537.7	524.5	524.5	576.4	524.5	524.5
6	547.02	538.48	538.48	595.22	538.48	538.48
7	554.79	546.25	546.25	636.25	546.25	546.25
8	566.14	555.56	555.56	656.77	555.56	555.56
9	576.4	567	567	672.16	567	567
10	584.96	577.26	577.26	694.39	577.26	577.26
11	595.22	584.1	584.1	713.02	584.1	584.1
12	636.25	596.07	596.07	748.93	596.07	596.07
13	656.77	604.62	604.62	771.16	604.62	604.62
14	672.16	611.46	611.46	783.13	611.46	611.46
15	682.43	625.14	625.14	846.4	625.14	625.14
16	694.39	637.11	637.11	866.92	637.11	637.11
17	701.24	643.95	643.95	884.02	643.95	643.95
18	713.02	655.92	655.92		655.92	655.92
19	742.09	662.76	662.76		662.76	662.76
20	748.93	674.73	674.73		674.73	674.73
21	771.16	681.57	681.57		681.57	681.57
22	783.13	693.54	693.54		693.54	693.54
23	846.4	700.38	700.38		700.38	700.38
24	866.92	712.16	712.16		712.16	712.16
25	884.02	741.23	741.23		741.23	741.23
26		749.78	749.78		749.78	749.78
27		772.01	772.01		772.01	772.01
28		782.27	782.27		782.27	782.27
29		799.37	799.37		799.37	799.37
30		813.05	813.05		813.05	813.05
31		830.15	830.15		830.15	830.15
32		845.54	845.54		845.54	845.54
33		866.06	866.06		866.06	866.06
34		874.61	874.61		874.61	874.61

### 3.3 Derivative of Reflectance Spectrum

#### 3.3.1 Functions of Derivative Spectra

Chlorophyll has a strong absorption at blue and red regions and a strong reflectance at green regions. A living green leaf has a typical spectral reflectance as described in Figure 2.3. The spectral reflectance from visible to near infrared regions could be represented by a third-order polynomial as equation 3.4:

$$y_1 = a_1 + b_1x + c_1x^2 + d_1x^3 \quad (3.4)$$

The spectral curve varies at the visible and near infrared regions with the difference of chlorophyll content. However, canopy spectral reflectance is also affected by soils and dead plant materials. The surface spectral reflectance of a bare soil increases with the enhancement of wavelengths at visible and near-infrared regions (Figure 3.10a). The soil spectral reflectance could be simulated as a straight line and expressed as equation 3.5

$$y_2 = a_2 + b_2x \quad (3.5)$$

The combination of equation 3.4 and 3.5 could represent a canopy with soil backgrounds and represented with equation (3.6) with parameters  $F_1$  and  $F_2$ .

$$Y = F_1y_1 + F_2y_2 \quad (3.6)$$

$$\text{then, } Y = F_1(a_1 + b_1x + c_1x^2 + d_1x^3) + F_2(a_2 + b_2x) \quad (3.7)$$

The first-order and second-order differentiating of equation 3.7 gives respectively as:

$$Y' = F_1(b_1 + 2c_1x + 3d_1x^2) + F_2b_2 \quad (3.8)$$

$$Y'' = 2F_1c_1 + 6F_1d_1x \quad (3.9)$$

Notice that the first-order derivative equation 3.8 has removed the variable  $x$  in equation 3.5 and the second derivative equation 3.9 has completely removed the parameters in equation 3.5 and is independent of the background noise. Higher order derivatives could remove more complicated noise; for example the fourth-order derivative can remove the interference caused by Rayleigh scattering in the atmosphere (Fell and Smith, 1982), but the signal to noise ratio becomes worse at higher derivative orders (O'Haver 1982)

Another application of differentiation in remote sensing is its effect in the resolution of overlapping spectra. It is found that if several spectral signals are overlapping, then the relative amplitudes of the derivative spectra with narrower bandwidths are greater and increase to a greater degree with increasing derivative order (Bulter and Hopkins 1970). Components can be more clearly separated in derivative spectrum than in the original reflectance spectrum.

### **3.3.2 Development of Derivative Spectra from Hyperspectral Reflectance**

Numerical methods are commonly used for generating derivative spectra (Demetriades-Shah *et al.* 1990). Derivative spectra can be simply obtained with numerical method by dividing the difference between successive spectral values with the wavelength interval. This process generates an approximation of the first-order derivative that represents the slope of zero-order spectrum between the two successive wavelengths.

The peak values of the first-order derivative represent the maximum slopes in the reflectance spectrum (Figure 3.10b). If the differentiation interval is very small, the differences between the successive spectral values may be small in comparison with noise and may generate a noise derivative spectrum. A larger differentiating interval can reduce noise and smooth the signal, but lose the sharp spectral features. The optimum differentiating interval depends on the level of noise in the data and the spectral bandwidth of the signal (Demetriades-Shah *et al.* 1990).

Convolution operations have long been used to smooth and generate derivative spectra (Savitzky and Golay 1964). The derivative spectra of hyperspectral reflectance in this research were derived by using a convolution operator with a five-point numerical differentiation technique (Burden and Fares 1985). The first-order derivative equations were given by:

$$f'(x_0) = \frac{1}{12h} [(f(x_0 - 2h) - 8f(x_0 - h) + 8f(x_0 + h) - f(x_0 + 2h))] \quad (3.10)$$

Higher order derivative spectra were recursively generated with equation 3.10. The vegetation spectra in zero-order (the reflectance curve), first-order, and second-order derivative were shown in Figure 3.11. As the higher order derivative spectra have noise generated from the derivative transform, a Gaussian filter was used to smooth the derivative spectra:

$$f(x_0) = 0.006f(x_0 - 3h) + 0.061f(x_0 - 2h) + 0.242f(x_0 - h) + 0.383f(x_0) + 0.242f(x_0 + h) + 0.061f(x_0 + 2h) + 0.006f(x_0 + 3h) \quad (3.11)$$

### 3.3.3 Development of Derivative Image from Hyperspectral Images

The derivative image were not generated with the numerical method but with the general difference of spectral divided by the wavelength interval. The first derivative image between two bands was generated from the spectral difference divided by the two bands interval with equation 3.12. The second derivative image was generated from two first-order derivative images.

$$DN'(\frac{Band2 + Band1}{2}) = \frac{DN_{Band2} - DN_{Band1}}{Band2 - Band1} \quad (3.12)$$

## 3.4 Data Analyses

A flowchart of the analysis in this dissertation shown in Figure 3.8. Leaf spectral reflectance collected with ASD was applied to estimate chlorophyll content. New spectral indices were derived from both spectral reflectance and derivative spectra to estimate leaf and canopy chlorophyll content. The new indices were compared with leaf chlorophyll content measured with convenient approaches. Three chlorophyll models were generated from original spectrum, first and second derivative spectra (Chapter Four).

Leaf chlorophyll content was measured with two traditional approaches: solvent extraction and a SPAD-502 meter. The relationship between chlorophyll contents measured with the two methods was determined with regression analysis. The correlation between chlorophyll content and hyper-spectral reflectance from visible region to far infrared wavelengths was analyzed. One new spectral index was generated for estimating leaf chlorophyll content based on high correlation between chlorophyll content and spectral reflectance. Meanwhile, two indices were derived from first and second

derivative spectra to estimate leaf chlorophyll content. All of the new spectral indices and other six previous vegetation indices from literature were compared with chlorophyll content measured with traditional methods in Chapter Four.

Chapter Five examines the experiment of the leaf Chl models extended into canopy scale to measure chlorophyll content. The spectral index and two derivative indices developed in Chapter Four were compared with field chlorophyll content measured with a SPAD-502 meter. The correlations between spectral indices and other canopy biophysical attributes including LAI, green cover were also analyzed to detect the effect of canopy structure on chlorophyll measurement. Canopy chlorophyll contents derived from the chlorophyll model generated in Chapter Four were validated with the field chlorophyll measurement.

Chapter Six is about the extension of the chlorophyll models generated in Chapter Four to hyperspectral aircraft images. Spectral index images were derived from hyperspectral images with the corresponding spectral wavelengths. The index images were also compared with field chlorophyll and LAI. Image chlorophyll converted from index image with the chlorophyll model developed in Chapter Four was validated with the field chlorophyll measurement.

Figure 3-11 Vegetation reflectance spectra in zero-order (a), first-order (b), and second-order (c) derivative in the visible and near-infrared ranges

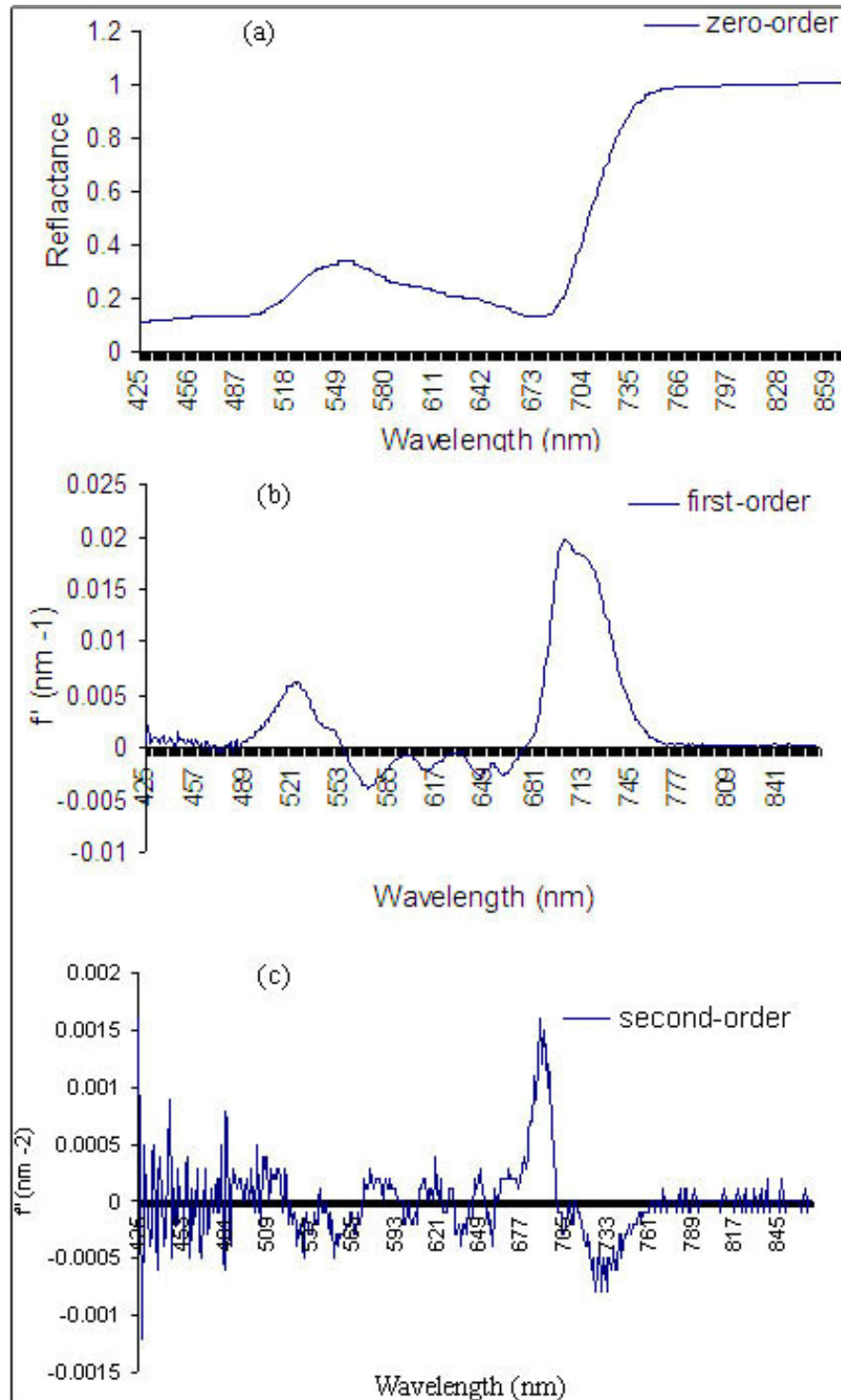
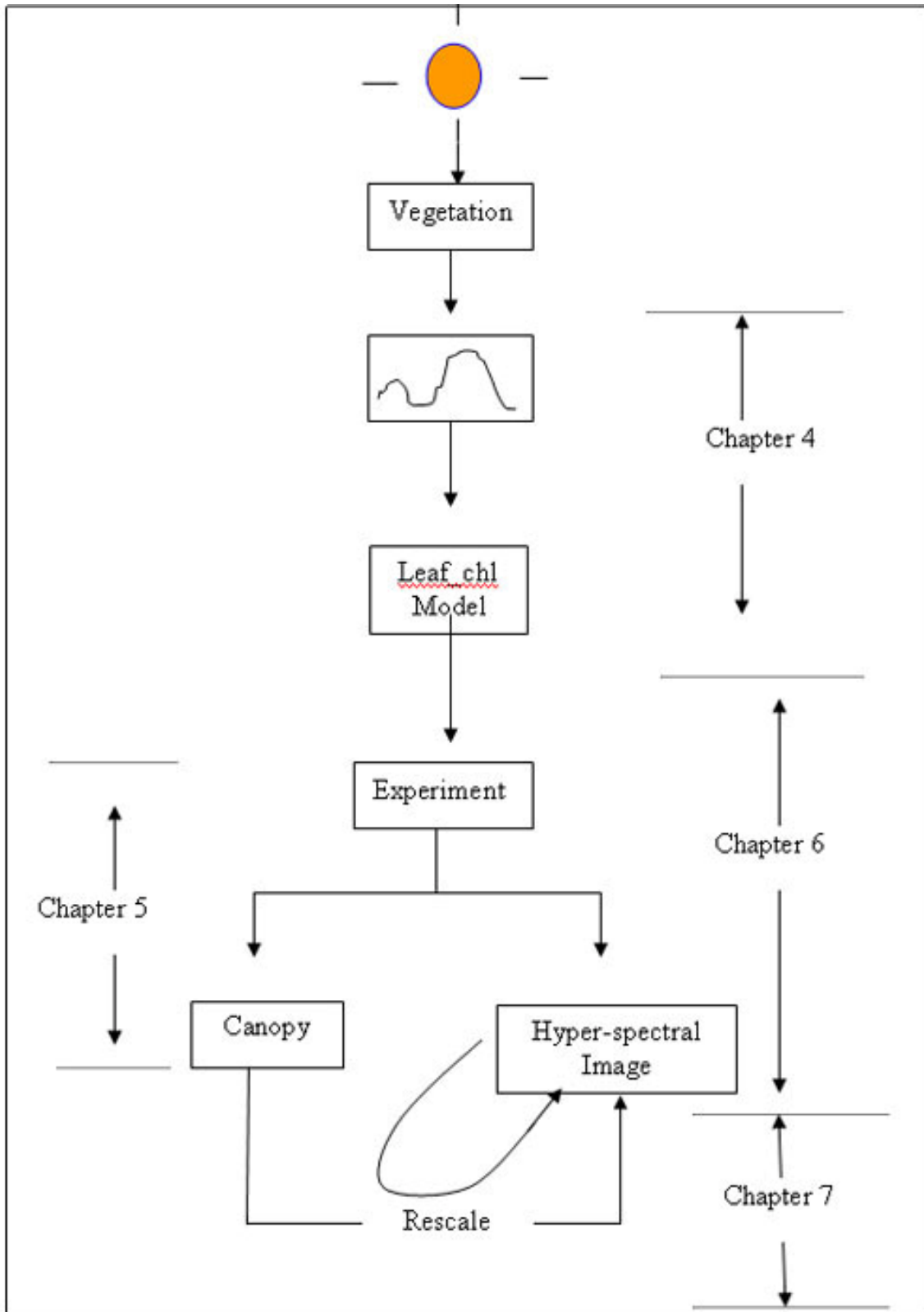


Figure 3-12 Data analysis flowchart and research framework



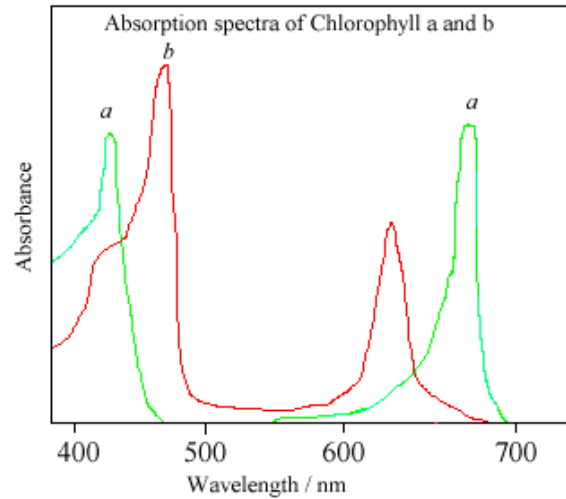
# CHAPTER 4 - LEAF REFLECTANCE MODEL TO ESTIMATE CHLOROPHYLL CONTENT USING HYPER-RESOLUTION SPECTROSCOPY

## 4.1 Introduction

Leaf pigments are strongly related to spectral reflectance. Chlorophyll strongly reflects green wavelength (around 550 nm), which is why plants appear green to the eyes, and strongly absorbs blue (400- 480 nm) and red (around 670 nm). Leaf cell structure is directly related to near infrared with high reflectance. Water content has a strong influence in far infrared region. Water molecules have a strong absorption at 1640 nm and 2130 nm (Chen *et al.* 2005).

There are two types of chlorophyll, designated *a* and *b*. Both of the two chlorophyll types have very strong absorption in blue and red wavelengths, but with slight differences (Figure 4.1). Chlorophyll *a* has strong absorption peaks at wavelengths around 410 nm and 663 nm, whereas chlorophyll *b* has strong absorption peaks at around 450 nm and 630 nm. The complement of the two type chlorophylls in absorbing sunlight can effectively obtain solar energy from blue and red regions (Ahmad *et al.* 1999).

**Figure 4-1 Absorption spectra of chlorophyll *a* and *b* (Ahmad *et al.* 1999)**



## 4.2 Spectral Indices

As chlorophyll *a+b* are strongly related to the visible spectrum and leaf cell structure is related to near infrared, most chlorophyll content indices are derived from spectral reflectance of narrow green, red, and near infrared wavelengths. The following six spectral indices have been proposed in the literature for estimating leaf chlorophyll content.

The Chlorophyll Absorption in Reflectance Index (CARI) was developed by Kim *et al.* (1994) from crop plants to minimize the effects of nonphotosynthetic materials on spectral estimates of absorbed photosynthetically active radiation.

$$CARI = \frac{R_{700}}{R_{670}} CAR = \frac{R_{700}}{R_{670}} \frac{670a + R_{670} + b}{\sqrt{a^2 + 1}} \quad (4.1)$$

$$\text{where } a = \frac{R_{700} - R_{550}}{150} \text{ and } b = R_{550} - 550a$$

CAR represents the distance from the baseline spanned by the green reflectance peak at 550 nm and the reflectance at 700 nm.

The Triangle Vegetation Index (TVI) was introduced by Broge and Leblance (2000) by comparing broadband and hyperspectral vegetation indices for estimating green leaf area index and canopy chlorophyll density. The TVI is the triangular area defined by green peak, red trough, and NIR shoulder in spectral space. It is calculated with the following formula:

$$TVI = \frac{120 * (R_{NIR} - R_{Green}) - 200 * (R_{Red} - R_{Green})}{2} \quad (4.2)$$

where Green = 550 nm, Red = 670 nm, and NIR = 750 nm

The Carotenoid Reflectance Index (CRI) was devised based on chlorophyll reflectance at green and near infrared wavelengths (Gitelson *et al.* 1996). Chlorophyll concentration was found to be linearly correlated with  $(R_{550})^{-1}$  and  $(R_{700})^{-1}$  (Gitelson *et al.* 2002), as well as  $(R_{715})^{-1}$  (Daughtry *et al.* 2000). The CRI is calculated with the inverse of reflectance in the green and near infrared wavelengths:

$$CRI = \frac{1}{R_{Green}} + \frac{1}{R_{NIR}} \quad (4.3)$$

where green band is 550 nm, and NIR band is 715 nm

The combination of Transformed Chlorophyll Absorption in Reflectance Index (TCARI) (Daughtry *et al.* 2000) and Optimized Soil-Adjusted Vegetation Index (OSAVI) (Rondeaux *et al.* 1996) has been used to estimate leaf chlorophyll concentration. The Ratio of TCARI and OSAVI was found more sensitive to chlorophyll content variations and was calculated with the following formula by (Haboudane *et al.* 2002):

$$TCARI = 3 * \{(R_{700} - R_{670}) - 0.2 * (R_{700} - R_{550}) * \frac{R_{700}}{R_{670}}\}$$

$$OSAVI = \frac{(1 + 0.16)(R_{800} - R_{670})}{R_{800} + R_{670} + 0.16}$$

$$Ratio = \frac{TCARI}{OSAVI} \quad (4.4)$$

The Normalized Difference Vegetation Index (NDVI) is the most popular vegetation index used in remote sensing. NDVI tends to enhance the contrast between soil and vegetation while minimizing the effects of illumination conditions (Baret and Guyot, 1991). NDVI is calculated from red and near infrared reflectance as:

$$NDVI = \frac{NIR_{800} - Red_{670}}{NIR_{800} + Red_{670}} \quad (4.5)$$

The Red Edge Position (REP) index was first introduced by Danson and Plummer (1995). The reflectance of an actively photosynthesizing vegetation canopy significantly increases at the boundary of red and near-infrared spectrum. The shift of REP is related to green vegetation density. This region is called the “red edge.” The REP index measured with several red-edge bands is positively related to leaf chlorophyll content. The REP index is calculated as (Guyot *et al.* 1992):

$$REP = 700 + \frac{R_i - R_{700}}{R_{740} - R_{700}} (740 - 700) \quad (4.6)$$

$$\text{where } R_i = 0.5 * R_{780} + 1.5 * R_{673}$$

## **4.3 Development of New Chlorophyll Index from Reflectance Spectrum**

### **4.3.1 Spectral Reflectance and Chlorophyll Content**

Using data from the June, July, and September 2004 field collection campaigns, a correlation spectrum was generated by correlating chlorophyll content measured with an optical chlorophyll meter with leaf reflectance spectrum. The correlation spectrum highlighted the relation between leaf chlorophyll content and spectral reflectance (Figure 4.2). High correlations between chlorophyll content and spectral reflectance are found at two regions. One was around 550 nm called the green edge between red and green wavelengths. The correlation was 0.65 at 550 nm in September and 0.6 at 610 nm in July. The other was around 700 nm called the red edge between red and near infrared wavelengths. The correlation was over 0.7 in July and September. However, the high correlations vary with the growing seasonal change and shift in opposite directions. One is shifted toward the shorter wavelength to the green edge and the other to the longer wavelength to the red edge. In July, the highest correlation ( $r > 0.7$ ) occurred around 710 nm and the second highest correlation ( $r > 0.5$ ) occurred around 620 nm. In September, the highest correlation occurred around 720 nm and the second highest correlation occurred around 570 nm.

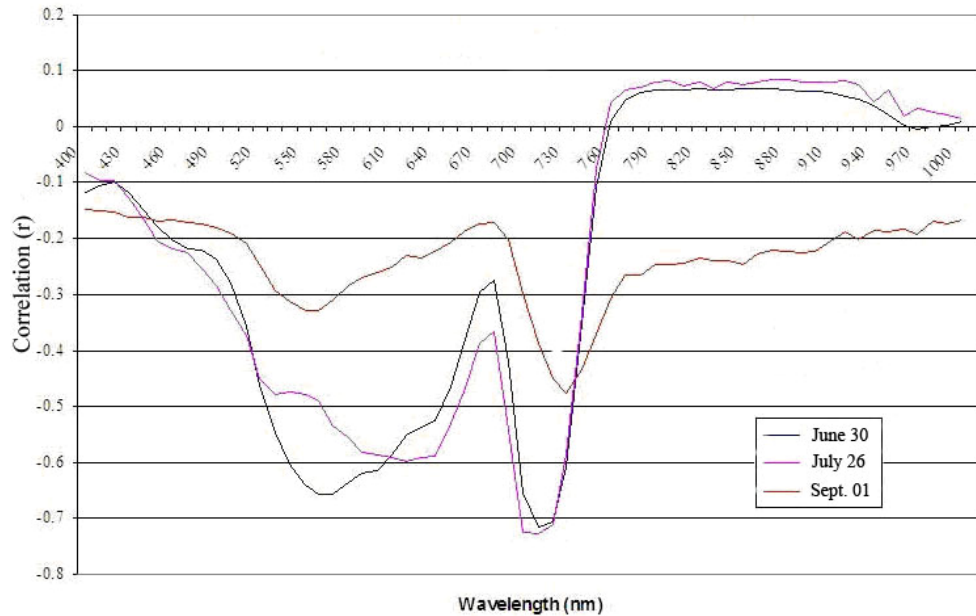
As the leaf area did not cover the whole white reference panel during the spectral measurement in June, the nongreen background resulted in the decreased reflectance at green region and the increased reflectance at near infrared regions. The correlation

between chlorophyll content and spectral reflectance was weak. The highest correlation occurred around 740 nm and 580 nm and shifted toward the green and red edges.

Chlorophyll content had a weak correlation with near infrared (NIR). The correlation between chlorophyll content and NIR at 740 –1000 nm was less than 0.1 from the sample data. The reflectance in near infrared region (over 740 nm) is not affected by chlorophyll content, but affected by leaf structure (Liang 2004).

Several spectral indices were developed with the green and red edge wavelengths and found the ratios of  $R_{750}/R_{700}$  and  $R_{750}/R_{550}$  were highly related to leaf chlorophyll content (Gitelson *et al.* 1996, Lichtenthaler *et al.* 1996). As the shift of spectral reflectance against chlorophyll content with the maturity of plant, the chlorophyll metrics should also be adjusted in different growing seasons. Thus, one new spectral index was developed from the leaf spectral reflectance based on the relationships between spectral reflectance and chlorophyll content.

**Figure 4-2 Correlation spectra between spectral reflectance and chlorophyll content on June 30, July 26, and September 1, 2004**



### **4.3.2 Triangle Chlorophyll Index (TCI)**

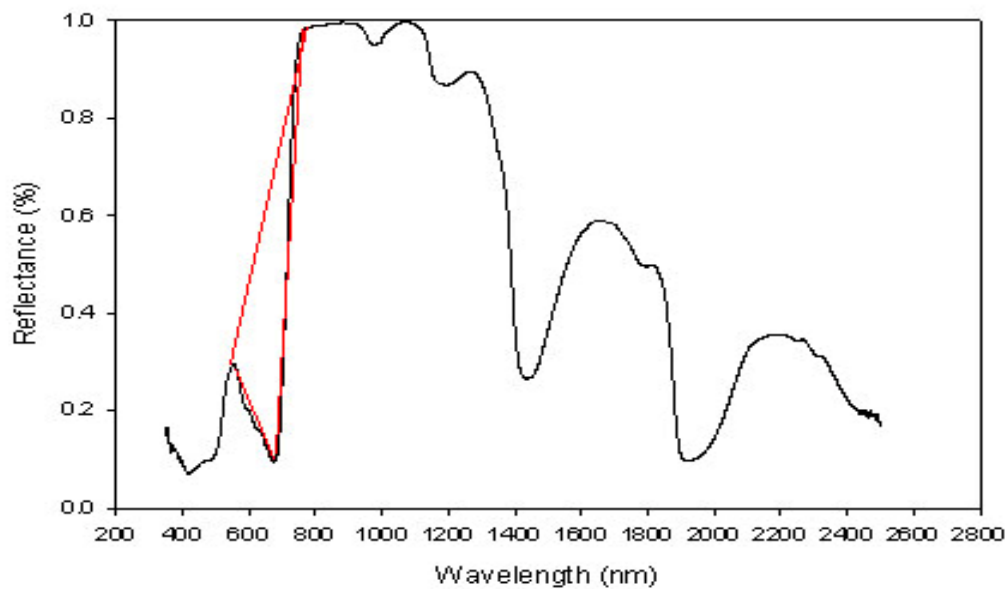
The TCI model is a new developed index in this research based on the correlation of chlorophyll content and spectral reflectance. It uses the integrated influence of green, red, and NIR on chlorophyll, the high reflectance in green and near infrared regions, and the high absorption in red regions. The peak reflectance at green (550 nm) and near infrared (800 nm), and the trough reflectance at 675 nm generate a triangle in the spectral reflectance. The triangle shape is determined by chlorophyll content (Figure 4.3). The bottom angle will reduce with increased concentrations of chlorophyll since the red edge wavelength (700nm) is sensitive to chlorophyll content. The TCI model with the four wavelengths reflects the sensitivity of chlorophyll in red edge region and enhances the

contrast between the reflectance in green region and the absorption in red region with increases in chlorophyll content.

$$TCI = \frac{R_i - R_{675}}{R_{800} - R_{700}} \quad (4.7)$$

where  $R_i = R_{800} + 1.5 * R_{550}$

**Figure 4-3 The triangle (red color) at the peak of green, trough of red, and shoulder of NIR regions from the reflectance spectrum of a fresh green leaf**



#### 4.4 Development of Derivative Spectral Indices

There are two noticeable peaks around 523 nm and 717 nm, and one trough at 571 nm in the first-order derivative spectra (Figure 3.10b). The two peaks represent the maximum slopes or maximum increasing gradient in the original spectral reflectance. The trough represents minimum slope or the maximum decreasing gradient in the spectral reflectance. The two peaks and one trough also represent three critical points that are

located at the edges of green and red regions. Spectral reflectance in those regions is actually sensitive to leaf chlorophyll content.

To identify the three critical points, the frequencies of wavelengths associated with the peaks and trough were generated from the first-order derivative spectra of the 80 leaf samples in each of the three growing seasons. The highest occurrence probabilities of the two peaks were located at wavelength 523 nm and 717 nm, and the highest probability of the trough was located at wavelength 571 nm (Figure 4.4). The peak occurrence frequencies of the first-order derivative spectra at 523 nm were more than 60 percent of the 80 samples in July and September, and over 40 percent in June. The peak occurrence frequencies at 717 nm were 20%, 21%, and 39% in June, July, and September, respectively. The maximum frequency of the trough occurred at 571 nm, the edge between the green and red regions, and the occurrence frequencies were 39%, 55%, and 64% in June, July, and September, respectively.

There is only one peak and one trough in the second derivative spectra (Figure 3.10c). The peak occurrence in the derivative spectra is located at 689 nm or 692 nm (Figure 4.5a). The occurrence frequencies at 692 nm were around 40 percent of the 80 samples in June, July, and September, and the frequencies at 689 nm were around 25% in the three growing seasons. The trough occurrence varied with the growing season. The trough occurred at 730 nm in June with 45%, and located at 733 nm in July and September with 35% and 45%, respectively (Figure 4.5b).

Three indices are derived from the first-order and second-order derivative spectra for measuring chlorophyll content. One is derived from the first-order derivative spectra (called FDI) with the ratio of the two peak derivatives at wavelength 717 nm and 523 nm.

Two indices are derived from the second derivative spectra (called SDI) with the peak derivative values at 689 nm or 692 nm.

$$FDI = \frac{R'_{717}}{R'_{535}} \quad (4.8)$$

$$SDI_1 = R''_{689} \quad (4.9)$$

$$SDI_2 = R''_{692} \quad (4.10)$$

**Figure 4-4** The peak occurrence (a and b) and the maximum trough (c) of the first derivative with 80 samples at visible and near infrared regions in different growing seasons

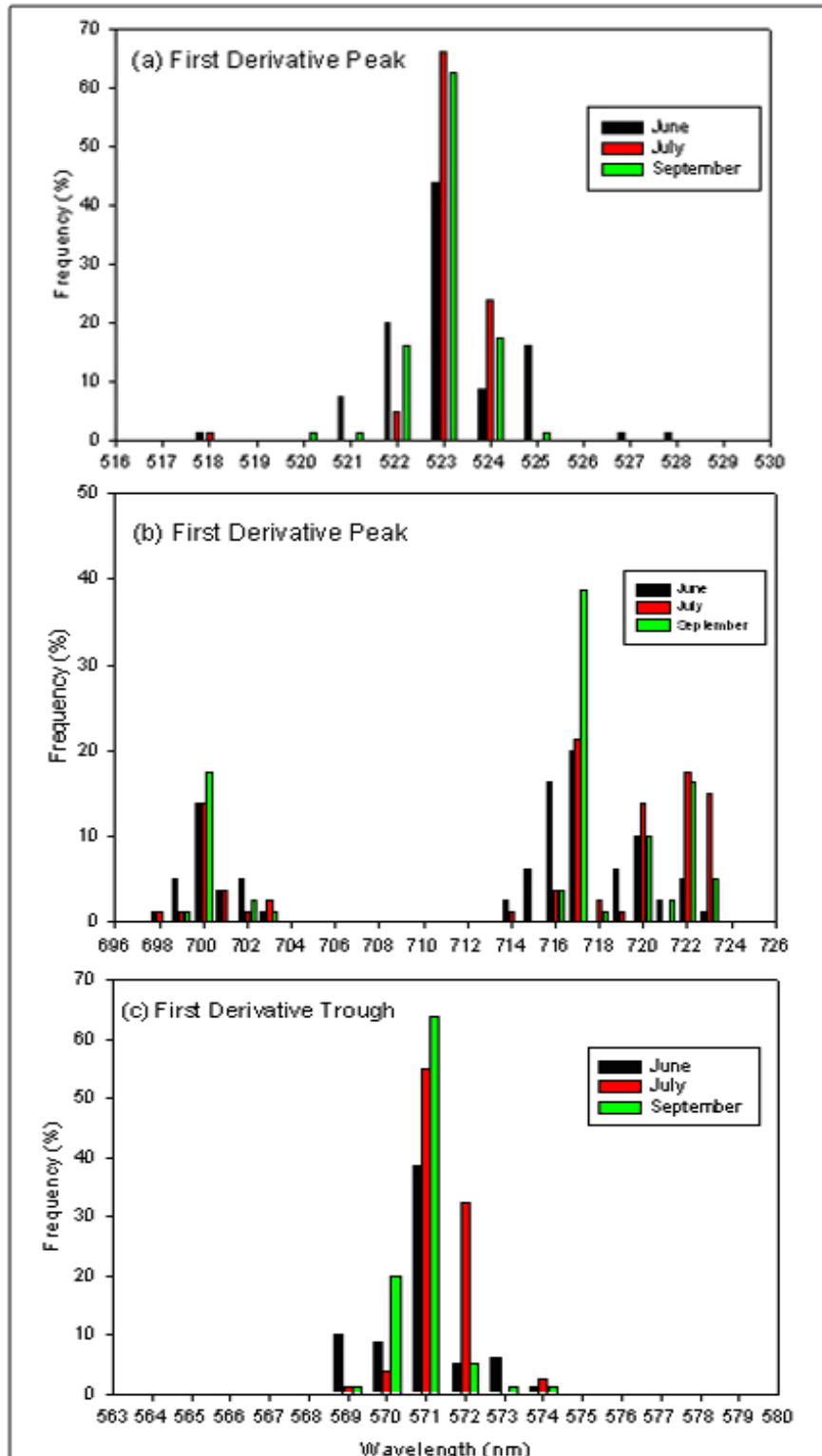
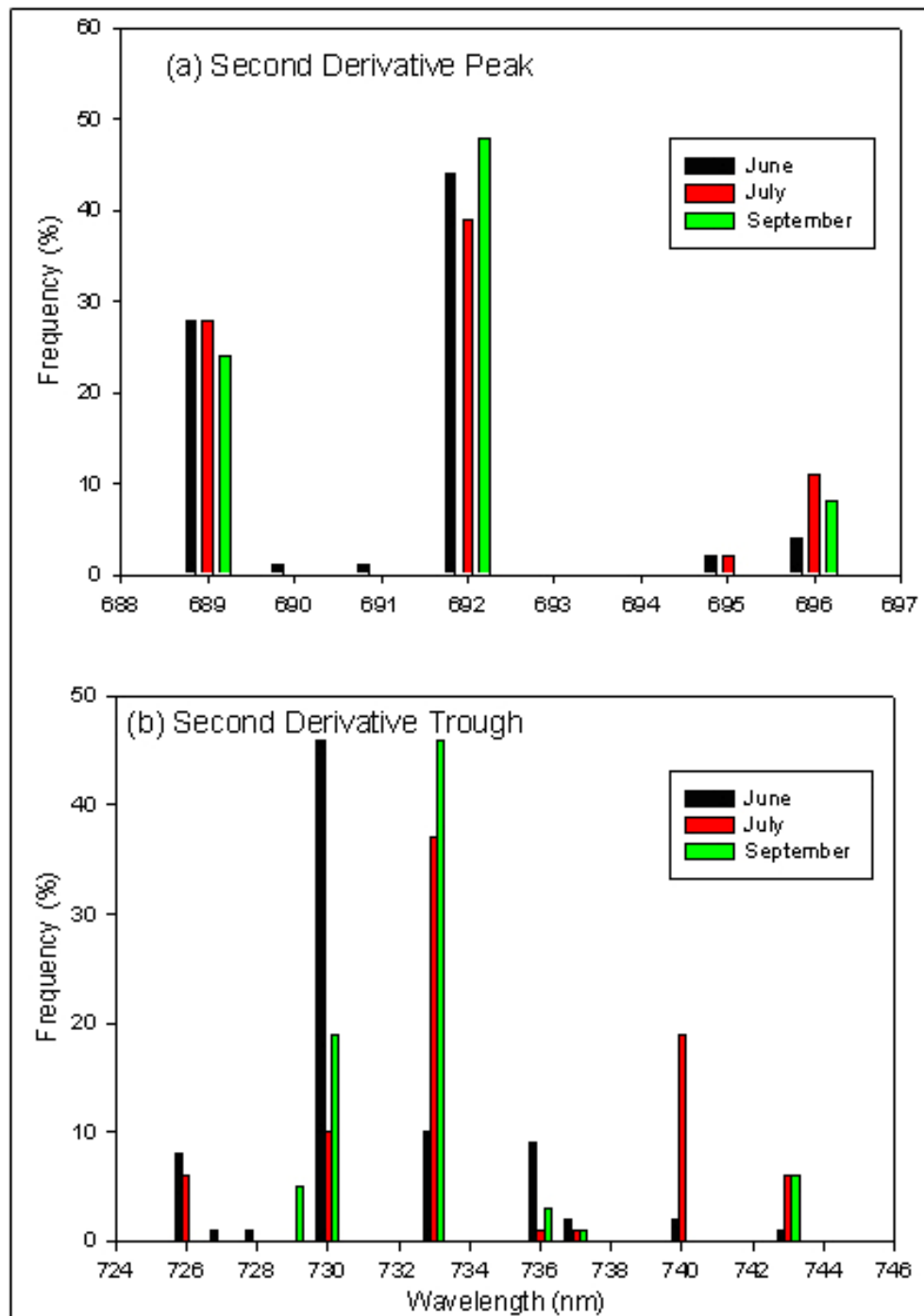


**Figure 4-5 The maximum peak (a) and maximum trough (b) of second derivative with 80 samples at visible and near infrared regions in different growing seasons**



## 4.5 Results and Analysis

### 4.5.1 Chlorophyll Contents of Solvent Extraction and Optical Measurement

The spot plot between the leaf chlorophyll content measured with solvent extraction and the optical measurements with a SPAD-502 meter shows high linear correlation, even though the two approaches used different spectral wavelengths. The correlations ( $r$ ) between the two measurements were 0.81 and 0.82 in July and September, respectively (Figure 4.6 and Figure 4.7). The significant linear relationship between optical measurement and solvent extraction indicates that the two methods could provide the same information of chlorophyll content. The regression of chlorophyll content with SPAD units was simulated with the 240 leaf samples collected from June, July, and September 2004, and shows in Figure 4.8. The R-square (0.66) indicates that the equation can explain 66 percent of the variance of chlorophyll content. The regression is significantly linear with  $F=290$ ,  $df=238$ , and  $P<0.001$ . The regression equation was listed as:

$$Chl = 2.885 * SPAD - 2.295 \quad (4.11)$$

### 4.5.2 Chlorophyll Content with the TCI Model

The correlation of the TCI index and the other six spectral indices with chlorophyll content measured with solvent extraction and a SPAD meter are listed in Table 4.1. The correlations between spectral indices and SPAD units are generally higher than those between spectral indices and chlorophyll content with solvent extraction. The correlation between chlorophyll content of solvent extraction with spectral indices ranged from  $r=0.1$  to  $r=0.75$ , but the correlation between SPAD units and spectral indices ranged from  $r=0.3$

to  $r=0.8$ . This demonstrates that the spectral indices derived from the hyperspectral reflectance are more highly correlated to optical measurement with a SPAD meter than that measured with solvent extraction. This may be because the SPAD meter uses the same spectral regions (red and near infrared) as the spectral indices, but the chlorophyll content with solvent extraction was analyzed with the absorption of green wavelengths.

**Figure 4-6 Correlation between optical measurement with a SPAD meter and solvent chlorophyll content (N=80), July 26, 2004**

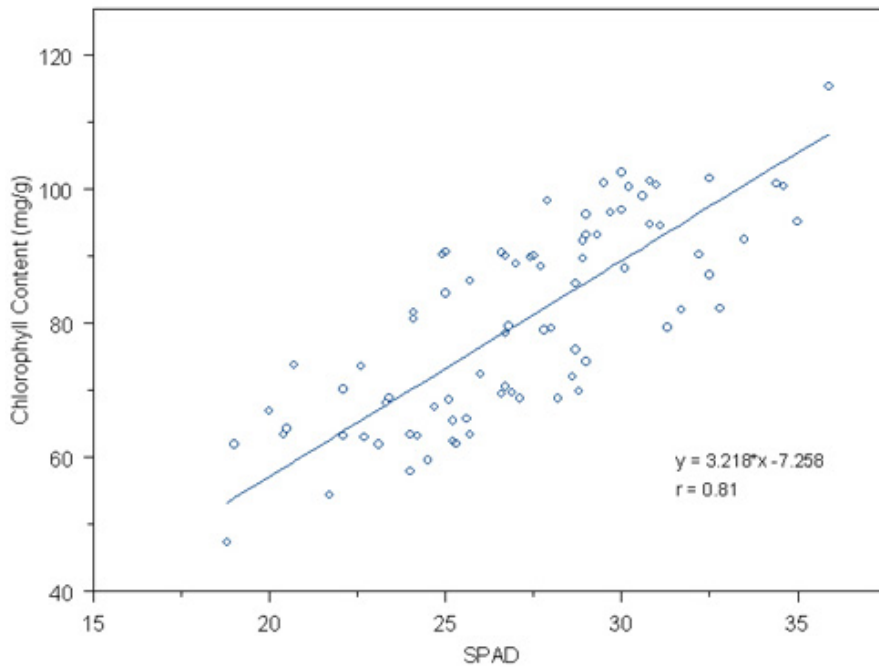


**Figure 4-7 Correlation between optical measurement with a SPAD meter and solvent chlorophyll content (N=80), September 1, 2004**

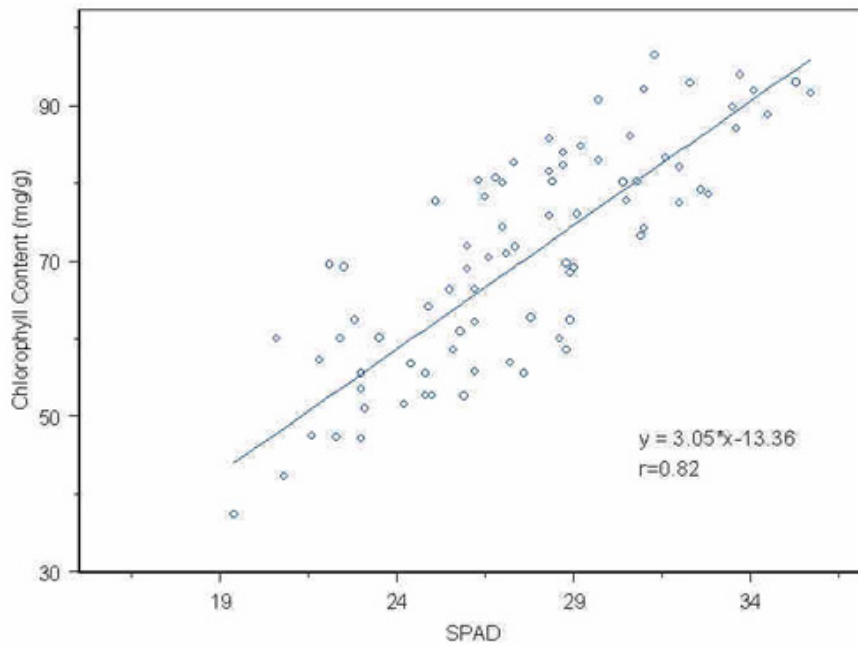
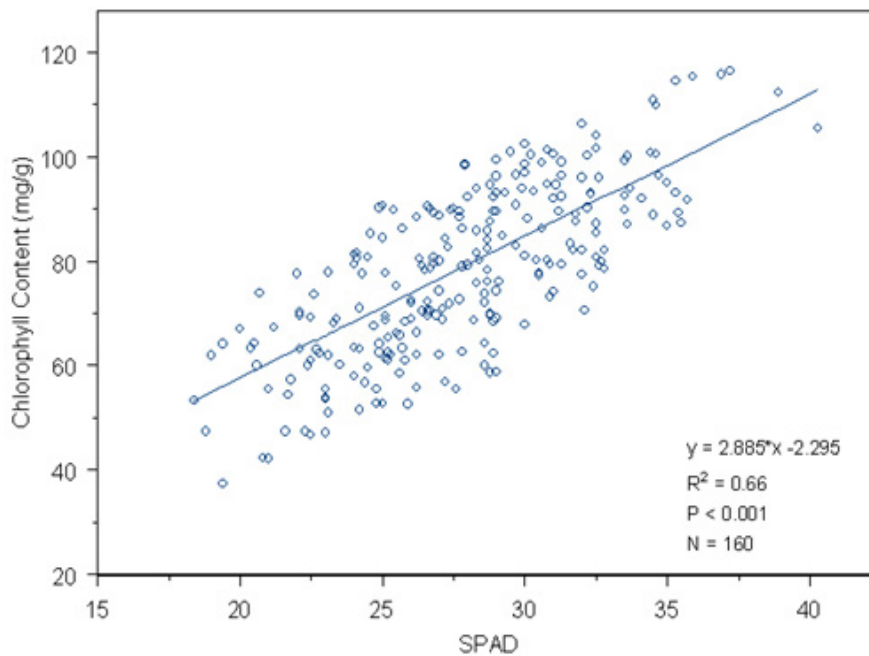


**Figure 4-8 Correlation between optical measurement with a SPAD meter and solvent chlorophyll content with 240 leaf samples collected in June, July, and September 2004**



The correlations between TCI and the leaf chlorophyll content are higher than those of other spectral indices. The ratio of TACI and OSAVI (Ratio) was highly correlated to the SPAD units in September with the highest correlation ( $r=0.802$ ), but the correlation was only 0.08 in July (Table 4.1). Both TVI and CRI were also highly correlated to SPAD units and solvent chlorophyll content in September, but low in July. The correlations for SPAD units with TVI and CRI were 0.76 and 0.63 respectively in September (Table 4.1), but only 0.61 and 0.56 in July, respectively. Only the TCI model showed strong correlations to SPAD units and chlorophyll content in both July and September. The correlations between SPAD unit and TCI were 0.782 in July and 0.775 in September. The correlations between chlorophyll content and TCI were 0.74 and 0.65 in July and September (Table 4.1).

The other spectral indices using only red and near infrared wavelengths are not strongly related to chlorophyll content. The correlations between NDVI and SPAD units were less than 0.4 in July and September. The red edge index (REIP) was also less than 0.44 in both July and September. These results demonstrate that TCI was relatively stable and highly correlated with chlorophyll content. TCI is the best spectral index that is highly related to leaf chlorophyll content. This result suggests that it is possible to estimate leaf chlorophyll content with hyperspectral spectrophotometer.

The TCI model was developed with the regression equations of TCI and chlorophyll content. The regression used leaf samples ( $n=160$ ) collected in July and September 2004 (Figure 4.9). As the strong influence of background in sample collection in June, the samples in June were not used in the regression. The regression shows significant linear relationship in July and September with  $P < 0.001$  and  $R^2 = 0.61$  (Table

4.2). These results indicate that TCI is relatively stable in measuring chlorophyll content in both July and September. The regression equation is listed as:

$$Chl = -0.447 * TCI + 156.475 \quad (4.12)$$

**Figure 4-9 Regression of leaf chlorophyll content with TCI within 160 leaf samples collected in July and September 2004**

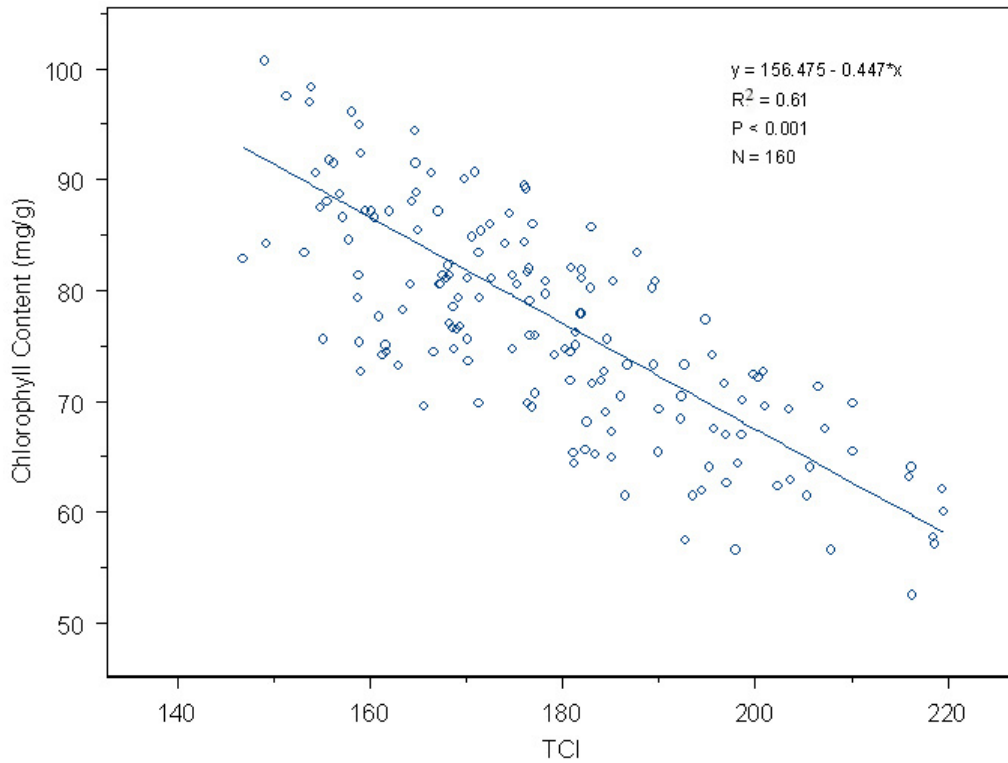


**Table 4-1 Correlation between spectral indices and chlorophyll content measured with dissolvent extraction and a SPAD chlorophyll meter**

		Chl.C	TVI	CRI	CARI	Ratio	NDVI	REP	TCI
July 26	Chl.C <sup>1</sup>	1	0.503	0.443	0.301	-0.163	0.352	-0.448	-0.739
	SPAD Unit	0.814	0.614	0.561	0.394	-0.079	0.422	-0.543	-0.782
Sept. 01	Chl.C	1	0.483	0.455	0.153	-0.594	0.076	-0.113	-0.649
	SPAD Unit	0.821	0.762	0.627	0.282	-0.802	0.296	-0.365	-0.775

<sup>1</sup>Chl.C – Chlorophyll Content (mg/g)

**Table 4-2 Regression equations and parameters of leaf chlorophyll content with SPAD units and spectral indices derived from original and derivative spectra**

Model Name	Regression equation	Intercept	Slope	RSE	R <sup>2</sup>	F-stat.	DF	P-value
SPAD	Chl=2.885*SPAD-2.295	-2.295	2.885	5.143	0.66	256.5	238	<0.001
TCI	Chl=-0.447*TCI+156.48	156.48	-0.447	6.803	0.61	212.6	158	<0.001
FDI	Chl=13.221*FDI+35.592	35.592	13.221	7.314	0.602	240.7	238	<0.001
SDI	Chl= 117.63-34.545*SDI	117.63	-34.545	6.431	0.628	290.8	238	<0.001

### 4.5.3 Chlorophyll Content with the FDI and SDI Models

The ratio of  $R'_{717}$  and  $R'_{523}$  in the first derivative (FDI) is found highly correlated to leaf chlorophyll content and the correlation varies with different growing seasons. The correlations between the FDI and SPAD units were approximate 0.7 in June, and over 0.80 in July and September (Table 4.3). The correlation between the FDI and chlorophyll content with chemical extraction was slightly low with 0.67, 0.58, and 0.65 in June, July, and September, respectively.

Chlorophyll content is also high correlated with the peak values of the second derivative. The two peaks of the second derivative are found to locate at 689 and 692 nm in the edge of visible and near infrared regions, which is consistent to the red edge of the original spectrum. The peak values are negatively correlated to chlorophyll content. The correlation between the peak at 689 nm and chlorophyll content are almost the same as that between the peak at 692 nm and chlorophyll content. The correlation between SDI and chlorophyll content measured with SPAD meter ranged from 0.61 to 0.80 in the growing seasons.

There is a deep trough at 730 nm in June or 733 nm in July and September in the second derivative spectrum (Figure 3.10c). Chlorophyll content is obviously weakly correlated to the trough values of the second derivative. The correlations between  $R''_{730}$  or  $R''_{733}$  and chlorophyll content are less than 0.5. However, the ratio of the maximum peak at 692 nm and the deepest valley at 730 nm is also highly related to chlorophyll content (Tables 4.3). The correlation of this ratio with the chlorophyll content with SPAD units was about 0.8.

The derivative models of chlorophyll content were developed with the first and second derivative spectra from leaf samples (n=240) collected in June, July, and September. The FDI model of chlorophyll content was developed from the first derivative spectra with the ratio of F'717 and F'523. The regression equation is described with formula 4.13 with R-square of 0.60 (Figure 4.10).

$$Chl = 13.221 * FDI + 35.592 \quad (4.13)$$

The SDI model of chlorophyll was developed with the second derivative spectra at 692 nm. The regression equation is listed in formula (4.14) with R-square of 0.628 (Figure 4.11).

$$Chl = 117.625 - 34.545 * SDI \quad (4.14)$$

**Figure 4-10 Regression of leaf chlorophyll content with first derivative index (FDI) within 240 leaf samples collected in June, July, and September 2004**

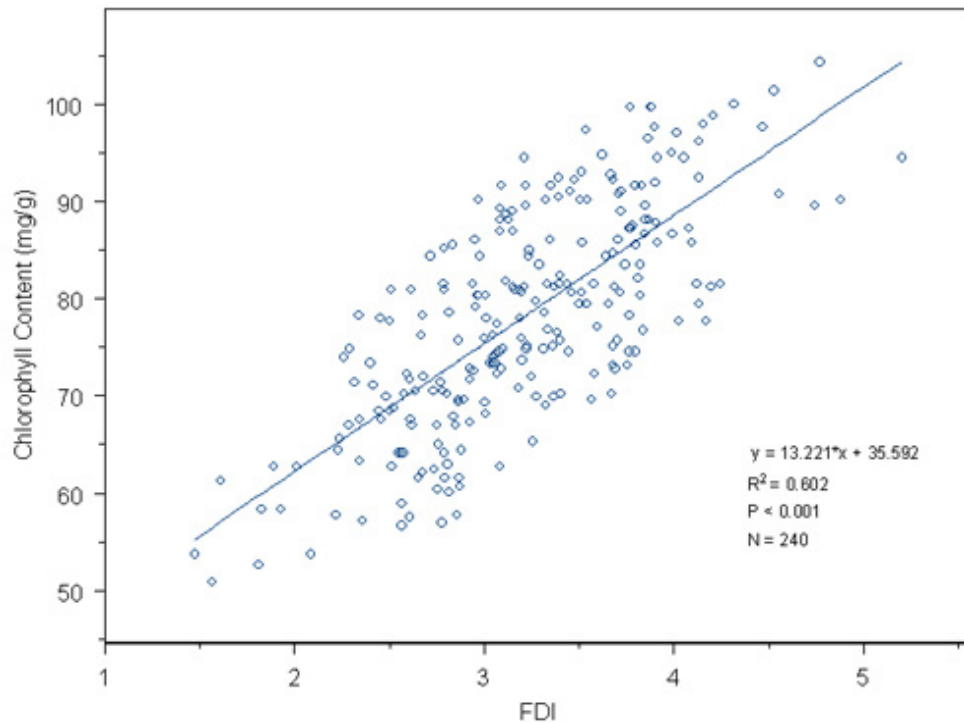


**Figure 4-11 Regression of leaf chlorophyll content with second derivative index (SDI) within 240 leaf samples collected in June, July, and September 2004**

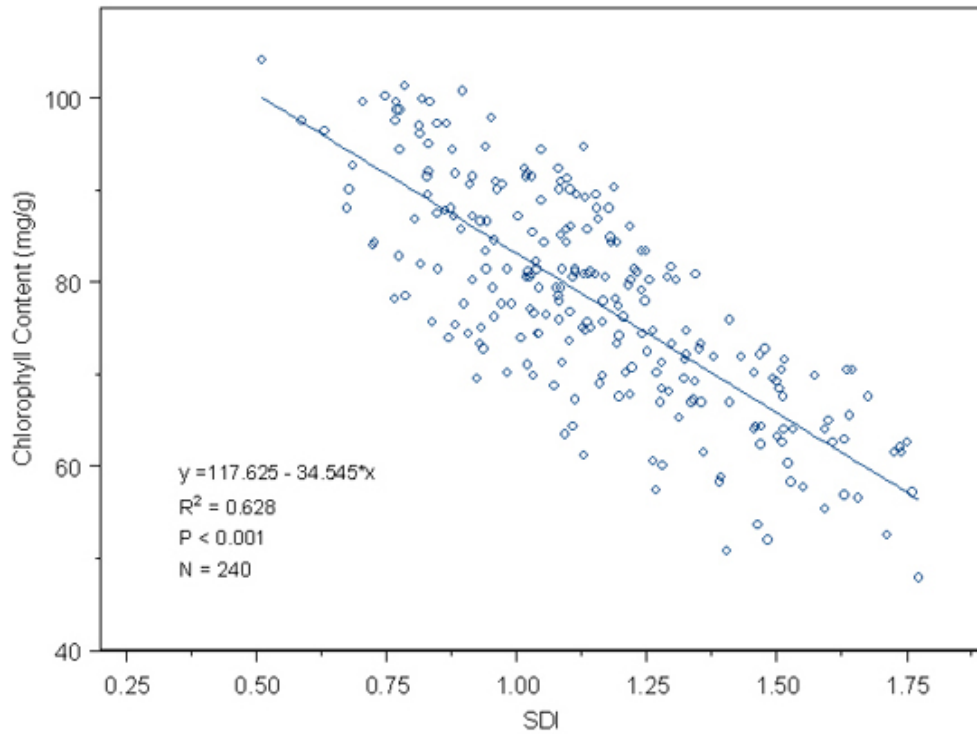


**Table 4-3 Correlations between derivative spectral indices and chlorophyll contents measured with dissolvent extraction and optical chlorophyll meter**

	June		July		September	
	SPAD	CHL	SPAD	CHL	SPAD	CHL
FDI	0.785	0.672	0.69	0.582	0.810	0.65
R''636	0.094	0.047	0.348	0.246	0.143	0.035
R''689	-0.764	-0.643	-0.793	-0.716	-0.801	-0.675
R''692	-0.722	-0.614	-0.762	-0.724	-0.782	-0.621
R''730*	-0.120	0.095	-0.468	-0.477	-0.392	-0.199
R''692/R''730*	0.719	0.437	0.683	0.633	0.742	0.483
R''689/R''730	0.710	0.467	0.705	0.651	0.783	0.532

\* R''730 was used in June and R''733 used in July and September

#### **4.5.4 Spectral Shift with Seasonal Change**

A noticeable characteristic is that the maximum correlation between leaf chlorophyll content and spectral reflectance shifted toward the two edges of red regions from July to September. One shift is toward the edge between green and red region and the other is toward the edge between red and near infrared. The shift phenomenon has been noticed from canopy reflectance (Collins 1978) and is regarded as the influence of green cover density (Broge and Leblanc 2000) and chlorophyll *a* (Campbell 1996). Causes of the shift appear to be complex and can not be completely understood. The shift may be related to the seasonal change of leaf structure or plant maturity, not only to leaf chlorophyll content, because the chlorophyll content was not changed in July and September. The average chlorophyll content of the 80 leaf samples was 27.1 SPAD units in July and 27.5 SPAD units in September. Chlorophyll components and leaf structure may contribute to the shift of spectral reflectance against chlorophyll content.

#### **4.6 Conclusions**

After the measurement of chlorophyll with three different methods, these results indicate that the chlorophyll contents measured with different approaches are highly correlated with each other. Solvent extraction of chlorophyll is a traditional approach widely used in crop nutrient and photosynthesis analysis, but this method is a time-consuming and labor intensive process. In contrast, optical chlorophyll meter - SPAD502, is a fast and easy-going method for leaf chlorophyll measurement. The correlation between SPAD units and chlorophyll content determined using solvent extraction is high ( $r > 0.6$ ). The results indicate that they are linearly correlated to each other. The SPAD

meter could replace solvent extraction for analysis of leaf chlorophyll content, especial in a single species or with a homogeneous canopy.

The spectral chlorophyll indices derived from the original spectral reflectance data from the ASD spectroradiometer are more correlated to chlorophyll measurement with SPAD meter than the measurement of solvent extraction. This may be because both spectroradiometer and SPAD chlorophyll meter use red and near infrared wavelengths to estimate chlorophyll content. Chlorophyll content with solvent extraction is calculated by using only green wavelengths. Among the seven spectral indices, only TCI model shows better correlations with leaf chlorophyll content for all sampling dates.

There is a significant seasonal shift in the wavelength of maximum correlation between chlorophyll content and spectral reflectance. With the senescence of the canopy, the peak of the correlation curve between spectral reflectance and chlorophyll content is shifted toward the longer wavelength called the red edge between the red and near infrared region and toward the shorter wavelength called the green edge between green and red region. The shift is related to the maturity of plant and may be related to change of leaf structure or chlorophyll component. Thus, chlorophyll indices should be adjusted based on the shifts. Otherwise, an index developed in the early growing season may not be as effective later in the growing season. For example, OSAVI is designed to remove the influence of soil background. The correlation coefficient between the SPAD measurements and the Ratio of TCARI and OSAVI was high in the late growing season. The correlation was over 0.8 in September, but it was low in the middle growing season with only 0.079 in July. Only the TCI model calculated with green, red, and near infrared wavelengths shows stability within the growing season. The correlation between SPAD

measurements and the TCI index was over 0.7 in both July and September. Thus, the TCI model shows more seasonal stability for estimating chlorophyll content than the other spectral indices and was effective for assessing leaf chlorophyll concentration.

The indices derived from derivative spectra were highly correlated to chlorophyll content. There are two obvious peaks in the first derivative at two red edge regions. The two peaks of first derivative mostly occurred at 523 nm and 717 nm in all growing seasons. The ratio of the two peak values at 717 nm and 523 nm in the first derivative spectra was highly correlated with chlorophyll content ( $r > 0.81$ ). The peak values of the second derivative spectra were also highly related with chlorophyll content with  $r > 0.8$  and showed small variability in the growing seasons. Those results indicate that the indices derived from derivative were more stable than the indices from the original spectral reflectance in the growing seasons.

Those results indicate that the hyper-spectroradiometer is an effective device to estimate leaf chlorophyll content. A more important application of hyperspectral spectrum is that it can be used to measure canopy chlorophyll content at different spatial scales, based on the regression of chlorophyll index with chlorophyll content at the leaf scale.

Three chlorophyll models are developed based on original and derivative spectra of leaf samplings collected in the whole growing season of 2004. The TCI model is derived from the original spectral reflectance of leaf based on the correlation between chlorophyll content and leaf reflectance spectrum. The FDI model is derived from ratio of the first derivative spectra at 717 nm and 523 nm. The SDI model is generated with the peaks of second derivative spectra at 692 nm. The regressions of

the three models with chlorophyll content were significant with  $P < 0.001$  and R-square  $> 0.6$ . This indicates that more than 60 percent predicted chlorophyll content can be explained with the field measured chlorophyll. The three models will be further validated with canopy and image estimation in the next two chapters.

# **CHAPTER 5 - APPLICATION OF LEAF-SCALE SPECTRAL MODELS FOR CANOPY CHLOROPHYLL ESTIMATION**

## **5.1 Introduction**

In the previous chapter, hyperspectral remote sensing was found effective to estimate leaf chlorophyll content. The TCI, FDI, and SDI indices derived from original and derivative reflectance spectra were significantly correlated to leaf chlorophyll content. Three chlorophyll models were generated based on the three indices. In this chapter, the three models are further validated with canopy chlorophyll measurements from field samples. Four other indices derived from the reflectance spectra including NDVI, TVI, CRI, and the ratio of TCARI and OSAVI (Ratio) are also used as reference to compare with TCI for estimating canopy chlorophyll content. NDVI is the most popular spectral index for monitoring vegetation and canopy structure (Liang 2004). The other three spectra indices were also found highly correlated to leaf chlorophyll content in Chapter 4.

All field canopy data were collected in HQC, a one-year burned treatment, on June 30, July 26, and September 1, 2004, the same days the leaf sample data were collected. Besides the canopy hyperspectral reflectance, canopy chlorophyll content data

were also collected from each plot in the four transects in HQC (Figure 3.4). Canopy spectral reflectance was measured using the ASD spectroradiometer with an 18° foreoptic suspended about one meter above canopy. Canopy reflectance is substantially influenced by the soil background, atmosphere conditions, and canopy shading, all of which could be ignored at the leaf scale because the leaf clip could isolate the leaf from the environmental conditions (see Chapter 3). TCI, FDI, and SDI indices derived from the reflectance and derivative spectra are compared with field measured canopy chlorophyll content, LAI, and greenness cover.

## **5.2 Correlation of Spectral Reflectance with Canopy Chlorophyll**

### **Content**

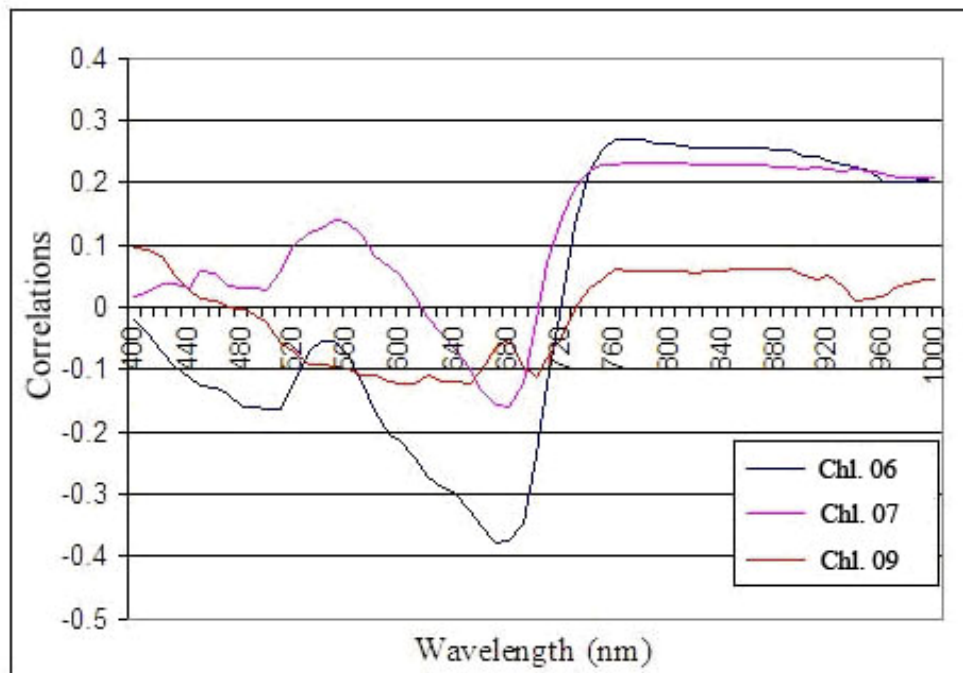
The canopy reflectance spectrum is strongly influenced by background and canopy structure. The correlation spectrum at the canopy scale (Figure 5.1) is obviously different from that at the leaf scale (Figure 4.2). The correlations were weaker and more seasonally variable. All correlations between spectral reflectance at all wavelengths and canopy chlorophyll content in the growing season were less than 0.35, which was much lower than those at the leaf scale (Figure 4.2). The correlation at the red edge was high at the leaf scale ( $r > 0.7$  see Figure 4.2), but lower at the canopy scale, and the peak correlations in the red edge region was shifted towards longer wavelengths as the canopy matured.

Unlike the results in the visible spectrum, the correlation spectrum at the canopy scale shows higher values than at the leaf scale. The correlation between canopy reflectance and chlorophyll content in NIR region was  $r=0.22$  in June and  $r=0.25$  in July

compared with  $r=0.1$  at the leaf scale, although none of the correlations were particularly high. NIR reflectance is mainly controlled by leaf structure (Campbell 1996). The slightly higher correlations between canopy chlorophyll and spectral reflectance in the NIR region of the spectrum could be caused by other factors which are confounding the chlorophyll signal. The factors may also be related to canopy structure and soil background, because they have strong reflectance in the NIR region.

Canopy spectral reflectance is controlled by many factors including leaf chlorophyll content, leaf scattering, canopy composition, greenness cover, and soil background. Canopy reflectance is not a simple aggregation of reflectance from individual leaves, but a complex function of reflectance and leaf scattering. Greater correlation between the NIR wavelengths and chlorophyll (compared to the red edge wavelengths) content could be related to canopy structure and scattering of leaves. Leaf density, canopy layers and shadowing would make the canopy reflectance complex. Dead material and yellowish leaves of canopy in the late growing season might also contribute to enhanced reflectance in the near infrared region. To summarize, the canopy spectral reflectance is complex and affected not only by individual leaves, but also by canopy structure and components.

**Figure 5-1 Correlation of spectral reflectance with chlorophyll content in June, July, and September 2004**



### 5.3 Canopy Derivative Spectral Indices

The wavelength occurrence frequencies of peaks and troughs in the derivative spectra at the canopy scale are different from those at the leaf scale. The derivative indices generated at the leaf scale may not work at the canopy scale.

Figure 5.2 shows the wavelength occurrence frequencies of peaks and troughs in the first derivative spectra of canopy. The occurrence frequency is the percentage of wavelengths at the peak or trough from the 80 canopy samples in each campaign. There are two peaks in the first-order derivative spectra of leaf reflectance (See Figure 3.10b in Chapter 3). One is at the green edge and the other is at the red edge. The two peaks are

found most frequently at 523 nm and 717 nm at the leaf scale. However, the peak occurrence at the canopy scale is found around the two wavelengths and varies in the growing season. The peak occurrence at the green edge is around 523 nm. The peak occurrence is at 530 nm in June with 97%, bimodal in July at 519 nm (42%) and 523 nm (36%), and at 521 nm (30%) in September. The peak occurrence at the green edge tends to shift toward the shorter wavelength with the maturity of vegetation.

The peak occurrence at the red edge is found around 717 nm at the canopy scale. The peak occurrence is at 719 nm in June with 43%, at 718 nm with frequency of 65% in July and 48% in September. The peak occurrence at the red edge at the canopy scale is almost the same as that at the leaf scale at 717 nm.

The trough occurrence at the canopy scale is different from that at the leaf scale. The trough occurrence at the leaf scale is at 571 nm, but is at 569 nm in June (with 100%), at 571 nm in July (38%) and at 661 nm in September (76%) at the canopy scale. The trough occurrence is shifted toward the longer wavelength with the maturity of vegetation. Thus, the wavelength occurrence of peaks and trough at the canopy scale was different from those at the leaf scale. Those results reflect the influence of canopy structure on canopy spectral reflectance in the growing season.

The occurrences of peak and trough in the second derivative spectra at the canopy scale are also different from those at the leaf scale (Figure 5.3). The peak occurrence occurs mostly at 689 nm and 692 nm at the leaf scale. The peak occurrence is only at 692 nm in June (with 53%) and is shifted toward longer wavelength at 722 nm in July (68%) and at 717 nm in September (with 54%) at the canopy scale (Figure 5.3a). This means that only in the early growing season does the canopy have the same derivative spectra

features as individual leaves. The second derivative spectra are substantially affected by canopy structure such as LAI and closure in the late growing season.

The trough occurrences in the second derivative spectra at the canopy scale also differ from those at the leaf scale and vary across the growing season. The frequency of trough around 733 nm at the leaf scale was only 45% in June, but was at 720 nm with 70% in July and 78% in September (Figure 5.3b). The consistence of trough occurrence at canopy and leaf scale in the early stage of vegetation suggests that the canopy in the early growing season has more similar spectral features as individual leaves. In the other words, the canopy spectral reflectance is more influenced by canopy composition and structure in the late growing season including the effect of stem, flower, and yellowish leaves.

**Figure 5-2 Wavelength occurrence frequency of peaks and trough in the first derivative spectra (N=80): (a) peak in the green edge around 523 nm, (b) peak in the red edge around 717 nm, and (c) trough around 570 nm**

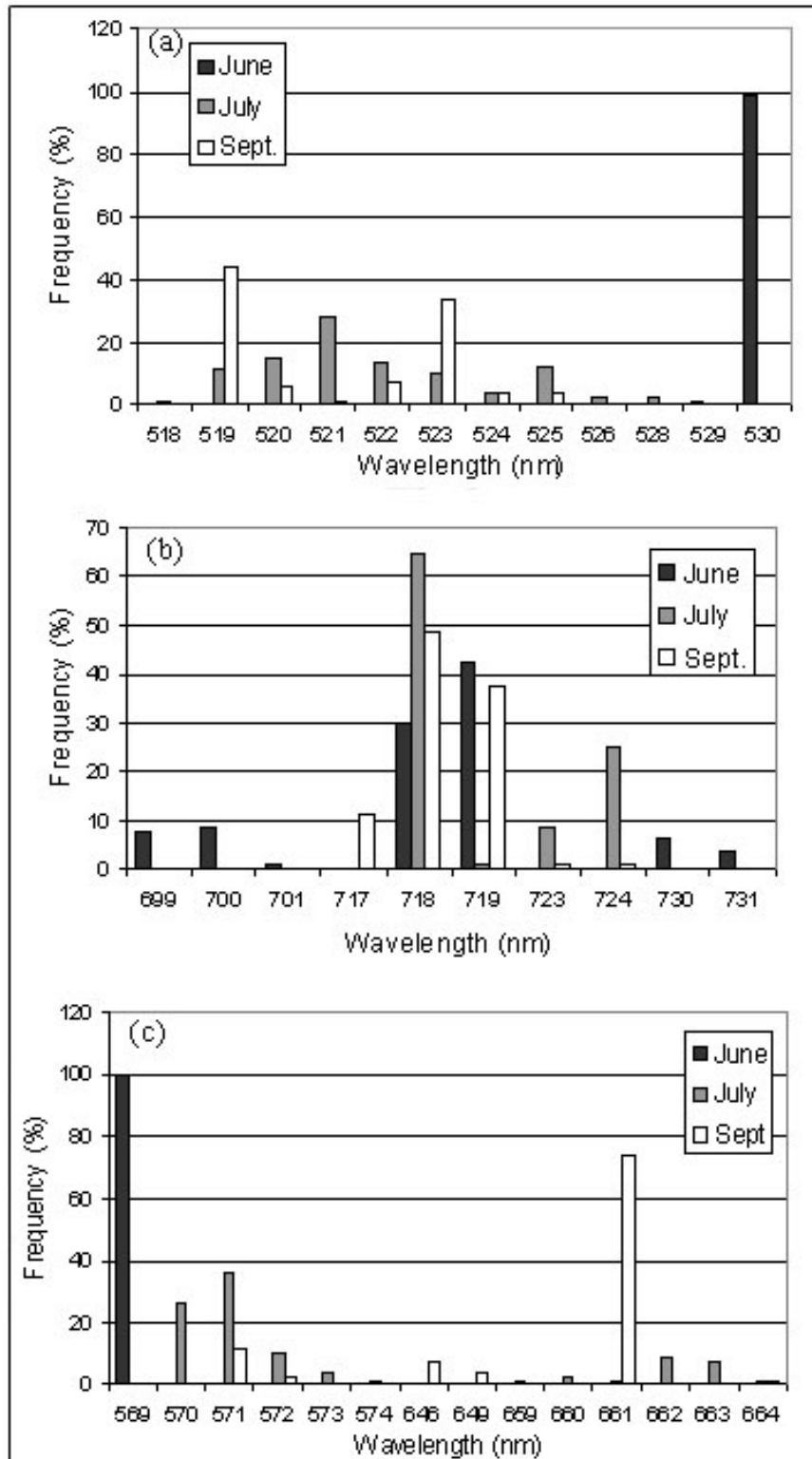
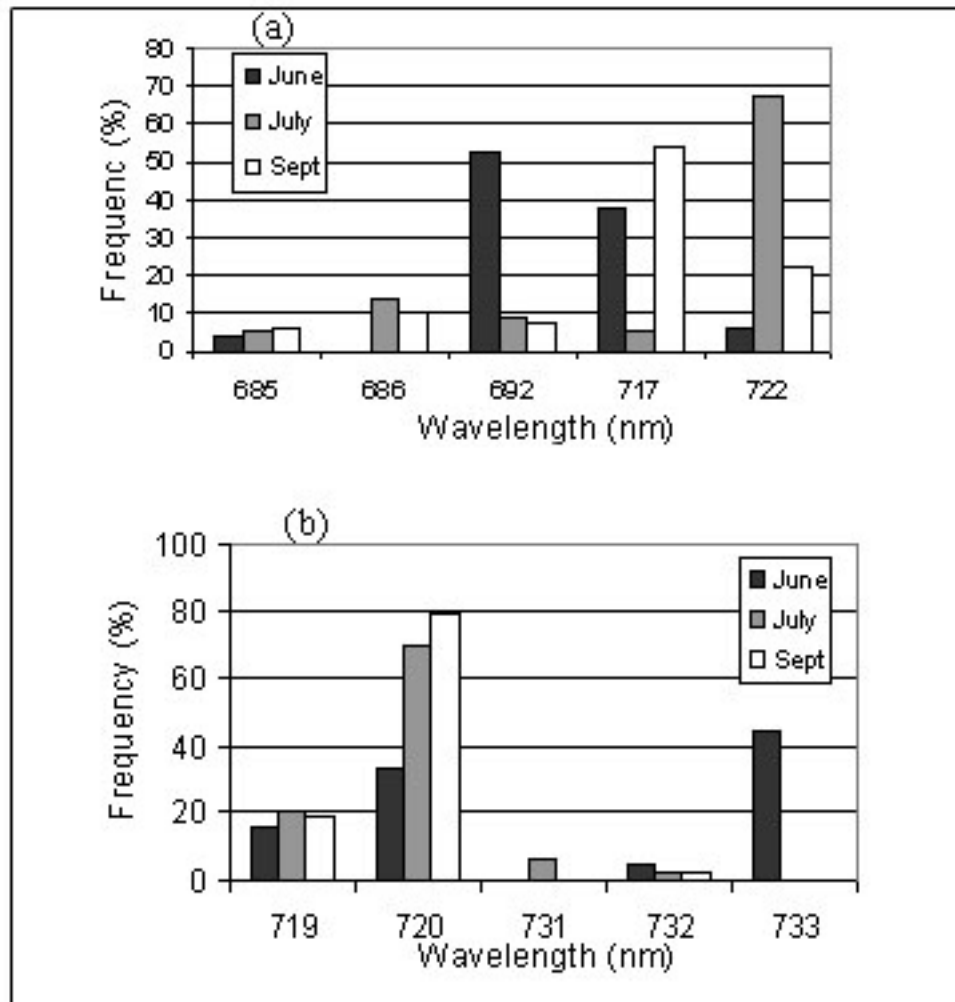


**Figure 5-3 Wavelength occurrence frequency of peak (a) and trough (b) in the second derivative spectra (N=80)**



Thus, the FDI derived from the ratio of first derivative spectrum at 717 nm and 523 nm and the SDIs derived from second derivative spectrum at 689 nm and 692 nm are still applied at the canopy scale. Meanwhile, the peak values at 717nm and 722 nm and the trough value at 733 nm in the second derivative spectra are also used as reference for the derivative spectral indices. The derivative spectral indices are compared with the field measurement of canopy chlorophyll content, LAI, and green cover.

## **5.4 Spectral Indices and Canopy Chlorophyll Content**

### **5.4.1 Correlation between Spectral Indices and Canopy Chlorophyll Content**

The spectral indices were derived from the canopy reflectance spectrum. The correlation between the spectral indices and canopy chlorophyll content are listed in Table 5.1. The spectral indices are weakly correlated with canopy chlorophyll content and vary across the growing season. Only TCI and NDVI show relatively high correlations with canopy chlorophyll content in the early growing season. The correlations of canopy Chl content with TCI and NDVI were  $-0.541$  and  $0.399$  in June, respectively. The correlations of Chl with TCI and NDVI were  $-0.514$  and  $0.467$ , respectively in July. The correlations of canopy Chl with the other three indices were low ( $r < 0.300$ ). In the later growing season, only TCI was relatively strongly correlated to canopy chlorophyll content. The correlation between TCI and Chl was  $-0.528$  in September. NDVI, TVI, CRI, and Ratio were weakly related to canopy chlorophyll in September with  $r < 0.200$ .

The seasonal analysis of spectral indices with canopy chlorophyll content indicates that TCI is relatively strongly related to canopy chlorophyll content. NDVI is only related to chlorophyll content in the early growing season. The low correlation of NDVI with chlorophyll content in the later growing season may be related to the influence of dead and yellowish leaves of canopy because they have strong reflectance in near infrared region. Only TCI has a relative stable correlation with canopy chlorophyll content in all growing seasons.

**Table 5-1 Correlations of spectral indices with canopy chlorophyll content measured with a SPAD chlorophyll meter and canopy LAI and greenness cover (n=80 for each sampling date)**

		TCI	TVI	CRI	Ratio	NDVI	Chl
June 30	Chl	-0.541	0.294	-0.044	-0.282	0.399	1
	Cover	-0.253	0.385	-0.321	-0.109	0.374	0.293
	LAI	-0.312	0.393	-0.177	-0.017	0.514	0.304
July 26	Chl	-0.514	0.240	-0.151	0.061	0.467	1
	Cover	-0.269	0.113	-0.009	-0.024	0.450	0.039
	LAI	-0.488	0.528	-0.303	0.083	0.475	0.220
September 01	Chl	-0.528	0.113	0.078	-0.217	0.190	1
	Cover	-0.152	0.186	-0.056	0.112	0.485	0.051
	LAI	-0.348	-0.022	0.326	-0.295	0.217	0.064

## 5.4.2 Correlation between Derivative Indices and Canopy Chlorophyll

### Content

The correlations between indices derived from the first and second derivative spectra and canopy chlorophyll content measured with a SPAD-502 chlorophyll meter are listed in Table 5.2. The ratios of  $F'_{717}$  and  $F'_{523}$  (FDI) derived from the first derivative spectra are more highly correlated to canopy chlorophyll content. The correlations between FDI and Chl were 0.541, 0.509, and 0.457 in June, July, and September, respectively. The correlations are consistently higher in all growing seasons compared with the correlations between the original spectral indices and chlorophyll content (see Table 5.1).

The derivative spectra are obviously affected by canopy structure, especially in the late growing season. The correlations between FDI and LAI were 0.21, 0.275, and 0.285 in June, July, and September, respectively. The FDI is weakly related to canopy greenness with  $r < 0.1$  in all of the growing season. Thus, the first derivative index (FDI) is still influenced by canopy structure (LAI), but not affected by canopy greenness cover.

The second derivative spectra at 689 nm and 692 nm are highly related to canopy chlorophyll content but vary in the growing season (Table 5.2). The second derivative spectra at 689 nm and 692 nm are highly related to canopy chlorophyll in the early growing season. The correlations between SPAD units and  $R''_{689}$  were 0.605 in June, 0.481 in July, and 0.334 in September. The correlations between  $R''_{692}$  and SPAD units were -0.538 in June, -0.479 in July, and -0.311 in September. The low correlation in the late growing season could be related to the canopy density and composition.

**Table 5-2 The correlations between derivative indices and canopy chlorophyll content, LAI, and greenness cover in 2004 (n=80 for each sampling date)**

	June 30			July 26			September 01		
	Chl	LAI	Cover	Chl	LAI	Cover	Chl	LAI	Cover
$R'_{717}/R'_{523}$	0.541	0.21	0.06	0.509	0.275	0.079	0.457	0.285	0.038
$R''_{636}$	0.052	0.08	0.043	0.044	0.152	0.09	0.183	0.108	0.036
$R''_{689}$	-0.605	0.164	-0.005	-0.481	0.281	0.049	-0.334	0.205	0.157
$R''_{690}$	-0.215	0.138	0.052	-0.189	0.148	0.027	-0.174	0.081	0.111
$R''_{692}$	-0.538	0.228	-0.015	-0.479	0.285	0.026	-0.311	0.257	0.22
$R''_{690}/R''_{730}$	0.045	0.227	0.017	0.16	0.265	0.069	0.161	0.175	0.131
$R''_{717}$	0.177	0.327	0.172	0.309	0.506	0.187	0.117	0.281	0.127
$R''_{722}$	0.259	0.263	0.435	0.276	0.382	0.267	0.194	0.15	0.219

The correlations between  $R''_{689}$  and canopy greenness cover were low throughout the growing season ( $r < 0.15$ ). The correlations between  $R''_{689}$  and LAI in July and September were higher than that in June. The correlation was 0.164 in June, 0.281 in July and 0.205 in September. This could be related to the canopy with high density and closure in the middle and late growing season in the tallgrass prairie. With the less influence of canopy structure, the second derivative index (SDI) was relatively strongly correlated to canopy chlorophyll content in the early growing season.

Canopy LAI was found strongly correlated to the peak of second-order derivative spectra at 717 nm. The correlation between LAI and  $R''_{717}$  were 0.42, 0.53, and 0.41 in June, July, and September, respectively. The peak spectra at 722 nm were relatively high

correlated to canopy greenness cover. The correlation between  $R'_{722}$  and greenness cover was 0.435 in June, 0.267 in July, and 0.219 in September. The spectra at 717 nm and 722 nm belong to the red edge region in the canopy reflectance spectrum. The spectral overlapping of chlorophyll and canopy structure in the red edge cannot be completely separated with the derivative transform.

## 5.5 Application of the Chlorophyll Models in Canopy

The three chlorophyll models, TCI, FDI, and SDI derived at the leaf scale, are applied to the canopy scale. Because of the seasonal change of vegetation, the three models are compared with the seasonal measurement of chlorophyll content. The estimated chlorophyll contents derived from the hyperspectral reflectance using the three models are compared with the field chlorophyll measurement made with the SPAD chlorophyll meter. For model testing purposes, the SPAD units were converted into absolute chlorophyll content (mg/g with fresh weight) using the conversion equation generated in Chapter 4. Linear regression, error index, and index of agreement were used to evaluate the chlorophyll models. The regression describes the linear functional relationships between two variables, but can not quantify the accuracy of a calibration (although it can characterize reliability). The root mean squared error (RMSE, Equation 5.1) is used to calculate the average error produced by model. Index of agreement ( $d$ , see Equation 5.2) was introduced to measure the degree to which a model's predictions are error free (Willmott 1981). The  $d$  value ranges from 0 to 1. The higher the  $d$ , the more close to error free the model.

$$RMSE = [N^{-1} \sum_{i=1}^N (P_i - O_i)^2]^{0.5} \quad (5.1)$$

where  $P_i$  is the predicted value,  $O_i$  is the observed value,  $N$  is sample numbers.

$$d = 1 - \frac{\sum_{i=1}^N (P_i + O_i)^2}{\sum_{i=1}^N (|P'| + |O'|)^2} \quad (5.2)$$

where  $P' = P_i - \bar{O}$  and  $O' = O_i - \bar{O}$ ,  $\bar{O}$  is the mean of observation

### 5.5.1 The TCI Model

Canopy chlorophyll content is estimated with the TCI model derived from the original spectral reflectance. The validation of canopy chlorophyll content from the TCI model is shown in Figure 5.4. The root mean square errors (RMSE) are lower less than 11 mg with chlorophyll content measurement ranged from 70 to 110 mg per gram of fresh leaves in all of the growing season. The RMSE is especially low in September with 8.00 mg. This means the TCI model is significant and reliable, especially in the later growing season.

Compared with the 1:1 line that has a slope of 1 and an intercept of 0 in the scatter plot, the TCI model in June is obviously below the error-free line. This means that the TCI model underestimates the canopy chlorophyll content in the early growing season. In contrast, the estimated chlorophyll contents in July and September are close to the measured chlorophyll. The index of agreement ( $d$ ) increased with the maturity of vegetation and was up to 0.622 in September. The  $d$  was 0.521 in June, 0.574 in July, and 0.622 in September. This indicates that the TCI model is more effective to predict canopy chlorophyll content in the later growing season. The underestimation of chlorophyll with

the TCI model in the early growing season could be affected by soil background because of the low closure of vegetation in June.

### 5.5.2 The FDI Model

The FDI model is generated with the ratio of the first derivative spectra at 717 nm and 523 nm (see equation 4.12). The validation of the chlorophyll content is shown in Figure 5.5. The RMSEs in the FDI model vary within the growing season. The RMSE is low in June with 8.0 mg, but it is high in July and September with 20 mg and 22 mg, respectively. This means that the FDI model works better in estimating chlorophyll content in the early growing season.

It is easily noticed that the estimated chlorophyll of FDI model in July and September are above the 1:1 line, which indicates that the estimated chlorophyll is higher than the measured chlorophyll. The estimated chlorophyll in June is close to the field measurement of chlorophyll. This suggests that the FDI models overstate the canopy chlorophyll content in July and September. Compared with the TCI model, the degree of agreement ( $d$ ) is higher in June, but lower in July and September (Table 5.3). The  $d$  was 0.603 in June, 0.399 in July, and 0.371 in September. The degree of agreements decreases in the late growing season. This indicates that the FDI model is more effective in the early growing season and less effective in the late stage of vegetation. The results also infer that canopy structure had strong influence on the FDI model in the late growing season. In the early growing season, the influence of soil background could be removed from the derivative transform.

The influence of canopy structure cannot be removed from the derivative transform. The influence of canopy structure on the FDI model could be reflected from the correlation between FDI and LAI. The correlations between LAI and FDI were relative high with 0.275 and 0.285 in July and September, respectively. The peaks of the first-order derivative spectra have been found related to the canopy structure (LAI) (Lamb *et al.* 2002). Thus, the FDI model is better than the TCI model to predict chlorophyll content in the early growing season in contrast with the TCI model that is better in the late growing season.

### **5.5.3. The SDI Model**

The SDI model is derived from the second derivative spectra at 689 nm. The estimated chlorophyll is created from the SDI model in equation 4.13. The validation of the chlorophyll content is shown in Figure 5.6.

Compared with the 1:1 line (Figure 5.6), the regressions of the estimated chlorophyll content are all above the error-free line in June, July, and September. This reflects the SDI model much overestimate the chlorophyll content. Only the SDI model in June is close to the chlorophyll measurement. The degree of agreement ( $d$ ) of the SDI model was relatively high with 0.500 in June, but it is lower than that of the FDI model ( $d=0.603$ ). The  $d$ -value of the SDI model decreased with the maturity of vegetation. It was 0.294 in July and 0.286 in September.

The RMSE of the SDI model is also high than the other two models. The RMSE ranged from 12 mg to 30 mg from June through September and is higher than that of the TCI and FDI models in the corresponding date. This means the SDI model generates

more errors than the other two models to estimate canopy chlorophyll content, although the second derivative spectra could remove more noises from canopy structure than the first derivative spectra. This could be reflected from the correlation between LAI and SDI ( $r=0.205$ ), which is lower than that of FDI with 0.285 in September (Table 5.2). The high order derivative could improve the discrimination of overlapping peaks of spectra (Fell and Smith 1982). However, the high derivative transform could also introduce some unknown information in the derivative spectrum and reduce the signal to noise ratio (Chadburn 1982).

**Table 5-3 Validation statistics of TCI, FDI, SDI chlorophyll models**

	Models	RMSE	Index of Agreement (d)	R-square	P-value
June 30	TCI	10.883	0.521	0.176	<0.001
	FDI	8.015	0.603	0.185	<0.001
	SDI	12.255	0.500	0.265	<0.001
July 26	TCI	8.640	0.574	0.256	<0.001
	FDI	19.793	0.399	0.204	<0.001
	SDI	28.598	0.294	0.173	<0.001
Sept. 01	TCI	7.981	0.622	0.276	<0.001
	FDI	22.659	0.371	0.265	0.003
	SDI	30.628	0.286	0.265	0.015

Figure 5-4 Regression (red line) of canopy Chl from TCI Model in June, July, and September 2004 (black solid line is 1:1 line)

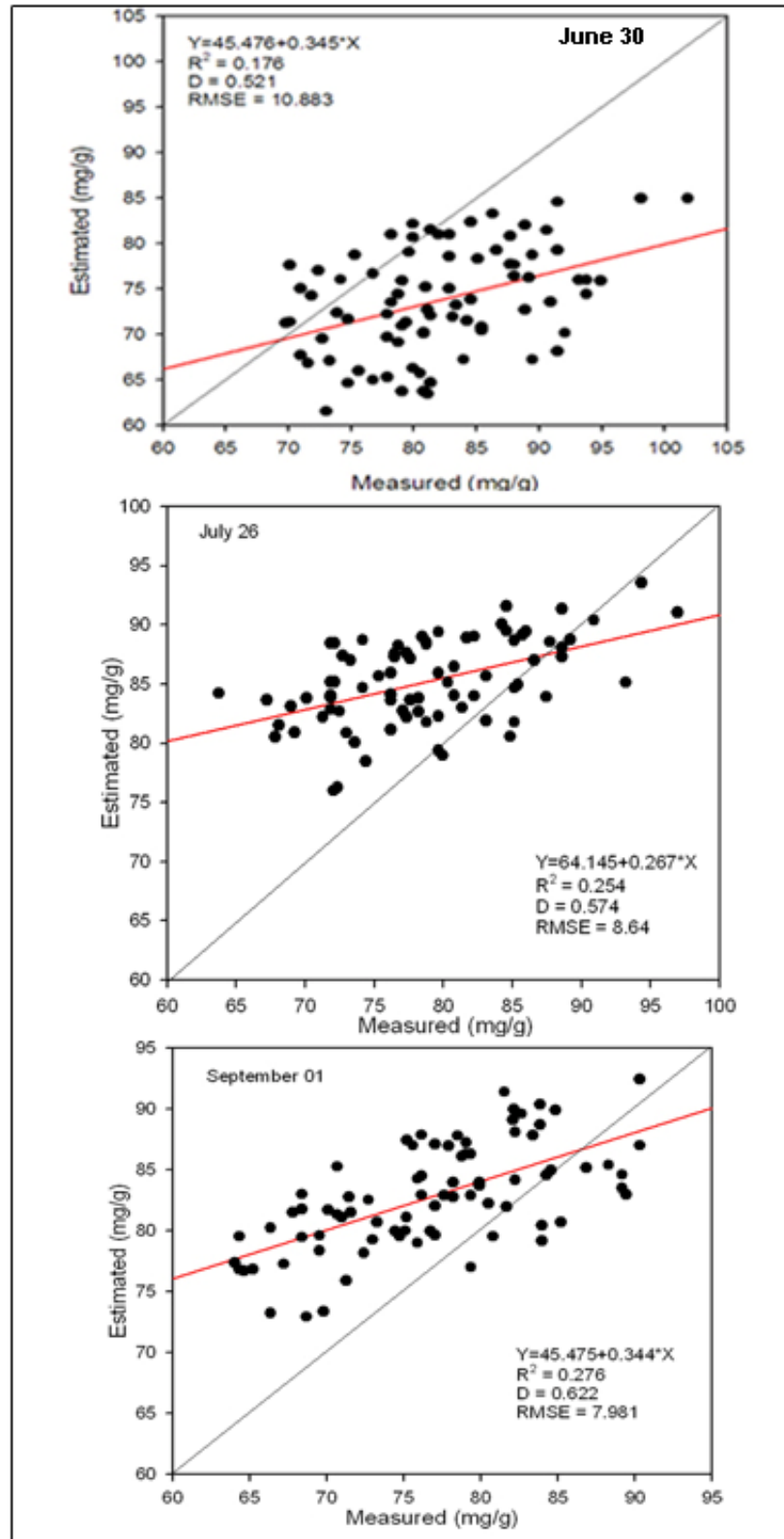


Figure 5-5 Regression (red line) of canopy Chl from FDI Model in June, July, and September 2004 (black solid line is the 1:1 line)

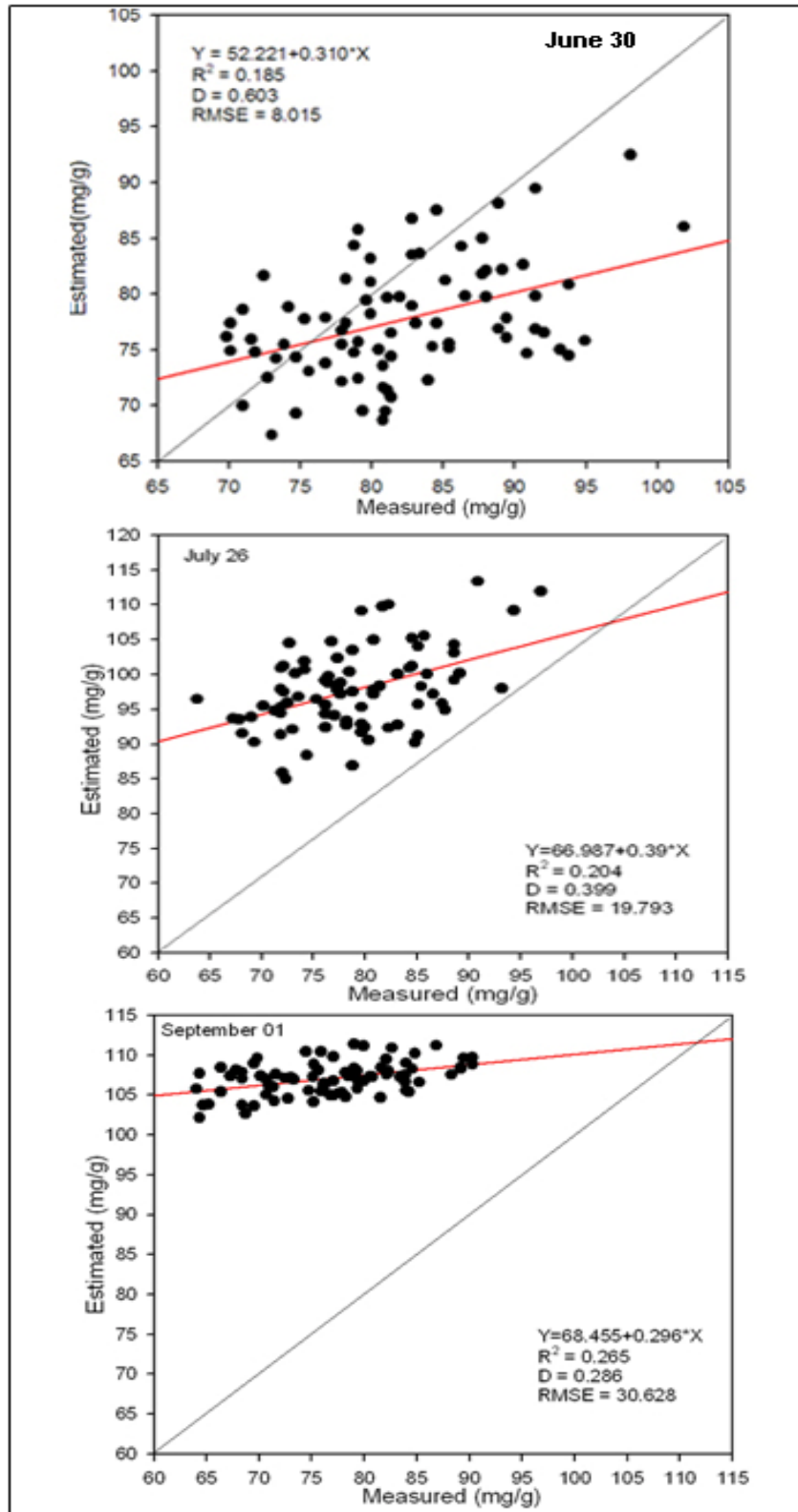
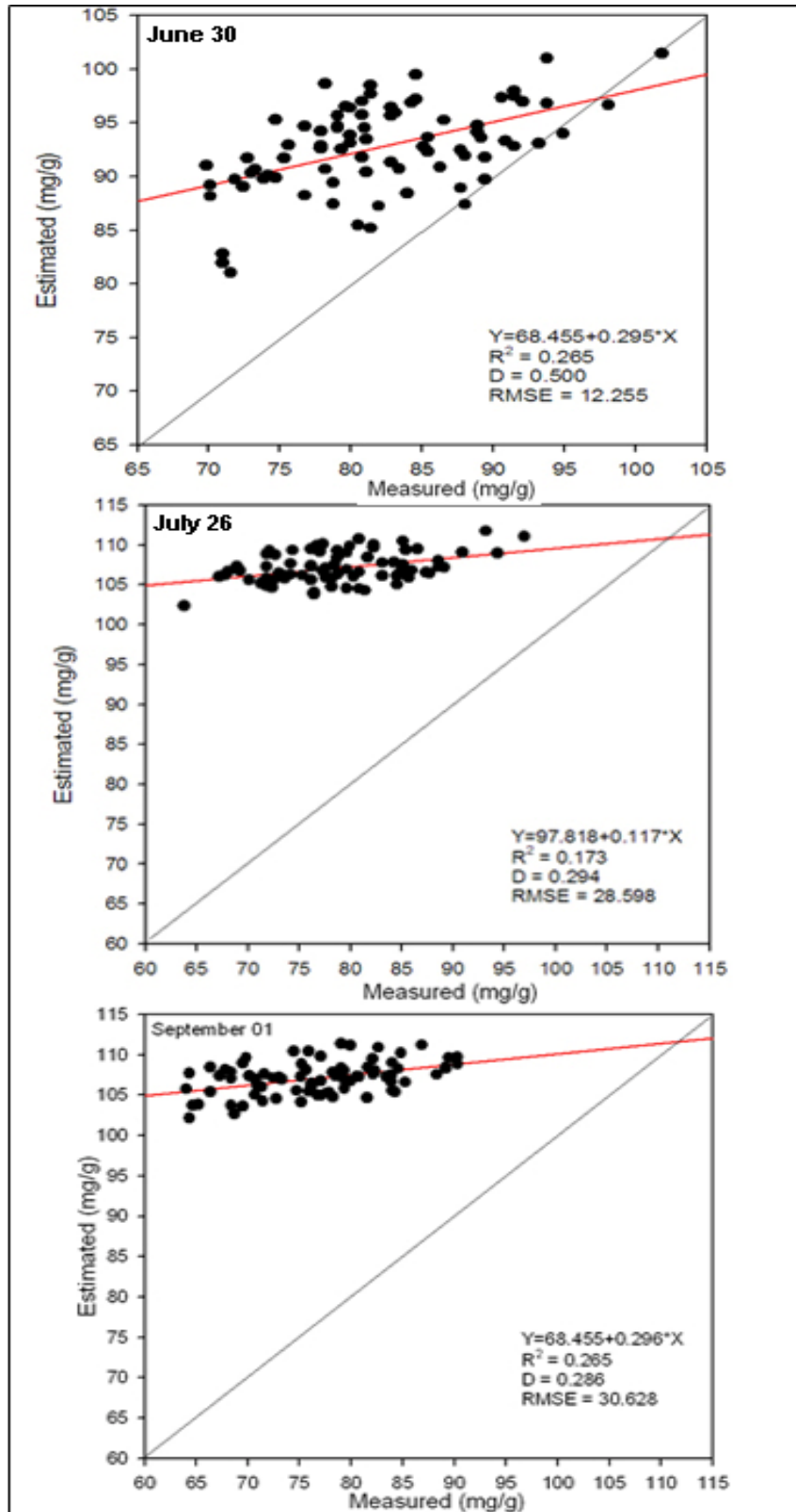


Figure 5-6 Regression (red line) of canopy chlorophyll from SDI Model in June, July, and September 2004 (black solid line is the 1:1 line)



#### **5.5.4 Analysis of the Chlorophyll Models**

A canopy is composed of many individual leaves that vary in size, shape, orientation, age, and biochemical properties. A canopy normally has several layers of leaves. The upper leaves shadow the lower leaves. Canopy reflectance is formed by a combination of reflectance and scattering of radiation by leaves, shadow, and backgrounds. It was found that the optical properties of individual leaves are not directly related to canopy reflectance (Curran and Milton 1983). The scattering of leaves is an important characteristic of canopy structure which is controlled by plant height, leaf density, layers, and canopy closure. The three chlorophyll models are obviously affected by canopy structure and soil background compared with those at the leaf scale.

The TCI model is substantially affected by soil background and canopy structure. The influence of soil background on the TCI model lowers the estimation of chlorophyll content in the early growing season. The influence of soil on the TCI model is ignored in the middle and late growing season because of the high density and closure of tallgrass in the July and September. The influence of canopy structure on the TCI model could be inferred from the relationship between TCI and LAI. LAI is an important vegetation parameter to estimate canopy structure. The correlation between TCI and LAI was -0.312 in June, -0.488 in July, and -0.358 in September (Table 5.1). The TCI model is more strongly affected by canopy structure in the middle and late growing season. This is related to the increase of canopy density and closure with the maturity of vegetation.

The influence of canopy structure is still reflected from the derivative spectra. The influence of LAI on the first derivative spectra increases with the maturity of vegetation. The correlations between LAI and FDI were 0.21, 0.275, and 0.285 in June, July, and

September, respectively (Table 5.2). The correlations between LAI and SDI were 0.164, 0.282, and 0.205 in June, July, and September, respectively. The correlations between the derivative spectral indices and LAI are obviously lower than those between TCI and LAI, especially in the middle and late growing season. This means the influence from canopy structure could be reduced from the derivative transform.

The TCI model is also affected by canopy greenness cover. The greenness cover is different from canopy closure, but they are closely related. The greenness cover is the proportion of greenness to contribute to the canopy spectral reflectance. Canopy closure is the percentage of vegetation covering ground. With the influence of shadow in canopy, the greenness cover is normally less than 100%, even the canopy closure is 100%. The correlation between TCI and the greenness cover was 0.253, 0.269, and 0.152 in June, July, and September, respectively. The TCI model is much more influenced by the greenness cover in the early growing season. In the late growing season, with the maturity of vegetation, more and more dead and yellowish leaves are dominant canopy vegetation. The influence of greenness cover was weak in the late growing season. The derivative models (FDI and SDI) are less influenced by the greenness cover. The correlation between FDI and greenness cover is less than 0.1 and the correlation between SDI and greenness cover are less than 0.15 in the growing season (Table 5.2).

The bias of sample collection should be an important factor to affect the validation of the chlorophyll model. The canopy chlorophyll content is measured with the SPAD meter to calculate average value with five leaves from the dominant grasses in a plot. The five leaf samples that were randomly selected depended on collector's experience and knowledge about species of the canopy. Leaf chlorophyll content varies

with growing stage and location of canopy. The chlorophyll content also varies in different part of a single grass leaf. The average of chlorophyll content from five leaf samples could not exactly represent the canopy chlorophyll content. The sampling error could seriously affect the measurement of canopy chlorophyll and further devaluate the validation of the simulated models.

## **5.6 Conclusions**

Canopy spectral reflectance is affected by canopy chlorophyll, canopy structure, and background. The correlations between canopy spectral reflectance and chlorophyll content vary with the growing season. There is a relatively high correlation between spectral reflectance and canopy chlorophyll content in the early growing season (in June and July), but the relationship is weak in the late growing season (in September). In the early growing season, the influence of canopy structure on reflectance is weak with the low leaf density and canopy closure. The influence of canopy chlorophyll on canopy reflectance decreases with the maturity of vegetation and the presence of standing dead material in the canopy.

With the comparison of five spectral indices derived from original spectral reflectance, the TCI shows stable correlation to canopy chlorophyll content in all of the growing season. NDVI is only correlated to canopy chlorophyll content in the early growing season. NDVI could be effective to estimate canopy chlorophyll content in the early growing season, but it is not effective in the late growing season. The TCI shows relatively effective in estimating canopy chlorophyll content in the whole growing season, but the TCI is obviously affected by soil background in the early growing season and affected by canopy structure in the late growing season.

The derivative transform of spectral reflectance could reduce the influence of canopy structure and backgrounds. The ratio of first derivative spectra at 717 nm and 523 nm is found high correlated to canopy chlorophyll and shows stable in all of the growing season. The second derivative spectra could further reduce the spectral noise caused by canopy structure and background. The second derivative spectra at 689 nm and 692 nm shows highly correlated to canopy chlorophyll content in the whole growing season, which is consistent with the results at the leaf scale. The peaks of second derivative spectra at 717 nm and 722 nm are found related to canopy structure such as LAI and greenness cover. Those results indicate that the derivative spectra could separate the influence of canopy chlorophyll from canopy structure. The ratio of  $F'_{717}$  and  $F'_{523}$  and the second derivative at 689 nm and 692 nm are high correlated to canopy chlorophyll content with low influence of LAI and greenness cover. Those derivative spectra could be more effectively to estimate chlorophyll content in both canopy and leaf scale than the spectral indices of original spectral reflectance.

The three chlorophyll models derived from original, first-order, and second-order derivative spectra are significantly related to the measured chlorophyll content. The TCI model derived from the original spectral is obviously affected by canopy structure and soil background and shows underestimated chlorophyll content in the early stage of vegetation. The FDI and SDI model derived from the first and second order derivative spectra could reduce the influence soil background and showed relatively highly correlation to the measured chlorophyll content in the early growing season. However, both FDI and SDI models are obviously influenced by canopy structure, especially in the middle and late growing seasons. The FDI and SDI models overestimate the canopy

chlorophyll content in the middle and late growing season. This could be related to the high density and closure of canopy with the maturity of vegetation in tallgrass prairie. The TCI model is better used for chlorophyll estimation in the middle and late growing season, but the derivative indices (FDI and SDI) are preferred used in the early growing season.

There are many factors affecting validation of the three models. The bias sampling of leaves could generate the measure error that could seriously affect the validation accuracy of the simulated models. The average chlorophyll content of five leaf samples could not exactly represent the canopy chlorophyll content, especially in the heterogeneous vegetation. The estimation of canopy chlorophyll content with a SPAD meter by measuring an average of dominant leaves may generate the measurement errors of canopy chlorophyll in a heterogeneous canopy. A SPAD chlorophyll meter is an efficient tool to measure canopy chlorophyll content in single species vegetation, but may be ineffective in a heterogeneous canopy with multiple species.

# CHAPTER 6 - APPLICATION OF LEAF-SCALE SPECTRAL MODELS FOR HYPERSPECTRAL IMAGES

## 6.1 Introduction

Extension of the chlorophyll models from leaf scale to canopy scale was studied in the previous chapter. Estimation of chlorophyll at the canopy scale was found not to be a simple aggregation of leaf-scale estimates, but a complex process affected by the canopy structure and the leaf chlorophyll content. Canopy spectral reflectance was substantially affected by canopy density and layers. In this chapter, the TCI, FDI, and SDI models of chlorophyll are extended to fine-scale images to further evaluate their ability to estimate canopy chlorophyll content.

The hyperspectral AISA images used for chlorophyll analysis were acquired in May and August 2002 with 1-m, 2-m, and 3-m spatial resolution. More spectral information of the images was listed in Table 3.1. All spectral index images were derived from the 1-m hyperspectral images. The TCI images were generated with four bands: 550 nm, 675 nm, 700 nm, and 800 nm (Figure 6.2). The derivative images could not be generated with the five-point numerical differentiation technique described in Chapter 3 with Equation 3.10 because of the spectral limitation and variety of band intervals in the hyperspectral images, but instead they were generated with the band difference method shown in Equation 3.12. The second derivative image was derived from two first derivative images with equation 3.12.

The FDI image was generated using the ratio of two first derivative bands at 722 nm and 526 nm instead of the derivative bands at 717 nm and 523 nm used at the leaf scale because the derivative bands at 717 nm and 523 nm could not be generated from the hyperspectral images. The first derivative images at band 526 nm were generated with bands at 537 nm and 516 nm bands in the May image and at 555 nm and 497 nm bands in the August image. The first derivative images at band 722 nm were generated with bands at 742 nm and 701 nm bands in the May image and at 749 nm and 694 nm bands in the August image.

The SDI images were derived from the second derivative band at 693 nm generated from bands at 682 nm, 694 nm, and 701 nm in the May image and with bands at 672 nm, 694 nm, and 713 nm in the August image. The chlorophyll contents from the spectral index images were converted from the TCI, FDI, and SDI models generated in Chapter 4.

Field samples were collected concurrently with the image acquisition and used to validate the image estimation of chlorophyll. Biannual burned treatment (002C) and unburned treatment (020B) were used to represent various vegetation types. Two grids were selected in each treatment, one on an east-facing slope (called West slope) and one on a west-facing slope (called East slope). Sixty measurement points were designed with a nested structure in each grid (see Figure 3.5). Each plot was associated with one pixel in image through its GPS coordinates (Figure 6.1). Canopy chlorophyll content in each plot was estimated from an average of measured chlorophyll from five dominant leaves using the SPAD chlorophyll meter. The canopy chlorophyll content was converted from SPAD units with equation 4.11.

**Figure 6-1 Ground sample location in 020B plotted on a 1-m false color image with bands of 508, 636, and 783 nm (black points represent the location of field sampling plots)**

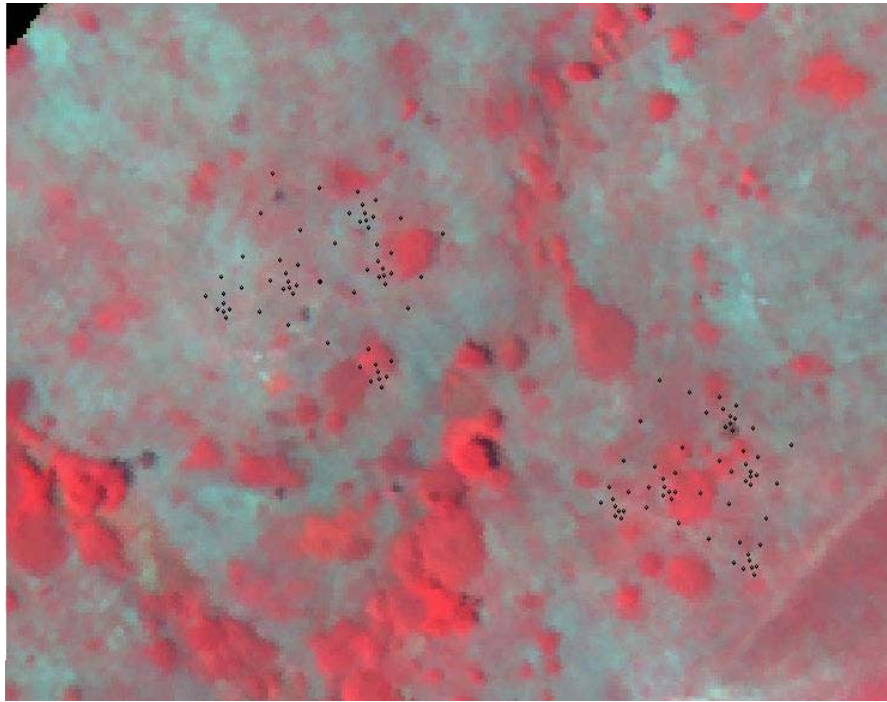
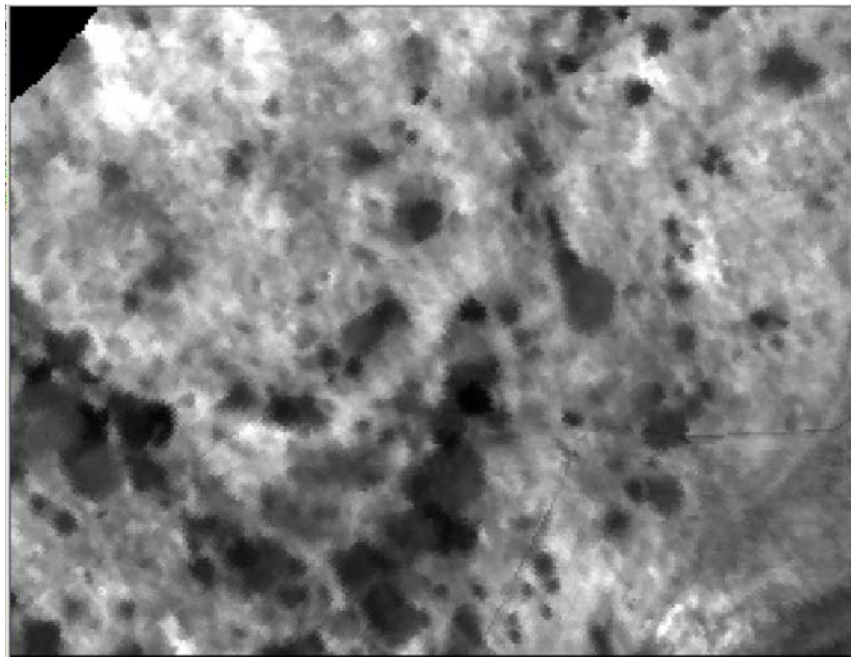


**Figure 6-2 The TCI image was derived from the spectral reflectance with green, red edge, and NIR bands of the hyperspectral image acquired in May 2002**



## **6.2 Relationship between Spectral Index Images and Field Canopy Chlorophyll Measurement**

### **6.2.1 Correlation between TCI image and Canopy Chlorophyll Content**

The TCI image was generated from the AISA images using the TCI formula (equation 4.7). Correlation analysis was conducted between TCI image and field sampling plots. The field canopy chlorophyll content was estimated with an average of chlorophyll content measured from five dominant leaves using the SPAD chlorophyll meter at each plot. Table 6.1 shows that the TCI images are highly correlated to canopy chlorophyll content. The correlations between the TCI image and estimated canopy chlorophyll were 0.608 at 002CW and 0.631 at 020BE in May. The correlation was up to 0.72 at 020BW in August, although the correlations were relatively low in the other three grids with  $r$  ranged from 0.47 to 0.52 in August.

The correlation between the TCI image and canopy chlorophyll content varies seasonally and topographically. The correlations are generally higher in the east slope than that in the west slope, and are higher in August than in May. This could be related to the change in species composition from May to August. In the early growing season, the vegetation is a complex of cool-season species ( $C_3$  species) and warm-season ( $C_4$ –species). In contrast,  $C_4$  plants are the dominant species of canopy in August as the  $C_3$  species become dormant due to heat in the later summer. The diversity of plant species can affect canopy heterogeneity and further affect canopy spectral reflectance and sampling errors. The spatial heterogeneity in the early growing season is higher than that in the later summer (Briggs and Nellis 1991). High spatial heterogeneity of canopy in

May could reduce the correlation between TCI and canopy chlorophyll. The topographic aspects could also affect ground surface reflectance of sunlight and further affect image magnitude.

The TCI image is obviously affected by canopy LAI that could diminish the relationship of TCI and canopy chlorophyll. As canopy structure has relatively strong reflectance in the NIR region (Liang 2001), the spectral reflectance at the red edge is affected by both canopy LAI and chlorophyll. The TCI index using green, red edge, and NIR regions is obviously affected by the spectral overlap caused by the canopy LAI and chlorophyll reflectance. The correlations between TCI and LAI were high with 0.636 in May and 0.421 in August at 020BE (Table 6.1). The correlations were  $r=0.421$  in May and  $r=0.378$  in August at 020BW. The correlations in the frequently burned treatment (002C) were relatively low with  $r=0.2$ . This reflects that canopy structure (LAI) also has an important influence on TCI images. This finding is consistent with the results from the canopy-scale analysis in Chapter 5.

### **6.2.2 Correlation between FDI Image and Canopy Chlorophyll Content**

The FDI image derived from the first derivative spectral image is highly related to canopy chlorophyll content, especially in August. The correlations between FDI image and chlorophyll content were  $r=0.45$  in May and  $r=0.618$  in August at 020BE. The  $r$ -values were 0.471 in May and 0.516 in August at 002CW. However, the correlations are relatively low at 020BW. The correlations at 020BW were  $r=0.323$  in May and  $r=0.457$  in August.

The influence of canopy structure on the FDI image is obviously lower than that on the TCI image. This could be reflected from the correlation between canopy LAI and

the FDI image. The correlations between the image FDI and LAI were less than 0.33 in all of the four grids. The results indicate the derivative transform can reduce the influence of canopy structure on spectral reflectance which is overlapped in spectra with canopy chlorophyll.

### **6.2.3 Correlation between SDI Image and Canopy Chlorophyll Content**

The SDI image was negatively correlated to the canopy chlorophyll content. The correlations are especially high in the unburned treatment (020B). The correlations between the SDI image and canopy measured chlorophyll were  $r = 0.683$  in May and  $r = 0.606$  in August at 020BE. The correlations were  $r = 0.459$  in May and  $r = 0.468$  in August at 020BW (Table 6.1). The correlations are relatively low in the frequently burned treatment (002C). The correlations were ranged from 0.396 to 0.655 at 002C treatment.

The influence of LAI on the second derivative image is weak compared with that on the first derivative image. The correlations between LAI and the SDI image were less than 0.25 in all grids. The correlations ( $r$ ) were close to zero in August at 020B and 002CW. This indicates that the SDI images had no linear relationship with the canopy structure (LAI).

## **6.3 Validation of Image Chlorophyll Content with Field Measurement**

### **6.3.1 The TCI Model**

The estimated chlorophyll derived from the TCI model applied to images is linearly related to the field canopy measurement, but the significance varies with different grids and seasons (Table 6.2). The prediction of chlorophyll from the TCI model

is significant in the May image, especially on the frequently burned treatment. The RMSE was less than 11 mg from canopy chlorophyll measurement ranged between 50 and 95 mg on the frequently burned treatment (002C) with in May and August. The RMSE is relatively higher in the unburned treatment (020B). The RMSE ranged from 12 to 17 mg at 020B with chlorophyll measurement ranged between 65 and 120 mg in May and August.

Degree of agreement ( $d$ ) is an index to measure the similarity of estimation from measurement. The  $d$ -value ranges from 0 to 1. High  $d$ -value means the regression line close to the 1:1 prediction line (see chapter 5 for definition). The  $d$ -values were generally low in all of the grids. The  $d$ -value was relative higher in May than in August at the frequently burned treatment, but it was the same on the unburned treatment (Table 6.2). The  $d$ -value on 020B east was relatively high with 0.5 and the RMSE was 15 mg in May and August. This means the TCI model works better on the unburned treatment than on the frequently burning treatment.

It is also noted that most measured chlorophyll on the other three grids is below the 1:1 line in the May image (Figure 6.3). This means the predicted chlorophyll from the TCI model was below the measurement. This suggests that the TCI model underestimates canopy chlorophyll content in May, which is consistent with the findings in Chapter 5 at the canopy scale.

**Table 6-1 The correlations (r) of canopy chlorophyll content and canopy LAI with the TCI, FDI, and SDI indices from hyperspectral images in May and August 2002 at 002C and 020B treatments on Konza Prairie**

		May		August	
		Chl	LAI	Chl	LAI
TCI	002CE	-0.416	-0.257	-0.473	-0.281
	002CW	-0.591	-0.236	-0.712	-0.311
	020BE	-0.615	-0.636	-0.475	-0.476
	020BW	-0.451	-0.421	-0.516	-0.378
FDI	002CE	0.539	0.249	0.336	0.388
	002CW	0.471	0.195	0.516	0.051
	020BE	0.450	0.283	0.618	0.326
	020BW	0.323	0.171	0.457	0.183
SDI	002CE	-0.396	-0.035	-0.655	0.210
	002CW	-0.562	-0.246	-0.241	-0.014
	020BE	-0.683	-0.213	-0.606	-0.030
	020BW	-0.459	-0.117	-0.468	-0.018

### 6.3.2 The FDI Model

The validation of canopy chlorophyll from the FDI model is shown in Figure 6.5 and Figure 6.6. The FDI model works better on the unburned treatment than on the frequently burned treatment, and works better in May than in August on the frequently burned treatment. The  $d$ -value was high on the unburned treatment with 0.611 on 020BE in May and 0.617 on 020BW in August. The  $d$ -values were also high on the frequently burned treatment in May with 0.589 and 0.587 on 002C east and west grids, respectively. The  $d$ -values were relatively low on 002C in August with 0.266 for east grid and 0.465 for west grid.

The RMSE was low in May for all grids with less than 11 mg. The RMSE was only 4.76 mg on 002C west and 7.76 mg on 002C east in May. However, the RMSE was high on 002C in August with about 26 mg in both grids. The RMSE was low on the unburned treatment in both May and August. The RMSE was 10 mg on 020B east and 9 mg on 020B west in May, and was 12 mg on 020B east and 14 mg on 020B west in August. Thus, the FDI model works better on the unburned treatment.

The regressions of chlorophyll content in the frequently burned treatment are obviously above the 1:1 line in May and August, and the regressions in the unburned treatment are below the 1:1 line in August (Figure 6.6). This indicates that the estimated FDI model overestimates canopy chlorophyll content of grass canopy and underestimates canopy chlorophyll content of woody canopy.

**Table 6-2 Validation of the TCI, FDI, and SDI models with field estimation of canopy chlorophyll in May and August hyperspectral images at 002C and 020B treatment on the Konza Prairie**

		May			August		
		RMSE	D	R <sup>2</sup>	RMSE	D	R <sup>2</sup>
002CE	TCI	7.714	0.500	0.217	11.436	0.397	0.138
	FDI	7.761	0.589	0.291	25.808	0.266	0.135
	SDI	25.428	0.282	0.134	26.085	0.242	0.429
002CW	TCI	9.904	0.416	0.238	8.727	0.458	0.127
	FDI	4.761	0.587	0.222	15.556	0.465	0.266
	SDI	16.006	0.254	0.203	22.859	0.331	0.058
020BE	TCI	15.228	0.485	0.398	14.993	0.494	0.226
	FDI	10.709	0.611	0.227	12.260	0.473	0.382
	SDI	13.030	0.520	0.466	10.276	0.443	0.368
020BW	TCI	17.471	0.424	0.213	12.700	0.434	0.103
	FDI	9.294	0.454	0.192	14.081	0.617	0.530
	SDI	11.985	0.481	0.280	13.688	0.469	0.209

The divergence of chlorophyll estimation from the FDI model is strongly controlled by the canopy component and structure. The effectiveness of the FDI model is related to the density and greenness cover of canopy (See Chapter 5). The litter from the previous year on 002C is an important component of canopy in the early growing season and has strong influence on canopy spectral reflectance. However, the derivative transform can diminish the spectral reflectance from litter and soil background. This is the reason why the FDI model works better on 002C in May. In the later summer, plants

are high and canopy becomes dense and closure. The influence of litter and soils on canopy spectral reflectance is minimized and the function of derivative transform is not significant.

### 6.3.3 The SDI Model

The validations of SDI model for canopy chlorophyll estimation are showed in Figure 6.7 and Figure 6.8. The estimation of chlorophyll content from the SDI model is obviously above the 1:1 line in both May and August images. This means that the SDI model overestimates the canopy chlorophyll content. The SDI model only works better on the unburned treatment. The RMSE was low on 020B in both May and August images. The RMSE was 13 mg on 020BE and 12 mg on 020BW in May, and was 10 mg on 020BE and 14 mg on 020BW in August. However, the RMSE was high on the frequently burned treatment. The RMSE was 25 mg on 02CE and 16 mg on 02CW in May, and was over 25 mg on both grids in August with chlorophyll measurement ranged from 50 to 95 mg. This means the SDI model is less effective on the frequently burned treatment.

The  $d$ -values of the SDI model were also low on the frequently burned treatment. The  $d$ -value was less than 0.33 on 002C in both May and August image. The  $d$ -value was relatively high on 020B with about 0.5 in May and August. The  $d$ -value on 020BE was 0.52 in May and 0.44 in August. The  $d$ -value on 020BW was 0.481 and 0.469 in May and August, respectively. Thus, the SDI model is more effective to estimate canopy chlorophyll on the unburned treatment than on the frequently burned treatment.

## 6.4 Factors Affecting the Three Models for Chlorophyll Estimation

From the previous data analysis, it is apparent that all of the three models are strongly affected by vegetation seasonal change. The variation of correlations between the predicted and measured chlorophyll content in May and August could be related to species composition and diversity. The canopy is dominated by cool- season grasses ( $C_3$ ) and warm-season grasses ( $C_4$ ), and woody species and forbs increase the canopy species diversity in the early growing season. In contrast, the canopy in the summer is dominated by warming-season ( $C_4$ ) grasses and woody species since the  $C_3$  grasses become dormant with high temperature. The species diversity is higher in the early growing season than that in the summer. Plant species composition and diversity in grasslands can significantly influence the ecosystem primary productivity and associated spatial heterogeneity (Collins and Steinauer 1998, Knapp *et al.*, 1999). The spectral reflectance is more complex in a heterogeneous canopy than that in a homogeneous canopy.

The relationship of the model prediction and canopy chlorophyll measurement obviously varied with burning treatments. Model performance is better on the unburned treatment (020B) compared to the frequently burned treatment (002C). This could be related to canopy composition, plant species, and sampling error. In the biannually burned treatment (002C), warm-season grasses are the dominant species with no or less woody species. However, the thick and dense dead materials at 002C take high percent of canopy cover in the early growing season. The spectral reflectance from the dead materials can influence the spectra model, especially for the TCI model. The influence is less from the derivative models because the derivative transformation could decrease the

background influence. Although a thick layer of standing dead material and litter also exists in the unburned treatment, it has less influence on canopy reflectance in the woody vegetation because the upper layer contributes most spectral reflectance. The standing dead plants could significantly affect spectral reflectance and further influence vegetation index (Rundquist 2000).

Sampling error cannot be ignored in the heterogeneous vegetation. The plant species composition was simple in the frequently burned treatment (002C), but the canopy composition was complex, including a combination of dead, yellow, and green leaves. It was difficult to collect leaf samples evenly to represent the canopy for chlorophyll measurement. However, as more shrub-land occupies on the unburned treatment (020B), the vegetation became more patchy and it was easier to collect leaf samples from the upper canopy layer in each patch to represent the entire canopy. The sampling errors could be reduced from the canopy of shrub land. This may be related to the higher correlations of the estimated and measured chlorophyll at 020BE.

## **6.5 Conclusions**

The TCI, FDI, and SDI derived from the hyperspectral image are found highly correlated to the canopy chlorophyll content. The correlation is obviously affected by the canopy composition and structure. The effect of the canopy LAI on the spectral indices could be clearly reflected from the correlation between spectra indices and LAI. The TCI derived from the original spectrum is strongly influenced by the canopy LAI. The influence could be reduced with derivative transform. The FDI derived from the first derivative has weak influence of LAI. The SDI generated from the second derivative has no relation with canopy LAI.

The validation of the TCI, FDI, and SDI models showed that the models are effective to estimate canopy chlorophyll content under different stages of vegetation. The TCI model is more effective with high greenness cover and density vegetation. The TCI could underestimate canopy chlorophyll content in a sparse canopy because of the influence of soil background. The derivative models (FDI and SDI models) are effective in sparse vegetation because derivative transformation can reduce the influence of soil backgrounds. The FDI model is more effective than the SDI model at the frequently burned treatment. In contrast, the SDI model is better than the FDI model to predict chlorophyll content at the unburned treatment. Both FDI and SDI models could overestimate the canopy chlorophyll in a density canopy because of the influence of the canopy structure. The findings from the image are consistent with the results found from the canopy in Chapter 5.

The application of the three models on images is more complex than that on the canopy. The image data is strongly affected by atmospheric absorption and refraction, topographic distortion and reflection, and surface albedo, but the field canopy data can ignore those influences and only consider the effect of the canopy structure and density. The validation of the three models on images was lower than that on the field canopy estimation. The low validation could also be affected by the sampling error. It is difficult to collect even samples of five leaves in a canopy with high species diversity. The bias sampling can affect the estimation of canopy chlorophyll and further affect the validation accuracy of the image estimation of chlorophyll.

**Figure 6-3 Regression of canopy chlorophyll content from the TCI model (Red line) in May image at 002C and 020B treatments in East and West slopes. The solid blank line represents the 1:1 line**

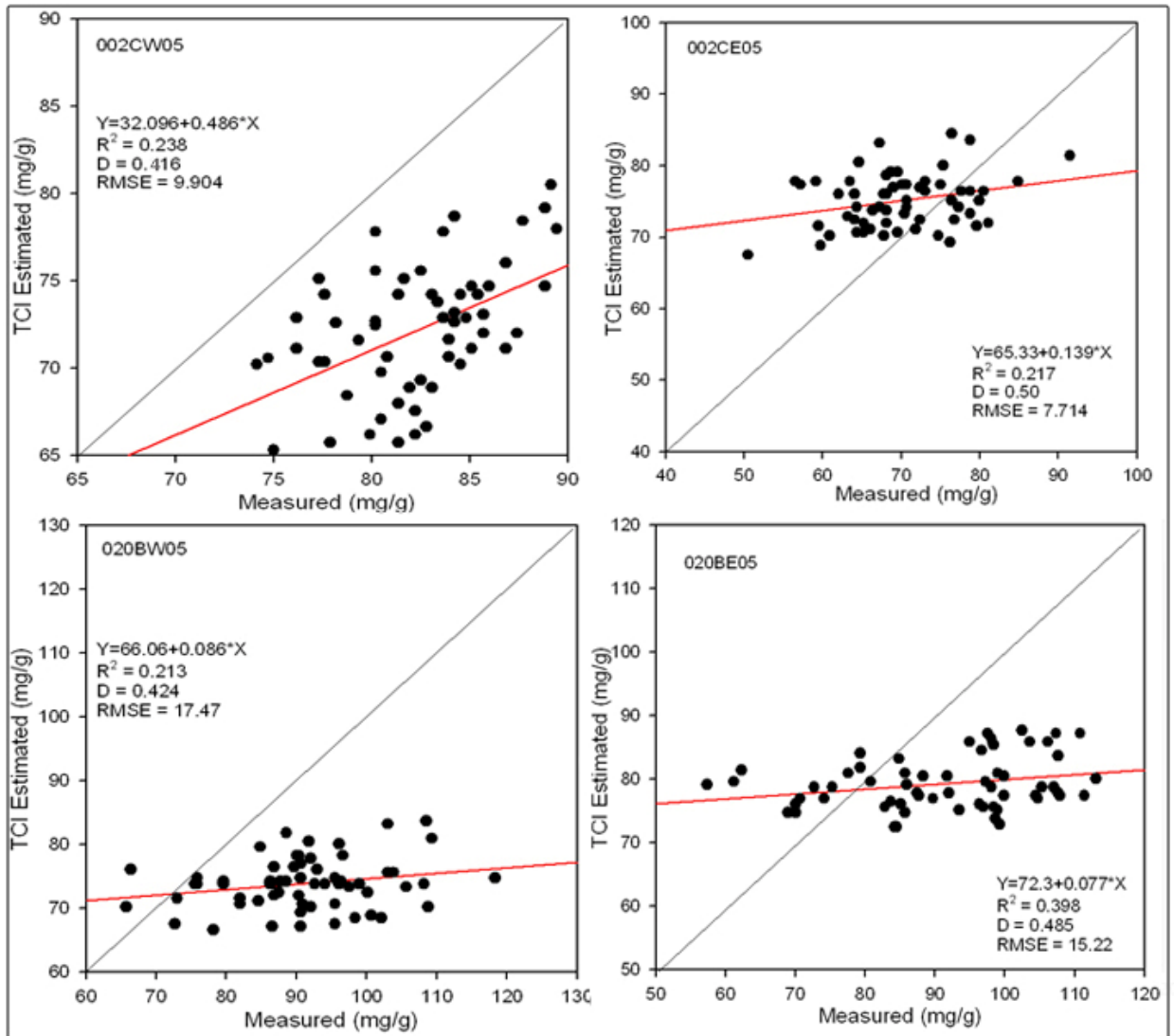


**Figure 6-4 Regression of canopy chlorophyll content from the TCI model (Red line) in August image at 002C and 020B treatments in the East and West slopes. The solid blank line represents the 1:1 line**

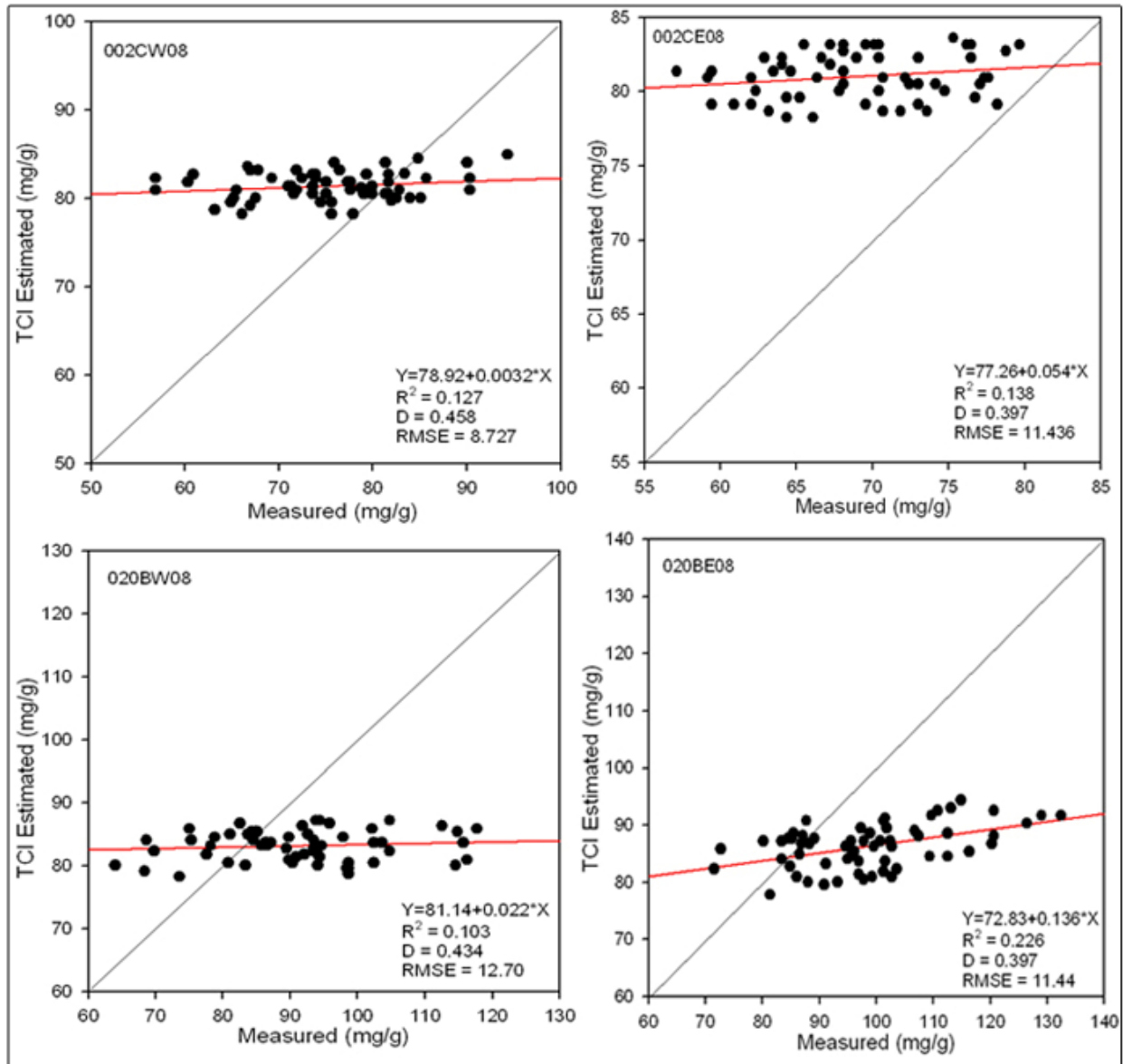


**Figure 6-5 Regression of canopy chlorophyll content from the FDI model (Red line) in May image at 002C and 020B treatments in East and West slopes. The solid blank line represents the 1:1 line**

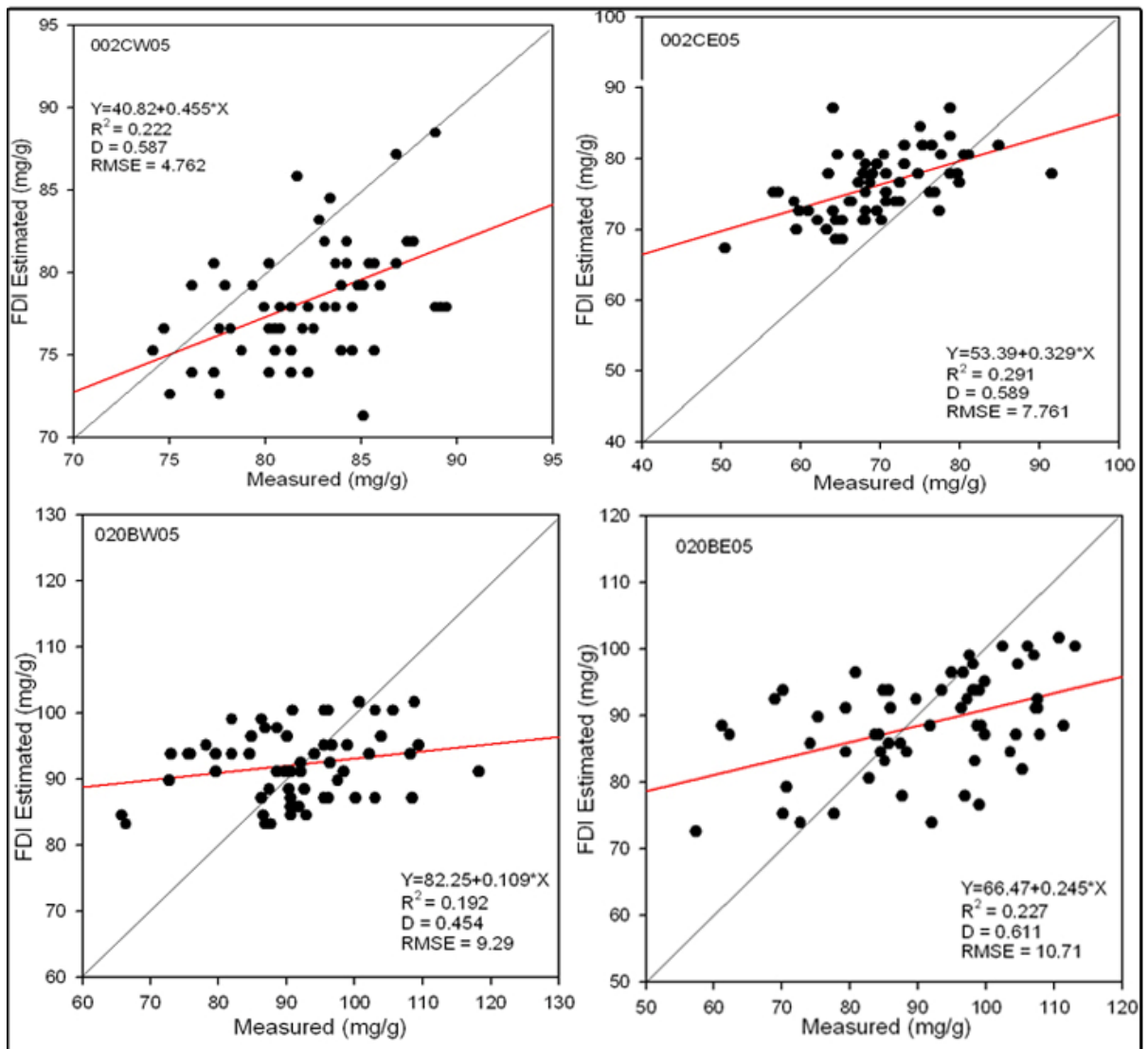


**Figure 6-6 Regression of canopy chlorophyll content from the FDI model (Red line) in August image at 002C and 020B treatments in East and West slopes. The solid blank line represents the 1:1 line**

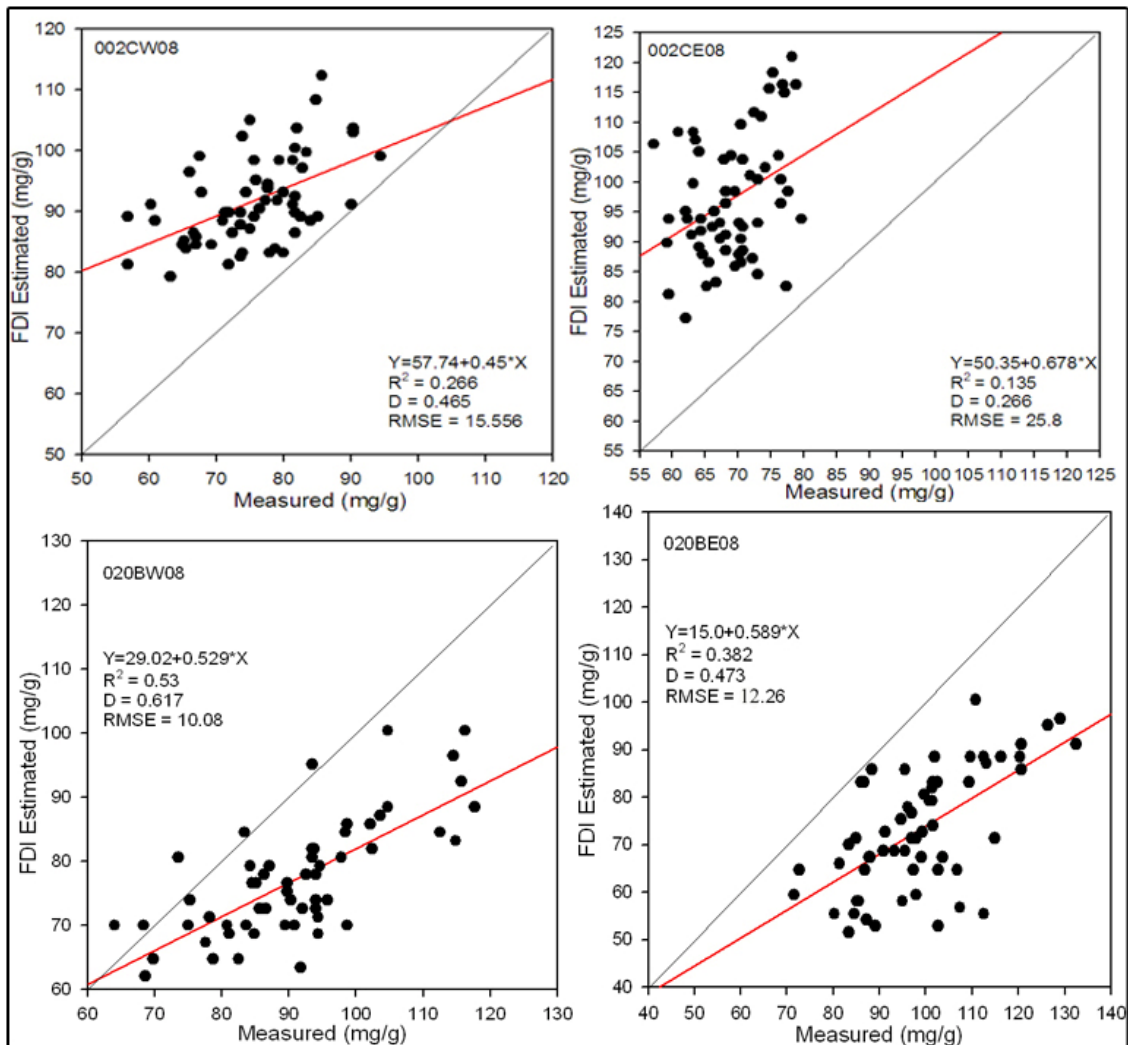


**Figure 6-7 Regression of canopy chlorophyll content from the SDI model (Red line) in May image at 002C and 020B treatments in East and West slopes. The solid black line represents the 1:1 line**

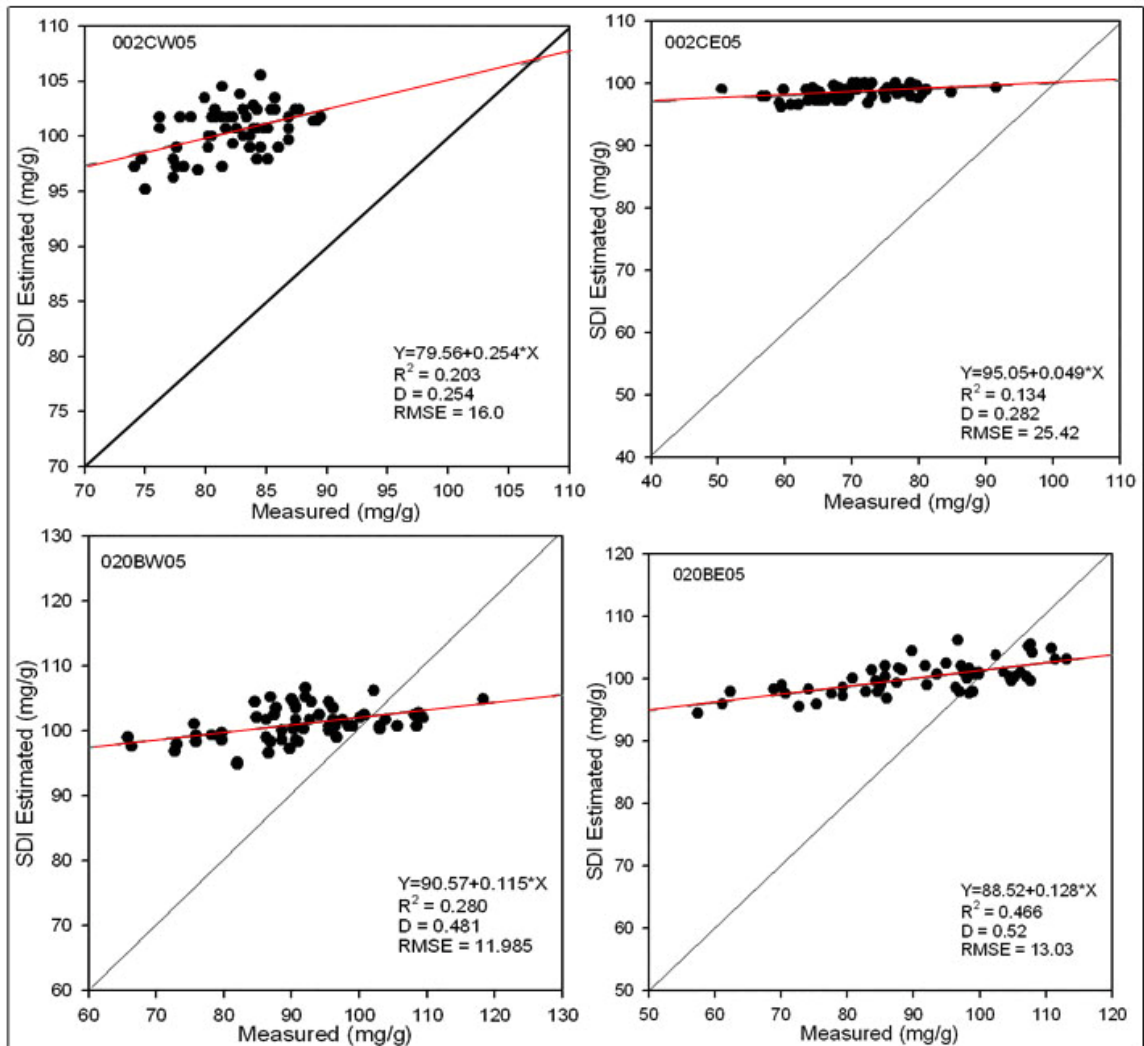
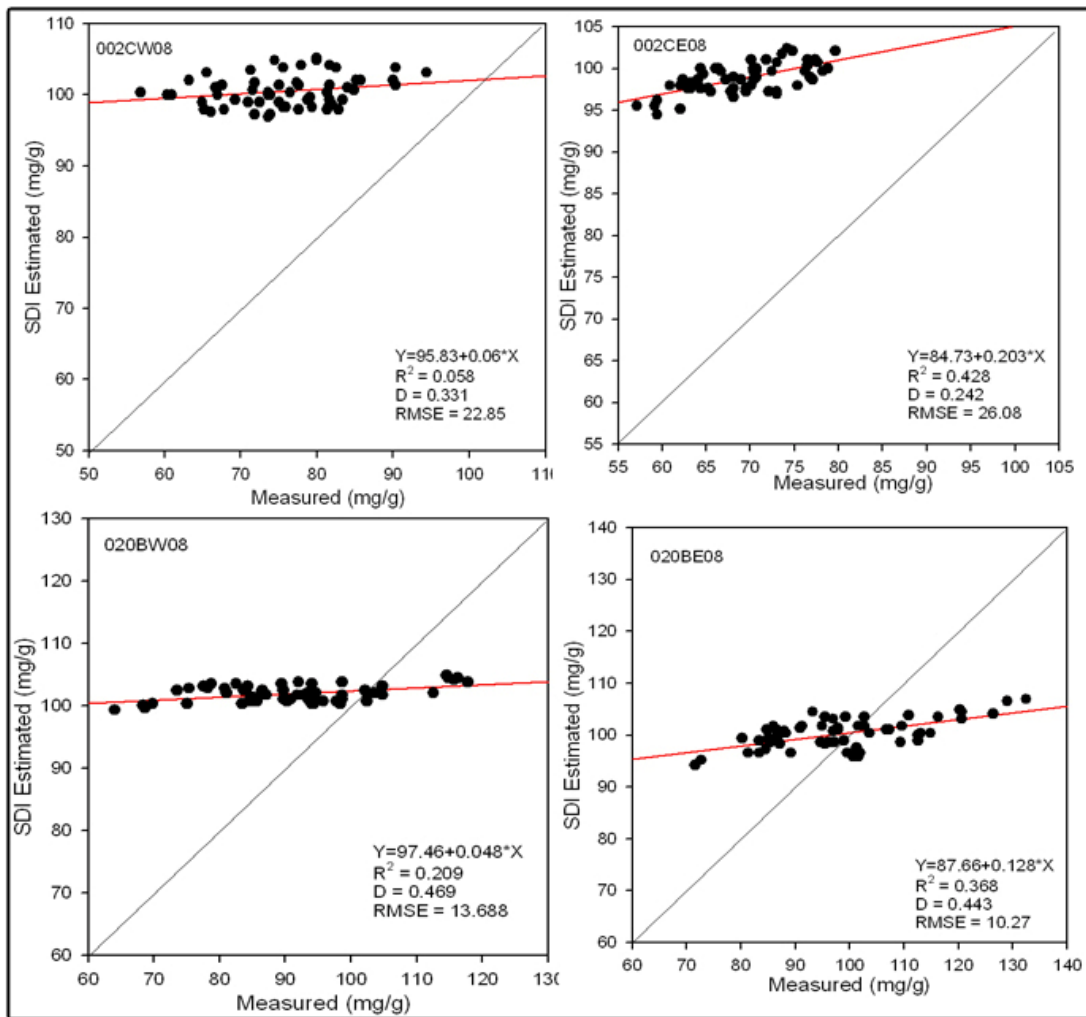


**Figure 6-8 Regression of canopy chlorophyll content from the SDI model (Red line) in August image at 002C and 020B treatments in East and West slopes. The solid blank line represents the 1:1 line**



## CHAPTER 7 - CONCLUSIONS

This dissertation presents an exploration of plant chlorophyll estimation using spectral reflectance data at different spatial scales. Three models were derived from reflectance spectrum and derivative spectra to estimate leaf chlorophyll content, and were compared with the measurement of chlorophyll (Chl) content with two conventional methods: solvent extraction and SPAD chlorophyll meter (Chapter 4). The three models derived from leaf scale were extended to canopy scale. Canopy spectral reflectance was measured with a hyperspectral photometer and was used to estimate canopy Chl content with the three models. The estimation of canopy Chl with the three models was further validated against field canopy Chl measured using a SPAD chlorophyll meter (Chapter 5). The three models were then applied to fine scale hyperspectral images to estimate Chl content over a larger area. The estimation of Chl content derived from the imagery was validated against canopy field Chl measurements (Chapter 6).

In addition to evaluating existing chlorophyll extraction methods, one new model was derived from the hyperspectral reflectance to estimate leaf chlorophyll content. Since the spectral response of green leaves varies with different growing stages, most spectral indices were not consistently effective for estimating chlorophyll content across seasons. A new triangle chlorophyll index (TCI) was developed in this research by using green, red, and near infrared data from hyperspectral reflectance curves. This new index shows relatively high correlation with leaf chlorophyll content in the growing seasons ( $r > 0.80$ ).

The spectral indices derived from the spectral reflectance curves were strongly influenced by the soil backgrounds and canopy litter. To remove or reduce the influence

of these background canopy components, derivative transformation of spectral reflectance was used. The first derivative spectrum was derived from the reflectance spectrum with 5-point numerical method. Two peaks were identified, which occur most commonly at  $\approx 523$  nm and  $\approx 717$  nm in the first derivative spectrum. The ratio of the first derivative spectra at 717 nm and at 523 nm was used as the first derivative index (FDI) and the index was found to be well correlated to leaf Chl content ( $r > 0.80$ ).

Second derivative spectra were further derived from the first derivative spectra using a 5-point numerical method. One peak most commonly occurs at  $\approx 689$  nm or  $\approx 692$  nm in the second derivative spectra. The peak values of the second derivative spectra at 689 nm and 692 nm were used to form the second derivative index (SDI). The SDI index was well correlated to leaf chlorophyll content in all the growing seasons ( $r = 0.8$ ). This suggests that TCI and the indices derived from the first and second derivative spectra could effectively estimate leaf chlorophyll content. Three models were derived from the TCI, FDI, and SDI indices to estimate chlorophyll content at leaf scale based on the field samples collected in all growing season in 2004.

With the canopy scattering and background influence, the spectral reflectance of canopy is more complex than that of individual leaves. Spectral reflectance from the canopy actually represents a combined response of leaf chlorophyll content, leaf area index, and soil backgrounds. The TCI index that was effective in estimating leaf chlorophyll content shows a relatively weak correlation with canopy Chl measurement. The correlation between TCI and canopy Chl was only up to  $r = 0.54$  in the early growing season. However, the TCI index was strongly correlated to canopy LAI ( $r \approx 0.5$ ). This

research shows that canopy structure and background have a significant influence on Chl estimations at the canopy scale, compared to the leaf scale.

The derivative transformation improved the relationship between remotely sensed Chl indices and canopy Chl content. The ratio of  $R'_{717}$  and  $R'_{523}$  was found to be well correlated to leaf Chl content. The correlation between the FDI and the canopy Chl content in canopy was relatively high throughout the growing season. The influence of LAI on FDI was also low.

The indices of second derivative spectra developed from leaf scale were found to be highly correlated to the canopy Chl content. The correlation between the second derivative spectra (SDI) at 689nm or 692 nm and the canopy Chl was over 0.60 in the early growing season. The second derivative spectra were obviously less influenced by the canopy LAI. The correlation between SDI and LAI was less than 0.15.

The low correlations between the spectral indices and canopy chlorophyll should also be affected by sampling errors in the heterogeneous vegetation. Average of five sample leaves cannot be efficient to represent canopy chlorophyll content at a spot because of the high species diversity. The canopy species on the Konza prairie are dominated by warm-season grasses, but forbs and woody species are also commonly distributed in the grassland. The high species diversity of canopy makes it difficult to evenly collect leaf samples at each plot, and further affects the accuracy of canopy chlorophyll estimation. Some previous researches have found effective indices to estimate canopy chlorophyll content, but the indices were used on crops with homogeneous canopy (Gitelson *et al.* 2003b).

The three Chl estimation models derived from the three spectral indices (TCI, FDI, and SDI) showed that the Chl models at the canopy scale are obviously affected by canopy structure and soil background. The TCI model normally underestimates the canopy Chl content in sparse vegetation, but is more effective to estimate canopy Chl in a dense and full greenness cover canopy. The FDI and SDI models normally overestimated canopy Chl content in the dense vegetation, but were more effective in the early growing season with sparse canopy because the derivative transformation could remove the influence of the soil background.

Application of the three Chl estimation models derived from the TCI, FDI, and SDI indices to fine-scale image data showed that the TCI model was most effective in the early growing season (May) compared to the later growing season (August). In contrast, the FDI model was more effective on the unburned treatment in all growing seasons and effective on the biannual burned treatment in the early growing season. This result reflected the difference of the vegetation in the unburned and the biannual burned treatments. The canopy is dominated by woody species on the unburned treatment, but mainly consists of grasses on the biannual burned treatment. On the biannual burned treatment, the canopy was sparse with less green cover in May because of the influence of litter from previous year, but the canopy was dense and closure with green cover in the late growing season. This suggests that the Chl models are strongly affected by the soil background and the canopy composition and structure. This research also shows that the application of the models derived from leaf scale is complicated at the image scale by the influence of atmosphere, sun angle, and topography.

The main contribution of this dissertation was the method to estimate the Chl content. One new index derived from the spectral reflectance and two indices from the derivative spectra were shown to be effective to estimate the leaf Chl content. These indices were correlated to the traditional Chl measurement in all growing seasons at the leaf scale. However, the three models were also shown to have limitations when applied to the canopy scale *in-situ* data and the fine-resolution imagery. These limitations are due to the influence of abiotic and non-living biotic components of the canopy, as well as to the canopy structure.

This research could be used in several applications. First, it provides additional insight into estimating the Chl content at various spatial scales using hyper-spectral remote sensing. Because of the difficulties inherent in the traditional, field-based methods for Chl estimation, remote sensing provides the only practical tool for making spatially extended estimation of this important canopy biophysical property. The majority of published literature in this field consists of studies applied to either the cropland or the forest, this research shows that similar methods can be applied to the grasslands. The FIFE project conducted on the Konza Prairie 20 years ago verified that remote sensing could be used to extract ground biophysical attributes on grassland with similar physiology. However, this research found the application of remote sensing has limitation to estimate canopy chlorophyll on heterogeneous canopy because of the influence of canopy structure and components. The results herein also suggest that these methods must be applied with caution due to the significant effects of canopy properties and seasonality on the accuracy of remotely sensed Chl estimation derived from the canopy level data or from the imagery. Within these limitations, the techniques developed here

provide a useful technique for nutrient management and biomass assessment in the grasslands.

Second, this research shows that the transformation from the leaf scale to the canopy scale is a complex process. Spectral metrics used at the leaf scale may not be used at the canopy scale because of the canopy scattering and the background noise.

Derivative transformation applied to reflectance spectra can minimize the effects of background and improve the correlation between the spectra indices and the Chl content to some extent, but again, the techniques must be applied with caution. Last, but not least, this research would provide useful information for selecting a rescaling factor and a method for the image rescale.

### **Limitation and Future Studies**

Since this research was conducted on the tallgrass prairie, all of the conclusions derived from the grasslands need to be also validated in other biomes (e.g. forests, savanna). The spectral metrics to extract the leaf Chl content were derived from green, red, and near infrared region based on healthy grass leaves. Further validations on different species such as broad-leaf forest and forbs are necessary. The validation of rescale from the canopy to the image is conducted on images with fine scale resolution and should be further tested on the coarse-scale resolution imagery.

The transformation of Chl extraction from the leaf scale to the canopy scale is a very important issue in contemporary remote sensing. Due to the complex canopy structure in the tallgrass prairie, it is difficult to equally collect field samples that will actually represent the canopy Chl content. The measurement errors of the canopy Chl

content exist. This research suggests that the model should be further validated on different heterogeneous canopy structure.

## References

Aase, J. K., J. P. Millard, and B. S. Brown, 1986. Spectral radiation estimates of leaf area and leaf phytomass of small grains and native vegetation. *IEEE Trans. Geosci. Remote Sens.* GE-24:685-692.

Ahmad I.S., J. F. Reid, N. Noguchi, and A. C. Hansen, 1999. Nitrogen sensing for precision agricultural using chlorophyll maps. *ASAE/CSAE-SCGR Annual International Meeting*, Toronto, ON, Canada, July 18-21.

Allen, W., A. V. Gayle, and A. J. Richardson, 1970. Pant-canopy irradiance specific photosynthetic radiation and leaf area index from spectral reflectance in wheat. *Agron. J.* 76:300-306.

Aman, A, H. P. Randriamanantena, A. Podaire, and R. Frouin, 1992. Upscale integration of normalized difference vegetation index: the problem of spatial heterogeneity, *IEEE Transactions on Geoscience and Remote Sensing* 30(2): 326-338.

Arnon, D. I., 1949. Copper enzymes in isolated chloroplasts. Polyphenoloxidases in *Beta vulgaris*. *Plant Physiol* 24:1-15.

Asrar, G., M. Fuchs, E. T. Kanemasu, and J. L. Hatfield, 1984. Estimating absorbed photosynthetic radiation and leaf area index from spectral reflectance in wheat. *Agron. J.* 76:300-306.

Badwhar, G. D., R. B. MacDonald, F. G. Hall, and J. C. Carnes, 1986. Spectral characterization of biophysical characteristics in a boreal forest: relationships between Thematic Mapper band reflectance and leaf area index for aspen. *IEEE Transactions of Geoscience and Remote Sensing* 24:322-6.

Baret, F., and G. Guyot, 1991. Potentials and limits of vegetation indices for LAI and APAR assessment. *Remote Sensing of Environment* 35:161-173

Bark, D. 1987. Konza Prairie Research Natural Area, Kansas. In *The Climates of the Long-Term Ecological Research Sites*, Ed. D. Greenland. University of Colorado: Institute of Arctic and Alpine Research.

Barnes, J. D., L. Balaguer, E. Manrique, S. Elvira, and A. W. Davison, 1992. A reappraisal of the use of DMSO for the extraction and determination of chlorophylls a and b in lichens and higher plants. *Environmental and Experimental Botany* 32:85-100.

Bartlett, D. S., G. J. Whiting, and J. M. Hartman, 1990. Use of vegetation indices to estimate intercepted solar radiation and net carbon dioxide exchange of a grass canopy. *Remote Sensing of Environment* 30:115-28.

Benedict, H. M., and R. Swidler, 1961. Non-destructive method for estimating chlorophyll content of leaves. *Science* 133:2015-2016.

Bian, L. 1997. Multiscale nature of spatial data in scaling up environmental models. In *Scale in Remote Sensing and GIS*, ed. D.A. Quattrochi and M. F. Goodchild, pp 13-16. Boca Raton, FL: CRC Press.

Bian, L. and R. Butler, 1999. Comparing effects of aggregation methods on statistical and spatial properties of simulated spatial data. *Photogrammetric Engineering & Remote Sensing* 65(1):73-84.

Blackmer, T. M., and J. S. Schepers, 1995. Use of a chlorophyll meter to monitor N status and schedule fertigation of corn. *J. Production Agriculture* 8:56-60.

Blackmer, T. M., and J. S. Schepers, and G. E. Varvel, 1994. Light reflectance compared with other nitrogen stress measurements in corn leaves. *Agronomy J.* 86:934-938.

Blackmer, T. M., and J. S. Schepers, G. E. Varvel, and E. A. Walter-Shea, 1996. Nitrogen deficiency detection using shortwave radiation from irrigated corn canopies. *Agronomy J.* 88:1-5.

Blonski, S., G. Gasser, J. Russell, R. Ryan, G. Terrie, and V. Zaroni, 2002. Synthesis of multispectral bands from hyperspectral data: validation based on images acquired by AVIRIS, Hyperion, ALI, and ETM+, *Proceedings, Annual AVIRIS Conference*, Pasadena: NASA Jet Propulsion Laboratory: Pasadena, <http://eis.jpl.nasa.gov/aviris/html/aviris.biblios.html#2002>.

Bonham-Carter, G. F. 1988. Numerical procedures and computer program for fitting an inverted Gaussian model to vegetation reflectance data, *Computer Geoscience* 14:339-356.

Bowyer, P., and F. M. Danson, 2004. Sensitivity of spectral reflectance to variation in live fuel moisture content at leaf and canopy level, *Remote Sensing of Environment* 92:297-308.

Bragg, T. B., and L. C. Hulbert, 1976. Woody plant invasion of unburned Kansas bluestem prairie. *Journal of Range Management* 29:19-23.

Briggs, J. M., and M. D. Nellis, 1991. Seasonal variation of heterogeneity in tallgrass prairie: a quantitative measure using remote sensing. *Photogrammetric Engineering and Remote Sensing* 57: 407-411.

Briggs, J. M., and A. K. Knapp, 1995. Interannual variability in primary production in tallgrass prairie: climate, soil moisture, topographic position and fire as determinants of aboveground biomass. *American Journal of Botany* 82: 1024-1030.

Briggs, J.M. and A. K. Knapp, 2001. Determinants of C3 forb growth and production in a C4 dominated grassland. *Plant Ecology* 152:93-100.

Broge, N. H., and E. L. Leblanc, 2000. Comparing prediction power and stability of broadband and hyperspectral vegetation indices for estimation of green leaf area index and canopy chlorophyll density, *Remote Sensing of Environment* 76:156-172.

Bunnik, N. J. J. 1978. *The Multispectral Reflectance of Shortwave Radiation by Agricultural Crops in Relation with Their Morphological and Optical Properties*. H. Vennman and Zonen, B. V. Waseningen. pp175.

Burden, R. L., and J. D. Fares, 1989. *Numerical Analysis*, 4<sup>th</sup> ed., PWS-Kent, Boston.

Buschman, C., and E. Nagel, 1993. In vivo spectroscopy and internal optics of leaves as a basis for remote sensing of vegetation. *International Journal of Remote Sensing* 14:711-722.

Butler, W. L., and D. W. Hopkins, 1970. Higher derivatives analysis of complex absorption spectra. *Photochem. Photobiol.* 12:439-450.

Campbell, G. S., 1986. Extinction coefficients for radiation in plant canopies calculated using an ellipsoidal inclination angle distribution. *Agric. For. Meteorol.* 36: 317.321.

Campbell, James B. 1996. *Introduction to Remote Sensing*, Second Edition. New York: The Guilford Press.

Card, D. H., D. L. Peterson, P. A. Matson, and J. D. Aber, 1988. Prediction of leaf chemistry by the use of visible and near infrared reflectance spectroscopy. *Remote Sensing of Environment* 26:123-147.

Carter, G. A. 1994. Ratios of leaf reflectance in narrow wavebands as indicators of plant stress. *International Journal of Remote Sensing* 15:697-703.

Ceccato, P., S. Flasse, S. Tarantola, S. Jacquemoud, and J. M. Gregoire, 2001. Detecting vegetation leaf water content using reflectance in the optical domain, *Remote Sensing of Environment* 77:22-33.

Chadburn, B. P. 1982. Derivative spectroscopy in the laboratory: advantages and trading rules. *Anal. Proc.* 54:42-45.

Chappelle, E. W., M. S. Kim, and J. E. McMurtrey, 1992. Ratio analysis of reflectance spectra (RARS): an algorithm for the remote estimation for the concentration of chlorophyll *a*, chlorophyll *b*, and carotenoids in soybean leaves. *Remote Sensing of Environment* 39:239-247.

Chen, D., J. Huang, and T. J. Jackson, 2005. Vegetation water content estimation for corn and soybeans using spectral indices derived from MODIS near- and short-wave infrared bands, *Remote Sensing of Environment* 98:225-236.

Collins, W., 1978. Remote sensing of crop type and maturity. *Photogrammetric Engineering and Remote Sensing* 44:43-55.

Collins, J. B., and C. E. Woodcock, 1999. Geostatistical estimation of resolution-dependent variance in remote sensed images. *Photogrammetric Engineering and Remote Sensing* 6(1):41-50.

Collins, S.L., 1992. Fire frequency and community heterogeneity in tallgrass prairie vegetation. *Ecology* 73:2001-2006.

Collins, S.L. and E.M. Steinauer, 1998. Disturbance, diversity and species interactions in tallgrass prairie. Pages 140-156 in A.K. Knapp, J.M. Briggs, D.C. Hartnett, and S.L.

Collins, (eds.) *Grassland Dynamics: Long-term Ecological Research in Tallgrass Prairie*. Oxford University Press. New York, NY.

Committee on Earth Sciences, 1989, *Our Changing Planet: The FY90 Research Plan*, The U.S. Global Change Research Program, U.S. Department of Interior, Reston, VA.

Craig, M. D. 1994. Minimum-volume transforms for remotely sensed data, *IEEE Trans. Geosci. Remote Sensing* 32:99-109.

Curran, P. J., 1980. Multispectral remote sensing of vegetation amount. *Progress in Physical Geography* 4:315-41.

Curran, P. J., and E. J. Milton 1983. The relationships between the chlorophyll concentration, LAI, and reflectance of a simple vegetation canopy, *International Journal of Remote Sensing* 4(2):247-55.

Curran, P. J., 1989. Remote sensing of foliar chemistry. *Remote Sensing of Environment*, 30:271-278.

Curran, P. J., J. L. Dungan, and H. L. Gholz, 1991. Exploring the relationship between reflectance red-edge and chlorophyll content in slash pine. *Tree Physiology*, 7:33-48.

Curran, P. J., J.L. Dungan, B. A. Macler, and S. E. Plummer, 1991. The effect of a red leaf pigment on the relationship between red edge and chlorophyll concentration. *Remote Sensing of Environment* 35:69-76.

Dall'Olmo, G., A. A. Gitelson, and D. C. Rundquist, 2003. Towards a unified approach for remote estimation of chlorophyll-a in both terrestrial vegetation and turbid productive waters, *Geophysical Research Letters*, 30(18),1938,doi:10.1029/2003GL018065

Darks, S. M., E. H. Evans, and P. A. Whittaker, 1983. *Photosynthetic Systems. Structure Function and Assembly*, Wiley, New York.

Datt, B., 1998. Remote sensing of chlorophyll *a*, chlorophyll *b*, chlorophyll *a+b*, and total carotenoid content in Eucalyptus leaves, *Remote Sensing of Environment* 66:111-121.

Daughtry, C. S. T., K. P. Gallo, S. N. Goward, S. D. Prince, and W. P. Kustas, 1992. Spectral estimates of absorbed radiation and phytomass production in corn and soybean canopies, *Remote Sensing of Environment* 19:2133-39

Daughtry, C. S. T., C. L. Walthall, M. S. Kim, E. Brown de Colstoun, and J. E. McMurtrey III, 2000, Estimating corn leaf chlorophyll concentration from leaf and canopy reflectance, *Remote Sensing of Environment* 74: 229-239.

Dawson, T., P. Curran, and S. Plummer, 1998. LIBRTY: Modeling the effects of leaf biochemistry on reflectance spectra, *Remote Sensing of Environment* 65:50-60.

De cola, L., 1994. Simulating and mapping spatial complexity using multiscale techniques. *International Journal of Geographic Information Systems* 8: 411-421.

Demetriades-Shah, T. H., M. D. Steven, and J. A. Clark, 1990. High resolution derivative spectra in remote sensing, *Remote Sensing of Environment* 33:55-64.

Fang, H, and S. Liang, 2003. Retrieve LAI from landsat 7 ETM + data with a neural network method: simulation and validation study, *IEEE Trans Geoscience and Remote Sensing* 41:2052-2062.

Fell, A. F., and G. Smith, 1982. Higher derivative methods in ultraviolet-visible and infrared spectrophotometry. *Anal. Proc.* 54:28-32.

Foody, G., and D. Cox, 1994. Sub-pixel land cover composition estimation using a linear mixture model and fuzzy membership model and fuzzy membership function, *Int. J. Remote Sensing* 15:619-631.

Fourty, T. and F. Baret, 1997. Vegetation water and dry matter contents estimate from top-of-atmosphere reflectance data: a simulation study, *Remote Sensing of Environment* 61:34-45.

Freeman, C.C. 1998. The flora of Konza Prairie: A historical review and contemporary patterns. In *Grassland Dynamics: Long-Term Ecological Research in Tallgrass Prairie*, ed. A. K. Knapp, J. M. Briggs, D. C. Hartnett, and S. L. Collins, pp. 3-15. New York: Oxford University Press.

Gao, B. C., 1996. NDWI: a normalized difference water index for remote sensing of liquid water from space, *Remote Sensing of Environment* 58:257-266.

Gao, J., and D. G. Goodin, 2004. Determining landscape structure and heterogeneity using image texture indices. *Papers and Proceedings of the Applied Geography Conferences* 27:187-197.

Gardner, B. R., and B. L. Blad, 1986. Evaluation of spectral reflectance models to estimate corn leaf area while minimizing the influence of soil background effects. *Remote Sensing of Environment* 20:183-193

Garrison, L. M., D. D. Doda, and A. E. S. Green, 1979. Total ozone determination by spectroradiometry in the middle ultraviolet, *Appl. Opt.* 18:850-854.

Gibson, P. J., and C. H. Power, 2000. *Introductory Remote Sensing: Digital Image Processing and Applications*, London: Routledge, 249 pp

Gilbert, M. A., S. Gandia, and J. Melia, 1996. Analysis of spectral- biophysical relationships for a corn canopy. *Remote Sensing of the Environment* 54:38-48.

Gilbert, M. A., M. N. Merzlyak, and H. K. Lichtenthaler, 1996. Detection of red edge position and chlorophyll content by reflectance measurement near 700 nm. *Journal of Plant Physiology* 148:501-508.

Gitelson, A. A., and M. N. Merzlyak, 1994. Spectral reflectance changes associated with autumn senescence of *Aesculus hippocastanum* L. and *Acer platanoides* L. leaves. Spectral features and relation to chlorophyll estimation. *Journal of Plant Physiology* 143:286-292.

Gitelson, A. A., and M. N. Merzlyak, 1996. Signature analysis of leaf reflectance spectra: algorithm development for remote sensing of chlorophyll, *Journal of Plant Physiology* 148:494-500.

Gitelson, A. A., C. Buschman, and H. K. Lichtenthaler, 1999. The chlorophyll fluorescence ratio F735/F700 as an accurate measure of chlorophyll content in plants, *Remote Sensing of Environment* 69:296-302.

Gitelson, A. A., Y. Zur, and M. N. Merzlyak, 2002. Assessing carotenoid content in plant leaves with reflectance spectroscopy. *Photochem. Photobiol.* 75:272-281.

Gitelson, A. A., U. Gritz, and M. N. Merzlyak 2003a, Relationships between leaf chlorophyll content and spectral reflectance and algorithms for non-destructive chlorophyll assessment in higher plant leaves, *J. Plant Physiol.*, 160, 271– 282.

Gitelson, A. A., A. Vina, V. Ciganda, D. C. Rundquist, and T. J. Arkebauer, 2003b. Remote estimation of canopy chlorophyll content in crops, *Geophysical Research Letters*, 32:L08403

Gitelson, A. A., A. Vina, S. B. Verma, D. C. Rundquist, T. J. Arkebauer, G. G. Burba, and A. E. Suyker, 2006. Relationship between gross primary production and chlorophyll content in crops: implications for the synoptic monitoring of vegetation productivity, *Journal of Geophysical Research, Atmosphere* (in press).

Goel, N. S., and R. L. Thompson, 1984. Inversion of vegetation canopy reflectance models for estimating agronomic variables. V. Estimation of leaf area index and average leaf angle using measured canopy reflectance, *Remote Sensing of Environment* 16:69-85.

Goel, N. S. 1988. Models of vegetation canopy reflectance and their use in estimation of biophysical parameters from reflectance data. *Remote Sensing Reviews* 4:1-212.

Gong, P., X. Mei, G.S. Biging Z. Zhang, 2002. Improvement of oak canopy model extracted from digital photogrammetry. *PE&RS*. 68(9): 919-924.

Goodin, D. G., L. Han, R. N. Fraser, D. C. Rundquist, and W. A. Stebbins, 1993. Analysis of suspended solids in water using remotely sensed high resolution derivative spectra, *Photogrammetric Engineering & Remote Sensing* 59(4):505-510.

Goodin, D. G., and G. M. Henebry, 1997. A technique for monitoring ecological disturbance in tallgrass prairie using seasonal NDVI trajectories and a discriminant function mixture model. *Remote Sensing of the Environment* 61: 270-278.

Goodin, D. G., and G. M. Henebry, 1998. Seasonality of finely-resolved spatial structure of NDVI and its component reflectances in tallgrass prairie, *International Journal of Remote Sensing* 19: 3213-3220.

Goodin, D. G., and G. M. Henebry, 2002. The effect of rescaling on fine spatial resolution NDVI data: a test using multi-resolution aircraft sensor data, *Int. J. Remote Sensing* 23(18):3865-3871.

Goodin, D. G., J. Gao, and G. M. Henebry, 2004, The effect of solar illumination angle and sensor view angle on observed patterns of spatial structure in tallgrass prairie. *IEEE Transactions on Geoscience and Remote Sensing*, 42(1):154-165.

Guyot, G., F. Baret, and S. Jacquemoud, 1992. Imaging spectroscopy for vegetation studies. In F. Toselli and J. Bodechtel, Eds. *Imaging Spectroscopy: Fundamentals and Prospective Applications*, pp 145-165.

Haboudane, D., J. R. Miller, N. Tremblay, P. J. Zarco-Tejada, and L. Dextraze, 2002. Integration of hyperspectral vegetation indices for prediction of crop chlorophyll content for application to precision agriculture. *Remote Sensing of Environment* 81: 416–426.

Hall, F. G., K. F. Huemmrich, S. J. Goetz, P.J. Sellers, and J. E. Nickeson 1992. Satellite remote sensing of surface energy balance: successes, failures and unresolved issues in FIFE . *Journal of Geophysical Research* 97: 19061-89.

Hartnett, D. C., K. R. Hickman, and L. E. F. Walter, 1996. Effects of bison grazing, fire and topography on floristic diversity in tallgrass prairie, *Journal of Range Management* 49:413-420.

Hartnett, D.C. and P.A. Fay, 1998. Plant populations: Patterns and processes. Pages 81-100 in Knapp, A. K., J. M. Briggs, D. C. Hartnett, and S. L. Collins (eds). *Grassland Dynamics: Long-Term Ecological Research in Tallgrass Prairie*. Oxford University Press. New York.

Hatfield, J. L., E. T. Kanemasu, G. Asrar, R. D. Jackson, P. J. Pinter, Jr., R. J. Reginato, and S. B. Idso, 1985. Leaf area estimates from spectral measurements over various planting dates of wheat, *Int J. Remote Sensing* 6:167-175.

Hay, G. J., K. O. Niemann, and D. G. Goodenough, 1997. Spatial thresholds, image-objects, and upscaling: a multiscale evaluation. *Remote Sensing of Environment* 62:1-19

Hay, G. J., D. J. Marceau, P. Dube, and A. Bouchard, 2001, A multiscale framework for landscape analysis: object-specific analysis and upscaling, *Landscape Ecology* 16:471-490.

Hiscox, J. D., and G. F. Israelstam, 1979. A method for the extraction of chlorophyll from leaf tissue without maceration, *Canada Journal of Botany* 57:1332-1334.

Hoffer, R. M., 1978. Biological and physical considerations in applying computer-aided analysis techniques to remote sensor data, In *Remote sensing: The Quantitative Approach*, P. H. Swain and S. M. Davis, eds, McGraw-Hill, pp. 227-289.

Holben, B. N., C. J. Tucker, and C. Fan, 1980. Spectral assessment of soybean leaf area and leaf biomass, *Photogramm. Eng. Remote Sens.* 46:651-656.

Horler, D. N. H., Dockray, M., and J. Barber, 1983. The red-edge of plant leaf reflectance. *International Journal of Remote Sensing* 4:273-288.

Hu, B., S. Qian, D. Haboudane, J. R. Miller, A. B. Hollinger, N. Tremblay and E. Pattey, 2004. Retrieval of crop chlorophyll content and leaf area index from decompressed hyperspectral data: the effects of data compression *Remote Sensing of Environment* 92:139-294.

Huang, Z., B. J. Turner, S. J. Dury, I. R. Wallis, and W. J. Foley, 2004. Estimating foliage nitrogen concentration from HYMAP data using continuum removal analysis *Remote Sensing of Environment* 93:18-29.

- Huete, A. C., 1988. A soil adjusted vegetation index (SAVI). *Remote Sensing of Environment* 17:37-53
- Huete, A. R., 1989. Soil influences in remotely sensed vegetation-canopy spectra, In: G. Asrar Ed. *Theory and Applications of Optical Remote Sensing* pp107-141. New York: Wiley.
- Huete, A. C, C. Justice, and H. Liu, 1994. Development of vegetation and soil indices for MODIS-EOS. *Remote Sensing of Environment* 49:224-234
- Hunt, E., Raymond, Jr., and N. R. Barrett, 1989. Detection of changes in leaf water content using near and middle infrared reflectance, *Remote Sensing of Environment* 30:43-54.
- Jacquemoud, S., 1993. Inversion of the PROSPECT + SAIL canopy reflectance model from AVIRIS equivalent spectra: Theoretical study, *Remote Sensing of Environment* 44:281-292.
- Jacquemoud, S., F. Baret, B. Andrieu, and F. M. Danson, 1995. Extraction of vegetation biophysical parameters by inversion of the PROSPECT + SAIL models on sugar beet canopy reflectance data. application to TM and AVIRIS sensors, *Remote Sensing of Environment* 52:163-172.
- Jenny, H. 1941. *Factors of Soil Formation*. McGraw-Hill, New York, USA.
- Jensen, J. R., 1983. Biophysical remote sensing, *Annals of the Association of American Geographers* 73(1):111-132.
- Jiang, Y., 2001. Physiological and biochemical responses of two cool-season turfgrasses to drought and heat stress, Thesis (Ph.D), Kansas State University.

Johnson, J. R. and J. R. Saunders, 2003. Evaluation of Chlorophyll Meter for Nitrogen Management in Cotton. Annual Report 2002 of the North Mississippi Research and Extension Center, *Mississippi Agriculture and Forestry Experiment Station Bulletin* 398:162-163. ,

Kaufman, Y. J., and D. Tanre, 1992. Atmospherically resistant vegetation index (ARVI) for EOS-MODIS. *IEEE Transactions in Geoscience and Remote Sensing* 30:261-270.

Kim, M. S., C. S.T. Daughtry, E. W. Chappelle, and J. E. McMurtrey, 1994. The use of high spectral resolution bands for estimating absorbed photosynthetically active radiation (APAR). In: *Proc. ISPRS'94*, Val d'Isere, France. pp. 299-306.

Kimes, D. S., B. L. Markham, C. J. Tucker, and J. E. McMurtrey, 1981. Temporal relationships between spectral responses and agronomic variables of a corn canopy. *Remote Sensing of Environment* 11:401-411.

Knapp, A. K., J. T. Fahnestock, S. P. Hamburg, L. J. Statland, T. R. Seastedt, and D. S. Schimel, 1993. Landscape patterns in soil-water relations and primary production in tallgrass prairie, *Ecology* 74: 549-560.

Knapp, A. K., and T. R. Seastedt, 1986. Detritus accumulation limits productivity in tallgrass prairie. *BioScience* 36:662-668.

Knapp, A. K., and T. R. Seastedt, 1998. Introduction : grasslands, Konza Prairie and long-term ecological research. In *Grassland Dynamics: Long-Term Ecological Research in Tallgrass Prairie*, ed. A. K. Knapp, J. M. Briggs, D. C. Hartnett, and S. L. Collins, pp. 3-15. New York: Oxford University Press.

- Knapp, A. K., and S. L. Conard, and J. M. Blair, 1998. Determinants of soil CO<sub>2</sub> flux from a sub-humid grassland: effect of fire and fire history. *Ecological Applications* 8:760-770.
- Knapp, A. K., J. M. Blair, J. M. Briggs, S. L. Collins, D. C. Hartnett, L. C. Johnson, and E. G. Towne, 1999. The Keystone role of bison in North American tallgrass prairie. *BioScience* 49:39-50.
- Knight, C. L., J. M. Briggs, and M. D. Nellis, 1994. Expansion of gallery forest on Konza Prairie Research Natural Area, Kansas, USA. *Landscape Ecology* 9:117-125.
- Knipling, E. B. 1970. Physical and physiological basis for the reflectance of visible and near infrared radiation for vegetation *Remote Sensing of Environment* 1:155-59.
- Knyazikhin, Y., J. V. Martonchik, R. B. Myneni, D. J. Diner, and S. W. Running, 1998. Synergistic algorithm for estimating vegetation canopy leaf index and fraction of absorbed photosynthetically active radiation from MODIS and MISR data, *J. Geophysical Research* 103:32257-32275.
- Kollenkark, J. C., C. S. T. Daughtry, M. E. Bause, and T. L. Housley, 1982. Effects of cultural practices on agronomic and reflectance characteristics of soybean canopies, *Agron. J.* 74:751-758.
- Kubelka, P., and F. Munk, 1931. Ein Beitrag zur optik der farbarstriche. *Z. Tech. Physik* 12, 593.
- Li, X. and A. Strahler, 1985. Geometric-optical modeling of a coniferous forest canopy, *IEEE Trans. Geosci. Remote Sensing* 23:705-721.
- Li, X. and A. Strahler, 1986. Geometric-optical bi-directional reflectance modeling of a coniferous forest canopy, *IEEE Trans. Geosci. Remote Sens.* 24:906-919.

- Liang, S. 2004. *Quantitative Remote Sensing of Land Surface*. John Wiley & Sons, Inc.
- Lichtenthaler, H. K., A. A. Gitelson, and M. Lang, 1996. Non destructive determination of chlorophyll content of leaves of a green and an aurea mutant of tobacco by reflectance measurements, *Journal of Plant Physiology* 148:483-493.
- Liu, J., J. M. Chen, J. Cihlar, and W. M. Pak, 1997. A process-based boreal ecosystem productivity simulator using remote sensing inputs, *Remote Sensing of Environment*, 62:158-175.
- Louchard, E. M., R. P. Reid, and C. F. Stephens, 2002. Derivative analysis of absorption features in hyperspectral remote sensing data of carbonate sediments. *Optics Express* 10 (26):1573-1584
- Lewis, Stacy L. 1996. Development of Water-usage Coefficients for the Tallgrass Prairie. Master thesis, Department of Civil Engineering, Kansas State University.
- Maas, S. J., and Dunlap 1989. Reflectance, transmittance, and absorption of light by normal, etiolated, and albino corn leaves. *Agronomy Journal* 81:105-10.
- Marsh, S. E., and R. J. Lyon 1980. Quantitative relationships of near-surface spectral to Landsat radiometric data. *Remote Sensing of Environment* 10:241-61.
- McLellan, T. M., J. D. Aber, M. E. Martin, J. M. Melillo, and K. J. Nadelhoffer, 1991. Determination of nitrogen, lignin, and cellulose content of decomposing leaf material by near infrared reflectance spectroscopy. *Canada Journal of Forestry Resource* 21:1684-1688.
- McMurtrey, J. E. III, E. W. Chappelle, and M. S. Kim, J. J. Meisinger, and L. A. Corp, 1994. Distinguishing nitrogen fertilization levels in field corn (*Zea mays* L.) with actively

induced fluorescence and passive reflectance measurements, *Remote Sensing of Environment* 47:36-44.

McNaughton, S. J. 1985. Ecology of a grazing ecosystem: the Serengeti. *Ecological Monographs* 55:259-294.

McArthur, D. E., Fuentes, R. W., and Devarajan, V. 2000. Generation of hierarchical multiresolution terrain database using wavelet filtering. *Photogrammetric Engineering & Remote Sensing*, 66(3):287-295.

Merzlyak, M. N., A. E. Solovchenko, and A. A. Gitelson, Reflectance spectral features and non-destructive estimation of chlorophyll, carotenoid and anthocyanin content in apple fruit, *Postharvest Biology and Technology*, 27, 197– 211, 2003.

Moody, A., and C. E. Woodcock, 1995. The influence of scale and the spatial characteristics of landscapes on land-cover mapping using remote sensing, *Landscape Ecology* 10:363-379.

MSR: Multispectral radiometer user's manual and technical reference, Cropscan, Inc, Rochester, MN, 1995.

Nellis, M. D., and J. M. Briggs, 1992. Transformed vegetation index for measuring spatial variation in drought impacted biomass on Konza Prairie, Kansas. *Transactions of the Kansas Academy of Science* 95: 93-99.

O'Havers, T. C. 1982. Derivative spectroscopy and its applications in analysis derivative spectroscopy: theoretical aspects. Plenary Lecture. *Anal. Proc.* 54:22-28.

O'Neill, R. V., C. T. Hunsaker, S. P. Timmins, B. L. Jackson, K. B. Jones, K. H. Riitters, and J. D. Wickham, 1996. Scale problems in reporting landscape pattern at the regional scale. *Landscape Ecology* 11:169-180.

Owensby, C. E., and K. L. Anderson. 1967. Yield responses to time of burning in the Kansas Flint Hills. *Journal of Range Management* 20:12-16.

Patel, N. K., T. P. Singh, B. Sahai, and M. S. Patel, 1983. Relationship between agronomic and spectral parameters in rice crop. *Proc. Int. Colloq. Spectral Signatures of Objects in Remote Sensing*, Bordeaux, France, pp.313-320.

Pearson, R. L., and L. D. Miller, 1972. Remote mapping of standing crop biomass for estimation of the productivity of the shortgrass prairie, Pawnee National Grasslands, Colorado. In *Proceedings of the 8<sup>th</sup> International Symposium on Remote Sensing of the Environment*, pp. 1355-79. Ann Arbor, MI: Environmental Research Institute of Michigan.

Penuelas, J., I. Fielella, C. Biel, L. Serrano, and R. Save, 1993. The reflectance at the 950-970 nm region as an indicator of plant water status, *International Journal of Remote Sensing* 14:1887-1905.

Peterson, T. A., T. M. Blackmer, D. D. Francis, and J. S. Schepers, 1993. Using a chlorophyll meter to improve N management. *Nebguide G93-1171A*. Coop. Ext. Serv., University of Nebraska, Lincoln.

Piekielek, W. P., R. H. Fox, J. D. Toth, and K. E. Macneal, 1995. Use of chlorophyll meter at the early dent stage of corn to evaluate nitrogen sufficiency, *Agron. J.* 87:403-408.

Printer, Jr. P. J., R. D. Jackson, S. B. Idso, and R. J. Reginato, 1983. Diurnal patterns of wheat spectral reflectance, *IEEE Trans. Geosci. Remote Sensing*, GE-21, 156-163.

Quattrochi, D. A., and M. F. Goodchild, 1997. *Scale in Remote Sensing and GIS*. Boca Raton, FL: CRC Press, Inc.

Rasmussen, M. S. 1998. Developing simple, operational, consistent NDVI-vegetation models by applying environmental and climatic information: Part I. Assessment of the net primary production. *International Journal of Remote Sensing* 19(1):97-117.

Richardson, A. J., and C. L. Wiegand, 1977. Distinguishing vegetation from soil background information. *Photogrammetric Engineering and Remote Sensing* 43:1541-1552.

Ridao, E., J. R. Conde, and M. I. Minguéz, 1998. Estimating FAPAR from nine vegetation indices for irrigated and non-irrigated faba bean and semileafless pea canopies, *Remote Sensing of Environment* 66:87-100.

Rundquist, B. C., 2000. *Fine-scale spatial and temporal variation in the relationship between spectral reflectance and a prairie vegetation canopy*, Dissertation, Kansas State University.

Rundquist, B. C., 2002. The influence of canopy green vegetation fraction on spectral measurements over native tallgrass prairie, *Remote Sensing of the Environment* 81: 129-135.

Roujean, J. L., and F. M. Breon, 1995. Estimating PAR absorbed by vegetation from bi-directional reflectance measurements. *Remote Sensing of Environment* 43:1541-1552.

Rouse, J. W., 1973. Monitoring the vernal advancement and retrogradation of natural vegetation. *NASA/GSFCT Type II Report*, Greenbelt, MD.

Running S. W., D. L. Peterson, M. A. Spanner, and K. B. Teuber, 1986. Remote Sensing of coniferous forest area. *Ecology* 67:273-6.

Runyon, J., R. H. R. H. Waring, S.N. Goward, and J. M. Welles, 1994. Environmental limits on net primary production and light-use efficiency across the Oregon Transect. *Ecological Applications* 4(2):226-37.

Sala, O. E., W. J. Parton, L. A. Joece, and W. K. Luenroth, 1988. Primary production of the central grassland region of the United States. *Ecology* 69:40-45.

Savitzky, A., and M. J. E. Golay, 1964. Smoothing and differentiation of data by simplified least squares procedures. *Anal. Proc.* 36:1627-1639.

Sellers, P. J., 1985. Canopy reflectance, photosynthesis and transpiration. *International Journal of Remote Sensing* 6(8):1335-72

Sellers, P. J., M. D. Heiser, and F. G. Hall, 1992. Relations between surface conductance and spectral vegetation indices at intermediate (100 m<sup>2</sup> to 15 km<sup>2</sup>) length scales, *Journal of Geophysical Research* 97(D17): 19033-059.

Sellers, P. J. and F. G. Hall 1992. FIFE in 1992: Results, scientific gains and future research directions. *Journal of Geophysical Research* 97(D17): 19091-109.

Shoaf W. T. and B. W. Lium, 1976. Improved extraction of chlorophyll a and b from algae using dimethyl sulphoxide. *Limnology Oceanogeography* 21: 926-928.

Sudduth, K. A., J. W. Hummel, and S. J. Birrell, 1997. Sensors for site-specific management. *The State of Site-Specific Management for Agriculture*. Editors: F. J. Pierce and E. J. Sadler. pp. 183-209. Madison, WI: ASA-CSSA-SSSA.

Suits, G. H. 1972. The calculation of the directional reflectance of a vegetative canopy. *Remote Sensing of Environment* 2:117-125.

Thenkabail, P.S., R. B. Smith, and E. De Paww, 2000. Hyperspectral vegetation indices and their relationships with agricultural crop characteristics, *Remote Sensing of Environment*, 71:158-182.

Thomas, J. R., and H. W. Gausman, 1977. Leaf reflectance versus leaf chlorophyll and carotenoids concentration for eight crops. *Agronomy Journal* 63:845-847.

Todd, S. W., R. M. Hofer, and D. G. Milchunas, 1998. Bioassessment on grazed and ungrazed rangelands using spectral indices. *International Journal of Remote Sensing* 19(3):427-38.

Tompkins, S., J. F. Mustard, C. M. Pieters, and D. W. Forsyth, 1997. Optimization of endmembers for spectral mixture analysis. *Remote Sensing of Environment* 59:472-489.

Tucker, C. J., L. D. Miller, and R. L. Pearson, 1975. Shortgrass prairie spectral measurements. *Photogrammetric Engineering and Remote Sensing* 41(9):1157-62.

Tucker, C. J., and E. L. Maxwell, 1976. Sensor design for monitoring vegetation. *Photogrammetric Engineering and Remote Sensing* 42(11):1139-410.

Tucker, C. J., 1979. Red and photographic infrared linear combinations for monitoring vegetation. *Remote Sensing of Environment* 8:127-50.

Tucker, C. J., 1980. Remote sensing of leaf water content in the near infrared. *Remote Sensing of Environment* 10:23-32.

Tucker, C. J., J. R. G. Townshend, and T. E. Goff, 1985. African land-cover classification using satellite data, *Science*, 227:369-375.

Turner, M. G., R. V. O'Neill, R. H. Gardner, and B. T. Milne, 1989. Effects of changing spatial scale on the analysis of landscape pattern. *Landscape Ecology* 3:153-162.

Turner, M. G., R. H. Gardner, and R. V. O'Neill, 2001. *Landscape Ecology in Theory and Practice – Pattern and Process*. Springer-Verlag.

Verhoef, W. 1984. Light scattering by leaf layers with application to canopy reflectance modeling: the SAIL model. *Remote Sensing of the Environment*, 16:125-141.

Veron, L. P., and G. R. Seely, Eds. 1966. *The Chlorophylls*, Academic, London.

Vogelman, T. C., B. N. Rock, and D. M. Moss, 1993. Red edge spectral measurements from sugar maple leaves. *International Journal of Remote Sensing* 14:1563-1575.

Walburg, G., M. E. Bauer, C. S. T. Daughtry, and T. L. Housley, 1982, Effects of nitrogen nutrition on the growth, yield, and reflectance characteristics of corn canopies. *Agron, J.* 74:677-683.

Wallihan, E. F., 1973. Portable reflectance meter for estimating chlorophyll concentrations in leaves. *Agronomy Journal* 65:659-662.

Walter-Shea, E. A., B. L. Blad, C. J. Hays, M. A. Mesarch, D. W. Deering, and E. A. Middleton, 1992. Biophysical properties affecting vegetative canopy reflectance and absorbed photosynthetically active radiation at the FIFE site. *Journal of Geophysical Research* 97:18925-34.

Wardley, N. W., and P. J. Curran, 1984. The estimation of green-leaf-area index from remotely sensed airborne multispectral scanner data. *Int. J. Remote Sensing* 5:671-679.

Weakly, H. E. 1962. History of drought in Nebraska. *Journal of Soil and Water Conservation* 17:271-273.

Wehmueller, W. A. 1996. Genesis and morphology of soils on the Konza Prairie Research Natural Area, Riley and Geary Counties, Kansas. M. S. thesis. Kansas State University, Manhattan, Kansas, USA.

Weiser, R. L., 1985. Assessing biophysical characteristics of grassland from spectral measurements. Master's Thesis, Department of Agronomy, Kansas State University.

Weiser, R. L., G. Asrar, G. P. Miller, and E. T. Kanemasu, 1986. Assessing grassland biophysical characteristics from spectral measurements. *Remote Sensing of Environment* 20:141-52.

Wellburn, A. R. 1994. The spectral determination of chlorophylls a and b, as well as total carotenoids, using various solvents with spectrophotometers of different resolution. *J. Plant Physiol.* 144:307-313.

Wessman, C. A., J. D. Aber, D. L. Peterson, and J. M. Melillo, 1988. Remote Sensing of canopy chemistry and nitrogen cycling in temperate forest ecosystems, *Nature* 335:154-156.

Whittaker, R. H., and P. L. Marks, 1975. Methods of assessing terrestrial productivity, in *Primary Productivity of the Biosphere* (H. Lieth and R. H. Whittaker, Eds), Springer-Verlag, New York, pp. 55-118.

White, J. D., S.W. Running, R. Nemani, R. E. Keane, and K. C. Ryan, 1997. Measurement and remote sensing of LAI in Rocky Mountain montane ecosystems, *Can. J. For Res.* 27:1714-1727.

Wiegand, C. L., A. J. Richardson, D. E. Escobar, and A. H. Gerbermann, 1991. Vegetation indices in crop assessment, *Remote Sensing of Environment* 35:105-119

Wiegand, C. L., S. J. Maas, J. K. Aase, J. L. Hatfield, P. J. J. Pinter, R. D. Jackson, E. T. Kanemasu, and R. L. Lapitan, 1992. Multisite analysis of spectral-biophysical data for wheat, *Remote Sensing of Environment* 42:1-21

Willmott, C. J. 1981. On the validation of models. *Physical Geography* 2:184-194.

Wood, C. W., D. W. Reeves, and D.G. Himelrick, 1993. Relationships between chlorophyll meter readings and leaf chlorophyll concentration, N status, and crop yield: a review. *Proc. Agronomy Soc. New Zealand* 23:1-9

Woodcock, C. E. and A. H. Strahler, 1987. The factor of scale in remote sensing. *Remote Sensing of Environment* 21:311-332.

Wylie, B.K., I. Denda, R. D. Pieper, J. A. Harrington, Jr., B. C. Reed, and G. M. Southward 1995. Satellite-based herbaceous biomass estimation in the pastoral zone of Niger. *Journal of Range Management* 48(2):159-64.

Yoder, B. J., and R. H. Waring, 1994. The normalized difference vegetation index of small Douglas-fir canopies with varying chlorophyll concentrations. *Remote Sensing of Environment* 49:81-91.

Yoder, B. J., and R. E. Pettigrew-Crosby, 1995. Predicting nitrogen and chlorophyll content and concentrations from reflectance spectra (400-2500 nm) at leaf and canopy scales. *Remote Sensing of Environment* 53:199-211.

Zhang, M. S. L. Ustin, E. Rejmankova, and E. W. Sanderson, 1997. Monitoring pacific coast salt marshes using remote sensing. *Ecological Applications* 7(3):1039-1053.

**Appendix A - Absorption Spectrum of Chlorophyll  
Content with Solvent Extraction in June 30, 2004**

ID	SPAD	Weight (g)	Wavelength (nm)				
			440	480	510	630	645
1	32.1	0.0698	0.7	0.357	0.123	0.084	0.118
2	32.4	0.0532	0.518	0.276	0.106	0.074	0.09
3	28.6	0.0675	0.533	0.243	0.079	0.05	0.07
4	32.5	0.0657	1.104	0.535	0.18	0.119	0.171
5	29	0.0633	0.856	0.45	0.171	0.104	0.145
6	27	0.0617	0.617	0.339	0.119	0.069	0.096
7	21	0.0589	0.336	0.158	0.052	0.032	0.046
8	31.3	0.0585	0.992	0.471	0.159	0.108	0.161
9	40.3	0.0636	1.101	0.547	0.191	0.138	0.204
10	26.8	0.0525	1.014	0.483	0.183	0.091	0.125
11	28.3	0.0848	1.225	0.659	0.258	0.141	0.189
12	38.9	0.0479	0.973	0.51	0.198	0.108	0.15
13	31.2	0.0573	0.823	0.455	0.178	0.096	0.13
14	30	0.0622	0.869	0.473	0.16	0.087	0.123
15	33.6	0.0572	1.263	0.349	0.415	0.325	0.368
16	32.5	0.0748	1.267	0.326	0.257	0.149	0.213
17	33.5	0.0513	0.786	0.486	0.155	0.085	0.119
18	30.3	0.0522	1.034	0.42	0.167	0.086	0.12
19	31.8	0.066	0.668	0.698	0.108	0.054	0.079
20	23	0.077	0.726	0.766	0.127	0.076	0.103
21	37.2	0.0478	0.838	0.483	0.169	0.1	0.149
22	27.2	0.0407	0.476	0.259	0.093	0.061	0.084
23	32	0.0514	0.747	0.437	0.159	0.086	0.12
24	34.7	0.0705	0.702	0.383	0.137	0.079	0.109
25	35.4	0.0625	0.804	0.455	0.168	0.093	0.135
26	32	0.0545	0.817	0.456	0.153	0.094	0.14
27	22.5	0.0703	0.53	0.278	0.095	0.054	0.075
28	31.8	0.0876	0.33	0.18	0.236	0.041	0.057
29	26.6	0.06	1.011	0.532	0.204	0.126	0.171
30	24.2	0.0624	0.639	0.39	0.172	0.102	0.121
31	30	0.0489	0.663	0.384	0.134	0.089	0.122
32	27.7	0.0785	0.903	0.543	0.196	0.1	0.145
33	34.6	0.0587	1.014	0.556	0.199	0.132	0.188
34	32.2	0.0617	0.711	0.433	0.217	0.152	0.18
35	30.5	0.0885	1.091	0.661	0.227	0.118	0.16

36	25.8	0.0611	0.669	0.371	0.144	0.078	0.103
37	24.3	0.0815	0.976	0.566	0.207	0.106	0.146
38	21.2	0.0392	0.393	0.227	0.082	0.043	0.064
39	29	0.0617	0.495	0.254	0.091	0.063	0.084
40	28.8	0.0499	0.822	0.464	0.177	0.095	0.13
41	25.4	0.0547	0.694	0.372	0.139	0.083	0.113
42	35.3	0.0801	1.286	0.707	0.249	0.152	0.217
43	28.6	0.0705	0.844	0.458	0.173	0.089	0.13
44	32.5	0.0874	1.08	0.611	0.213	0.119	0.173
45	28.7	0.0649	1.064	0.593	0.214	0.137	0.19
46	26.4	0.0632	0.713	0.388	0.144	0.077	0.105
47	35.5	0.0537	0.635	0.332	0.129	0.078	0.112
48	32.7	0.0807	0.942	0.521	0.183	0.108	0.152
49	25.1	0.0807	0.85	0.501	0.176	0.085	0.119
50	22.5	0.0579	0.607	0.328	0.13	0.065	0.087
51	36.9	0.0736	1.265	0.707	0.251	0.152	0.227
52	35	0.0699	0.838	0.43	0.145	0.098	0.141
53	34.5	0.0584	0.854	0.456	0.175	0.113	0.163
54	30	0.0666	0.697	0.407	0.144	0.075	0.108
55	24.6	0.0725	0.939	0.547	0.212	0.112	0.151
56	30.9	0.0701	1.031	0.552	0.208	0.133	0.186
57	24	0.035	0.53	0.268	0.101	0.075	0.106
58	26.2	0.0607	0.737	0.382	0.149	0.091	0.122
59	31.3	0.0613	0.81	0.458	0.165	0.093	0.136
60	29	0.0894	1.455	0.796	0.29	0.178	0.25
61	29.9	0.0208	0.319	0.168	0.059	0.034	0.05
62	27.9	0.0519	0.959	0.482	0.167	0.109	0.157
63	25.1	0.0728	1.144	0.631	0.225	0.132	0.182
64	26.4	0.0473	0.627	0.337	0.116	0.061	0.088
65	28	0.0435	0.577	0.29	0.106	0.065	0.09
66	28.8	0.0531	0.907	0.524	0.25	0.094	0.123
67	24.5	0.0495	0.745	0.419	0.16	0.084	0.117
68	24	0.0688	0.912	0.505	0.34	0.112	0.152
69	32.6	0.0541	0.942	0.51	0.182	0.097	0.138
70	22	0.0381	0.445	0.248	0.073	0.048	0.069
71	23.1	0.0627	0.405	0.206	0.086	0.038	0.053
72	24.9	0.0682	0.777	0.498	0.185	0.073	0.106
73	27.8	0.0568	0.906	0.601	0.192	0.262	0.288
74	32.3	0.0756	1.247	0.696	0.247	0.139	0.201
75	18.4	0.0552	0.574	0.33	0.123	0.05	0.069
76	21	0.0719	0.694	0.426	0.157	0.067	0.095
77	19.4	0.0374	0.428	0.245	0.094	0.04	0.058
78	25.2	0.0693	0.688	0.408	0.134	0.068	0.1
79	27.7	0.0476	0.688	0.372	0.148	0.073	0.102
80	25.5	0.0666	0.753	0.427	0.151	0.081	0.117

**Appendix B - Absorption Spectrum of Chlorophyll  
Content with Solvent Extraction in July, 2004**

ID	SPAD	Weight(g)	Wavelength (nm)					
			440	480	510	630	645	663
1	22.6	0.0593	0.661	0.373	0.136	0.073	0.104	0.356
2	24.7	0.0677	0.667	0.35	0.132	0.076	0.109	0.373
3	34.6	0.0623	0.845	0.39	0.155	0.105	0.145	0.521
4	28.6	0.0562	0.529	0.269	0.104	0.062	0.09	0.3
5	24.1	0.0657	0.758	0.401	0.149	0.09	0.128	0.437
6	24.9	0.0674	0.854	0.433	0.166	0.102	0.144	0.499
7	32.5	0.0732	0.85	0.4	0.15	0.1	0.14	0.479
8	25.6	0.0542	0.446	0.214	0.083	0.051	0.072	0.247
9	35.0	0.0523	0.557	0.252	0.1	0.071	0.099	0.344
10	25.1	0.073	0.717	0.373	0.141	0.085	0.121	0.405
11	27.5	0.0574	0.867	0.426	0.172	0.102	0.142	0.489
12	26.7	0.0701	0.728	0.38	0.145	0.084	0.117	0.406
13	26.9	0.0714	0.745	0.374	0.149	0.087	0.121	0.4
14	30.0	0.0535	0.904	0.442	0.173	0.113	0.158	0.531
15	25.0	0.0551	0.736	0.381	0.148	0.089	0.127	0.418
16	23.4	0.0877	0.857	0.436	0.158	0.102	0.144	0.494
17	26.6	0.0671	0.641	0.31	0.116	0.079	0.11	0.384
18	28.0	0.0646	0.685	0.33	0.125	0.086	0.122	0.418
19	27.0	0.0548	0.698	0.349	0.133	0.083	0.117	0.395
20	27.4	0.0564	0.703	0.36	0.132	0.085	0.121	0.413
21	29.5	0.0644	1.014	0.508	0.192	0.119	0.167	0.573
22	22.1	0.0758	0.728	0.375	0.141	0.082	0.112	0.397
23	30.8	0.0553	0.75	0.379	0.136	0.094	0.134	0.456
24	25.2	0.0665	0.534	0.281	0.105	0.063	0.086	0.306
25	24.2	0.0627	0.614	0.327	0.124	0.067	0.093	0.327
26	35.9	0.0628	0.976	0.501	0.184	0.121	0.173	0.591
27	31.7	0.0612	0.605	0.33	0.118	0.073	0.108	0.353
28	21.7	0.0843	0.549	0.294	0.112	0.063	0.087	0.311
29	32.8	0.0858	0.923	0.454	0.171	0.117	0.17	0.571
30	23.1	0.0702	0.649	0.34	0.122	0.074	0.104	0.354
31	26.6	0.0608	0.792	0.371	0.14	0.099	0.139	0.49
32	31.3	0.0817	0.969	0.47	0.176	0.11	0.154	0.531
33	32.5	0.0645	0.89	0.456	0.168	0.109	0.157	0.533
34	34.4	0.0689	1.009	0.498	0.186	0.127	0.182	0.624
35	33.5	0.0562	0.739	0.384	0.148	0.087	0.122	0.429
36	29.0	0.0612	0.958	0.48	0.179	0.117	0.165	0.566
37	32.2	0.0598	0.729	0.367	0.138	0.09	0.13	0.437
38	30.8	0.0797	1.097	0.541	0.196	0.129	0.182	0.612
39	27.7	0.0643	0.808	0.397	0.147	0.096	0.136	0.464

40	27.9	0.0572	0.781	0.4	0.151	0.095	0.132	0.464
41	28.9	0.0719	0.907	0.453	0.167	0.111	0.159	0.54
42	28.7	0.065	1.014	0.52	0.191	0.125	0.178	0.619
43	31.1	0.0625	0.862	0.389	0.148	0.1	0.14	0.485
44	28.8	0.0722	0.693	0.352	0.133	0.08	0.114	0.387
45	26.8	0.0696	0.794	0.371	0.134	0.093	0.135	0.445
46	25.7	0.0547	0.696	0.336	0.125	0.08	0.112	0.387
47	24.0	0.0861	0.867	0.382	0.144	0.086	0.121	0.402
48	29.3	0.055	0.741	0.366	0.138	0.086	0.123	0.416
49	28.2	0.096	0.903	0.454	0.166	0.103	0.147	0.497
50	25.7	0.0566	0.524	0.257	0.096	0.061	0.085	0.294
51	26.7	0.0512	0.588	0.308	0.117	0.068	0.095	0.33
52	25.2	0.0607	0.59	0.311	0.118	0.068	0.094	0.301
53	27.1	0.0597	0.593	0.316	0.116	0.069	0.099	0.333
54	20.7	0.0599	0.717	0.369	0.141	0.085	0.116	0.419
55	27.8	0.0453	0.504	0.263	0.099	0.06	0.085	0.293
56	22.7	0.0559	0.528	0.27	0.104	0.06	0.084	0.288
57	26.7	0.0585	0.731	0.361	0.135	0.088	0.126	0.429
58	31.0	0.0526	0.747	0.38	0.136	0.088	0.127	0.43
59	22.1	0.0703	0.711	0.366	0.138	0.083	0.117	0.404
60	18.8	0.0541	0.425	0.232	0.088	0.044	0.063	0.205
61	28.7	0.0624	0.808	0.401	0.169	0.085	0.117	0.378
62	30.0	0.0579	0.755	0.387	0.145	0.094	0.136	0.453
63	29.0	0.0619	0.84	0.437	0.16	0.1	0.138	0.496
64	24.5	0.0647	0.632	0.291	0.11	0.066	0.093	0.312
65	26.0	0.0544	0.838	0.416	0.155	0.102	0.145	0.502
66	20.0	0.0638	0.638	0.325	0.124	0.073	0.103	0.346
67	24.0	0.0511	0.706	0.352	0.129	0.088	0.13	0.422
68	30.6	0.0638	0.882	0.447	0.163	0.106	0.152	0.512
69	28.9	0.0696	0.889	0.416	0.153	0.105	0.151	0.504
70	23.3	0.0553	0.601	0.31	0.118	0.065	0.093	0.3
71	30.2	0.0641	0.978	0.464	0.173	0.109	0.155	0.521
72	30.1	0.0764	0.996	0.48	0.183	0.115	0.162	0.547
73	24.1	0.0609	0.726	0.356	0.132	0.083	0.119	0.396
74	25.0	0.0603	0.794	0.395	0.152	0.093	0.131	0.445
75	29.0	0.0632	0.693	0.324	0.124	0.078	0.11	0.388
76	20.4	0.0539	0.495	0.248	0.099	0.059	0.081	0.28
77	19.0	0.0558	0.496	0.252	0.098	0.058	0.082	0.283
78	29.7	0.0519	0.661	0.311	0.121	0.083	0.119	0.41
79	20.5	0.0618	0.563	0.289	0.121	0.067	0.097	0.319
80	25.3	0.0573	0.527	0.27	0.105	0.061	0.085	0.29

**Appendix C - Absorption Spectrum of Chlorophyll  
Content with Solvent Extraction in September 1, 2004**

ID	SPAD	Weight (g)	Wavelength (nm)					
			440	480	510	630	645	663
1	27.2	0.0564	0.358	0.176	0.071	0.045	0.064	0.214
2	24.8	0.0539	0.378	0.177	0.072	0.047	0.067	0.234
3	25.9	0.0644	0.44	0.195	0.077	0.057	0.08	0.279
4	20.8	0.0632	0.415	0.22	0.081	0.045	0.066	0.213
5	24.4	0.051	0.383	0.191	0.073	0.048	0.07	0.234
6	29.2	0.0709	0.827	0.402	0.157	0.101	0.145	0.487
7	28.9	0.057	0.501	0.244	0.094	0.065	0.094	0.317
8	28.6	0.0526	0.289	0.138	0.055	0.035	0.051	0.17
9	29.1	0.0568	0.402	0.193	0.074	0.052	0.078	0.255
10	25.0	0.0611	0.273	0.133	0.052	0.034	0.049	0.16
11	25.5	0.0567	0.53	0.258	0.106	0.064	0.09	0.306
12	28.3	0.0906	1.065	0.517	0.207	0.139	0.197	0.679
13	28.9	0.0733	0.423	0.209	0.0787	0.053	0.076	0.249
14	30.9	0.0504	0.465	0.218	0.084	0.061	0.089	0.299
15	22.8	0.0631	0.541	0.267	0.102	0.066	0.095	0.319
16	29.7	0.0622	0.697	0.352	0.132	0.086	0.125	0.417
17	31.6	0.0594	0.954	0.416	0.154	0.13	0.189	0.647
18	32.8	0.0521	0.526	0.255	0.1	0.067	0.099	0.331
19	32.3	0.0504	0.587	0.275	0.107	0.077	0.114	0.377
20	28.8	0.0562	0.446	0.215	0.084	0.055	0.079	0.268
21	33.5	0.0598	0.396	0.189	0.073	0.049	0.072	0.241
22	23.0	0.0513	0.357	0.171	0.068	0.045	0.067	0.221
23	28.	0.0555	0.535	0.249	0.094	0.069	0.102	0.34
24	22.5	0.064	0.607	0.313	0.129	0.078	0.109	0.354
25	35.7	0.0617	0.714	0.33	0.129	0.093	0.134	0.464
26	34.1	0.0559	0.636	0.294	0.114	0.085	0.124	0.416
27	26.2	0.0641	0.478	0.236	0.091	0.059	0.087	0.288
28	26.5	0.0701	0.75	0.341	0.132	0.092	0.129	0.453
29	32.0	0.0718	0.482	0.235	0.091	0.062	0.091	0.301
30	35.3	0.0709	0.563	0.257	0.097	0.074	0.105	0.368
31	32.0	0.0742	0.756	0.364	0.139	0.095	0.136	0.472
32	29.0	0.0845	0.865	0.403	0.158	0.1	0.14	0.475
33	30.6	0.0635	0.721	0.378	0.135	0.091	0.134	0.438
34	28.4	0.0583	0.608	0.289	0.112	0.077	0.112	0.381
35	31.8	0.0554	0.692	0.335	0.13	0.092	0.133	0.452
36	23.0	0.0581	0.221	0.113	0.048	0.026	0.037	0.13
37	25.6	0.0645	0.498	0.248	0.096	0.063	0.092	0.304
38	32.6	0.067	0.688	0.317	0.122	0.089	0.122	0.444
39	31.0	0.0634	0.615	0.3	0.113	0.078	0.114	0.38

40	27.3	0.0546	0.593	0.297	0.111	0.074	0.108	0.368
41	29.7	0.0543	0.668	0.348	0.139	0.081	0.118	0.401
42	26.0	0.0595	0.588	0.285	0.112	0.07	0.099	0.332
43	28.7	0.0661	0.731	0.346	0.13	0.092	0.133	0.452
44	24.2	0.0852	0.641	0.335	0.131	0.073	0.105	0.358
45	34.5	0.0629	0.78	0.352	0.131	0.093	0.136	0.45
46	27.1	0.0667	0.66	0.314	0.121	0.079	0.113	0.386
47	31.3	0.0625	0.767	0.382	0.142	0.1	0.148	0.482
48	33.7	0.0543	0.631	0.301	0.114	0.084	0.122	0.416
49	25.8	0.0651	0.51	0.238	0.093	0.066	0.095	0.323
50	28.8	0.063	0.572	0.289	0.107	0.073	0.107	0.353
51	25.1	0.0562	0.591	0.299	0.12	0.073	0.104	0.357
52	23.1	0.0598	0.427	0.214	0.082	0.051	0.074	0.246
53	27.6	0.0549	0.406	0.208	0.079	0.051	0.074	0.246
54	27.4	0.0533	0.762	0.358	0.146	0.099	0.138	0.497
55	26.8	0.0621	0.652	0.315	0.132	0.084	0.117	0.415
56	24.9	0.0632	0.543	0.266	0.103	0.068	0.097	0.33
57	22.4	0.0508	0.424	0.208	0.081	0.051	0.072	0.251
58	27.8	0.0668	0.57	0.285	0.105	0.07	0.102	0.337
59	31.0	0.061	0.872	0.412	0.162	0.114	0.159	0.568
60	26.2	0.0715	0.611	0.277	0.107	0.081	0.113	0.388
61	26.2	0.061	1.079	0.532	0.216	0.134	0.187	0.671
62	23.0	0.0704	0.555	0.298	0.12	0.064	0.098	0.308
63	26.0	0.0512	0.548	0.291	0.12	0.062	0.087	0.303
64	21.6	0.0623	0.775	0.366	0.142	0.103	0.144	0.498
65	28.3	0.052	0.58	0.29	0.108	0.074	0.109	0.358
66	26.6	0.0553	0.524	0.264	0.097	0.065	0.096	0.311
67	24.8	0.0618	0.537	0.281	0.12	0.059	0.082	0.28
68	17.4	0.0742	0.473	0.255	0.107	0.048	0.066	0.227
69	21.8	0.0556	0.44	0.23	0.086	0.055	0.078	0.255
70	22.3	0.0728	0.525	0.264	0.107	0.059	0.083	0.28
71	26.3	0.0627	0.649	0.323	0.119	0.083	0.122	0.407
72	27.0	0.0553	0.575	0.284	0.108	0.069	0.097	0.338
73	23.5	0.0551	0.492	0.256	0.102	0.056	0.08	0.268
74	20.6	0.0565	0.475	0.24	0.098	0.057	0.081	0.277
75	30.5	0.0638	0.706	0.365	0.144	0.083	0.12	0.401
76	28.7	-	-	-	-	-	-	-
77	33.6	0.0564	0.497	0.242	0.092	0.063	0.091	0.307
78	30.4	0.0545	0.558	0.278	0.101	0.072	0.106	0.352
79	27.0	0.064	0.741	0.368	0.135	0.095	0.138	0.463
80	22.1	0.0644	0.685	0.349	0.135	0.085	0.122	0.419

## Appendix D - Leaf Reflectance in Visible and Near Infrared, June 30, 2004

ID	Wavelength (nm)												
	550	570	590	610	630	650	680	700	720	740	760	780	800
1	0.337	0.308	0.256	0.231	0.208	0.174	0.136	0.344	0.713	0.939	0.990	0.998	1.002
2	0.290	0.262	0.217	0.196	0.177	0.151	0.124	0.276	0.605	0.866	0.930	0.937	0.939
3	0.226	0.196	0.155	0.136	0.121	0.103	0.090	0.191	0.512	0.876	0.990	1.004	1.007
4	0.263	0.237	0.191	0.168	0.148	0.117	0.085	0.252	0.579	0.820	0.883	0.893	0.898
5	0.243	0.213	0.167	0.145	0.127	0.102	0.079	0.216	0.559	0.869	0.958	0.972	0.977
6	0.247	0.219	0.175	0.154	0.136	0.114	0.089	0.210	0.508	0.808	0.903	0.917	0.922
7	0.246	0.217	0.176	0.157	0.140	0.122	0.105	0.209	0.503	0.799	0.888	0.901	0.906
8	0.298	0.265	0.209	0.182	0.157	0.126	0.091	0.261	0.622	0.889	0.957	0.967	0.971
9	0.242	0.214	0.173	0.153	0.137	0.117	0.099	0.202	0.505	0.846	0.958	0.975	0.981
10	0.243	0.210	0.162	0.140	0.122	0.099	0.077	0.205	0.547	0.866	0.956	0.968	0.971
11	0.232	0.214	0.172	0.150	0.130	0.105	0.070	0.230	0.575	0.842	0.918	0.933	0.940
12	0.248	0.223	0.176	0.154	0.134	0.108	0.076	0.242	0.599	0.847	0.911	0.922	0.928
13	0.212	0.189	0.154	0.138	0.123	0.104	0.081	0.202	0.499	0.797	0.891	0.907	0.913
14	0.203	0.179	0.145	0.129	0.117	0.101	0.087	0.183	0.485	0.820	0.930	0.950	0.959
15	0.282	0.246	0.194	0.170	0.149	0.123	0.099	0.239	0.586	0.894	0.977	0.987	0.990
16	0.275	0.250	0.206	0.184	0.165	0.133	0.101	0.276	0.621	0.874	0.936	0.945	0.949
17	0.251	0.222	0.176	0.154	0.135	0.109	0.087	0.228	0.558	0.867	0.954	0.966	0.971
18	0.278	0.240	0.187	0.162	0.141	0.114	0.091	0.231	0.578	0.902	0.992	1.003	1.006
19	0.226	0.197	0.157	0.137	0.123	0.102	0.086	0.198	0.522	0.858	0.960	0.975	0.980
20	0.259	0.225	0.174	0.149	0.128	0.103	0.079	0.221	0.570	0.861	0.937	0.948	0.953
21	0.184	0.168	0.138	0.124	0.113	0.097	0.078	0.180	0.478	0.805	0.917	0.939	0.948
22	0.336	0.311	0.256	0.227	0.200	0.163	0.114	0.333	0.700	0.919	0.971	0.981	0.988
23	0.212	0.188	0.150	0.132	0.117	0.095	0.080	0.198	0.508	0.781	0.861	0.878	0.889
24	0.282	0.253	0.198	0.170	0.144	0.110	0.073	0.280	0.662	0.908	0.966	0.976	0.982
25	0.339	0.308	0.249	0.218	0.190	0.156	0.110	0.307	0.683	0.933	0.994	1.005	1.010
26	0.234	0.204	0.162	0.143	0.127	0.108	0.093	0.202	0.539	0.891	0.997	1.011	1.016
27	0.279	0.246	0.194	0.169	0.146	0.118	0.086	0.255	0.621	0.903	0.977	0.988	0.992
28	0.263	0.248	0.216	0.202	0.187	0.159	0.117	0.320	0.688	0.942	1.006	1.020	1.027
29	0.227	0.204	0.169	0.155	0.144	0.125	0.107	0.235	0.551	0.867	0.966	0.984	0.993
30	0.127	0.123	0.120	0.129	0.141	0.128	0.099	0.309	0.653	0.868	0.925	0.940	0.951
31	0.258	0.224	0.176	0.154	0.136	0.114	0.094	0.216	0.561	0.891	0.985	0.998	1.003
32	0.243	0.217	0.174	0.154	0.137	0.114	0.088	0.233	0.585	0.887	0.971	0.985	0.991
33	0.222	0.192	0.146	0.125	0.107	0.084	0.065	0.192	0.536	0.860	0.954	0.969	0.976
34	0.232	0.200	0.156	0.135	0.119	0.099	0.085	0.195	0.524	0.880	0.987	1.002	1.007
35	0.266	0.240	0.189	0.162	0.138	0.110	0.074	0.253	0.640	0.897	0.961	0.973	0.980
36	0.232	0.206	0.165	0.145	0.129	0.109	0.087	0.210	0.542	0.853	0.947	0.965	0.973
37	0.205	0.181	0.144	0.126	0.112	0.091	0.075	0.191	0.510	0.819	0.912	0.929	0.937
38	0.239	0.208	0.163	0.141	0.124	0.102	0.082	0.205	0.540	0.881	0.986	1.003	1.009
39	0.241	0.216	0.176	0.157	0.141	0.117	0.097	0.231	0.575	0.893	0.987	1.003	1.010

40	0.231	0.207	0.163	0.141	0.122	0.099	0.074	0.225	0.592	0.874	0.951	0.967	0.976
41	0.246	0.223	0.182	0.162	0.145	0.121	0.096	0.230	0.541	0.807	0.885	0.903	0.914
42	0.271	0.240	0.194	0.172	0.155	0.132	0.108	0.241	0.585	0.897	0.985	0.999	1.004
43	0.227	0.193	0.147	0.125	0.109	0.088	0.071	0.190	0.524	0.872	0.974	0.987	0.992
44	0.305	0.276	0.226	0.201	0.178	0.151	0.117	0.265	0.567	0.796	0.856	0.866	0.870
45	0.256	0.221	0.172	0.148	0.131	0.107	0.087	0.212	0.551	0.887	0.984	0.997	1.002
46	0.277	0.250	0.204	0.182	0.162	0.134	0.099	0.281	0.646	0.906	0.971	0.982	0.988
47	0.324	0.297	0.245	0.219	0.195	0.161	0.115	0.308	0.640	0.882	0.946	0.958	0.965
48	0.249	0.219	0.173	0.152	0.134	0.110	0.082	0.225	0.560	0.849	0.930	0.943	0.949
49	0.286	0.248	0.191	0.164	0.142	0.113	0.084	0.247	0.608	0.897	0.971	0.980	0.984
50	0.305	0.267	0.206	0.176	0.151	0.118	0.082	0.273	0.654	0.934	1.000	1.008	1.012
51	0.271	0.245	0.196	0.171	0.149	0.121	0.085	0.253	0.594	0.848	0.916	0.929	0.936
52	0.314	0.285	0.229	0.200	0.175	0.139	0.095	0.304	0.683	0.934	0.995	1.004	1.009
53	0.286	0.251	0.194	0.166	0.143	0.109	0.079	0.259	0.647	0.930	1.000	1.009	1.013
54	0.273	0.252	0.201	0.174	0.150	0.117	0.074	0.278	0.632	0.842	0.894	0.905	0.912
55	0.298	0.266	0.214	0.188	0.167	0.139	0.108	0.266	0.614	0.887	0.957	0.966	0.971
56	0.325	0.306	0.257	0.231	0.206	0.163	0.102	0.359	0.725	0.921	0.964	0.971	0.976
57	0.253	0.220	0.169	0.144	0.124	0.099	0.074	0.215	0.556	0.847	0.925	0.935	0.940
58	0.241	0.210	0.165	0.144	0.128	0.105	0.084	0.216	0.564	0.887	0.979	0.992	0.998
59	0.296	0.275	0.227	0.201	0.179	0.143	0.102	0.308	0.672	0.899	0.954	0.966	0.974
60	0.275	0.259	0.232	0.220	0.211	0.176	0.141	0.349	0.687	0.907	0.962	0.972	0.979
61	0.261	0.229	0.179	0.155	0.135	0.110	0.085	0.227	0.557	0.869	0.967	0.981	0.988
62	0.355	0.320	0.268	0.244	0.223	0.196	0.165	0.320	0.651	0.925	0.999	1.010	1.015
63	0.260	0.235	0.192	0.172	0.155	0.128	0.096	0.257	0.599	0.869	0.941	0.954	0.961
64	0.318	0.281	0.219	0.188	0.161	0.126	0.086	0.281	0.655	0.905	0.965	0.973	0.978
65	0.249	0.214	0.164	0.140	0.122	0.099	0.080	0.206	0.561	0.902	0.998	1.010	1.016
66	0.264	0.243	0.206	0.191	0.176	0.143	0.104	0.307	0.659	0.879	0.931	0.941	0.948
67	0.326	0.296	0.246	0.222	0.200	0.168	0.132	0.309	0.644	0.891	0.953	0.962	0.966
68	0.275	0.242	0.193	0.170	0.151	0.126	0.098	0.249	0.602	0.895	0.974	0.986	0.991
69	0.270	0.235	0.182	0.157	0.136	0.108	0.081	0.234	0.595	0.913	1.002	1.014	1.019
70	0.309	0.270	0.211	0.183	0.159	0.125	0.087	0.287	0.681	0.954	1.020	1.029	1.034
71	0.274	0.239	0.186	0.160	0.139	0.113	0.088	0.235	0.593	0.891	0.972	0.984	0.990
72	0.240	0.206	0.157	0.134	0.116	0.095	0.073	0.194	0.531	0.868	0.969	0.984	0.989
73	0.276	0.249	0.200	0.176	0.155	0.123	0.086	0.267	0.609	0.857	0.920	0.930	0.935
74	0.269	0.243	0.197	0.173	0.153	0.125	0.093	0.245	0.571	0.843	0.919	0.932	0.940
75	0.265	0.232	0.183	0.159	0.140	0.115	0.089	0.225	0.564	0.872	0.960	0.972	0.977
76	0.294	0.271	0.223	0.199	0.176	0.143	0.094	0.302	0.649	0.862	0.915	0.927	0.936
77	0.511	0.485	0.430	0.401	0.373	0.336	0.276	0.495	0.789	0.948	0.984	0.992	0.998
78	0.222	0.187	0.139	0.118	0.101	0.079	0.066	0.181	0.525	0.871	0.971	0.984	0.988
79	0.304	0.280	0.231	0.205	0.181	0.144	0.098	0.305	0.666	0.895	0.952	0.962	0.968
80	0.288	0.256	0.204	0.181	0.162	0.134	0.107	0.262	0.620	0.900	0.972	0.983	0.988

## Appendix E - Leaf Reflectance in Visible and Near Infrared, July 26, 2004

ID	Wavelength (nm)												
	550	570	590	610	630	650	680	700	720	740	760	780	800
1	0.337	0.308	0.256	0.231	0.208	0.174	0.136	0.344	0.713	0.939	0.990	0.998	1.002
2	0.290	0.262	0.217	0.196	0.177	0.151	0.124	0.276	0.605	0.866	0.930	0.937	0.939
3	0.226	0.196	0.155	0.136	0.121	0.103	0.090	0.191	0.512	0.876	0.990	1.004	1.007
4	0.263	0.237	0.191	0.168	0.148	0.117	0.085	0.252	0.579	0.820	0.883	0.893	0.898
5	0.243	0.213	0.167	0.145	0.127	0.102	0.079	0.216	0.559	0.869	0.958	0.972	0.977
6	0.247	0.219	0.175	0.154	0.136	0.114	0.089	0.210	0.508	0.808	0.903	0.917	0.922
7	0.246	0.217	0.176	0.157	0.140	0.122	0.105	0.209	0.503	0.799	0.888	0.901	0.906
8	0.298	0.265	0.209	0.182	0.157	0.126	0.091	0.261	0.622	0.889	0.957	0.967	0.971
9	0.242	0.214	0.173	0.153	0.137	0.117	0.099	0.202	0.505	0.846	0.958	0.975	0.981
10	0.243	0.210	0.162	0.140	0.122	0.099	0.077	0.205	0.547	0.866	0.956	0.968	0.971
11	0.232	0.214	0.172	0.150	0.130	0.105	0.070	0.230	0.575	0.842	0.918	0.933	0.940
12	0.248	0.223	0.176	0.154	0.134	0.108	0.076	0.242	0.599	0.847	0.911	0.922	0.928
13	0.212	0.189	0.154	0.138	0.123	0.104	0.081	0.202	0.499	0.797	0.891	0.907	0.913
14	0.203	0.179	0.145	0.129	0.117	0.101	0.087	0.183	0.485	0.820	0.930	0.950	0.959
15	0.282	0.246	0.194	0.170	0.149	0.123	0.099	0.239	0.586	0.894	0.977	0.987	0.990
16	0.275	0.250	0.206	0.184	0.165	0.133	0.101	0.276	0.621	0.874	0.936	0.945	0.949
17	0.251	0.222	0.176	0.154	0.135	0.109	0.087	0.228	0.558	0.867	0.954	0.966	0.971
18	0.278	0.240	0.187	0.162	0.141	0.114	0.091	0.231	0.578	0.902	0.992	1.003	1.006
19	0.226	0.197	0.157	0.137	0.123	0.102	0.086	0.198	0.522	0.858	0.960	0.975	0.980
20	0.259	0.225	0.174	0.149	0.128	0.103	0.079	0.221	0.570	0.861	0.937	0.948	0.953
21	0.184	0.168	0.138	0.124	0.113	0.097	0.078	0.180	0.478	0.805	0.917	0.939	0.948
22	0.336	0.311	0.256	0.227	0.200	0.163	0.114	0.333	0.700	0.919	0.971	0.981	0.988
23	0.212	0.188	0.150	0.132	0.117	0.095	0.080	0.198	0.508	0.781	0.861	0.878	0.889
24	0.282	0.253	0.198	0.170	0.144	0.110	0.073	0.280	0.662	0.908	0.966	0.976	0.982
25	0.339	0.308	0.249	0.218	0.190	0.156	0.110	0.307	0.683	0.933	0.994	1.005	1.010
26	0.234	0.204	0.162	0.143	0.127	0.108	0.093	0.202	0.539	0.891	0.997	1.011	1.016
27	0.279	0.246	0.194	0.169	0.146	0.118	0.086	0.255	0.621	0.903	0.977	0.988	0.992
28	0.263	0.248	0.216	0.202	0.187	0.159	0.117	0.320	0.688	0.942	1.006	1.020	1.027
29	0.227	0.204	0.169	0.155	0.144	0.125	0.107	0.235	0.551	0.867	0.966	0.984	0.993
30	0.127	0.123	0.120	0.129	0.141	0.128	0.099	0.309	0.653	0.868	0.925	0.940	0.951
31	0.258	0.224	0.176	0.154	0.136	0.114	0.094	0.216	0.561	0.891	0.985	0.998	1.003
32	0.243	0.217	0.174	0.154	0.137	0.114	0.088	0.233	0.585	0.887	0.971	0.985	0.991
33	0.222	0.192	0.146	0.125	0.107	0.084	0.065	0.192	0.536	0.860	0.954	0.969	0.976
34	0.232	0.200	0.156	0.135	0.119	0.099	0.085	0.195	0.524	0.880	0.987	1.002	1.007
35	0.266	0.240	0.189	0.162	0.138	0.110	0.074	0.253	0.640	0.897	0.961	0.973	0.980
36	0.232	0.206	0.165	0.145	0.129	0.109	0.087	0.210	0.542	0.853	0.947	0.965	0.973
37	0.205	0.181	0.144	0.126	0.112	0.091	0.075	0.191	0.510	0.819	0.912	0.929	0.937
38	0.239	0.208	0.163	0.141	0.124	0.102	0.082	0.205	0.540	0.881	0.986	1.003	1.009
39	0.241	0.216	0.176	0.157	0.141	0.117	0.097	0.231	0.575	0.893	0.987	1.003	1.010

40	0.231	0.207	0.163	0.141	0.122	0.099	0.074	0.225	0.592	0.874	0.951	0.967	0.976
41	0.246	0.223	0.182	0.16	0.145	0.121	0.096	0.230	0.541	0.807	0.885	0.90	0.914
42	0.271	0.240	0.194	0.12	0.155	0.132	0.10	0.241	0.585	0.897	0.985	0.999	1.004
43	0.227	0.193	0.147	0.25	0.109	0.088	0.071	0.190	0.524	0.872	0.974	0.987	0.992
44	0.305	0.276	0.226	0.201	0.178	0.151	0.117	0.265	0.567	0.796	0.856	0.866	0.870
45	0.256	0.221	0.172	0.148	0.131	0.107	0.087	0.212	0.551	0.887	0.984	0.997	1.002
46	0.277	0.250	0.204	0.182	0.162	0.134	0.099	0.281	0.646	0.906	0.971	0.982	0.988
47	0.324	0.297	0.245	0.219	0.195	0.161	0.115	0.308	0.640	0.882	0.946	0.958	0.965
48	0.249	0.219	0.173	0.152	0.134	0.110	0.082	0.225	0.560	0.849	0.930	0.943	0.949
49	0.286	0.248	0.191	0.164	0.142	0.113	0.084	0.247	0.608	0.897	0.971	0.980	0.984
50	0.305	0.267	0.206	0.176	0.151	0.118	0.082	0.273	0.654	0.934	1.000	1.008	1.012
51	0.271	0.245	0.196	0.171	0.149	0.121	0.085	0.253	0.594	0.848	0.916	0.929	0.936
52	0.314	0.285	0.229	0.200	0.175	0.139	0.095	0.304	0.683	0.934	0.995	1.004	1.009
53	0.286	0.251	0.194	0.166	0.143	0.109	0.079	0.259	0.647	0.930	1.000	1.009	1.013
54	0.273	0.252	0.201	0.174	0.150	0.117	0.074	0.278	0.632	0.842	0.894	0.905	0.912
55	0.298	0.266	0.214	0.188	0.167	0.139	0.108	0.266	0.614	0.887	0.957	0.966	0.971
56	0.325	0.306	0.257	0.231	0.206	0.163	0.102	0.359	0.725	0.921	0.964	0.971	0.976
57	0.253	0.220	0.169	0.144	0.124	0.099	0.074	0.215	0.556	0.847	0.925	0.935	0.940
58	0.241	0.210	0.165	0.144	0.128	0.105	0.084	0.216	0.564	0.887	0.979	0.992	0.998
59	0.296	0.275	0.227	0.201	0.179	0.143	0.102	0.308	0.672	0.899	0.954	0.966	0.974
60	0.275	0.259	0.232	0.220	0.211	0.176	0.141	0.349	0.687	0.907	0.962	0.972	0.979
61	0.261	0.229	0.179	0.155	0.135	0.110	0.085	0.227	0.557	0.869	0.967	0.981	0.988
62	0.355	0.320	0.268	0.244	0.223	0.196	0.165	0.320	0.651	0.925	0.999	1.010	1.015
63	0.260	0.235	0.192	0.172	0.155	0.128	0.096	0.257	0.599	0.869	0.941	0.954	0.961
64	0.318	0.281	0.219	0.188	0.161	0.126	0.086	0.281	0.655	0.905	0.965	0.973	0.978
65	0.249	0.214	0.164	0.140	0.122	0.099	0.080	0.206	0.561	0.902	0.998	1.010	1.016
66	0.264	0.243	0.206	0.191	0.176	0.143	0.104	0.307	0.659	0.879	0.931	0.941	0.948
67	0.326	0.296	0.246	0.222	0.200	0.168	0.132	0.309	0.644	0.891	0.953	0.962	0.966
68	0.275	0.242	0.193	0.170	0.151	0.126	0.098	0.249	0.602	0.895	0.974	0.986	0.991
69	0.270	0.235	0.182	0.157	0.136	0.108	0.081	0.234	0.595	0.913	1.002	1.014	1.019
70	0.309	0.270	0.211	0.183	0.159	0.125	0.087	0.287	0.681	0.954	1.020	1.029	1.034
71	0.274	0.239	0.186	0.160	0.139	0.113	0.088	0.235	0.593	0.891	0.972	0.984	0.990
72	0.240	0.206	0.157	0.134	0.116	0.095	0.073	0.194	0.531	0.868	0.969	0.984	0.989
73	0.276	0.249	0.200	0.176	0.155	0.123	0.086	0.267	0.609	0.857	0.920	0.930	0.935
74	0.269	0.243	0.197	0.173	0.153	0.125	0.093	0.245	0.571	0.843	0.919	0.932	0.940
75	0.265	0.232	0.183	0.159	0.140	0.115	0.089	0.225	0.564	0.872	0.960	0.972	0.977
76	0.294	0.271	0.223	0.199	0.176	0.143	0.094	0.302	0.649	0.862	0.915	0.927	0.936
77	0.511	0.485	0.430	0.401	0.373	0.336	0.276	0.495	0.789	0.948	0.984	0.992	0.998
78	0.222	0.187	0.139	0.118	0.101	0.079	0.066	0.181	0.525	0.871	0.971	0.984	0.988
79	0.304	0.280	0.231	0.205	0.181	0.144	0.098	0.305	0.666	0.895	0.952	0.962	0.968
80	0.288	0.256	0.204	0.181	0.162	0.134	0.107	0.262	0.620	0.900	0.972	0.983	0.988

## Appendix F - Leaf Reflectance in Visible and Near Infrared, September 1, 2004

ID	Wavelength (nm)												
	550	570	590	610	630	650	680	700	720	740	760	780	800
1	0.292	0.258	0.206	0.182	0.158	0.129	0.098	0.255	0.605	0.898	0.977	0.986	0.989
2	0.318	0.283	0.231	0.209	0.187	0.157	0.118	0.288	0.650	0.926	0.996	1.005	1.008
3	0.328	0.297	0.246	0.222	0.197	0.161	0.124	0.291	0.625	0.872	0.937	0.947	0.952
4	0.376	0.349	0.292	0.263	0.233	0.183	0.127	0.381	0.752	0.962	1.010	1.016	1.020
5	0.280	0.248	0.196	0.174	0.152	0.121	0.087	0.261	0.626	0.904	0.975	0.983	0.985
6	0.303	0.273	0.232	0.215	0.202	0.180	0.161	0.274	0.586	0.906	1.003	1.015	1.019
7	0.307	0.271	0.219	0.196	0.173	0.143	0.111	0.265	0.623	0.916	0.997	1.010	1.016
8	0.305	0.276	0.224	0.199	0.174	0.140	0.098	0.275	0.628	0.892	0.964	0.980	0.988
9	0.261	0.227	0.174	0.150	0.127	0.096	0.068	0.228	0.595	0.869	0.941	0.951	0.955
10	0.388	0.351	0.294	0.267	0.242	0.205	0.167	0.358	0.722	0.961	1.017	1.023	1.026
11	0.442	0.411	0.367	0.346	0.332	0.302	0.276	0.408	0.690	0.920	0.982	0.990	0.992
12	0.222	0.192	0.150	0.131	0.114	0.093	0.074	0.188	0.525	0.836	0.928	0.944	0.950
13	0.261	0.229	0.180	0.159	0.138	0.108	0.083	0.232	0.580	0.881	0.965	0.976	0.980
14	0.332	0.300	0.250	0.228	0.204	0.175	0.143	0.299	0.642	0.920	0.998	1.009	1.014
15	0.280	0.252	0.209	0.190	0.171	0.144	0.116	0.250	0.571	0.866	0.954	0.968	0.974
16	0.251	0.224	0.182	0.164	0.145	0.117	0.089	0.247	0.613	0.903	0.982	0.996	1.001
17	0.351	0.317	0.274	0.257	0.238	0.215	0.198	0.335	0.676	0.953	1.026	1.034	1.038
18	0.263	0.229	0.180	0.157	0.137	0.108	0.085	0.226	0.580	0.878	0.961	0.973	0.977
19	0.273	0.241	0.194	0.173	0.152	0.126	0.101	0.236	0.575	0.867	0.951	0.965	0.970
20	0.288	0.263	0.220	0.204	0.187	0.159	0.123	0.305	0.657	0.911	0.977	0.988	0.993
21	0.243	0.215	0.173	0.154	0.139	0.114	0.094	0.216	0.551	0.860	0.950	0.964	0.970
22	0.332	0.310	0.264	0.241	0.223	0.185	0.143	0.332	0.656	0.848	0.901	0.915	0.925
23	0.253	0.222	0.176	0.156	0.137	0.110	0.083	0.214	0.540	0.841	0.932	0.948	0.955
24	0.290	0.263	0.206	0.178	0.149	0.113	0.067	0.275	0.654	0.872	0.925	0.934	0.940
25	0.271	0.237	0.191	0.172	0.155	0.132	0.114	0.231	0.561	0.881	0.975	0.988	0.991
26	0.228	0.199	0.160	0.142	0.127	0.105	0.088	0.194	0.500	0.833	0.944	0.962	0.967
27	0.311	0.283	0.234	0.211	0.185	0.153	0.109	0.279	0.614	0.871	0.945	0.960	0.968
28	0.291	0.256	0.202	0.178	0.153	0.125	0.090	0.248	0.608	0.907	0.988	0.999	1.004
29	0.284	0.261	0.220	0.201	0.182	0.153	0.117	0.269	0.606	0.883	0.964	0.978	0.985
30	0.261	0.231	0.190	0.172	0.156	0.132	0.112	0.227	0.538	0.870	0.974	0.989	0.995
31	0.267	0.231	0.180	0.158	0.137	0.110	0.087	0.225	0.584	0.897	0.983	0.994	0.998
32	0.252	0.218	0.169	0.148	0.127	0.100	0.075	0.219	0.576	0.888	0.975	0.986	0.989
33	0.280	0.254	0.212	0.194	0.175	0.149	0.127	0.268	0.615	0.905	0.985	0.997	1.003
34	0.280	0.247	0.196	0.174	0.152	0.122	0.095	0.249	0.611	0.896	0.971	0.982	0.987
35	0.278	0.258	0.222	0.207	0.188	0.164	0.129	0.276	0.593	0.836	0.907	0.924	0.934
36	0.264	0.247	0.202	0.179	0.153	0.120	0.068	0.268	0.612	0.811	0.866	0.882	0.894

37	0.298	0.268	0.214	0.189	0.164	0.126	0.086	0.277	0.635	0.866	0.924	0.933	0.939
38	0.222	0.188	0.143	0.125	0.108	0.086	0.070	0.181	0.518	0.861	0.964	0.978	0.983
39	0.228	0.202	0.163	0.145	0.128	0.105	0.087	0.202	0.511	0.822	0.921	0.937	0.944
40	0.26	0.229	0.182	0.161	0.140	0.114	0.088	0.227	0.565	0.886	0.982	0.996	1.001
41	0.286	0.261	0.216	0.195	0.172	0.141	0.105	0.26	0.607	0.859	0.924	0.935	0.941
42	0.283	0.258	0.211	0.190	0.168	0.137	0.098	0.24	0.628	0.903	0.974	0.985	0.990
43	0.252	0.214	0.164	0.142	0.122	0.097	0.077	0.206	0.554	0.892	0.987	0.997	0.999
44	0.347	0.315	0.254	0.225	0.192	0.151	0.095	0.311	0.692	0.930	0.986	0.995	0.999
45	0.225	0.195	0.153	0.135	0.118	0.096	0.075	0.190	0.484	0.816	0.930	0.947	0.953
46	0.289	0.253	0.199	0.176	0.153	0.125	0.096	0.242	0.599	0.908	0.990	1.000	1.003
47	0.218	0.185	0.141	0.122	0.104	0.082	0.065	0.177	0.505	0.843	0.949	0.965	0.971
48	0.220	0.193	0.156	0.140	0.124	0.100	0.080	0.201	0.505	0.832	0.942	0.961	0.970
49	0.325	0.290	0.233	0.207	0.179	0.143	0.102	0.290	0.643	0.896	0.956	0.964	0.968
50	0.276	0.243	0.194	0.171	0.150	0.120	0.092	0.241	0.581	0.872	0.950	0.960	0.963
51	0.313	0.279	0.222	0.196	0.169	0.129	0.088	0.294	0.671	0.913	0.968	0.976	0.981
52	0.309	0.286	0.237	0.213	0.187	0.150	0.104	0.300	0.656	0.901	0.961	0.970	0.975
53	0.324	0.295	0.248	0.227	0.205	0.174	0.137	0.298	0.634	0.897	0.966	0.977	0.984
54	0.237	0.212	0.171	0.153	0.134	0.111	0.085	0.210	0.534	0.815	0.893	0.906	0.913
55	0.294	0.262	0.212	0.189	0.165	0.138	0.101	0.248	0.591	0.878	0.954	0.966	0.972
56	0.389	0.362	0.318	0.302	0.282	0.256	0.218	0.392	0.719	0.939	0.992	1.001	1.005
57	0.350	0.317	0.262	0.236	0.209	0.172	0.127	0.309	0.664	0.919	0.984	0.995	1.001
58	0.293	0.263	0.216	0.194	0.172	0.141	0.108	0.265	0.610	0.898	0.978	0.990	0.996
59	0.231	0.204	0.163	0.145	0.126	0.104	0.079	0.196	0.500	0.777	0.862	0.879	0.887
60	0.308	0.276	0.226	0.203	0.180	0.147	0.110	0.277	0.630	0.895	0.965	0.977	0.983
61	0.210	0.184	0.142	0.124	0.106	0.085	0.062	0.187	0.537	0.849	0.942	0.958	0.965
62	0.329	0.302	0.253	0.229	0.203	0.167	0.119	0.309	0.650	0.883	0.941	0.951	0.957
63	0.310	0.294	0.253	0.233	0.210	0.176	0.122	0.321	0.655	0.864	0.918	0.930	0.937
64	0.396	0.367	0.320	0.299	0.277	0.249	0.218	0.370	0.683	0.918	0.980	0.990	0.996
65	0.271	0.237	0.188	0.166	0.146	0.118	0.094	0.232	0.581	0.899	0.984	0.994	0.997
66	0.301	0.265	0.211	0.187	0.164	0.132	0.102	0.264	0.628	0.933	1.013	1.023	1.027
67	0.313	0.295	0.252	0.232	0.209	0.174	0.123	0.322	0.663	0.886	0.947	0.961	0.969
68	0.380	0.362	0.314	0.288	0.257	0.217	0.144	0.376	0.694	0.864	0.904	0.913	0.919
69	0.302	0.266	0.211	0.186	0.162	0.131	0.096	0.259	0.625	0.917	0.995	1.006	1.010
70	0.333	0.320	0.278	0.257	0.230	0.191	0.126	0.360	0.710	0.908	0.957	0.969	0.975
71	0.265	0.228	0.177	0.154	0.133	0.103	0.079	0.220	0.561	0.879	0.974	0.987	0.992
72	0.254	0.227	0.182	0.161	0.140	0.111	0.083	0.232	0.585	0.887	0.970	0.984	0.991
73	0.341	0.304	0.241	0.210	0.179	0.134	0.086	0.309	0.684	0.911	0.965	0.973	0.977
74	0.343	0.321	0.270	0.245	0.217	0.173	0.118	0.350	0.713	0.920	0.968	0.976	0.981
75	0.249	0.238	0.212	0.203	0.190	0.166	0.127	0.286	0.593	0.832	0.902	0.919	0.929
76	0.257	0.229	0.187	0.170	0.154	0.127	0.099	0.250	0.589	0.870	0.948	0.960	0.965
77	0.256	0.225	0.182	0.164	0.146	0.118	0.090	0.242	0.605	0.905	0.985	0.997	1.002
78	0.237	0.209	0.167	0.148	0.130	0.104	0.082	0.216	0.552	0.859	0.949	0.965	0.974
79	0.289	0.264	0.219	0.199	0.176	0.147	0.110	0.265	0.599	0.869	0.944	0.957	0.964
80	0.370	0.347	0.303	0.284	0.261	0.231	0.193	0.360	0.677	0.884	0.937	0.947	0.952

## Appendix G - Canopy Reflectance and Biophysical Attributes on HQC, June 30, 2004

ID	Wavelength (nm)						LAI	fPAR	SPAD	Cover (%)	Soil water	Water content
	470	510	550	675	700	800						
1	0.061	0.076	0.156	0.080	0.178	0.496	0.9	0.326	38.0	0.72	0.63	1.79
2	0.065	0.081	0.173	0.081	0.185	0.507	0.9	0.328	32.0	0.76	0.58	1.72
3	0.069	0.085	0.179	0.087	0.196	0.565	1.4	0.184	37.0	0.76	0.6	1.62
4	0.066	0.084	0.185	0.080	0.187	0.593	0.8	0.354	36.0	0.71	0.39	1.59
5	0.062	0.078	0.174	0.076	0.183	0.585	1.3	0.188	41.0	0.78	0.6	1.60
6	0.065	0.081	0.171	0.085	0.193	0.482	1.3	0.197	48.0	0.80	0.72	1.72
7	0.061	0.080	0.194	0.065	0.181	0.730	1.4	0.183	40.0	0.85	0.6	1.69
8	0.067	0.085	0.189	0.076	0.185	0.603	1.4	0.185	47.0	0.85	0.6	1.79
9	0.075	0.097	0.224	0.084	0.216	0.896	2.4	0.063	42.0	0.83	0.6	1.84
10	0.088	0.103	0.192	0.100	0.208	0.701	1.4	0.181	52.0	0.80	0.58	1.46
11	0.073	0.093	0.220	0.078	0.207	0.807	1.6	0.147	54.0	0.91	0.67	1.52
12	0.065	0.079	0.172	0.073	0.182	0.733	1.1	0.243	39.0	0.84	0.58	1.60
13	0.056	0.068	0.138	0.068	0.153	0.503	1.6	0.143	43.0	0.67	0.63	1.41
14	0.058	0.073	0.161	0.068	0.163	0.623	1.4	0.180	42.0	0.83	0.63	1.75
15	0.051	0.064	0.134	0.064	0.149	0.483	1.6	0.140	41.0	0.78	0.6	1.56
16	0.071	0.084	0.166	0.085	0.183	0.592	1.3	0.205	51.0	0.77	0.65	1.69
17	0.054	0.069	0.163	0.060	0.168	0.715	2.1	0.093	46.0	0.72	0.65	1.73
18	0.072	0.092	0.208	0.084	0.215	0.658	1.2	0.222	45.0	0.82	0.7	1.63
19	0.064	0.078	0.165	0.077	0.208	0.660	1.7	0.134	41.0	0.73	0.7	1.61
20	0.065	0.080	0.180	0.071	0.185	0.600	2.1	0.090	48.0	0.75	0.65	1.61
21	0.062	0.077	0.165	0.074	0.190	0.610	1.2	0.236	34.0	0.80	0.77	1.51
22	0.058	0.073	0.160	0.076	0.180	0.556	2	0.104	36.0	0.78	0.67	1.57
23	0.059	0.076	0.183	0.064	0.166	0.608	1.2	0.228	51.0	0.88	0.7	1.57
24	0.061	0.076	0.176	0.067	0.181	0.726	2.2	0.084	48.0	0.79	0.67	1.53
25	0.073	0.094	0.220	0.080	0.215	0.739	2.2	0.083	52.0	0.82	0.65	1.70
26	0.065	0.082	0.187	0.074	0.185	0.683	1.9	0.114	40.0	0.86	0.6	1.61
27	0.058	0.076	0.165	0.074	0.174	0.465	1.8	0.128	41.0	0.89	0.67	1.75
28	0.094	0.113	0.218	0.105	0.218	0.796	1.5	0.185	36.0	0.92	0.67	1.64
29	0.073	0.094	0.208	0.082	0.207	0.706	1.6	0.155	35.0	0.89	0.63	1.76
30	0.072	0.088	0.190	0.079	0.197	0.655	2	0.110	42.0	0.83	0.6	1.37
31	0.059	0.077	0.178	0.075	0.183	0.515	1.5	0.186	35.0	0.77	0.75	1.63
32	0.063	0.074	0.146	0.074	0.191	0.668	2.1	0.097	51.0	0.60	0.57	1.62
33	0.065	0.080	0.174	0.074	0.189	0.681	1.7	0.146	54.0	0.89	0.65	1.65
34	0.063	0.078	0.175	0.064	0.156	0.596	2.1	0.101	51.0	0.76	0.7	1.80
35	0.052	0.065	0.150	0.057	0.151	0.613	1.9	0.116	49.0	0.87	0.72	1.57
36	0.065	0.079	0.159	0.071	0.161	0.770	2	0.112	56.0	0.91	0.77	1.83
37	0.067	0.084	0.183	0.079	0.193	0.622	2.4	0.072	48.0	0.87	0.83	1.61

38	0.061	0.078	0.184	0.067	0.182	0.676	2.8	0.051	47.0	0.86	0.83	1.51
39	0.058	0.072	0.169	0.061	0.164	0.723	1.4	0.214	50.0	0.81	0.83	1.67
40	0.061	0.077	0.172	0.069	0.171	0.558	1.5	0.177	47.0	0.88	0.75	1.51
41	0.041	0.054	0.130	0.044	0.112	0.500	2	0.111	53.0	0.91	0.6	1.50
42	0.064	0.080	0.184	0.065	0.171	0.648	1.5	0.190	58.0	0.84	0.72	1.60
43	0.053	0.067	0.152	0.055	0.150	0.594	2.4	0.081	55.0	0.80	0.72	1.66
44	0.053	0.067	0.152	0.055	0.150	0.593	1.8	0.143	53.0	0.74	0.75	1.65
45	0.052	0.067	0.169	0.054	0.154	0.594	2.6	0.067	61.0	0.84	0.78	1.62
46	0.061	0.077	0.174	0.065	0.165	0.567	2.5	0.075	49.0	0.88	0.7	1.69
47	0.055	0.069	0.149	0.062	0.148	0.441	1.5	0.190	42.0	0.83	0.75	1.81
48	0.046	0.058	0.139	0.047	0.121	0.638	2.2	0.099	65.0	0.85	0.67	1.62
49	0.064	0.079	0.170	0.067	0.171	0.650	1.9	0.134	52.0	0.89	0.65	1.56
50	0.061	0.077	0.172	0.072	0.183	0.525	1.7	0.159	52.0	0.77	0.78	1.59
51	0.062	0.077	0.169	0.072	0.166	0.466	1.9	0.126	46.0	0.84	0.77	1.57
52	0.059	0.079	0.187	0.068	0.183	0.536	1.8	0.142	44.0	0.82	0.72	1.62
53	0.066	0.085	0.198	0.078	0.214	0.571	2.8	0.056	47.0	0.86	0.65	1.59
54	0.052	0.070	0.173	0.063	0.180	0.536	2.1	0.104	41.0	0.87	0.63	1.52
55	0.072	0.095	0.239	0.077	0.230	0.747	2.1	0.107	54.0	0.83	0.7	1.58
56	0.052	0.069	0.162	0.061	0.177	0.626	2.6	0.070	48.0	0.75	0.65	1.67
57	0.065	0.083	0.190	0.071	0.197	0.652	2	0.123	48.0	0.74	0.75	1.61
58	0.056	0.076	0.191	0.063	0.200	0.715	1.8	0.139	41.0	0.79	0.63	1.59
59	0.052	0.066	0.154	0.053	0.132	0.646	2.3	0.090	59.0	0.90	0.81	1.58
60	0.076	0.092	0.197	0.078	0.179	0.633	2.3	0.093	47.0	0.89	0.83	1.49
61	0.064	0.082	0.177	0.074	0.174	0.586	1.6	0.182	65.0	0.84	0.78	1.72
62	0.051	0.069	0.179	0.054	0.158	0.720	2.8	0.057	60.0	0.94	0.81	1.94
63	0.056	0.073	0.156	0.075	0.167	0.408	1.1	0.306	29.0	0.66	0.81	1.64
64	0.059	0.073	0.164	0.062	0.166	0.748	2.8	0.058	54.0	0.88	0.75	1.49
65	0.058	0.081	0.199	0.065	0.184	0.751	2.2	0.107	58.0	0.91	0.77	1.59
66	0.070	0.087	0.182	0.079	0.198	0.675	1.5	0.202	55.0	0.78	0.78	1.50
67	0.061	0.075	0.164	0.065	0.155	0.531	1.8	0.145	53.0	0.87	0.83	1.55
68	0.056	0.076	0.182	0.071	0.190	0.555	1.6	0.178	51.0	0.86	0.86	2.23
69	0.063	0.084	0.190	0.073	0.181	0.547	1.3	0.239	35.0	0.81	0.88	1.58
70	0.059	0.079	0.174	0.075	0.179	0.484	1.8	0.153	39.0	0.80	0.91	1.55
71	0.062	0.084	0.202	0.070	0.200	0.654	2	0.123	41.0	0.86	0.99	1.72
72	0.048	0.064	0.154	0.060	0.152	0.510	1.2	0.281	51.0	0.84	0.83	1.55
73	0.058	0.078	0.184	0.075	0.196	0.593	1.4	0.251	52.0	0.78	1.01	1.69
74	0.057	0.075	0.156	0.077	0.181	0.513	0.9	0.408	46.0	0.73	0.93	1.54
75	0.063	0.081	0.180	0.075	0.176	0.574	1.6	0.208	44.0	0.87	0.93	1.88
76	0.068	0.084	0.183	0.078	0.197	0.693	1.9	0.151	65.0	0.83	1.09	1.66
77	0.076	0.097	0.213	0.088	0.251	0.730	2.7	0.079	48.0	0.83	1.06	1.55
78	0.066	0.084	0.189	0.071	0.189	0.703	1.8	0.160	52.0	0.85	0.88	1.48
79	0.065	0.082	0.180	0.073	0.178	0.564	2.2	0.121	54.0	0.77	0.78	1.68
80	0.066	0.084	0.182	0.079	0.198	0.589	1.7	0.182	58.0	0.78	0.88	1.51

## Appendix H - Canopy Reflectance and Biophysical Attributes on HQC, July 26, 2004

ID	Wavelength (nm)						LAI	fPAR	SPAD	Cover (%)	Soil water	Water content
	470	510	550	675	700	800						
1	0.024	0.032	0.063	0.037	0.085	0.300	3.1	0.158	27.6	0.79	0.48	1.57
2	0.029	0.038	0.072	0.044	0.096	0.293	4	0.094	29	0.73	0.6	1.90
3	0.027	0.035	0.074	0.033	0.090	0.359	3.7	0.114	31.1	0.72	0.63	1.57
4	0.030	0.039	0.074	0.047	0.095	0.279	3	0.173	22.3	0.68	0.45	1.49
5	0.024	0.032	0.066	0.034	0.081	0.333	3.5	0.126	27.2	0.75	0.65	1.50
6	0.029	0.039	0.080	0.039	0.099	0.376	3	0.166	31.9	0.79	0.45	1.49
7	0.023	0.032	0.072	0.029	0.082	0.411	5.3	0.045	20	0.86	0.72	1.74
8	0.024	0.031	0.065	0.030	0.072	0.324	4.7	0.063	30.8	0.86	0.65	1.66
9	0.029	0.038	0.082	0.034	0.094	0.449	5.3	0.044	26.5	0.86	0.63	1.59
10	0.031	0.041	0.088	0.036	0.096	0.403	4.2	0.086	27.2	0.78	0.57	1.55
11	0.035	0.047	0.103	0.044	0.115	0.527	5.7	0.036	27.3	0.90	0.58	1.38
12	0.028	0.036	0.072	0.037	0.090	0.404	4.4	0.076	26.1	0.74	0.57	1.35
13	0.022	0.029	0.058	0.028	0.070	0.307	3.5	0.127	31.5	0.79	0.6	1.47
14	0.029	0.038	0.081	0.034	0.089	0.427	6.1	0.028	30.4	0.81	0.55	1.56
15	0.027	0.036	0.078	0.035	0.094	0.374	4.3	0.079	25.1	0.80	0.53	1.70
16	0.032	0.042	0.085	0.043	0.108	0.417	3.9	0.101	23.8	0.71	0.57	1.58
17	0.026	0.033	0.068	0.033	0.087	0.397	5.4	0.044	38.4	0.75	0.7	1.66
18	0.020	0.028	0.065	0.027	0.078	0.364	4.2	0.084	30.3	0.76	0.63	1.53
19	0.027	0.036	0.075	0.037	0.099	0.380	5	0.052	30.7	0.72	0.7	1.63
20	0.025	0.033	0.075	0.030	0.088	0.392	4.8	0.061	28.8	0.85	0.6	1.70
21	0.028	0.037	0.075	0.038	0.092	0.357	3.3	0.146	23.7	0.68	0.48	1.71
22	0.024	0.031	0.060	0.034	0.076	0.308	4.7	0.066	26.8	0.69	0.57	1.47
23	0.022	0.030	0.068	0.027	0.074	0.365	4.4	0.077	28	0.82	0.57	1.46
24	0.022	0.030	0.067	0.027	0.076	0.367	5	0.056	33.7	0.72	0.65	1.39
25	0.029	0.039	0.086	0.036	0.098	0.445	5.6	0.038	32.2	0.76	0.6	1.46
26	0.030	0.041	0.090	0.038	0.099	0.401	5.6	0.039	35.7	0.84	0.65	1.65
27	0.025	0.035	0.079	0.031	0.091	0.376	3.7	0.115	24.1	0.84	0.6	1.69
28	0.028	0.039	0.089	0.033	0.097	0.410	3.5	0.126	27.9	0.83	0.67	1.39
29	0.026	0.036	0.074	0.033	0.082	0.333	3.9	0.102	24.7	0.75	0.6	1.64
30	0.031	0.040	0.082	0.037	0.097	0.435	4.6	0.069	27.6	0.75	0.53	1.60
31	0.028	0.037	0.073	0.040	0.091	0.323	3.9	0.100	26.1	0.64	0.58	1.63
32	0.032	0.044	0.096	0.041	0.116	0.473	5.4	0.044	32.9	0.77	0.63	1.55
33	0.029	0.039	0.083	0.036	0.097	0.465	4.8	0.061	36.5	0.75	0.6	1.58
34	0.027	0.035	0.073	0.031	0.080	0.380	5.3	0.046	38.5	0.74	0.63	1.66
35	0.025	0.032	0.070	0.032	0.085	0.403	4.9	0.059	30.1	0.75	0.78	1.44
36	0.024	0.032	0.072	0.029	0.082	0.391	4.8	0.060	28.1	0.76	0.78	1.78

37	0.025	0.034	0.076	0.031	0.092	0.410	5.1	0.051	27.7	0.71	0.93	1.67
38	0.028	0.038	0.085	0.033	0.099	0.455	5.1	0.051	27.3	0.76	0.91	1.81
39	0.030	0.038	0.075	0.037	0.092	0.422	5.1	0.051	29.3	0.70	0.78	1.63
40	0.033	0.043	0.091	0.039	0.100	0.432	4.9	0.057	25.7	0.69	0.81	1.45
41	0.023	0.031	0.069	0.027	0.072	0.399	6	0.032	33.5	0.89	0.7	1.58
42	0.027	0.036	0.078	0.034	0.087	0.378	5	0.057	26.9	0.88	0.7	1.54
43	0.028	0.038	0.083	0.035	0.097	0.420	6.1	0.030	28.4	0.81	0.7	1.76
44	0.030	0.040	0.084	0.045	0.107	0.379	4.2	0.088	22.8	0.84	0.67	1.78
45	0.021	0.027	0.060	0.022	0.062	0.381	5.4	0.044	23.5	0.97	0.77	1.64
46	0.033	0.042	0.086	0.038	0.099	0.379	4.9	0.061	24.4	0.90	0.75	1.66
47	0.025	0.032	0.066	0.034	0.083	0.336	4.3	0.082	29.6	0.80	0.78	1.52
48	0.027	0.037	0.079	0.032	0.087	0.433	4.9	0.059	30.6	0.85	0.81	1.80
49	0.034	0.045	0.096	0.044	0.113	0.417	4.5	0.076	33.2	0.90	0.43	1.76
50	0.029	0.038	0.075	0.042	0.099	0.333	4	0.099	28.4	0.84	0.75	1.69
51	0.025	0.034	0.074	0.035	0.094	0.351	5.1	0.053	25.5	0.89	0.65	1.53
52	0.024	0.033	0.070	0.034	0.093	0.327	4	0.099	24.3	0.88	0.7	1.63
53	0.021	0.030	0.069	0.025	0.078	0.376	6.5	0.024	25.7	0.96	0.65	1.64
54	0.021	0.028	0.059	0.030	0.073	0.292	3.3	0.152	22.4	0.87	0.7	1.56
55	0.033	0.045	0.099	0.040	0.111	0.442	4.1	0.092	28.4	0.82	0.7	1.61
56	0.023	0.029	0.061	0.032	0.086	0.324	4.2	0.091	26.5	0.89	0.67	1.59
57	0.027	0.036	0.074	0.039	0.107	0.358	3.6	0.122	26.3	0.73	0.7	1.71
58	0.022	0.029	0.055	0.032	0.071	0.254	3.4	0.140	38.8	0.88	0.72	1.83
59	0.019	0.025	0.053	0.026	0.071	0.333	4.7	0.068	26.3	0.84	1.17	1.17
60	0.031	0.037	0.060	0.053	0.101	0.301	4.1	0.095	21.4	0.46	1.2	1.29
61	0.028	0.038	0.081	0.036	0.095	0.390	2.9	0.191	31.2	0.81	0.81	1.55
62	0.023	0.033	0.082	0.028	0.084	0.480	4.1	0.095	30.1	0.89	0.67	1.56
63	0.024	0.031	0.056	0.039	0.076	0.223	2.5	0.240	22.1	0.70	0.75	1.62
64	0.028	0.037	0.078	0.032	0.088	0.477	4.4	0.081	29.6	0.85	0.77	1.82
65	0.024	0.034	0.081	0.032	0.091	0.389	4.9	0.061	30.3	0.86	0.77	1.72
66	0.023	0.032	0.065	0.030	0.079	0.350	3.7	0.117	25	0.82	0.88	1.54
67	0.025	0.033	0.066	0.033	0.078	0.322	5.1	0.055	25.8	0.93	0.78	1.72
68	0.021	0.029	0.061	0.030	0.075	0.297	3.8	0.112	25.7	0.90	1.01	3.93
69	0.025	0.033	0.066	0.036	0.086	0.288	3.7	0.122	24.5	0.83	1.06	0.60
70	0.022	0.032	0.070	0.031	0.079	0.305	4.3	0.085	33.1	0.86	0.81	1.61
71	0.025	0.036	0.079	0.035	0.096	0.371	4.6	0.072	27.9	0.84	0.88	1.43
72	0.020	0.028	0.062	0.029	0.073	0.295	3.9	0.106	29.3	0.85	0.86	1.80
73	0.024	0.032	0.066	0.034	0.083	0.312	3.8	0.112	23.5	0.78	0.83	1.59
74	0.024	0.033	0.068	0.037	0.087	0.309	4.2	0.089	27.2	0.81	0.77	1.50
75	0.021	0.029	0.060	0.030	0.076	0.334	5.1	0.055	23.4	0.90	0.91	1.60
76	0.030	0.039	0.078	0.043	0.106	0.397	6.7	0.022	27.2	0.74	0.88	1.76
77	0.029	0.042	0.086	0.049	0.123	0.376	4.8	0.063	26.8	0.70	0.93	1.45
78	0.024	0.032	0.068	0.035	0.089	0.389	6.9	0.020	28.1	0.78	1.01	1.62
79	0.031	0.042	0.087	0.040	0.112	0.428	4.7	0.068	29	0.74	0.91	1.52
80	0.023	0.031	0.058	0.035	0.078	0.271	5.3	0.050	30.3	0.75	0.96	1.73

## Appendix I - Canopy Reflectance and Biophysical Attributes on HQC, September 01, 2004

ID	Wavelength (nm)						LAI	fPAR	SPAD	Cover (%)	Soil water	Water content
	470	510	550	675	700	800						
1	0.024	0.031	0.054	0.042	0.082	0.240	1.6	0.151	24.1	0.38	0.5	1.34
2	0.026	0.033	0.055	0.046	0.083	0.221	1.6	0.156	25	0.45	0.58	1.43
3	0.028	0.036	0.061	0.046	0.095	0.277	2.4	0.067	28.3	0.42	0.38	1.43
4	0.032	0.041	0.071	0.056	0.107	0.280	1.7	0.145	25.5	0.43	0.29	1.28
5	0.029	0.038	0.071	0.047	0.103	0.340	1.5	0.169	25.3	0.52	0.46	1.24
6	0.021	0.027	0.052	0.034	0.107	0.280	2	0.098	26.6	0.71	0.39	1.45
7	0.030	0.039	0.075	0.045	0.076	0.344	3	0.040	29.7	0.60	0.57	1.34
8	0.031	0.043	0.087	0.051	0.097	0.415	2.2	0.086	27.8	0.61	0.45	1.49
9	0.026	0.035	0.065	0.044	0.119	0.318	3.2	0.034	29.6	0.46	0.48	1.53
10	0.026	0.035	0.065	0.044	0.102	0.318	2	0.105	28.8	0.53	0.45	1.41
11	0.021	0.028	0.058	0.031	0.084	0.336	2.1	0.088	27.5	0.46	0.39	1.21
12	0.027	0.034	0.061	0.045	0.091	0.297	2	0.102	29.1	0.40	0.43	1.33
13	0.023	0.030	0.054	0.037	0.078	0.265	2.3	0.075	27.2	0.44	0.48	1.44
14	0.027	0.036	0.068	0.041	0.100	0.364	2.4	0.067	27.2	0.37	0.45	1.17
15	0.028	0.035	0.062	0.048	0.101	0.326	2.1	0.096	27.7	0.47	0.45	1.39
16	0.028	0.036	0.063	0.050	0.101	0.321	2.2	0.088	27.5	0.43	0.46	1.29
17	0.019	0.025	0.045	0.035	0.078	0.285	2.7	0.050	29.3	0.61	0.53	1.46
18	0.023	0.030	0.059	0.038	0.087	0.319	2.2	0.084	31.4	0.48	0.46	1.54
19	0.025	0.033	0.064	0.038	0.098	0.352	3.2	0.034	30	0.62	0.48	1.64
20	0.020	0.028	0.058	0.031	0.081	0.335	2.8	0.046	28	0.60	0.65	1.49
21	0.022	0.029	0.052	0.037	0.078	0.262	1.6	0.165	32.3	0.44	0.5	1.31
22	0.020	0.026	0.050	0.036	0.078	0.287	1.9	0.120	32.1	0.41	0.48	1.36
23	0.023	0.031	0.061	0.038	0.079	0.300	2.6	0.061	30.1	0.62	0.45	1.39
24	0.023	0.030	0.057	0.038	0.080	0.285	2.1	0.099	28.5	0.50	0.41	1.50
25	0.028	0.039	0.078	0.045	0.109	0.362	2.7	0.056	24.9	0.52	0.43	1.43
26	0.025	0.034	0.066	0.038	0.088	0.324	2.5	0.065	32.5	0.66	0.45	1.42
27	0.027	0.036	0.069	0.048	0.108	0.335	2.2	0.091	26.7	0.58	0.39	1.45
28	0.027	0.038	0.076	0.046	0.111	0.340	2.2	0.087	23.2	0.65	0.46	1.31
29	0.026	0.035	0.064	0.044	0.086	0.276	1.8	0.136	26.1	0.52	0.43	1.47
30	0.027	0.034	0.061	0.046	0.094	0.321	2.5	0.070	29.3	0.51	0.43	1.25
31	0.028	0.036	0.060	0.051	0.093	0.271	1.9	0.123	27.1	0.43	0.5	1.36
32	0.028	0.036	0.068	0.044	0.110	0.366	3.6	0.024	26	0.55	0.46	1.59
33	0.020	0.027	0.055	0.031	0.075	0.292	2	0.107	28.1	0.57	0.41	1.63
34	0.017	0.022	0.040	0.030	0.064	0.256	3.4	0.029	30.2	0.40	0.57	1.59
35	0.024	0.032	0.063	0.039	0.094	0.344	2.4	0.076	25.3	0.40	0.55	1.52
36	0.027	0.037	0.081	0.037	0.104	0.436	2.3	0.083	28.3	0.54	0.55	1.56
37	0.019	0.026	0.055	0.030	0.075	0.314	3.1	0.038	27.2	0.50	0.67	1.51
38	0.024	0.032	0.060	0.039	0.089	0.319	3.5	0.028	31.7	0.60	0.58	1.46

39	0.030	0.038	0.067	0.051	0.104	0.348	2.8	0.055	31.7	0.46	0.77	1.47
40	0.032	0.041	0.074	0.051	0.106	0.360	2.8	0.053	27.9	0.41	0.48	1.71
41	0.017	0.023	0.048	0.026	0.066	0.300	2.4	0.079	26.4	0.50	0.46	1.25
42	0.024	0.031	0.055	0.042	0.106	0.342	2.5	0.076	27.9	0.37	0.41	1.57
43	0.020	0.025	0.044	0.038	0.084	0.285	3.1	0.041	27	0.41	0.5	1.48
44	0.027	0.035	0.061	0.051	0.099	0.287	1.9	0.131	24.9	0.42	0.63	1.50
45	0.009	0.012	0.024	0.013	0.032	0.165	3.9	0.021	29.4	0.73	0.57	1.66
46	0.027	0.035	0.066	0.042	0.101	0.330	3.5	0.028	25.4	0.49	0.57	1.69
47	0.021	0.027	0.050	0.034	0.070	0.287	2.5	0.074	25.8	0.42	0.53	1.48
48	0.027	0.039	0.088	0.046	0.126	0.398	2.4	0.078	25.1	0.42	0.53	1.72
49	0.030	0.041	0.081	0.045	0.117	0.363	2.2	0.100	26.4	0.39	0.53	1.51
50	0.022	0.029	0.052	0.039	0.083	0.249	2.1	0.114	29.9	0.47	0.55	1.51
51	0.025	0.033	0.062	0.039	0.089	0.293	2.9	0.053	23.4	0.60	0.57	1.38
52	0.027	0.036	0.064	0.048	0.114	0.303	2.7	0.060	23.8	0.55	0.58	1.39
53	0.021	0.028	0.053	0.035	0.080	0.259	3.3	0.036	26.2	0.67	0.48	1.48
54	0.028	0.036	0.062	0.047	0.097	0.298	2.7	0.065	25.1	0.53	0.45	1.47
55	0.018	0.022	0.040	0.032	0.066	0.231	4	0.020	28.2	0.54	0.41	1.56
56	0.023	0.029	0.051	0.038	0.080	0.237	2.5	0.077	25.9	0.38	0.53	1.51
57	0.019	0.025	0.045	0.036	0.071	0.227	2.4	0.088	28.7	0.47	0.34	1.45
58	0.026	0.034	0.056	0.046	0.086	0.264	2.5	0.079	32.1	0.56	0.27	1.55
59	0.016	0.021	0.038	0.030	0.056	0.253	2.7	0.064	28.4	0.57	0.53	1.13
60	0.020	0.027	0.046	0.040	0.071	0.253	2.7	0.065	28.2	0.24	0.5	1.18
61	0.029	0.039	0.072	0.050	0.104	0.333	2.4	0.154	27.4	0.49	0.45	1.27
62	0.023	0.032	0.065	0.042	0.102	0.390	3.6	0.072	22	0.57	0.55	1.28
63	0.022	0.029	0.050	0.041	0.077	0.231	1.3	0.342	24.5	0.35	0.43	1.27
64	0.021	0.028	0.055	0.034	0.081	0.332	3	0.109	26.4	0.54	0.5	1.48
65	0.023	0.031	0.063	0.033	0.081	0.372	3.3	0.087	25.8	0.58	0.43	1.57
66	0.024	0.032	0.059	0.041	0.096	0.330	3	0.110	27.1	0.51	0.41	1.62
67	0.017	0.022	0.045	0.027	0.061	0.246	3	0.109	23.4	0.58	0.53	1.66
68	0.022	0.031	0.063	0.039	0.089	0.277	2.1	0.189	23	0.60	0.67	1.37
69	0.018	0.025	0.047	0.031	0.067	0.224	2.1	0.189	24.5	0.52	0.65	1.44
70	0.021	0.030	0.061	0.035	0.081	0.282	2.4	0.154	21.3	0.60	0.7	1.54
71	0.020	0.026	0.048	0.038	0.076	0.239	3.1	0.097	25.1	0.39	0.58	1.45
72	0.026	0.033	0.059	0.047	0.094	0.282	2.4	0.159	27.5	0.44	0.67	1.40
73	0.017	0.023	0.042	0.033	0.065	0.213	2.1	0.192	24.5	0.46	0.67	1.39
74	0.020	0.027	0.046	0.041	0.080	0.233	2	0.215	22.9	0.36	0.48	1.53
75	0.021	0.027	0.049	0.040	0.080	0.255	3.3	0.089	31.8	0.44	0.58	1.37
76	0.020	0.026	0.043	0.040	0.068	0.226	4.1	0.054	30.9	0.32	0.86	1.48
77	0.018	0.024	0.043	0.033	0.067	0.208	4.1	0.055	23.8	0.35	0.77	1.53
78	0.020	0.027	0.046	0.041	0.074	0.224	4.1	0.053	25.6	0.29	0.7	1.55
79	0.021	0.029	0.052	0.039	0.086	0.259	3.4	0.081	23.1	0.38	0.6	1.42
80	0.022	0.029	0.050	0.040	0.075	0.228	3.5	0.080	26.6	0.52	0.58	1.32

**Appendix J - Canopy Reflectance and Biophysical  
Attributes on 020BE, May 29, 2002**

ID	COOR-X	COOR-Y	Wavelength (nm)					SPAD	Height (cm)	fPAR	LAI
			480	560	660	830	1650				
11	709716.94	4327465.00	5.46	9.39	7.85	43.45	50.07	31.2	28	0.475	1.3
111	709713.50	4327463.00	6.33	10.35	9.16	45.1	54.84	30.3	25	0.546	1.1
112	709715.50	4327469.00	7.13	11.88	9.9	51.46	66.33	27.7	20	0.487	1.3
113	709720.50	4327467.00	7.07	11.76	9.71	49.3	62.71	28.3	19	0.419	1.5
114	709718.88	4327461.50	3.69	7.7	4.67	51.8	46.82	25.3	65	0.159	3.3
1141	709717.75	4327460.50	4.71	10.4	5.44	62.74	51.4	22	50	0.080	4.6
1142	709717.94	4327463.00	5.75	10.78	7.32	55.39	53.65	26.5	25	0.568	1
1143	709720.31	4327462.50	4.79	9.28	6.02	53.95	50.11	26	55	0.146	3.5
1144	709719.75	4327460.00	3.1	7.52	3.42	53.7	40.21	30.5	60	0.121	3.8
12	709726.25	4327462.50	5.85	11.62	7.28	59.8	54.94	32.6	23	0.279	2.3
13	709736.31	4327458.50	7.51	11.28	9.46	46.02	54.74	34.8	25	0.457	1.4
14	709745.00	4327454.00	6.19	10.74	8.87	44.57	53.12	29.8	17	0.318	2.1
15	709755.75	4327449.00	5.75	10.88	8.06	47.74	56.22	25.1	26	0.060	5.1
151	709752.31	4327446.50	6.64	10.45	9.39	45.2	56.25	28.3	30	0.605	0.9
152	709753.94	4327452.50	7.66	11.34	11.7	43.11	67.17	37.1	20	0.512	1.2
153	709759.56	4327451.00	5.13	10.15	6.54	51.07	52.54	20.7	38	0.246	2.5
154	709757.81	4327445.00	4.75	10.26	6.15	52.87	51.02	34.5	38	0.485	1.3
1541	709755.81	4327444.00	4.57	11.54	5.7	64.03	51.38	22.4	44	0.133	3.7
1542	709759.75	4327445.50	6.12	11.17	8.84	52.08	59.14	31.1	25	0.361	1.8
1543	709759.75	4327445.50	6.46	11.19	8.85	53.83	58.26	34.2	19	0.482	1.3
1544	709758.50	4327443.00	7.26	11.31	10.4	43.94	60.48	37	23	0.477	1.4
21	709720.63	4327475.50	5.83	9.87	8.49	42.21	55.05	38.2	28	0.688	0.7
22	709731.31	4327471.50	3.43	8.08	3.91	60.58	41.25	38	130	0.021	7.2
221	709728.19	4327468.50	6.09	10.44	8.49	46.65	57.58	38.1	75	0.342	2
222	709729.13	4327475.00	6.42	11.21	8.16	50.72	54.87	36.7	25	0.346	2
223	709735.00	4327473.50	4.65	9.89	5.6	72.53	49.74	34.6	140	0.115	4
224	709732.50	4327467.00	3.68	7.51	4.47	52.86	35.84	37.6	200	0.075	4.8
2241	709730.81	4327467.00	2.59	6.56	3.39	50.81	32.34	39.2	150	0.068	5

2242	709732.00	4327469.50	3.28	5.47	3.45	41	29.96	34.3	180	0.035	6.2
2243	709734.06	4327468.00	4.64	8.82	6.01	64.59	42.88	34.9	200	0.010	8.6
2244	709732.88	4327465.50	3.46	7.4	4.19	52.85	35.95	34.8	185	0.025	6.9
23	709741.63	4327468.00	3.93	7.5	5.44	47.16	44.54	33.7	80	0.364	1.9
24	709749.31	4327464.00	5.73	10.13	7.48	46.98	46	31.4	21	0.333	2
25	709759.31	4327461.50	4.91	8.64	7.01	44.74	45.15	33.2	45	0.296	2.3
31	709725.63	4327486.50	7.46	11.72	10.56	43.59	63.15	25.1	25	0.272	2.4
32	709737.38	4327483.50	7.54	10.91	10.91	38.49	65.04	30.2	24	0.140	3.7
33	709748.31	4327479.00	3.9	9.91	4.7	73.34	47.21	36.3	84	0.138	3.7
34	709755.88	4327474.50	5.93	9.09	8.63	37.86	52.07	31.9	30	0.482	1.3
341	709752.06	4327473.00	6.38	10.77	8.82	49.91	57.41	35.4	28	0.303	2.2
342	709754.94	4327478.50	5.75	10.89	7.64	55.33	55.77	30.6	28	0.234	2.7
343	709759.56	4327476.50	5.4	10.41	7.31	51.77	54.44	35.1	54	0.402	1.7
344	709757.06	4327470.50	6.52	10.88	8.92	45.81	54.22	39.4	20	0.354	1.9
3441	709755.38	4327470.00	6.53	10.49	9.57	45.15	59.51	38.1	24	0.507	1.3
3442	709756.50	4327472.50	6.89	10.44	9.42	42.72	54.93	37.9	25	0.347	2
3443	709758.81	4327471.50	6.76	10.86	10.16	42.66	54.94	35.4	20	0.387	1.8
3444	709757.75	4327469.00	6.43	10.77	9.45	46.19	56.36	30	20	0.490	1.3
35	709765.06	4327469.50	7.39	11.64	11.09	43.32	63.18	35	24	0.437	1.5
41	709731.25	4327498.50	6.59	10.77	9.44	39.8	57.03	26.9	35	0.257	2.5
42	709739.94	4327495.50	7.23	11.19	10.27	41.33	59.18	40	35	0.511	1.2
43	709749.31	4327491.00	6.3	10.42	9.45	41.85	60.66	29.5	31	0.508	1.3
431	709745.38	4327490.00	8.29	12.17	10.7	61.5	47.51	37.3	29	0.060	5.3
432	709747.56	4327494.50	7.3	10.86	10.92	37.57	62.2	34.9	25	0.550	1.1
433	709753.25	4327492.00	7.48	11.11	11.38	42.6	63.98	32.7	39	0.556	1.1
434	709751.13	4327487.00	4.97	9.9	6.92	57.33	56.09	30.5	30	0.375	1.8
4341	709749.31	4327486.50	3.21	7.66	4.03	48.92	36.41	28.8	80	0.184	3.2
4342	709750.31	4327489.00	6.55	10.29	9.38	44.61	56.28	34.4	20	0.683	0.7
4343	709752.63	4327488.00	6.34	9.89	9.69	38.15	56.62	35.1	26	0.647	0.8
4344	709751.75	4327485.00	3.82	11.12	4.87	71.61	50.53	24.7	30	0.546	1.1
44	709758.00	4327485.50	5.57	10.57	7.61	49.51	48.47	30.1	30	0.263	2.5
45	709769.44	4327479.50	7.29	12.03	10.33	48.85	64.39	35.2	25	0.502	1.3

**Appendix K - Canopy Reflectance and Biophysical  
Attributes on 020BW, May 29, 2002**

ID	COOR-X	COOR-Y	Wavelength (nm)					SPAD	Height (cm)	fPAR	LAI
			480	560	660	830	1650				
11	709603.75	4327524	6.59	10.6	9.69	43.58	58.93	30.9	19	0.305	2
111	709599.125	4327523	6.8	10.29	10.3	38.04	60.25	33.9	16	0.116	3.6
112	709603.625	4327528.5	5.83	9.93	8.68	44.52	54.79	36.2	25	0.275	2.2
113	709609.625	4327525.5	7.35	11.46	10.7	44.73	62.91	27.9	15	0.460	1.3
114	709603.875	4327519.5	8.33	12.54	11.44	45.62	66.68	31.1	22	0.259	2.3
1141	709601.875	4327519.5	8.33	12.09	12.81	40.88	67.63	32.1	21	0.762	0.4
1142	709603.813	4327521.5	7.38	11.5	10.81	44.24	62.38	34.1	29	0.348	1.8
1143	709605.813	4327519.5	7.58	11.98	11.43	46.75	66.27	35.5	16	0.518	1.1
1144	709603.938	4327517.5	7.4	11.24	11.23	44.02	65.51	32.7	11	0.411	1.5
12	709614.438	4327519.5	6.06	10.27	8.98	50.17	60.78	32.3	24	0.391	1.6
13	709623.125	4327515	8.86	13.09	12.92	47.88	72.7	33.9	25	0.472	1.2
14	709633.875	4327510	6.83	11.3	9.81	44.91	61.73	36.5	44	0.384	1.6
15	709648.563	4327503	7.32	12.15	10.04	55.56	65.34	24.2	30	0.194	2.8
151	709643.938	4327502.5	6.57	11.28	9.73	47.65	59.12	27	43	0.063	4.7
152	709646.438	4327507	4.55	8.16	6.11	38.2	41.16	30.9	200	0.064	4.7
153	709652.5	4327504	8.05	11.85	12.21	41.17	70.24	29.2	20	0.116	3.7
154	709649.313	4327499	6.73	11.06	9.87	46.28	62.11	23.8	25	0.333	1.9
1541	709647.813	4327498.5	6.86	10.65	10.36	43.6	63.39	32.6	30	0.046	5.3
1542	709648.813	4327501	7.87	12.45	11.55	48.88	66.52	32.1	41	0.220	2.6
1543	709651.313	4327499.5	7.14	11.36	10.52	47.79	62.84	32.2	34	0.386	1.6
1544	709649.75	4327497.5	6.93	11.15	10.67	49.92	68.16	31.9	23	0.356	1.7
21	709609.375	4327536	8.98	13.48	13.39	48.38	72.4	38.5	26	0.129	3.5
22	709622.063	4327530	8.15	12.44	11.73	47.59	62.07	33.9	30	0.358	1.7
221	709618.75	4327528.5	8.82	13.38	13.14	46.77	73.02	37.4	18	0.195	2.8
222	709620.438	4327533.5	7.31	11.6	10.95	48.12	65.1	36.8	25	0.149	3.3
223	709625.25	4327532	7.64	12.79	10.65	47.97	63.38	30.2	29	0.298	2.1
224	709623.313	4327526.5	8.7	14.1	13.45	58.14	75.49	28.4	19	0.607	0.8
2241	709621.625	4327525.5	8.1	12.56	12.49	46.72	67.9	30.7	24	0.545	1
2242	709622.5	4327528	7.88	12.3	12.13	51.04	69.92	32.2	24	0.182	2.9

2243	709624.75	4327527.5	8.31	13.21	12.28	50.38	71.18	35.1	20	0.353	1.8
2244	709623.938	4327524.5	9.08	13.29	14.22	44.85	74.27	31.5	19	0.445	1.4
23	709632.063	4327527.5	7.18	11.37	9.74	51.21	54.8	31.2	27	0.239	2.4
24	709643.438	4327522	8.17	12.26	12.03	48.6	71.67	33.4	31	0.196	2.8
25	709654.75	4327517.5	7.26	11.55	10.64	46.97	64.87	34.9	39	0.080	4.4
31	709614.313	4327548	5.6	9.2	7.78	45.11	48.59	41.8	19	0.304	2
32	709625.688	4327543	7.83	11.96	11.3	48.36	66	35.7	28	0.370	1.7
33	709636.375	4327540	8.16	12.64	12.24	46.09	69.36	30.8	26	0.380	1.6
34	709649.063	4327534.5	5.88	10.79	7.68	55.78	55.03	21.6	32	0.348	1.8
341	709645.563	4327532.5	7.44	11.37	10.54	46.99	62.92	32	25	0.250	2.4
342	709647.563	4327538	6.12	9.81	8.95	46.3	58.19	32.7	30	0.289	2.1
343	709652.563	4327536	4.38	9.68	5.57	54.45	45.1	31.5	175	0.057	5
344	709650.313	4327530.5	7.78	11.34	11.52	40.94	67.71	26.1	24	0.347	1.8
3441	709648.75	4327529.5	7.95	12.01	11.6	47.31	68.22	23.6	19	0.314	2
3442	709649.75	4327532.5	7.17	11.47	10.02	49.47	64.04	36.5	18	0.329	1.9
3443	709651.875	4327531	7.38	11.65	10.75	44.48	64.26	27.1	20	0.342	1.8
3444	709650.875	4327528.5	8.55	12.71	13.08	43.8	71.42	22.4	28	0.260	2.3
35	709661.688	4327530	6.64	10.71	9.44	42.48	58.28	34.6	40	0.344	1.8
41	709619.688	4327560	5.23	9.71	6.74	52.63	50.99	34.2	30	0.421	1.5
42	709631.313	4327555.5	7.81	11.44	10.63	44.74	58.8	38.4	30	0.691	0.6
43	709644	4327551	7.79	11.48	11.24	45.2	67.95	32.9	29	0.522	1.1
431	709640.375	4327548.5	10.1	13.52	15.76	37.58	81.25	32.2	28	0.820	0.3
432	709642.5	4327555	7.6	11.21	10.67	43.68	61.33	34.3	24	0.239	2.5
433	709647.938	4327552	6.53	10.88	8.61	48.02	56.48	30.7	25	0.916	0.1
434	709644.688	4327546.5	8.58	12.63	12.37	43.88	68.85	30.1	18	0.730	0.5
4341	709642.813	4327546	8.69	11.89	12.92	36.15	69.76	33	20	0.678	0.7
4342	709644.188	4327548.5	9.21	12.65	13.83	39.62	72.64	38.3	23	0.510	1.1
4343	709646.438	4327547.5	7.3	10.75	10.36	40.6	60.62	34.1	25	0.499	1.2
4344	709645.5	4327544.5	9.83	13.6	14.71	44.9	78.02	32.2	16	0.523	1.1
44	709654.688	4327547	2.59	5.73	3.26	44.73	28.22	38.7	200	0.031	6.1
45	709667.313	4327542	7.94	12.14	12.34	41.77	68.87	29.2	25	0.500	1.2

**Appendix L - Canopy Reflectance and Biophysical  
Attributes on 002CE, May 29, 2002**

ID	COOR-X	COOR-Y	Wavelength (nm)				SPAD	Height (cm)	fPAR	LAI
			560	660	830	1650				
11	709427.13	4327063.00	10.71	9.4	42.64	53.56	30.5	30	0.109	4.2
111	709431.75	4327063.00	9.91	9.19	40.43	52.57	30.7	20	0.210	3
112	709426.56	4327058.50	11.22	10.43	43.61	56.76	29.8	21	0.130	3.9
113	709423.19	4327062.50	10.68	9.36	43.47	54.88	30.9	24	0.071	5
114	709427.69	4327067.00	10.34	9.03	42.23	52.96	31.3	30	0.087	4.7
1141	709429.63	4327066.50	10.12	8.53	44.16	52.55	32.1	30	0.045	5.9
1142	709427.44	4327065.00	10.12	8.69	48.67	54.57	34.7	31	0.078	4.9
1143	709425.81	4327067.00	9.73	8.31	43.2	48.66	29.8	31	0.038	6.3
1144	709427.75	4327069.00	10.08	8.87	40.84	52.63	29.8	38	0.055	5.5
12	709418.31	4327071.00	10.11	9.3	42.5	52.33	30.1	28	0.094	4.5
13	709409.50	4327079.00	9.97	9.86	41.99	54.59	29.6	30	0.129	3.9
14	709400.69	4327087.50	10.34	8.27	45.73	54.07	32.5	28	0.098	4.4
15	709393.88	4327095.00	11.25	10.52	42.75	54.19	30.6	15	0.033	6.5
151	709397.31	4327095.50	10.6	9.41	42.81	50.88	31	21	0.055	5.5
152	709393.94	4327091.50	10.78	9.66	47.28	52.73	31.2	21	0.085	4.7
153	709390.56	4327095.50	14.69	15.26	45.17	67.75	31.3	15	0.079	4.8
154	709393.13	4327099.00	11.17	9.99	43.18	54.28	28.5	12	0.051	5.7
1541	709395.06	4327099.50	12.38	10.35	46.96	55.06	35.6	15	0.031	6.6
1542	709391.25	4327098.50	11.54	10.46	48.44	59.28	33	20	0.118	4.1
1543	709391.25	4327098.50	13.93	13.31	46.76	59.35	33.2	20	0.095	4.5
1544	709392.31	4327101.00	10.17	8.75	44.24	47.89	30.4	13	0.227	2.8
21	709416.00	4327058.00	11.04	9.55	44.51	54.13	27.9	28	0.119	4
22	709408.56	4327065.50	10.26	9.76	42.61	53.89	28.6	26	0.155	3.5
221	709412.50	4327065.50	10.8	9.62	41.62	52.86	27.3	27	0.154	3.5
222	709407.31	4327061.50	10.26	9.12	43.69	51.15	26.6	32	0.141	3.7
223	709403.25	4327065.50	12.99	11.86	60.59	75.99	28.1	31	0.230	2.8
224	709409.06	4327070.50	10.56	10.26	38.93	54.15	27.6	23	0.780	0.5
2241	709411.06	4327071.00	10.14	9.32	42.06	51.85	32.4	26	0.148	3.6
2242	709409.13	4327068.50	9.95	9.94	37.35	52.59	29	30	0.356	1.9

2243	709407.06	4327071.00	10.44	10.17	38.17	55.05	31.3	28	0.344	2
2244	709409.00	4327072.50	9.31	7.74	44	48.28	31.1	26	0.033	6.4
23	709400.38	4327073.50	9.17	9.18	38.7	50.72	30.5	31	0.071	5
24	709392.25	4327081.50	9.78	9.17	43.79	56.47	29.3	34	0.100	4.3
25	709383.44	4327090.00	11.46	10.52	42.59	53.13	27.9	27	0.064	5.2
31	709406.19	4327054.00	9.71	7.74	47.01	48.42	31.1	39	0.030	6.6
32	709398.75	4327061.00	9.92	9.71	40.29	53.52	26	28	0.068	5
33	709390.63	4327069.00	9.83	7.74	45.44	50.22	30.4	36	0.164	3.4
34	709383.13	4327076.50	10.07	7.85	48.09	54.42	30.4	41	0.080	4.7
341	709387.13	4327075.50	10.11	8.9	40.04	53.78	24.2	28	0.065	5.1
342	709382.38	4327073.00	11.39	9.49	44.9	53.31	28.7	28	0.091	4.5
343	709379.63	4327076.50	10.84	9.78	41.05	57.71	30.2	36	0.110	4.1
344	709384.44	4327080.00	10.58	9.45	41.32	52.44	26	25	0.419	1.6
3441	709387.00	4327080.00	10.52	9.06	45.08	55.45	30.9	23	0.224	2.8
3442	709383.75	4327078.00	11.87	10.69	43.31	57.75	30.3	30	0.086	4.6
3443	709382.38	4327081.00	10.84	9.78	43.24	54.29	32.1	30	0.108	4.2
3444	709385.00	4327082.00	13.61	13.79	44.33	62.42	28.4	24	0.712	0.6
35	709374.31	4327085.50	11.19	10.55	42.28	57.1	30	30	0.035	6.3
41	709393.13	4327048.50	10.07	8.29	46.7	51.41	28.8	35	0.163	3.4
42	709386.31	4327056.50	9.44	7.23	42.48	47.4	27.8	46	0.147	3.6
43	709381.56	4327062.50	9.87	8.28	45.96	51.88	31.3	33	0.097	4.4
431	709385.50	4327063.00	9.78	8.78	42.38	49.77	28.1	38	0.188	3.1
432	709379.00	4327059.00	9.42	7.7	44.18	48.75	31.8	37	0.053	5.5
433	709376.88	4327063.50	10.24	8.71	45.16	54.62	33.7	34	0.094	4.4
434	709382.06	4327067.00	10.48	9.1	44.19	52.34	29	32	0.051	5.5
4341	709383.94	4327066.50	9.76	8.93	43.49	50.48	31.1	34	0.360	1.9
4342	709381.69	4327065.00	16.77	18.12	44.24	73.44	26.4	25	0.091	4.5
4343	709380.50	4327067.50	10.34	8.59	44.29	51.54	27.3	31	0.009	8.8
4344	709382.25	4327068.50	10.1	8.38	45.62	51.63	28	33	0.090	4.5
44	709373.38	4327072.00	9.3	6.43	51.72	47.48	34.5	53	0.050	5.6
45	709367.31	4327078.50	10.97	9.88	44.99	57.9	33.8	34	0.627	0.8

**Appendix M - Canopy Reflectance and Biophysical  
Attributes on 002CW, May 29, 2002**

ID	COOR-X	COOR-Y	Wavelength (nm)				SPAD	Height (cm)	fPAR	LAI
			560	660	830	1650				
11	709350.25	4326924.00	11.39	11.76	42.03	61.48	23.5	30	0.114	4
111	709351.00	4326919.50	11.13	10.04	45.12	58.41	30	20	0.132	3.7
112	709345.00	4326922.00	10.22	9.68	37.93	50.88	28.8	21	0.165	3.3
113	709346.81	4326927.50	10.97	11.24	36.19	55.58	29.3	24	0.115	4
114	709354.81	4326925.50	11.1	10.19	40.05	52.83	29.4	30	0.162	3.3
1141	709355.75	4326924.00	11.52	10.75	39.68	54.99	29.3	30	0.140	3.6
1142	709352.88	4326924.50	11.38	11.34	40.03	58.22	31.2	31	0.084	4.5
1143	709353.38	4326927.50	10.84	10.31	39.12	53.94	29	31	0.100	4.2
1144	709356.06	4326927.00	11.3	10.14	42.04	53.89	28.7	38	0.111	4
12	709366.94	4326967.00	10.23	10.58	40.32	55.9	28.8	28	0.146	3.5
13	709360.25	4326969.00	10.64	10.27	38.65	54.97	29.6	30	0.066	5
14	709362.69	4326976.00	10.58	10.54	40.67	55.46	26.1	28	0.229	2.7
15	709369.44	4326972.50	12.21	12.61	39.38	60.1	32.9	15	0.291	2.2
151	709369.44	4326970.50	11.69	12.43	36.14	59.68	30.1	21	0.394	1.7
152	709367.13	4326972.50	12.38	12.9	39.34	60.66	24	21	0.481	1.3
153	709369.25	4326975.00	9.5	8.81	38.3	49.85	26.8	15	0.591	0.9
154	709371.38	4326973.00	9.51	7.65	42.81	48.24	29	12	0.899	0.2
1541	709372.06	4326972.00	9.99	6.78	51.26	46.59	30.9	15	0.199	2.9
1542	709356.69	4326926.00	10.01	7.1	48.82	47.66	28.6	20	0.409	1.6
1543	709370.50	4326972.00	10.31	7.56	47.88	49.8	26.5	20	0.307	2.1
1544	709355.25	4326926.50	10.9	8.85	46.52	52.56	27.6	13	0.230	2.7
21	709339.00	4326927.50	10.15	9.07	41.89	51.53	31.1	28	0.103	4.1
22	709341.19	4326940.00	9.82	9.54	37.75	52.31	29.9	26	0.427	1.5
221	709343.31	4326935.50	10.98	11.54	36.77	54.55	33.6	27	0.204	2.9
222	709337.31	4326938.50	11.37	10.65	40.52	56.6	30.6	32	0.136	3.6
223	709339.13	4326943.50	9.93	9.18	37.9	51.95	30.2	31	0.948	0.1
224	709345.13	4326940.50	10.2	11.63	34.91	56.23	31.8	23	0.213	2.8
2241	709345.38	4326938.50	9.99	10.78	33.46	52.75	29.2	26	0.438	1.5
2242	709343.00	4326940.00	9.73	10.54	35.43	53.4	27.2	30	0.266	2.4

2243	709344.75	4326942.50	10.05	10.35	35.67	52.32	29.9	28	0.325	2
2244	709347.13	4326941.00	11.13	12.18	38.32	59.28	36.5	26	0.165	3.2
23	709344.88	4326952.00	11.27	12.28	36.59	56.43	27.8	31	0.156	3.3
24	709348.50	4326963.50	11.22	11.52	39.59	56.31	26.2	34	0.163	3.3
25	709352.19	4326975.00	10.6	10.19	39.61	53.4	29.5	27	0.241	2.5
31	709326.88	4326933.50	10.48	7	60.71	51.66	35.7	39	0.076	4.6
32	709330.50	4326945.00	10.5	8.4	41.82	49.01	27.6	28	0.299	2.1
33	709333.50	4326957.50	10.77	9.68	38.89	51.85	29.4	36	0.075	4.6
34	709337.81	4326968.00	11.39	11.8	38.06	58.22	30.3	41	0.035	6
341	709338.56	4326964.00	10.18	10.44	36.82	54.4	28.7	28	0.108	4
342	709334.19	4326967.00	10.87	10.63	36.92	53.57	30.5	28	0.103	4.1
343	709336.38	4326971.00	11.52	10.74	41.89	55.22	28.6	36	0.239	2.5
344	709340.94	4326968.50	11.2	10.8	39.69	54.67	27.7	25	0.416	1.5
3441	709341.00	4326967.00	10.5	11.72	36.06	55.59	30.3	23	0.318	2
3442	709339.69	4326968.00	10.51	10.66	36.7	54.22	30.1	30	0.144	3.5
3443	709340.56	4326970.00	11.02	10.7	39.18	55.52	24.6	30	0.375	1.7
3444	709342.38	4326969.00	11.28	12.03	36.09	56.93	37.9	24	0.474	1.3
35	709340.19	4326978.50	11.71	10.69	43.07	55.24	31.6	30	0.277	2.3
41	709315.44	4326939.00	12.04	10.83	43.01	53.82	33.4	35	0.188	3
42	709319.19	4326949.50	12.26	11.37	41.72	57.01	29.6	46	0.068	4.8
43	709322.13	4326961.00	9.76	7.03	42.66	42.37	29.8	33	0.193	2.9
431	709323.94	4326957.50	9.58	5.61	51.66	42.68	32.6	38	0.156	3.3
432	709318.19	4326960.00	9.68	7.58	45.03	46.96	26.7	37	0.081	4.4
433	709320.19	4326964.50	10.69	8.04	45.85	51.09	29.8	34	0.106	4
434	709325.19	4326963.00	9.99	7.36	45.81	47.66	27.9	32	0.196	2.9
4341	709326.00	4326961.00	9.43	6.59	49.01	45.13	28.3	34	0.161	3.2
4342	709323.56	4326962.00	9.96	7.7	41.77	45.5	27.7	25	0.590	0.9
4343	709324.06	4326964.50	10.45	6.35	58.86	47.25	30	31	0.138	3.5
4344	709326.69	4326964.00	9.24	6.62	48.91	46.59	28.6	33	0.063	4.9
44	709324.50	4326971.00	10.81	10.66	38.23	52.54	25.7	53	0.013	7.7
45	709326.94	4326980.50	9.68	7.43	44.78	49.33	29.1	34	0.294	2.1

**Appendix N - Canopy Reflectance and Biophysical  
Attributes on 020BE, August 22, 2002**

ID	COOR-X	COOR-Y	Wavelength (nm)					SPAD	Height (cm)	fPAR	LAI
			480	560	660	830	1650				
11	709716.94	4327465.00	5.06	9.18	7.68	47.45	49.23	36.4	50	1.374	4
111	709713.50	4327463.00	5.56	9.96	8.21	49.59	50.75	31	34	1.097	2.8
112	709715.50	4327469.00	7.31	12.35	11.23	59.07	67.61	31.7	49	1.546	3
113	709720.50	4327467.00	5.32	9.12	7.35	47.35	48.79	30.4	41	1.349	2.3
114	709718.88	4327461.50	4.64	7.54	7.06	39.59	52.73	29.7	90	3.030	2.2
1141	709717.75	4327460.50	4.52	8.32	6.83	42.04	53.61	30.1	58	1.927	5.8
1142	709717.94	4327463.00	5.42	9.22	7.65	51.55	52.34	39.8	45	1.131	5
1143	709720.31	4327462.50	5.21	9.41	7.28	52.04	50.89	28.6	71	2.483	4
1144	709719.75	4327460.00	3.48	6.92	4.35	53.81	46.33	38	90	2.368	4.3
12	709726.25	4327462.50	5.44	9.32	7.49	48.33	49.54	37.8	42	1.111	4.3
13	709736.31	4327458.50	6.23	9.62	8.01	47.39	51.84	30.9	30	0.971	1.8
14	709745.00	4327454.00	6.34	9.53	9.74	36.7	54.08	30.2	31	1.026	1.8
15	709755.75	4327449.00	5.1	8.49	7.56	45.43	52.43	36.4	50	1.374	3.7
151	709752.31	4327446.50	5.42	8.46	7.87	40.15	51.66	35.2	34	0.966	3
152	709753.94	4327452.50	6.72	9.75	10.03	42.98	57.7	36	34	0.944	2.7
153	709759.56	4327451.00	5.66	8.59	8.08	43.7	58.41	36.7	46	1.253	3.7
154	709757.81	4327445.00	5.36	9.71	7.45	54.98	53.18	31.3	50	1.597	3.3
1541	709755.81	4327444.00	4.72	9.09	6.13	56.58	54.39	29.7	54	1.818	3.3
1542	709759.75	4327445.50	6.55	10.45	9.72	50.23	65.18	25.6	51	1.992	2.6
1543	709759.75	4327445.50	7.23	10.83	10.96	47.77	63.87	32.3	30	0.929	1.2
1544	709758.50	4327443.00	7.17	10.77	10.22	47.32	60.23	29	28	0.966	1.4
21	709720.63	4327475.50	5.4	8.98	8.1	44.9	52.49	42.5	65	1.529	2.2
22	709731.31	4327471.50	3.36	7.03	4.72	60.73	43.06	45.5	110	2.418	5.4
221	709728.19	4327468.50	4.82	8.16	6.88	47.22	48.66	44.6	70	1.570	4.5
222	709729.13	4327475.00	5.66	8.69	7.58	42.35	50.21	36.3	30	0.826	1.5
223	709735.00	4327473.50	4.26	8.02	5.69	76.19	52.47	39.2	200	5.102	6.5
224	709732.50	4327467.00	3.97	8.45	5.05	66.17	51.77	38.8	170	4.381	4
2241	709730.81	4327467.00	2.2	4.34	2.52	37.75	30.11	46.7	120	2.570	6
2242	709732.00	4327469.50	2.33	3.69	3.18	27.64	31.27	42.6	160	3.756	4

2243	709734.06	4327468.00	4.55	7.81	6.05	77.53	54.1	36	220	6.111	5.5
2244	709732.88	4327465.50	3.32	5.16	4.38	39.91	35.69	35.9	210	5.850	5.3
23	709741.63	4327468.00	3.23	5.57	4.01	46.63	38.67	40	82	2.050	5.4
24	709749.31	4327464.00	5.8	8.85	8.48	38.77	49.31	33.7	40	1.187	2.8
25	709759.31	4327461.50	5.64	8.58	8.17	36.82	47.16	34.7	53	1.527	4
31	709725.63	4327486.50	6.04	10.48	8.01	58.96	56.34	30.3	50	1.650	1.3
32	709737.38	4327483.50	4.64	7.84	6.09	40.5	45.24	34.5	40	1.159	3.8
33	709748.31	4327479.00	3.34	6.74	4.35	50.23	45.08	40.6	76	1.872	2.6
34	709755.88	4327474.50	3.89	6.54	5.74	41.01	39.24	42.6	41	0.962	3.9
341	709752.06	4327473.00	5.54	9.72	8.26	52.04	53.98	38.7	39	1.008	2
342	709754.94	4327478.50	4.89	9.3	7.36	58.19	54.29	35.1	48	1.368	2.9
343	709759.56	4327476.50	5.35	8.47	7.54	41.97	53.8	41.1	41	0.998	3.6
344	709757.06	4327470.50	7.06	11.32	10.44	47.88	58.87	34.4	37	1.076	1.6
3441	709755.38	4327470.00	5.59	9.01	7.81	49.17	50.71	33.9	51	1.504	3
3442	709756.50	4327472.50	5.54	9.54	8.21	50.85	53.85	34.7	36	1.037	1.4
3443	709758.81	4327471.50	7.57	11.08	11.78	39.55	62.52	32.4	35	1.080	2.2
3444	709757.75	4327469.00	6.66	9.87	10.01	42.42	57.31	34.4	30	0.872	1.6
35	709765.06	4327469.50	7.22	11.4	10.78	49.67	64.08	33.1	37	1.118	2.4
41	709731.25	4327498.50	6.75	10.25	10.19	40.47	57.53	26	30	1.154	2.3
42	709739.94	4327495.50	5.46	9.32	7.44	46.25	48.96	39.8	44	1.106	2.7
43	709749.31	4327491.00	4.36	7.46	6.28	41.28	44.94	31.4	50	1.592	3.1
431	709745.38	4327490.00	3.52	5.04	4	26.86	26.38	35.7	43	1.204	5.3
432	709747.56	4327494.50	5.69	8.79	8.82	36.29	55.57	31.2	52	1.667	3
433	709753.25	4327492.00	4.96	9.97	7.15	63.24	52.08	30.8	59	1.916	5.5
434	709751.13	4327487.00	3.01	5.74	4.42	39.31	36.25	33.9	36	1.062	4.5
4341	709749.31	4327486.50	3.18	6.82	3.84	49.04	36.94	36.1	95	2.632	7.4
4342	709750.31	4327489.00	4.99	8.1	7.67	42.34	50.62	33.6	53	1.577	2.4
4343	709752.63	4327488.00	4.59	7.95	7.04	49.85	51.23	35.3	40	1.133	2.4
4344	709751.75	4327485.00	3.65	9.02	4.57	68.06	50.92	34.1	102	2.991	2.5
44	709758.00	4327485.50	5.34	8.95	7.56	46.83	48.15	35.9	39	1.086	4.7
45	709769.44	4327479.50	7.11	11.89	11.23	49.38	65.64	30.6	36	1.176	1.3

**Appendix O - Canopy Reflectance and Biophysical  
Attributes on 020BW, August 22, 2002**

ID	COOR-X	COOR-Y	Wavelength (nm)					SPAD	Height (cm)	fPAR	LAI
			480	560	660	830	1650				
11	709603.75	4327524	7.13	10.48	11.53	41.64	63.99	32.1	22	0.289	2.3
111	709599.125	4327523	6.4	9.76	10.33	39.41	60.4	35	30	0.255	2.6
112	709603.625	4327528.5	6.41	10.47	10.7	44.98	56.99	44.5	33	0.160	3.5
113	709609.625	4327525.5	6.92	10.71	10.06	46.11	62.12	44.9	30	0.288	2.3
114	709603.875	4327519.5	6.82	10.69	10.74	47.66	60.94	33.5	25	0.169	3.4
1141	709601.875	4327519.5	6.51	10.37	10.88	49.27	62.92	37.1	33	0.050	5.8
1142	709603.813	4327521.5	6.84	10.61	11.39	45.49	63.08	33.4	29	0.192	3.1
1143	709605.813	4327519.5	7.22	10.86	12.19	45.25	69.37	32.7	22	0.503	1.2
1144	709603.938	4327517.5	7.11	10.27	12.31	44.48	71.62	32.3	15	0.419	1.6
12	709614.438	4327519.5	7.11	10.37	11.39	39.19	67.22	10.2	47	0.376	1.8
13	709623.125	4327515	7.64	11.89	11.08	51.99	65.07	24.5	28	0.250	2.6
14	709633.875	4327510	6.23	9.38	9.89	40.48	58.7	37.1	43	0.262	2.5
15	709648.563	4327503	5.28	8.84	7.83	54.29	51.15	33.2	42	0.090	4.6
151	709643.938	4327502.5	5.23	8.91	7.54	48.85	49.36	29.7	44	0.232	2.8
152	709646.438	4327507	5.28	6.72	6.7	59.58	34.67	26.3	33	0.059	5.5
153	709652.5	4327504	7.25	10.68	11.17	44.15	66.95	27.9	42	0.399	1.7
154	709649.313	4327499	5.96	9.25	9.13	48.55	56.96	33.5	44	0.216	2.9
1541	709647.813	4327498.5	4.97	8.51	6.66	51.46	44.91	34	54	0.257	2.6
1542	709648.813	4327501	5.82	10.33	8.94	57.13	56.8	30.1	46	0.101	4.4
1543	709651.313	4327499.5	5.82	9.65	7.67	52.48	47.41	40.6	51	0.287	2.4
1544	709649.75	4327497.5	5.25	8.79	8.3	49.49	55.23	28.9	47	0.183	3.2
21	709609.375	4327536	6.41	11.4	10.57	62.65	61.43	31.8	52	0.177	3.3
22	709622.063	4327530	6.39	10	8.95	48.73	52.36	33.4	47	0.135	3.8
221	709618.75	4327528.5	7.95	12.4	12.31	53.33	71.44	41.1	35	0.388	1.8
222	709620.438	4327533.5	7.59	11.19	11.8	50.61	67.57	33.6	27	0.306	2.2
223	709625.25	4327532	7.31	11.46	10.79	50.05	62.63	27.7	46	0.329	2.1
224	709623.313	4327526.5	7.6	12.75	11.41	59.97	69.22	35	48	0.346	2

2241	709621.625	4327525.5	8.22	10.91	13.08	31.53	66.23	35	20	0.448	1.5
2242	709622.5	4327528	6.52	10.19	10.72	49.97	64.72	34.9	46	0.287	2.3
2243	709624.75	4327527.5	7.32	12.35	10.93	59.24	66.86	36.3	32	0.245	2.7
2244	709623.938	4327524.5	8.28	12.13	13.18	48.77	72.42	31.9	30	0.618	0.9
23	709632.063	4327527.5	7.5	11.2	10.78	41.8	61.52	36.7	33	0.327	2.1
24	709643.438	4327522	6.35	10.06	10.01	51.84	58.14	26.9	49	0.285	2.4
25	709654.75	4327517.5	6.13	9.69	9.36	47.62	57.13	33.2	56	0.094	4.5
31	709614.313	4327548	5.44	9.58	7.27	50.2	44.24	30	50	0.121	4
32	709625.688	4327543	7.23	11.06	11.3	49.57	63.18	33.2	41	0.524	1.1
33	709636.375	4327540	7.24	11.25	11.66	47.8	64.55	25	42	0.239	2.6
34	709649.063	4327534.5	4.99	8.51	7.27	50.85	49.04	29.4	51	0.161	3.4
341	709645.563	4327532.5	6.88	10.58	10.17	50.29	61.15	39.8	34	0.488	1.3
342	709647.563	4327538	4.46	7.67	6.41	44.02	42.51	41.6	62	0.103	4.3
343	709652.563	4327536	2.89	5.74	4.06	48.74	36.48	28.8	150	0.091	4.5
344	709650.313	4327530.5	6.5	10.26	9.26	52.06	57.32	30.7	42	0.233	2.7
3441	709648.75	4327529.5	6.28	10.03	8.56	54.14	54.87	26.8	39	0.246	2.6
3442	709649.75	4327532.5	6.41	10.79	9.34	52.52	58.55	32.6	52	0.174	3.2
3443	709651.875	4327531	7.34	11.39	11.55	48.14	65.39	33.3	68	0.170	3.3
3444	709650.875	4327528.5	5.29	8.47	8.53	45.16	50.54	36.3	48	0.168	3.3
35	709661.688	4327530	5.84	9.94	7.99	49.65	47.95	31	47	0.299	2.2
41	709619.688	4327560	6.19	9.81	9.46	47.13	55.52	30.8	60	0.108	4.2
42	709631.313	4327555.5	7.28	11.55	10.45	51.45	57.45	30.5	43	0.248	2.6
43	709644	4327551	7.79	11.93	10.94	52.58	62.23	31.9	52	0.121	3.9
431	709640.375	4327548.5	7.4	10.81	11.76	44.64	64.71	33.4	52	0.287	2.3
432	709642.5	4327555	6.52	10.98	9.48	56.51	58.07	30.3	56	0.109	4.1
433	709647.938	4327552	6.11	9.94	8.65	52.12	55.74	36.2	34	0.366	1.8
434	709644.688	4327546.5	6.24	10.54	8.92	60.13	54.65	32.9	47	0.146	3.5
4341	709642.813	4327546	7.26	11.74	10.84	52.9	64.89	28.1	48	0.137	3.7
4342	709644.188	4327548.5	7.15	11.13	10.88	53.26	66.39	30.8	53	0.193	3
4343	709646.438	4327547.5	5.86	9.33	8.24	50.97	54.01	30.2	60	0.250	2.5
4344	709645.5	4327544.5	7.23	11.66	9.71	57.47	61.21	34.7	48	0.511	1.2
44	709654.688	4327547	2.54	3.36	2.98	31.51	23.77	29.8	170	0.032	6.4
45	709667.313	4327542	6.22	9.77	8.71	47.99	55.54	24.6	46	0.326	2

**Appendix P - Canopy Reflectance and Biophysical  
Attributes on 002CE, August 22, 2002**

ID	COOR-X	COOR-Y	Wavelength (nm)					SPAD	Height (cm)	fPAR	LAI
			480	560	660	830	1650				
11	709427.13	4327063.00	7.31	11.83	11.87	45.92	64.34	28.1	40	0.219	2.4
111	709431.75	4327063.00	5.98	9.33	9.4	39.65	54.45	30.2	45	0.190	2.6
112	709426.56	4327058.50	6.37	10.58	10.82	42.11	60.24	24.1	42	0.144	3.1
113	709423.19	4327062.50	6.27	10.11	9.92	43.51	57.83	24.4	52	0.180	2.7
114	709427.69	4327067.00	7.05	11.62	11.45	45.92	62.53	28.5	50	0.061	4.5
1141	709429.63	4327066.50	6.15	10.76	9.49	48.28	58.3	25.1	48	0.113	3.5
1142	709427.44	4327065.00	6.14	9.7	9.53	41.63	57.01	27.3	47	0.057	4.6
1143	709425.81	4327067.00	5.98	9.72	9.91	39.18	57.82	27.7	54	0.078	4.1
1144	709427.75	4327069.00	5.74	10.34	9.73	43.14	57.67	22.3	60	0.083	4
12	709418.31	4327071.00	6.3	10.18	10.36	41.76	57.47	24.4	40	0.184	2.7
13	709409.50	4327079.00	5.85	9.41	9.82	37.34	56.08	24.9	40	0.147	3
14	709400.69	4327087.50	6.82	11.95	9.91	54.06	59.68	27.3	43	0.032	5.5
15	709393.88	4327095.00	7.41	11.4	12.09	44.8	62.93	21.4	30	0.219	2.4
151	709397.31	4327095.50	7.13	11.16	11.73	44.43	60.6	28.4	30	0.213	2.4
152	709393.94	4327091.50	7.62	11.49	12.55	43.38	63.03	27.2	31	0.614	0.7
153	709390.56	4327095.50	8.1	12.12	12.48	46.53	63.16	21.5	29	0.370	1.5
154	709393.13	4327099.00	7.34	12.38	11.52	52.41	63.5	24.4	30	0.401	1.4
1541	709395.06	4327099.50	8.17	12.45	12.05	47.31	63.39	26.9	31	0.225	2.3
1542	709391.25	4327098.50	7.75	12.04	12.5	47	64.84	25.9	34	0.403	1.4
1543	709391.25	4327098.50	10.01	13.01	14.35	42.06	66.72	27.4	32	0.490	1.1
1544	709392.31	4327101.00	6.52	10.4	9.83	42.89	53.79	25.3	32	0.373	1.5
21	709416.00	4327058.00	6.51	12.78	10.09	54.67	58.46	17.6	45	0.159	2.9
22	709408.56	4327065.50	6.07	9.66	10.25	42.3	61.43	23.7	35	0.210	2.4
221	709412.50	4327065.50	6.33	10.51	10.2	43.32	58.06	22.7	42	0.216	2.4
222	709407.31	4327061.50	6.09	10.3	9.66	45.22	56.05	19.4	48	0.087	3.8
223	709403.25	4327065.50	5.77	9.84	9.93	42.07	58.22	23.1	40	0.245	2.2
224	709409.06	4327070.50	6.48	10.62	10.82	41.93	61.08	23.4	38	0.193	2.5
2241	709411.06	4327071.00	6.59	10.17	10.57	42.28	60.32	25.3	25	0.252	2.1

2242	709409.13	4327068.50	6.46	9.76	10.72	40.45	61.99	25.7	40	0.195	2.5
2243	709407.06	4327071.00	6	9.36	9.58	40.43	55.39	26.7	40	0.181	2.6
2244	709409.00	4327072.50	6.19	10.02	10.07	42.78	60.14	24.3	34	0.093	3.7
23	709400.38	4327073.50	5.78	9.08	9.66	36.6	54.88	26.1	38	0.492	1.1
24	709392.25	4327081.50	6.7	9.97	10.64	40.24	57.67	22.8	38	0.086	3.8
25	709383.44	4327090.00	6.36	9.09	9.74	32.89	46.14	23	32	0.279	1.9
31	709406.19	4327054.00	5.46	10.38	9.44	49.85	57.04	24.7	34	0.127	3.1
32	709398.75	4327061.00	5.88	9.64	9.95	40.91	57.57	23.8	35	0.154	2.8
33	709390.63	4327069.00	6.2	10.18	10.13	43.56	59	19.6	38	0.098	3.5
34	709383.13	4327076.50	5.89	10.48	9.42	47.84	57.77	25.9	57	0.049	4.6
341	709387.13	4327075.50	5.98	9.77	9.64	40.71	57.76	23.1	31	0.097	3.5
342	709382.38	4327073.00	6.05	10.05	9.2	45.23	55.49	28.7	50	0.073	4
343	709379.63	4327076.50	6.44	10.4	10.19	43.73	55.86	20.6	43	0.114	3.3
344	709384.44	4327080.00	6.73	10.34	10.86	42.93	60.41	18.3	29	0.351	1.5
3441	709387.00	4327080.00	6.53	10.02	9.77	42.45	58.64	32.5	32	0.272	1.9
3442	709383.75	4327078.00	6.69	11.24	9.98	48.54	59.57	28.9	39	0.286	1.9
3443	709382.38	4327081.00	6.75	10.28	10.65	40.99	56.74	28.1	36	0.483	1.1
3444	709385.00	4327082.00	9.23	13.26	14.33	45.83	69.91	21.9	27	0.555	0.9
35	709374.31	4327085.50	6.85	10.95	11.22	42.98	61.14	15.2	41	0.352	1.5
41	709393.13	4327048.50	5.64	10.36	8.91	51.72	57.03	24.9	46	0.140	2.9
42	709386.31	4327056.50	5.78	10.52	9.68	47.65	57.14	23	53	0.039	4.9
43	709381.56	4327062.50	5.8	10.01	8.84	48.54	56.14	21.3	46	0.096	3.5
431	709385.50	4327063.00	5.68	9.55	9.01	43.53	52.98	25.3	43	0.183	2.5
432	709379.00	4327059.00	6.24	10.29	9.67	48.54	58.91	20.4	54	0.027	5.5
433	709376.88	4327063.50	6.32	11.21	9.65	51.28	56.46	24.1	49	0.135	3
434	709382.06	4327067.00	6.34	10.74	10.14	47.53	61.84	23.2	38	0.158	2.7
4341	709383.94	4327066.50	5.73	9.68	9.28	46.39	55.39	24.4	33	0.251	2
4342	709381.69	4327065.00	8.63	12.1	11.82	46.05	63.02	25.2	34	0.538	0.9
4343	709380.50	4327067.50	6.07	9.98	9.12	45.26	56.82	26.1	42	0.128	3
4344	709382.25	4327068.50	6.09	9.68	9.75	43.92	60.27	26.8	39	0.089	3.6
44	709373.38	4327072.00	5.97	9.68	9.15	43.67	57	28.1	51	0.060	4.2
45	709367.31	4327078.50	6.67	11.1	9.83	50.56	57.44	24.3	47	0.107	3.3

**Appendix Q - Canopy Reflectance and Biophysical  
Attributes on 002CW, August 22, 2002**

ID	COOR-X	COOR-Y	Wavelength (nm)					SPAD	Height (cm)	fPAR	LAI
			485	560	660	830	1650				
11	709350.25	4326924.00	6.69	11.31	9.6	49.78	59.76	29.1	65	0.064	4.7
111	709351.00	4326919.50	7.67	13.12	11.4	62.69	66.62	27.3	60	0.042	5.5
112	709345.00	4326922.00	6.32	11.64	8.89	56.86	55.3	27.7	72	0.007	8.7
113	709346.81	4326927.50	7.45	12.07	11.6	46.93	65.93	29.9	58	0.084	4.3
114	709354.81	4326925.50	6.26	12.28	8.35	60.17	54.13	28.1	69	0.016	7.2
1141	709355.75	4326924.00	5.71	10.75	8.29	53.11	52.69	29.7	74	0.006	8.7
1142	709352.88	4326924.50	6.23	11.96	8.93	59.54	58.56	29	63	0.013	7.5
1143	709353.38	4326927.50	7.68	14.76	10.4	68.17	64.73	30.3	67	0.032	5.9
1144	709356.06	4326927.00	5.38	10.87	7.46	58.14	49.21	29.1	77	0.042	5.4
12	709366.94	4326967.00	6.28	11.1	10.3	53.96	64.52	26.8	58	0.058	4.9
13	709360.25	4326969.00	6.11	10.56	9.92	43.6	55.49	27	60	0.145	3.3
14	709362.69	4326976.00	6.42	11.69	9.98	50.68	56.61	26.6	61	0.038	5.6
15	709369.44	4326972.50	6.68	10.26	9.86	45.39	56.7	24.8	82	0.007	8.4
151	709369.44	4326970.50	5.81	10.87	8.77	48.84	53.57	25.7	72	0.049	5.1
152	709367.13	4326972.50	6.46	12.39	10.2	53.48	61.1	21.9	60	0.028	6.1
153	709369.25	4326975.00	6.09	10.7	8.95	50.73	55.85	26.8	71	0.066	4.6
154	709371.38	4326973.00	5.56	10.41	7.72	58.21	52.09	33.5	82	0.008	8.2
1541	709372.06	4326972.00	5.53	10.57	7.47	57.68	50.35	26.4	80	0.023	6.4
1542	709356.69	4326926.00	5.39	9.73	7.85	50.01	50.63	27	72	0.020	6.7
1543	709370.50	4326972.00	5.87	11.02	8.42	54.99	52.93	24	59	0.080	4.3
1544	709355.25	4326926.50	5.91	10.79	9	48.38	52.83	23.9	57	0.135	3.4
21	709339.00	4326927.50	7.1	12.39	10.9	56.36	66.03	27.6	70	0.067	4.6
22	709341.19	4326940.00	6.82	11.27	10.5	46.8	58.06	28.5	50	0.085	4.2
221	709343.31	4326935.50	6.35	10.14	9.73	42.66	55.32	29.1	60	0.074	4.4
222	709337.31	4326938.50	6.35	13.02	10.3	58.13	65.41	28.5	73	0.053	5
223	709339.13	4326943.50	5.49	9.39	8.46	42.77	52.62	29.1	71	0.045	5.2
224	709345.13	4326940.50	6.47	10.53	9.5	48.36	54.96	26.3	55	0.134	3.4
2241	709345.38	4326938.50	5.21	8.8	8.56	38.58	50.36	23.5	66	0.129	3.4
2242	709343.00	4326940.00	5.73	9.41	9.15	39.46	54.71	27.8	72	0.225	2.5

2243	709344.75	4326942.50	7.18	11.45	11.1	45.14	60.79	29.4	56	0.174	2.9
2244	709347.13	4326941.00	6.71	10.94	9.48	49.05	56.65	32	58	0.035	5.7
23	709344.88	4326952.00	5.86	9.88	9.91	41.46	56.02	22.7	65	0.212	2.6
24	709348.50	4326963.50	6.63	10.9	10.6	41.9	56.38	25.6	50	0.123	3.5
25	709352.19	4326975.00	6.27	10.85	9	48.93	54.65	30.5	75	0.051	5
31	709326.88	4326933.50	8.36	13.91	13	61.74	74.57	25.5	68	0.125	3.4
32	709330.50	4326945.00	6.74	11.3	10.4	45.24	55.88	27.7	50	0.171	2.9
33	709333.50	4326957.50	6.61	11.74	9.77	46.47	58.13	23.4	60	-	-
34	709337.81	4326968.00	6.83	11.52	10.1	49.29	56.72	29.2	58	0.068	4.5
341	709338.56	4326964.00	6.35	10.62	9.51	46.06	54.64	23.3	51	0.157	3.1
342	709334.19	4326967.00	6.83	11.35	10.6	44.54	57.28	26.3	63	0.189	2.7
343	709336.38	4326971.00	6.06	9.83	9.13	42.28	51.74	29	56	0.117	3.5
344	709340.94	4326968.50	6.13	10.47	9.74	43.09	56.3	20.5	52	0.125	3.4
3441	709341.00	4326967.00	7.11	12.32	11.8	57.89	77.29	26.3	44	0.094	3.9
3442	709339.69	4326968.00	6.61	11.34	9.98	47.13	56.13	29.5	54	0.238	2.4
3443	709340.56	4326970.00	7	11.42	11.3	49.33	64.82	25.4	49	0.185	2.8
3444	709342.38	4326969.00	6.05	9.86	9.51	40.03	53.75	26.4	50	0.108	3.7
35	709340.19	4326978.50	6.94	12.23	10	54.81	58.05	24.2	62	0.061	4.6
41	709315.44	4326939.00	8.14	12.06	12.1	44.8	61.04	32.1	30	0.382	1.6
42	709319.19	4326949.50	7.16	11.12	10.7	45.72	58.53	28.3	41	0.112	3.6
43	709322.13	4326961.00	5.74	10.16	7.71	48.84	48.02	24	48	0.051	4.9
431	709323.94	4326957.50	6.38	10.76	9.15	48.45	53.22	24.3	50	0.088	4
432	709318.19	4326960.00	5.85	10.22	8.89	45.23	52.67	25.7	42	0.106	3.7
433	709320.19	4326964.50	6.78	12.93	9.86	55.22	58.76	23.7	53	0.135	3.3
434	709325.19	4326963.00	6.75	11.58	10	51.77	53.75	21.7	62	0.127	3.4
4341	709326.00	4326961.00	5.87	10.42	9.33	47.8	52.81	30.2	35	0.145	3.1
4342	709323.56	4326962.00	6.1	10.31	9.14	45.65	51.46	20.5	42	0.133	3.3
4343	709324.06	4326964.50	6.4	11.26	9.23	51.44	52.16	32.1	83	0.018	6.6
4344	709326.69	4326964.00	5.9	10.6	9.08	49.69	54.66	27.1	62	0.058	4.7
44	709324.50	4326971.00	5.98	9.55	9.3	35.97	51.9	25.9	63	0.081	4.1
45	709326.94	4326980.50	5.78	10.07	7.81	51.26	50.03	28.2	75	0.016	6.8